

**Synthesis and investigation of the chemosensing properties of  
novel fluorescent triazolyl coumarin-based polymers**

By

J.M.V NGORORABANGA

A dissertation submitted in fulfillment of the requirements for the PhD  
degree in Chemistry to be awarded at the Nelson Mandela Metropolitan  
University

April 2017

Supervisor: Dr N. Mama

---

## Dedication

Unto God, in whom all is possible; and my parents, the late Mr Mpatabanga and Ms Mukagakwisi.

---

## Abstract

Environmental pollution by ionic species has become one of the greatest challenges to the sustainable development of communities. Increasing amounts of these ionic species in the environment is associated with several detrimental effects to human health and ecological systems. Proper detection and monitoring of these ionic species is essential. Considering the diversity of the ions and the fact that the available sensors are limited, it is clear that there is need for a rapid and low-cost method for recognition and monitoring of these ions. Fluorescence based methods are ranked among the most powerful transduction systems to signal chemical recognition events. Fluorescent polymers containing triazolyl coumarin units in the polymer backbone or as pendant groups were therefore designed and investigated as potential sensors for these ions.

Three methods were used to incorporate triazolyl coumarin units into the polymers. The first method involved polymerization of the vinyl monomer containing the triazolyl coumarin unit. The second method involved AA-BB step-grow click polymerization of diazide and dialkyne-functionalized monomers. The third method involved post-polymerization functionalization of an azide-functionalized polymer with an alkyne functionalized coumarin derivative. In each method, formation of the triazole ring was achieved using a Cu(I)-catalyzed 1,3-dipolar cycloaddition (CuAAC) reaction.

The photophysical properties of the polymers and their starting monomers were investigated and compared. Polymers with triazolyl coumarin units in the backbone or as pendant groups were found to have higher absorption and emission intensities than their corresponding monomers while polymers resulting from functionalization of azide-functionalized polymer were found to exhibit improved photophysical properties compared to the starting azide-functionalized polymer.

The chemosensing potential of the polymers was investigated through absorption and emission. The polymers were found to be selective towards different metal ions ( $\text{Fe}^{3+}$ ,  $\text{Hg}^{2+}$  and  $\text{Al}^{3+}$ ) and anions ( $\text{OH}^-$  and  $\text{F}^-$ ). The mechanisms of interaction between the polymers and ions were investigated by comparing the absorption and emission spectra of the polymers to those of their monomers in the presence of an ion of interest. In some cases the mechanism of interaction was supported by  $^1\text{H}$  NMR and FT-IR.

---

---

## Acknowledgements

I would like to acknowledge the following people and institutions that made it possible for me to complete this project;

- The almighty God for the gift of life.
- My supervisor, Dr N. Mama for her constant guidance and support.
- Nelson Mandela Metropolitan University (NMMU) for funding and giving the opportunity and facilities to carry out this project.
- Mr H. Schalekamp, Dr. E. Hosten, Mr H. Marchant, Ms Kina Miller, and Mr E. Bashman for their technical assistance.
- André Adams, Nadia Adams, Lynn Cristalla, Dr Felix Odame and Tendai Dembaremba for their treasured friendship, assistance and advice.
- Fellow students and friends at Nelson Mandela Metropolitan University.
- My mother, siblings, daughter and fiancée for their endless love and motivation to strive for my dream

---

---

## Table of Contents

Dedication.....	i
Abstract.....	ii
Acknowledgements.....	iii
Table of contents.....	iv
List of figures.....	viii
List of Schemes.....	xiv
Selected Abbreviations.....	xvi
Selected Abbreviations.....	xvi
1.1 Background.....	0
1.2 Human and ecological significance of ions and their detection.....	1
1.2.1 Examples of pollutant ionic species.....	2
1.3 Aim of the study.....	4
1.4 Organization of the thesis.....	4
1.5 References.....	5
Chapter 2 Signal transduction modes and polymer based chemosensors.....	8
2.1 Introduction.....	8
2.2 Optical chemosensors.....	9
2.2.1 Fluorogenic chemosensors.....	10
2.2.2 Mechanism of fluorescence sensing.....	12
2.2.2.1 Photo-induced electron transfer (PET).....	12
2.2.2.2 Intramolecular charge transfer (ICT).....	17
2.2.2.3 Energy transfer (ET).....	19
2.2.2.4 Excimer and exciplex formation.....	25
2.2.2.5 Aggregation-induced emission.....	26
2.2.2.6 C=N isomerization.....	27
2.2.2.7 Excited state intramolecular proton transfer (ESIPT).....	29
2.3 Fluorescent polymers.....	30
2.3.1 Side-chain polymer based chemosensors.....	32
2.3.2 Conjugated polymers based-chemosensors.....	34
2.3.3 Molecular imprinted polymer based-chemosensors.....	36
2.3.4 Dendrimer-based chemosensors.....	38

2.4	Triazole-based chemosensors .....	38
2.5	Coumarin derivatives.....	43
2.6	References .....	44
<b>Chapter 3 Polymers with conjugated triazolyl coumarin units as pendant group.....</b>		<b>52</b>
3.1	Introduction .....	52
3.2	Monomer synthesis .....	54
3.2.1	Absorption and fluorescence properties of the monomers.....	57
3.3	Polymer synthesis.....	58
3.4	Absorption and fluorescence properties of the polymers .....	60
3.4	Chemosensing studies of polymer 18 and 19 .....	62
3.4.1	UV-Vis analysis .....	63
3.4.3	Titration experiments of polymer 18 and 19 with Fe <sup>3+</sup> ions .....	66
3.4.4	Competitive studies .....	68
3.4.5	Sensing mechanism of polymers 18 and 19 toward metal ions .....	69
3.4	Conclusion.....	71
3.5	Experimental.....	71
3.5.1	General information.....	71
3.5.1	Synthesis of vinyl monomer (10).....	72
3.5.2	Synthesis of vinyl monomer (16).....	74
3.5.3	7-(Diethylamino)-2 <i>H</i> -chromen-2-one (17).....	75
3.5.4	Radical polymerization of monomer 10 and 16.....	75
3.6	References .....	75
<b>Chapter 4 Polymers with bridged triazolyl coumarin units as pendant group.....</b>		<b>77</b>
4.1	Introduction .....	77
4.2	Synthesis of the poly(4-vinylbenzyl azide) polymer (P0).....	78
4.3	Triazolyl coumarin based polymers with hydroxyethylene linkages between triazole and coumarin units.....	81
4.3.1	Triazolyl coumarin based polymers with the hydroxyethylene linkage at position 3 of the coumarin motif (P1) .....	82
4.3.1.1	Synthesis of alkynylated coumarin derivative 7 .....	82
4.3.1.3	Functionalization of polymer P0 using alkynylated coumarin derivative 7.....	83
4.3.1.3	Absorption and emission studies of functionalized polymer P0.....	85
4.3.1.4	Chemosensing studies.....	86
4.3.2	Triazolyl coumarin based polymers with the hydroxyethylene linkage at position 8 of the coumarin motif (P2) .....	104

4.3.2.1	Synthesis of alkynylated coumarin derivative 11 .....	104
4.3.2.2	Functionalization of polymer P0 using alkynylated coumarin derivative 11.....	106
4.3.2.3	Absorption and emission studies on functionalized of polymer P0.....	108
4.3.2.4	Chemosensing studies.....	109
4.4	Triazolyl coumarin-based polymers with amino-methylene linkages between triazole and coumarin units (P3).....	125
4.4.1	Synthesis of the alkynylated coumarin derivative 15 .....	125
4.4.2	Functionalization of polymer P0 with alkynylated coumarin derivative 15 .....	126
4.4.3	Absorption and emission studies on polymer P0 functionalization .....	128
4.4.4	Chemosensing studies of polymer P3.....	131
4.4.4.1	Absorption and emission studies.....	131
4.4.4.2	Titration experiments.....	132
4.4.4.3	Competitive studies .....	133
4.4.4.4	Sensing mechanism of the polymer P3 with F <sup>-</sup> ions.....	134
4.5	Conclusion.....	135
4.6	Experimental.....	135
4.6.1	General information .....	135
4.6.2	Synthesis of the poly(4-vinylbenzyl azide) (P0) .....	135
4.6.3	Synthesis of 7-(diethylamino)-3-(1-hydroxybut-3-ynyl)-2 <i>H</i> -chromen-2-one (7).....	136
4.6.4	Synthesis of 7-hydroxy-8-(1-hydroxybut-3-ynyl)-4-methyl-2 <i>H</i> -chromen-2-one(11)....	137
4.6.5	Synthesis of 7-(diethylamino)-3-(prop-2-ynylamino)-2 <i>H</i> -chromen-2-one (15) .....	137
4.6.5.2	General procedure for functionalization of poly(4-vinylbenzyl azide) .....	138
4.7	References .....	138
Chapter 5	Linear triazolyl coumarin-based polymers .....	140
5.1	Introduction .....	140
5.2	Monomer synthesis .....	141
5.2.1	AA-type monomer synthesis .....	141
5.2.2	BB-type monomer synthesis.....	143
5.3	AA-BB step-growth click polymerization.....	146
5.4	The effect of click polymerization on photophysical properties of the monomers .....	148
5.5	Photophysical properties of polymers 18 and 19 .....	149
5.6	Chemosensing studies of polymer 18.....	152
5.6.1	Absorption studies.....	152
5.6.2	Emission studies .....	153

---

---

5.6.3	Titration experiments.....	154
5.6.4	Competitive studies .....	155
5.6.5	Sensing mechanism of polymer 18 with Hg <sup>2+</sup> .....	156
5.7	Quaternarization of polymer 18 .....	157
5.7.1	Emission studies .....	158
5.7.2	Effect of solvent on the emission of the quaternarized polymer 20.....	159
5.7.3	Effect of metal ions on the emission of the quaternarized polymer 20 .....	160
5.7.4	Competitive studies .....	161
5.8	Conclusion.....	162
5.9	Experimental.....	163
5.9.1	General information.....	163
5.9.2	Synthesis of AA-type monomer.....	163
5.9.3	Synthesis of BB-type monomer .....	164
5.9.3.1	Synthesis of diazide functionalized coumarin monomer (12).....	164
5.9.4	General procedure for AA-BB step-growth click polymerization .....	166
5.9.5	Quaternarization of polymer 18.....	166
5.10	References .....	167
Chapter 6	Summary, conclusions and recommendations.....	168
	for future work .....	168
6.1	Summary and conclusions .....	168
6.2	Recommendations for future work.....	170
Appendices.....		171
Appendices.....		174



---

---

## List of Figures

<b>Figure 2.1:</b> A schematic representation of a chemosensor binding to an analyte .....	8
<b>Figure 2.2:</b> Coumarin based polymeric chemosensor for cyanide ions detection.....	10
<b>Figure 2.3:</b> Examples of different fluorogenic sensing systems based on chemodosimeter approach.....	11
<b>Figure 2.4:</b> PET mechanism showing the interaction between LUMO and HOMO of the fluorophore and the external molecular orbital of the receptor.....	13
<b>Figure 2.5:</b> Fluorescent “turn-on” type PET chemosensor in terms of frontier molecular orbitals.....	14
<b>Figure 2.6:</b> Fluorescent “turn-on” type PET chemosensor in terms of frontier molecular orbitals.....	16
<b>Figure 2.7:</b> Shifts in ICT mechanism due to analyte binding.....	18
<b>Figure 2.8:</b> Förster type and Dexter energy transfer.....	20
<b>Figure 2.9:</b> Schematic representation of FRET mechanism from a donor to an acceptor.....	21
<b>Figure 2.10:</b> FRET spectral overlap.....	22
<b>Figure 2.11:</b> Dexter type energy transfer between a donor and an acceptor.....	24
<b>Figure 2.12:</b> Pyrene-coumarin based calix fluorophore emitting exciplex for F <sup>-</sup> ions detection.....	26
<b>Figure 2.13:</b> AIE-based chemosensors.....	27
<b>Figure 2.14:</b> Mode of analyte interactions which lead to the inhibition of C=N isomerization.....	28
<b>Figure 2.15:</b> ESIPT-based polymeric chemosensor for anions.....	30
<b>Figure 2.16:</b> Comparison between small molecule based chemosensors and conjugated polymer based chemosensors in term of sensitivity.....	31
<b>Figure 2.17:</b> CPs signal amplification upon analyte binding.....	35
<b>Figure 2.18:</b> Examples of CPs with chemosensing applications.....	36
<b>Figure 2.19:</b> Summary of polymer imprinting process.....	37
<b>Figure 2.20:</b> Poly(amine ester) dendrimer for Al <sup>3+</sup> , Cu <sup>2+</sup> and Zn <sup>2+</sup> detection.....	38
<b>Figure 1.21:</b> Triazole-containing polymer for Hg <sup>2+</sup> and Zn <sup>2+</sup> recognition.....	40
<b>Figure 2.22:</b> Triazole-containing chromogenic chemosensor for F <sup>-</sup> ions.....	41
<b>Figure 2.23:</b> Triazole-containing fluorogenic chemosensor for citrate ions.....	42
<b>Figure 2.24:</b> Triazole-based polymer for the detection of explosive compounds.....	42

---

<b>Figure 2.25:</b> Coumarin structure showing the numbering of carbons.....	43
<b>Figure 2.26:</b> Coumarin “push-pull” $\pi$ -electron system.....	44
<b>Figure 3.1:</b> 1,2,3-Triazole-coumarin-based fluorescent probe for hydrogen peroxide detection.....	53
<b>Figure 3.2:</b> Triazolyl coumarin substituted glycoligands for selective recognition of $\text{Ag}^+$ ions in aqueous solution.....	53
<b>Figure 3.3:</b> $^1\text{H}$ NMR spectrum of the monomer <b>10</b> .....	56
<b>Figure 3.4:</b> $^1\text{H}$ NMR spectrum of the monomer <b>16</b> .....	56
<b>Figure 3.5:</b> Absorption and Emission spectra of monomers <b>10</b> and <b>16</b> , and 7-diethylamionocoumarin <b>17</b> . .....	58
<b>Figure 3.6:</b> $^1\text{H}$ NMR spectrum for polymer <b>18</b> .....	59
<b>Figure 3.7:</b> $^1\text{H}$ NMR spectrum for polymer <b>19</b> .....	60
<b>Figure 3.8:</b> Comparative FT-IR spectra of monomer <b>10</b> and <b>16</b> with their corresponding polymers <b>18</b> and <b>19</b> .....	60
<b>Figure 3.9:</b> Absorption and emission spectra of monomer <b>10</b> and <b>16</b> with their corresponding polymers <b>18</b> and <b>19</b> .....	61
<b>Figure 3.10:</b> Absorption and emission spectra of polymers <b>18</b> and <b>19</b> .....	62
<b>Figure 3.11:</b> Absorption spectra of polymer <b>18</b> in the presence of metal ions and anions ...	64
<b>Figure 3.12:</b> Absorption spectra of polymer <b>19</b> in the presence of metal ions and anions ...	64
<b>Figure 3.13:</b> Emission spectra of polymer <b>18</b> in the presence of metal ions and anions .....	65
<b>Figure 3.14:</b> Emission spectra of polymer <b>19</b> in the presence of metal ions and anions....	66
<b>Figure 3.15:</b> Changes in the absorption spectra of polymer <b>18</b> and polymer <b>19</b> upon addition of $\text{Fe}^{3+}$ aliquots. ....	67
<b>Figure 3.16:</b> Emission spectra of polymer <b>18</b> and polymer <b>19</b> in DMF in the presence of increasing amounts of $\text{Fe}^{3+}$ .....	67
<b>Figure 3.17:</b> Fluorescence responses of polymer and polymer <b>19</b> in the presence of other metal ion.....	68
<b>Figure 3.18:</b> Emission spectra of 7-diethylamionocoumarin <b>17</b> , monomer <b>10</b> and monomer <b>16</b> in the presence of $\text{Fe}^{3+}$ , $\text{Cu}^{2+}$ , $\text{Hg}^{2+}$ and $\text{Co}^{2+}$ .....	70
<b>Figure 3.19:</b> Changes in the FT-IR spectra of polymers <b>18</b> and <b>19</b> with addition of aliquots of $\text{Fe}^{3+}$ .....	71
<b>Figure 4.1:</b> $^1\text{H}$ NMR spectrum of monomer <b>2</b> .....	79
<b>Figure 4.2:</b> FT-IR spectra of 4-vinylbenzyl chloride and monomer <b>2</b> .....	80

---

<b>Figure 4.3:</b> $^1\text{H}$ NMR spectrum of the polymer <b>P0</b> .....	80
<b>Figure 4.4:</b> FT-IR spectra of monomer <b>2</b> and polymer <b>P0</b> .....	81
<b>Figure 4.5:</b> Structures of alkynylated coumarin derivatives <b>7</b> , <b>11</b> .....	81
<b>Figure 4.6:</b> $^1\text{H}$ NMR spectrum of alkynylated coumarin derivative <b>7</b> .....	83
<b>Figure 4.7:</b> $^1\text{H}$ NMR spectra of <b>P0</b> , the alkynylated coumarin derivative <b>7</b> and the polymer <b>P1</b> .....	84
<b>Figure 4.8:</b> Comparison of FT-IR spectra of polymer <b>P0</b> and functionalized polymer <b>P1</b> ....	85
<b>Figure 4.9:</b> Absorption and emission spectra of alkynylated coumarin derivative <b>7</b> , polymer <b>P0</b> and <b>P1</b> .....	86
<b>Figure 4.10:</b> Absorption spectra of alkynylated coumarin <b>7</b> in the presence of different metal ions and anions.....	87
<b>Figure 4.11:</b> The absorption spectra of alkynylated coumarin derivative <b>7</b> upon addition of increasing amount of $\text{Hg}^{2+}$ .....	88
<b>Figure 4.12:</b> Emission spectra of alkynylated coumarin <b>7</b> in the presence of different metal ions and anions.....	89
<b>Figure 4.13:</b> The emission spectra of alkynylated coumarin derivative <b>7</b> upon addition of increasing amount of $\text{Hg}^{2+}$ .....	90
<b>Figure 4.14:</b> Fluorescence response of alkynylated coumarin derivative <b>7</b> in the presence of mixture of $\text{Hg}^{2+}$ with other metal ions.....	91
<b>Figure 4.15:</b> A Job plot and Benesi-Hildebrand plot of alkynylated coumarin derivative <b>7</b> with $\text{Hg}^{2+}$ . .....	92
<b>Figure 4.16:</b> Changes in the $^1\text{H}$ NMR signal of the alkynylated coumarin <b>7</b> with increasing amounts of $\text{Hg}^{2+}$ in $\text{DMSO-d}_6$ .....	92
<b>Figure 4.15:</b> Absorption spectra of polymer <b>P1</b> in the presence of different metal ions.....	94
<b>Figure 4.18:</b> Emission spectra and emission response of polymer in the presence of metal ions .....	94
<b>Figure 4.19:</b> The absorption spectra of polymer <b>P1</b> upon addition of increasing amount of $\text{Fe}^{3+}$ and $\text{Hg}^{2+}$ .....	95
<b>Figure 4.20:</b> Emission spectra of polymer <b>P1</b> upon addition of increasing amount of $\text{Fe}^{3+}$ and $\text{Hg}^{2+}$ .....	96
<b>Figure 4.21:</b> Fluorescence response of <b>P1</b> in the presence $\text{Hg}^{2+}/\text{Fe}^{3+}$ and other metal ions ..	97
<b>Figure 4.22:</b> Absorption spectra of polymer <b>P1</b> in the presence of different anion.....	98

---

<b>Figure 4.23:</b> Emission spectra and fluorescence response of polymer <b>P1</b> in the presence of various anions .....	98
<b>Figure 4.24:</b> The absorption spectra of polymer <b>P1</b> upon addition of OH <sup>-</sup> aliquots... ..	99
<b>Figure 4.25:</b> Fluorescence response of polymer <b>P1</b> in the presence of mixture of OH <sup>-</sup> and other anions.....	100
<b>Figure 4.26:</b> Absorption spectra of the alkynylated coumarin derivative <b>7</b> and polymer <b>P1</b> in the presence of Hg <sup>2+</sup> .....	102
<b>Figure 4.27:</b> <sup>1</sup> H NMR spectrum of the alkynylated coumarin derivative <b>11</b> .....	106
<b>Figure 4.28:</b> <sup>1</sup> H NMR spectra of <b>P0</b> , the alkynylated coumarin derivative <b>11</b> and the polymer <b>P2</b> . .....	107
<b>Figure 4.29:</b> FT-IR spectra of polymer <b>P0</b> and the functionalized polymer <b>P2</b> .....	108
<b>Figure 4.30:</b> Absorption and emission spectra of the alkynylated coumarin derivative <b>11</b> , polymer <b>P0</b> and polymer <b>P2</b> .....	109
<b>Figure 4.31:</b> Absorption spectra of alkynylated coumarin derivative <b>11</b> in the presence of various metal ions anions .....	110
<b>Figure 4.32:</b> Emission spectra of the alkynylated coumarin derivative <b>11</b> in the presence of various metal ions and anions .....	111
<b>Figure 4.33:</b> Absorption and emission spectra of alkynylated coumarin derivative <b>11</b> upon addition of Hg <sup>2+</sup> .....	112
<b>Figure 4.34:</b> Fluorescence response of alkynylated coumarin <b>11</b> in the presence of mixture of Hg <sup>2+</sup> and other metal ions .....	113
<b>Figure 4.35:</b> Job plot and Benesi-Hildebrand plot of alkynylated coumarin <b>11</b> derivative with Hg <sup>2+</sup> .....	114
<b>Figure 4.36:</b> Changes in the <sup>1</sup> H NMR signal of the alkynylated coumarin derivative <b>11</b> with increasing amounts of Hg <sup>2+</sup> in DMSO <sub>d6</sub> .....	115
<b>Figure 4.37:</b> Absorption spectra of polymer <b>P2</b> in the presence of various metal ions anions.....	116
<b>Figure 4.38:</b> Emission spectra polymer <b>P2</b> in the presence of different metal ions and anions .....	117
<b>Figure 4.39:</b> Absorption spectra of polymer <b>P2</b> upon addition of increasing amount of Hg <sup>2+</sup> and Fe <sup>3+</sup> .....	118
<b>Figure 4.40:</b> Emission spectra of polymer <b>P2</b> upon addition of increasing amount of Hg <sup>2+</sup> and Fe <sup>3+</sup> .....	119

---

---

<b>Figure 4.41:</b> Changes in the emission spectra of polymer <b>P2</b> with increasing amounts of $\text{Al}^{3+}$ .....	120
<b>Figure 4.42:</b> Fluorescence response of polymer <b>P2</b> in the presence of a mixture of $\text{Al}^{3+}$ and other metal ions .....	121
<b>Figure 4.43:</b> Fluorescence response of polymer <b>P2</b> in the presence of a mixture of $\text{Hg}^{2+}$ and other metal ions .....	122
<b>Figure 4.44:</b> $^1\text{H}$ NMR spectrum of alkynylated coumarin derivative <b>15</b> .....	126
<b>Figure 4.45:</b> Comparative $^1\text{H}$ NMR spectra for polymer <b>P0</b> , alkynylated coumarin derivative <b>15</b> , polymer <b>P3</b> .....	127
<b>Figure 4.46:</b> Comparative FT-IR spectra of polymer <b>P0</b> and the functionalized polymer <b>P3</b> .....	128
<b>Figure 4.47:</b> Absorption and emission spectra of the alkynylated coumarin derivative <b>15</b> , polymer <b>P0</b> and polymer <b>P3</b> .....	128
<b>Figure 4.48:</b> Emission spectra of polymer <b>P3</b> in the presence of various metal ions. ... ..	131
<b>Figure 4.49:</b> Absorption and emission spectra of polymer <b>P3</b> in the presence of various anions.....	132
<b>Figure 4.50:</b> Absorption and emission spectra of polymer <b>P3</b> in DMF upon addition of $\text{F}^-$ .....	133
<b>Figure 4.51:</b> Fluorescence responses of polymer <b>P3</b> in the presence of mixture of $\text{F}^-$ and other anions .....	133
<b>Figure 5.1:</b> Different types of monomers for the synthesis of polytriazoles.....	140
<b>Figure 5.2:</b> $^1\text{H}$ NMR spectrum of the monomer precursor <b>6</b> .....	142
<b>Figure 5.3:</b> $^1\text{H}$ NMR spectrum of monomer <b>7</b> .....	142
<b>Figure 5.4:</b> $^1\text{H}$ NMR spectrum of monomer <b>12</b> in DMSO.....	144
<b>Figure 5.5:</b> FT-IR spectrum of monomer <b>12</b> .....	144
<b>Figure 5.6:</b> $^1\text{H}$ NMR spectrum of monomer <b>17</b> .....	145
<b>Figure 5.7:</b> FT-IR spectrum of monomer <b>17</b> .....	146
<b>Figure 5.8:</b> $^1\text{H}$ NMR spectrum of polymer <b>18</b> in DMSO.....	147
<b>Figure 5.9:</b> $^1\text{H}$ NMR spectrum of polymer <b>19</b> in DMSO.....	147
<b>Figure 5.10:</b> Comparative FT-IR spectra between monomers <b>12</b> and <b>17</b> with their corresponding polymers <b>18</b> and <b>19</b> .....	148
<b>Figure 5.11:</b> Absorption and emission spectra of monomers <b>7</b> , <b>12</b> and polymer <b>18</b> .....	149
<b>Figure 5.12:</b> Absorption and emission spectra of polymers <b>18</b> and <b>19</b> .....	150
<b>Figure 5.13:</b> Emission spectra of polymer <b>18</b> in DMF at different the excitation wavelengths .....	

---

---

.....	151
<b>Figure 5.14:</b> Absorption spectra of polymer <b>18</b> in the presence of various metal ions and anions	.....153
<b>Figure 5.15:</b> Emission spectra of polymer <b>18</b> in the presence of various metal ions and anions	.....154
<b>Figure 5.16:</b> Absorption and emission spectra of polymer <b>18</b> upon addition of Hg <sup>2+</sup> aliquots.....	155
<b>Figure 5.17:</b> Emission spectra of polymer <b>18</b> in the presence of mixture of Hg <sup>2+</sup> and other metal ions.....	156
<b>Figure 5.18:</b> The proposed binding sites of Hg <sup>2+</sup> and other metal ions.....	157
<b>Figure 5.19:</b> Comparative <sup>1</sup> H NMR spectra between polymer <b>18</b> and the quaternarized polymer <b>20</b> .....	158
<b>Figure 5.20:</b> Comparative emission spectra between polymer <b>18</b> and the quaternarized polymer <b>20</b> . .....	158
<b>Figure 5.21:</b> Changes in the emission spectra of the quaternarized polymer <b>20</b> with different DMF/H <sub>2</sub> O ratios. ....	159
<b>Figure 5.22:</b> Emission spectra of the quaternarized polymer <b>20</b> in the presence of metal ions	.....160
<b>Figure 5.23</b> Changes in the emission spectra of the quaternarized polymer <b>20</b> with increasing amounts of Hg <sup>2+</sup> .....	161
<b>Figure 5.24:</b> Fluorescence responses of the quaternarized polymer <b>20</b> in the presence of a mixture of Hg <sup>2+</sup> and other metal ions .....	162

---

## List of Schemes

<b>Scheme 2.1:</b> A fluorescent “turn-on” PET polymeric chemosensor for detection of proton and Ni <sup>2+</sup> .....	15
<b>Scheme 2.2:</b> A fluorescent “turn-on” PET polymeric chemosensors for F <sup>-</sup> ions.....	16
<b>Scheme 2.3:</b> ICT-based polymeric chemosensor for Cd <sup>2+</sup> , H <sup>+</sup> and Zn <sup>2+</sup> .....	19
<b>Scheme 2.4:</b> Polyfluorene-bearing boronate-protected fluorescein (peroxyfluoro-1) for the detection of (H <sub>2</sub> O <sub>2</sub> ) and glucose in serum. ....	23
<b>Scheme 2.5:</b> Coumarin-rhodamin TBET system for ratiometric detection of Hg <sup>2+</sup> .....	25
<b>Scheme 2.6:</b> Different types of C=N isomerization based chemosensors.....	29
<b>Scheme 2.7:</b> A reusable thermoresponsive co-polymer with coumarin-spyropropan conjugate for cyanide ions detection.....	33
<b>Scheme 2.8:</b> Highly sensitive and selective turn-on fluorescent polymeric chemosensor for Hg <sup>2+</sup> in pure water.....	33
<b>Scheme 2.9:</b> Representation of imprinted process for Al <sup>3+</sup> -imprinted polymer.....	37
<b>Scheme 2.10:</b> Cu(I) catalyzed 1,3-dipolar cycloaddition reaction of azide and alkyne.....	39
<b>Scheme 3.1:</b> Synthesis of vinyl monomer <b>10</b> .....	54
<b>Scheme 3.2:</b> Synthesis of vinyl monomer <b>16</b> .....	55
<b>Scheme 3.3:</b> Synthesis of the 7-diethylaminocoumarin.....	57
<b>Scheme 3.4:</b> Uncontrolled free radical polymerization of monomer <b>10</b> and <b>16</b> .....	58
<b>Scheme 3.5:</b> RAFT polymerization of monomer <b>10</b> and <b>16</b> .....	59
<b>Scheme 4.1:</b> A summary for the synthesis of triazolyl coumarin based polymers with functionalized linkages.....	78
<b>Scheme 4.2:</b> Synthesis of poly(4-vinylbenzyl azide) <b>P0</b> .....	79
<b>Scheme 4.3:</b> Synthesis of alkynylated coumarin <b>7</b> .....	82
<b>Scheme 4.4:</b> Functionalization of Polymer <b>P0</b> with alkynylated coumarin <b>7</b> . ....	83
<b>Scheme 4.5:</b> A proposed binding mode of alkynylated coumarin derivative <b>7</b> with Hg <sup>2+</sup> ....	93
<b>Scheme 4.6:</b> Proposed hydrogen bonding interactions in the alkynylated coumarin derivative <b>7</b> and polymer <b>P1</b> .....	101
<b>Scheme 4.7:</b> A proposed binding mode of polymer <b>P1</b> with Hg <sup>2+</sup> .....	103
<b>Scheme 4.8:</b> A proposed binding mode of polymer <b>P1</b> with OH <sup>-</sup> .....	104
<b>Scheme 4.9:</b> Synthesis of alkynylated coumarin <b>11</b> .....	105
<b>Scheme 4.10:</b> Functionalization of <b>P0</b> with the alkynylated coumarin derivative <b>11</b> .....	106

---

<b>Scheme 4.11:</b> A proposed binding mode of coumarin derivative <b>11</b> with Hg <sup>2+</sup> .....	115
<b>Scheme 4.12:</b> The proposed binding modes of polymer <b>P2</b> in the presence of Hg <sup>2+</sup> .....	124
<b>Scheme 4.13:</b> The proposed binding modes of polymer <b>P2</b> in the presence of Al <sup>3+</sup> .....	124
<b>Scheme 4.14:</b> Synthesis of the alkynylated coumarin derivative <b>15</b> .....	125
<b>Scheme 4.15:</b> Functionalization of Polymer <b>P0</b> with alkynylated coumarin derivative <b>15</b> ...	126
<b>Scheme 4.16:</b> Schematic representation of the ESIPT mechanism in polymer <b>P3</b> .....	130
<b>Scheme 4.16:</b> A proposed inhibition of the ESIPT mechanism in polymer <b>P3</b> .....	134
<b>Scheme 5.1:</b> Synthesis of the dialkyne monomer <b>7</b> .....	141
<b>Scheme 5.2:</b> Synthesis of the diazide-functionalized coumarin monomer <b>12</b> .....	143
<b>Scheme 5.3:</b> Synthesis of the diazide coumarin monomer <b>17</b> .....	145
<b>Scheme 5.4:</b> AA-BB step-growth click polymerization of dialkyne-functionalized monomer <b>7</b> with diazide-functionalized coumarin monomers <b>12</b> and <b>17</b> .....	146
<b>Scheme 5.5:</b> Schematic representation of ESIPT in polymer <b>18</b> .....	151
<b>Scheme 5.6:</b> Quaternarization of polymer <b>18</b> .....	157



---

---

## Selected Abbreviations

AIBN	azobisisobutyronitrile
CuAAC	copper(I) catalyzed azide alkyne cycloaddition
CP	conjugated polymer
CPDB	2-(2-cyanopropyl)-dithiobenzoate
DCC	N,N'-dicyclohexylcarbodiimide
DMF	dimethylformamide
DMSO	dimethylsulfoxide
ET	charge transfer
FRET	fluorescence resonance energy transfer
FT-IR	fourier-transform infra-red
HOMO	highest occupied molecular orbital
LUMO	lowest occupied molecular orbital
NMR	nuclear magnetic resonance
OLED	organic light-emitting diode
PET	photoinduced electron transfer
PMDETA	N,N,N',N'',N'''-pentamethyldiethylenetriamine
TBAB	tetrabutylammonium bromide
TBAF	tetrabutylammonium fluoride
TBET	through bond electron transfer
THF	tetrahydrofuran
TLC	thin layer chromatography
UV-Vis	ultraviolet visible

# Introduction

## 1.1 Background

Due to growing interest in understanding natural biochemical mechanisms and the rate of release of toxic contaminants into the environment, chemical sensing has become a prerequisite in our technology-driven society. Several other fields such as security, chemical processing, food processing and pharmaceuticals also require sensor systems for continuous monitoring of chemical species.<sup>1,2,3</sup> Chemical sensors are generally considered to be miniaturized devices that can qualitatively and quantitatively detect the presence of specific compounds, classes of chemicals or specific chemical reactions.<sup>4</sup> On the other hand, molecular sensors (chemosensors), some of which form a basis for chemical sensor devices, are defined as abiotic molecules that reversibly bind an analyte and signal its presence by some physical means.<sup>5</sup> It has been reported that chemical sensing can be employed as a simple and sensitive method for detecting a variety of analytes, which cannot be normally detected using traditional methods. Such analytes include complex samples and biological systems.<sup>6</sup> Chemical sensing employs different transduction methods to signal the presence of an analyte. Commonly used methods include optical absorption, fluorescence and redox potentials.<sup>7</sup>

Information regarding various neutral and ionic species (cations and ions) which are of great importance, and those which are harmful, is now better understood. Of great need are sensors that can sense and monitor those chemical species over a broad range of often-regulated concentration in environment and biological systems. Typical techniques that have been developed and employed for the detection of ions are mainly based on flame photometry, atomic absorption spectroscopy, inductively coupled plasma mass spectroscopy, ion sensitive electrodes, electron microprobe analysis and neutron activation analysis.<sup>8,9</sup> However, some of these techniques are costly, destructive, often require large samples and continuous monitoring is a challenge.

In an attempt to find inexpensive, reliable and simple ways of detecting ions in different environments, fluorescence-based methods were found to be promising methods for chemical recognition and monitoring.<sup>10</sup> These methods are often much simpler to use and offer many benefits compared to other techniques which, include high sensitivity, high selectivity, short response time and local observation (fluorescent imaging spectroscopy). Furthermore, by using fluorescence, remote chemical monitoring can also be performed.<sup>11</sup>

---

Due to several adverse physiological and environmental effects associated with high concentrations of some chemicals, they have become an object of strict regulation. Major research efforts have been recently dedicated to the design of novel fluorescent sensors with improved sensing capabilities towards analytes in different environmental conditions. Despite the notable evolution of molecular and ionic probe design, an efficient detection system remains a huge challenge.

Most of the current molecular and ionic probes are of low molecular weight and only a few qualify to be in the macromolecule range. Due to low chemical and thermal resistance, as well as difficulties in separation and recovery associated with the low molecular weight chemosensors, a physical immobilization support is often needed for their applicability. A physical support does not only contribute to the good mechanical properties, but also minimizes the tendency of the sensing molecules to migrate. To avoid complications associated with synthesizing probes and immobilizing them on a physical support, polymers with host binding sites as part of their backbone, or as part of their pendant structure, were found to be more suitable alternatives. These polymeric materials have good thermal and mechanical properties and they also offer an outstanding and permanent immobilization method which allows them to be processed into end-user materials such as coatings and films.<sup>12-14</sup>

## **1.2 Human and ecological significance of ions and their detection**

Environmental pollution by ionic species has been recognized as one of the biggest challenges to the sustainable development of communities.<sup>15</sup> A tremendous increase in global energy usage, the widespread use of organic and inorganic chemical products, and the unwanted release of toxic inorganic and organic chemical species in the form of industrial waste, have led to a serious need for advanced monitoring technologies for environment protection, remediation and restoration.

It has been highlighted by experts that industrial processes release millions of different pollutants into the ground, atmosphere and to the aquatic ecosystem.<sup>16</sup> Among the listed pollutants, ionic species make up the majority of human and environmental contaminants. Most of the pollution can be attributed to industrial activities, mining, refinery, farming and chemical storage. In addition, most of these contaminants are not biodegradable and can reach water resources, where they may present ecological and human-health threats.

---

### 1.2.1 Examples of pollutant ionic species

Highly toxic lead ( $\text{Pb}^{2+}$ ) ions are discharged into the environment from materials such as batteries, gasoline and pigments.<sup>17</sup> Pb poisoning is one of the most prevalent metal contamination to human health and the environment. Pb exposure may lead to damage of neurological and reproductive systems, cardiovascular diseases and developmental disorders, especially in young children.<sup>18</sup>

Cadmium ( $\text{Cd}^{2+}$ ) is a highly toxic transition metal, commonly used in paints, solar panels, corrosive resistant steel electroplating, batteries and as a plastic stabilizer.<sup>19</sup> The Comprehensive Environmental Response, Compensation and Liability Act (CERCLA) in the USA has listed Cd as seventh in its priority list of top 275 hazardous materials.<sup>20</sup> The main source of exposure to Cd is tobacco and through food. However, inhalation of Cd-containing dust is considerably much more dangerous. The occupational exposure standards of Cd were previously set at 100-200  $\mu\text{g}/\text{m}^3$ , but have been narrowed down to 2-50  $\mu\text{g}/\text{m}^3$  in the last 40 years.<sup>21</sup> Exposure to Cd is associated with increased risk of cardiovascular diseases, cancer and damage to the liver and kidneys.<sup>22</sup>

Mercury (Hg) is one of the most toxic and widespread pollutants in the environment, and bio-accumulates through the food chain. It is released into the environment from natural sources and human activities such as gold production, coal plants, thermometers, barometers, caustic soda and mercury lamps. Mercuric ion ( $\text{Hg}^{2+}$ ) is a caustic and carcinogenic material with high cellular toxicity.<sup>23</sup> Natural biomethylation of  $\text{Hg}^{2+}$  ions in an aquatic environment can lead to the formation of methylmercury, a primary form of mercury.<sup>24</sup> The latter bio-accumulates in animal and human bodies through food chains, and can cause brain damage and other chronic diseases. Levels of  $\text{Hg}^{2+}$  are therefore an object of strict regulation. A provisional tolerable weekly intake for methylmercury set by a meeting of the joint Food and Agriculture Organization and World Health Organization (FAO/WHO) Expert Committee on Food Additive (JECFA) is 1.6  $\mu\text{g}/\text{kg}$  body weight.<sup>25</sup>

Aluminium ions ( $\text{Al}^{3+}$ ) are widely spread ions in natural water and many plants. Most exposure is through food and water. High levels of exposure to  $\text{Al}^{3+}$  may cause Alzheimer's disease, Guamanian amyotrophic lateral sclerosis and Parkinsonism dementia.<sup>26</sup> The limiting concentration of these ions in drinking water was set by WHO technical reports in 2010 between 0.1-0.2  $\text{mg}/\text{L}$ .<sup>27</sup>

---

Some metals can be classified as “trace elements” in human and other mammals due to their essentiality and very limited quantities in the body. These metals include vanadium (V), iron (Fe), manganese (Mn), chromium (Cr), copper (Cu), zinc (Zn), cobalt (Co) and molybdenum (Mo). Trace elements act as essential part of biological structures, but can be toxic at concentrations beyond those necessary for their biological functions. Similarly, some anions are essential and are required at limited quantities in humans and animals. Some of them can be even toxic at low concentrations. Fluoride ions ( $F^-$ ) are common in biological systems and are clinically useful for osteoporosis treatment and enhance mineral deposition in bones.<sup>28</sup> Excess  $F^-$  ions can be associated to many pathologies in humans, such as dental and skeleton fluorosis, osteoporosis, metabolism dysfunctions and cancers.<sup>29</sup>

Recurrent use of highly toxic cyanide ( $CN^-$ ) in industrial processes such as gold mining, electroplating, and manufacture of organic chemicals and polymers, results in unwanted discharge of this pollutant into the environment.<sup>30</sup> Furthermore, cyanide can be generated from biochemical processes and natural substances found in some foods and plants such as cassava, lima beans and almonds.<sup>31</sup> Cyanide in the blood stream of the humans can lead to vomiting, loss of conscious and eventually death.<sup>30</sup>

Some anions can be used in environmental monitoring by measuring their levels in the medium. For example, chloride ions ( $Cl^-$ ) measurement which helps in monitoring of landfills for leaks, tracing the movement of pollutants within natural water bodies and detection of salt water intrusion into drinkable ground or surface water.<sup>32</sup> Measurement of nitrate ion ( $NO_3^-$ ) levels is widely used to trace pollution from agriculture,<sup>33</sup> in aquaculture to check waste build-up and in surveying nutrient levels in natural water body.<sup>34</sup>

From above discussion and examples, it is clear that a need exists for reliable, inexpensive and simple methods for detecting and quantifying ions in different media for real-time monitoring of the environment, biological and industrial samples.

---

### 1.3 Aim of the study

Fluorescent polymers incorporating triazolyl coumarin systems in the backbone or as pendant units form the basis of this project. In addition to the inherent fluorescent properties, the polymers possess well-defined binding sites for ions.<sup>35</sup> Binding of specific ions on the sites alters the inherent spectral properties of the polymers, resulting in detectable changes in their absorption and emission. The aims of the study were to synthesize fluorescent triazolyl coumarin-based polymers from azide and alkyne functionalized monomers, triazole-containing vinyl monomers and an azide-functionalized polymer with alkyne functionalized coumarin molecules. In all the cases, a Cu(I) catalyzed 1,3-dipolar cycloaddition reaction of azides and alkynes (click reaction) was used to introduce the triazole ring in polymerizable vinyl monomers or as linkage in the case of linear polymers and azide-functionalized polymers. Three different methods such as radical polymerization, step-growth click polymerization system and post-polymerization functionalization were applied in the synthesis of polymers.

The photophysical properties of each polymer and its starting monomer/materials were investigated and compared. The chemosensing potential of the synthesized polymers for metal ions and anions were investigated using absorption, emission, FT-IR and NMR spectral analysis.

### 1.4 Organization of the thesis

This work is divided into five chapters. In chapter one, the background of this study is discussed and aims are briefly underlined.

Chapter two gives a summary of the reported literature related to this work. This summary includes: signal transduction modes in chemosensor systems, different mechanisms that are used in chemosensing and typical examples, an account on chemosensors that use the triazole ring as a receptor unit, a coumarin fluorophore and the effect of substituents on its absorption and emission.

Chapter three deals with polymers with pendant triazolyl coumarin systems, in which the triazole and the coumarin are in direct conjugation. The full synthesis, characterization and chemosensing studies will be discussed.

---

Chapter four gives an account on polymers with pendant bridged triazolyl coumarin units in which the triazole and the coumarin are linked with functional linkages. Hydroxyethylene and amino-methylene are two functional linkages which are investigated in this chapter. The synthesis and the effect of functional linkages on the chemosensing of the polymer will be discussed in detail.

Chapter five deals with linear polymers with conjugated triazolyl coumarin units in the backbones. Their synthesis using AA-BB step-growth click polymerization using diazide-functionalized coumarin monomers and dialkyne-functionalized monomer and how their functionalization affects their photophysical properties, as well as their chemosensitivity will be discussed.

## 1.5 References

1. K. J. Albert and D. R. Walt, *Anal. Chem.*, **2000**, 72, 1947–1955.
2. R. J. Colton and J. N. Russell, *Science*, **2003**, 299, 1324–1325.
3. E. Kress-Rogers and C. J. B. Brimelow, *Instrumentation and sensors in the food industry*, **2001**, Woodhead Publishing Ltd, Cambridge, 2<sup>nd</sup> edn.
4. J. R. Stetter, W. R. Penrose and S. Yao, *J. Electrochem. Soc.*, **2003**, 150, S11-S16.
5. G. Orellana and M. C. Moreno-Bondi, *Frontiers in chemical sensors: novel principles and techniques*, **2005**, Springer: New York.
6. a) B. C. Dickinson, D. Srikun and C. J. Chang, *Curr. Opin. Chem. Biol.*, **2010**, 14, 50-56.  
b) H. Kobayashi, M. Ogawa, R. Alford, P. L. Choyke and Y. Urano, *Chem. Rev.*, **2010**, 110, 2620-2640. c) R. W. Sinkeldam, N. J. Greco and Y. Tor, *Chem. Rev.*, **2010**, 110, 2579-2619.
7. C. McDonagh, C. S. Burke and B. D. MacCraith, *Chem. Rev.*, **2008**, 108, 400-422.
8. V. Iyengar and J. Wolttlez, *Clin. Chem.*, **1988**, 34, 474-481.
9. A. T. Townsend, K. A. Miller, S. Mclean and S. Aldous, *J. Anal. At. Spectrom.*, **1998**, 13, 1213-1219.
10. J. R. Lakowicz, *Topics in fluorescence spectroscopy*, **1994**, 4, Plenum Press, New York.
11. D. J. Irvine, M. A. Purbhoo, M. Krosgaard and M. M. Davis, *Nature*, **2002**, 419, 845–849.
12. J. M. García, F. C. García, F. Serna and J. L. de la Peña, *Prog. Polym. Sci.*, **2010**, 35, 623–686.
13. P. Anzenbacher, Y. Liu and M. E. Kozelkova, *Curr. Opin. Chem. Biol.*, **2010**, 14, 693–704.

- 
14. V. Rotello and S. Thayumanavan, *Molecular recognition and polymers; control of polymer structure and self-assembly*; **2008**, Wiley: Hoboken, NJ.
  15. Q. Ashton Acton, *Issues in Global Environment-Pollution and Waste Management: 2013 Edition*, Atlanta, GA: Scholarly Edition, USA.
  16. United State Environment Protection Agency, (EPA, Washington, DC, **2007**).
  17. A. R. Flegal and D. R. Smith, *Environ. Res.*, **1992**, 58, 125-133.
  18. P. A. Meyer, T. Pivetz, T. A. Dignam, D. M. Homa, J. Schoonover, D. Brody, *Morbidity and mortality weekly report CDC Surveillance Summaries*, **2003**, 52, 1-21.
  19. T. C. Jennings, *Cadmium Environmental Concerns*, **2005**. PVC handbook. Hanser Verlag. p. 149. ISBN 9781569903797.
  20. G. F. Nordberg, R. F. M. Herber and L. Alessio, *Cadmium in the human environment*, **1992**, Oxford University Press, Oxford, UK.
  21. National Institute for Occupational Safety and Health. *NIOSH Current Intelligence Bulletin 42: Cadmium (Cd)*. 1984, DHHS (NIOSH) Publication No. 84-116.
  22. C. N. McFarland, L. I. Bendell-Young, C. Guglielmo and T. D. Williams, *J. Environ. Monit.*, **2002**, 4, 791-795.
  23. J. S. Lee, M. S. Han and C. A. Mirkin, *Angew. Chem., Int. Ed.*, **2007**, 46, 4093–4096.
  24. I. Onyido, A. R. Norris and E. Buncl, *Chem. Rev.*, **2004**, 104, 5911–29.
  25. S.C. Bondy, *Neurotoxicology*, 2010, 31, 575-581.
  26. JECFA (Joint FAO/WHO Expert Committee on Food Additives), *Joint FAO/WHO Expert Committee on Food Additives*, **2003**, Sixty-first Meeting, Rome, 10-19 June.
  27. World Health Organization (**2010**) *Aluminium in Drinking-water*. Background document for development of WHO Guidelines for Drinking-water Quality.
  28. R. Waddington and M. Langley, *Connective Tissue Res.*, **2003**, 44, 88-95.
  29. E. Gazzano, L. Bergandi, C. Riganti, E. Aldieri, S. Doublier, C. Costamagna, A. Bosia and D. Ghigo, *Curr. Med. Chem.*, **2010**, 17, 2431-2441.
  30. G. C. Miller and C. A. Pritsos, *Cyanide: Soc., Ind. Econ. Aspects, Proc. Symp. Annu. Meet. TMS*, **2001**, Vol 73.
  31. World Health Organization, Geneva, **1996**, *Guidelines for Drinking-Water Quality*, 2<sup>nd</sup> edn, vol 2.
  32. a) G. Venkatesan and G. Swaminathan, *J. Environ. Eng. Landsc.* **2009**, 17, 1-7. b) S.V. Panno, K. C. Hackley, H. H. Hwang, S. Greenberg, I. G. Krapac, S. Landsberger and D. J. O'Kelly, Source identification of sodium and chloride contamination in natural waters:



- 
- preliminary results. In Proceedings, 12th *Annual Illinois Groundwater Consortium Symposium*. Illinois Groundwater Consortium, **2002**.
33. P. Saccon, A. Leis, A. Marca, J. Kaiser, L. Campisi, M.E. Böttcher, J. Savarino, P. Escher, A. Eisenhauer and J. Erbland, *Proced. Earth Plan. Sc.*, **2013**, 7, 758-761.
34. D. Kirkwood, **1996**, *Nutrients: Practical notes on their determination in sea water* (No. 17). International Council for the Exploration of the Sea.
35. a) Y. Li, J. C. Huffman and A. H. Flood, *Chem. Commun.*, **2007**, 26, 2692-2694. b) M. C. González, F. Oton, A. Espinosa, A. Tarraga and P. Molina, *Org. Biomol. Chem.*, **2015**, 13, 1429-1438. c) Z. Xu, J. Yoon and D. R. Spring, *Chem. Soc. Rev.*, **2010**. 39, 1996-2006.

---

## Chapter 2 Signal transduction modes and polymer based chemosensors

### 2.1 Introduction

A chemosensor, as a molecule that signals the presence of the analyte through changes in its macroscopic properties, must possess the ability to selectively recognize a given analyte and allow a quantitative and qualitative determination of the analyte. A typical chemosensor consists of two major components; a signalling and a receptor units, which are connected together either by linkage or integration (**Figure 2.1**).<sup>1</sup>

The signalling subunit acts as a signal transducer which translates the recognition events into a measurable signal. The signal arises from the perturbation of electronic and photoinduced processes such as: electron transfer, charge transfer, energy transfer, and excimer formation or disappearance, due to the binding of the guest analyte to the sensing molecule.

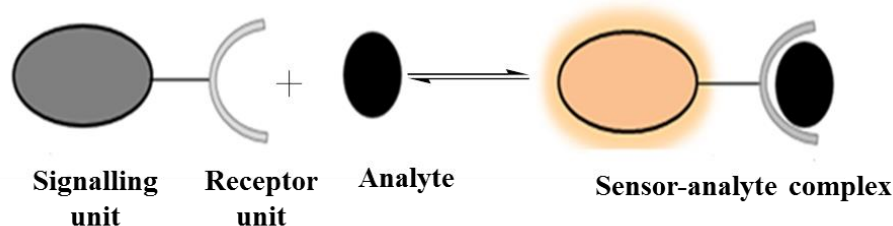


**Figure 2.1:** A schematic representation of a chemosensor binding to an analyte

The receptor subunit is responsible for recognizing and binding an analyte of interest with high selectivity and efficiency. Recognition involves the formation of weak interactions such as reversible covalent interactions and non-covalent interactions (hydrophobic interaction, hydrogen bond, electrostatic and metal-analyte interaction) between receptor and target.<sup>2</sup> Those interactions are usually governed by receptor topology, characteristics of the analyte, and the nature of the solvent.<sup>3</sup>

Depending on the operating principle of transducer, chemosensors can be categorized into two major classes: electrochemical chemosensors and optical chemosensors.<sup>4</sup> The former are characterized by the presence of a redox active unit in the binding site of the sensor and signals are reported as changes in electrochemical properties, while the latter report the binding events as change in optical properties.

---

## 2.2 Optical chemosensors

Optical chemosensors can be split into two categories; fluorogenic (fluorescent) chemosensors and chromogenic (colorimetric) chemosensors. The former is extensively used and it signals the presence of analytes by emission of light, while the latter signal through the absorption of light. Although colorimetric chemosensors offer qualitative and quantitative information of the analyte through the change in colour of receptor molecules, their sensitivity is lower compared to fluorogenic chemosensors. In fluorescence measurements, emitted light is proportional to the concentration of the analyte, whereas in absorption measurements analyte concentration is proportional to the absorbance. The latter compares the ratio between the light intensity measured before and after passing through the sample. Fluorescence looks at the light emitted after applying an incident light on the molecule. The fluorescent signal can be optimized by increasing the intensity of the incident light which is not the case for absorbance. This feature enables fluorescence methods to detect analyte concentration at picomolar levels, while absorbance measurements can only detect analyte concentration up to the micromolar scale. Furthermore, fluorogenic chemosensors are known for their high speed, simplicity and safety parameters, which make them suitable for biological systems.<sup>5</sup>

Recently, there has been a lot of research interest in finding new optical chemosensors with improved sensitivity and selectivity, which can be applied either in solutions or in biological medium. Some researchers in this field have also turned their attention to polymer-based optical chemosensors. The latter exhibited improved sensitivity and selectivity due to their inherent collective properties that enable them to be sensitive even to minor perturbations. Recent examples include the coumarin-based polymeric chemosensor **1** for cyanide ions in biological solution developed by El Acharia and co-workers.<sup>6</sup> (**Figure 2.2**). This water soluble chemosensor was obtained from a radical copolymerization of a coumarin-dicyano vinyl monomer containing both sensing and receptor units and a glycol-conjugated methacrylate derivative which enhanced water solubility of the polymer. The detection limit for cyanide ions was determined to be  $1.17 \mu\text{mol L}^{-1}$  and the polymer showed both colorimetric and fluorometric changes in biological solutions.

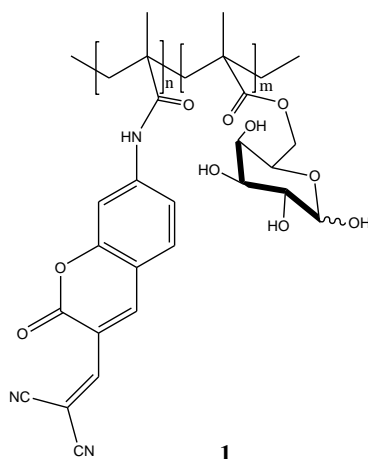


**Figure 2.2:** Coumarin-based polymeric chemosensor **1** for cyanide ion detection.

### 2.2.1 Fluorogenic chemosensors

Fluorescent chemosensors are systems that change their fluorescence properties in response to analytes binding with their receptors. They are mainly organic materials that can interact with target analytes actively or passively.<sup>7</sup> Active interaction refers to a sensing system in which the analyte-receptor complex occurs in the ground state, while passive interaction refers to any kind of excited-state photophysical interaction between the analyte and receptor molecule.

Fluorescent systems that ‘actively’ sense the analyte can be designed in different ways depending on the arrangements of the signalling unit (fluorophore) and binding site or reactive site. It can also be designed based on the mode of interaction between the analyte and receptor. From the design of the chemosensor, one can predict the changes in the fluorescence signal which may occur when interacting with target analyte. Those changes can mostly be detected as amplification or quenching of the fluorescent signal and/or shifting in the emission wavelength.

Five different approaches have been applied in pursuing synthetic receptors design. These are listed below:

*i) Fluorescent ligand:* This approach mostly involves aromatic or heterocyclic ring systems, usually substituted with potentially analyte-chelating functional groups. This system acts simultaneously as a recognition and a signaling unit (see for example compound **2** in **Figure 2.3**).<sup>8</sup>

*ii) Intrinsic fluorescent probe:* The approach involves a receptor which is in direct electronic conjugation with a signalling subunit (compound **3** in **Figure 2.3**).<sup>9</sup>

*iii) Composite “Fluorophore-spacer-receptor”:* In this approach the receptor and signalling subunits are largely separated by a spacer (compound **4** in **Figure 2.3**).<sup>10</sup>

*iv) Displacement approach:* This approach is based on a competitive assay in which a receptor-fluorophore ensemble is selectively dissociated in the presence of specific competitive analyte capable of interacting efficiently with a receptor. The dissociation is accompanied by a change in optical properties of the fluorophore.<sup>11</sup>

*v) Chemodosimeter:* This approach relies on specific analyte-induced chemical reactions which result in new chemical compounds with concomitant changes in chromogenic or fluorogenic behaviour.<sup>12</sup> Owing to the irreversibility of the reaction which occurs during the process, this sensing technique cannot be strictly categorized as chemosensing, therefore the terms chemodosimeters or chemoreactants is mostly applied. Nevertheless, in all sensing processes chemosensing terminology is preferred. Compound **5** in **Figure 2.3** is an example of a chemodosimeter used for CN<sup>-</sup> detection.<sup>13</sup>

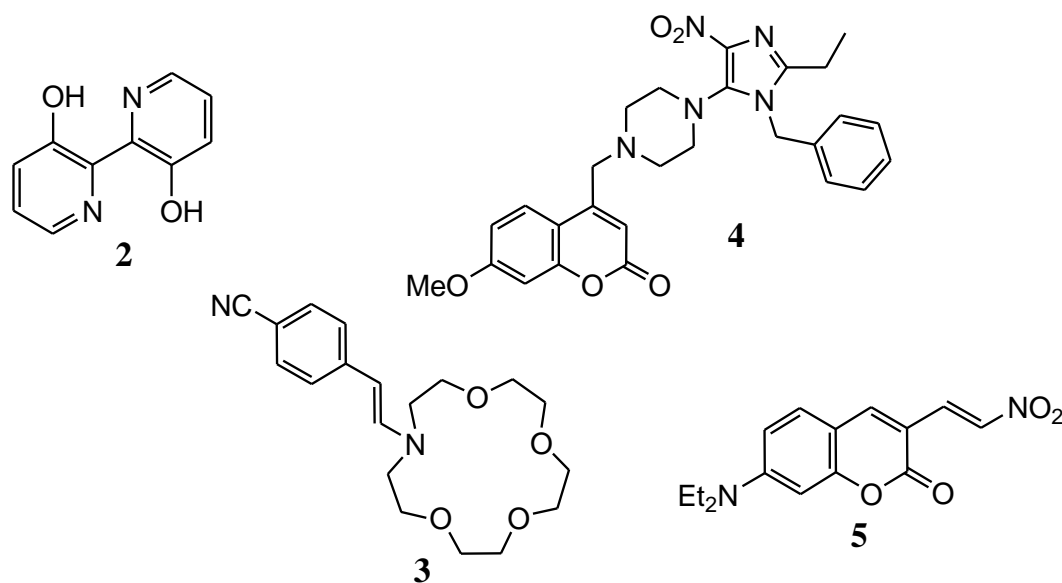


**Figure 2.3:** Examples of different synthetic receptors systems.

---

## 2.2.2 Mechanism of fluorescence sensing

Considering the critical roles that fluorogenic chemosensors play in many fields which include environmental monitoring, process control and medical diagnosis, it is clear that there is a large gap between the analytes that need to be detected and the availability of chemosensors. With that in mind, a clear understanding of chemosensor structure and functionality at the molecular level is important. This can help illuminate and improve the design of previously reported fluorogenic chemosensors.

The recent designs explore novel mechanisms of interaction between recognition and signalling subunits or utilise basic photophysical mechanisms at molecular level combined with some supramolecular chemistry principles. Several conventional mechanisms have been developed and widely used in the detection of chemical stimulus through changes in fluorescence properties. Typical ones are photoinduced electron transfer (PET),<sup>14</sup> charge transfer (CT),<sup>15</sup> energy transfer (ET),<sup>16</sup> and excimer/exciple formation.<sup>17</sup> As supramolecular chemistry is still a fertile discipline, a number of emerging novel design principles have been currently investigated.

It has been shown that the photophysical properties of the molecule can be affected by conformation restriction in different environments. Many researchers have used this phenomenon and a number of small molecules have been recently designed and applied as fluorogenic chemosensors. So far, the emerging sensing mechanisms emanating from the conformation restriction phenomenon include aggregation induced emission (AIE),<sup>18</sup> and C=N isomerization.<sup>19</sup> In addition to these novel mechanisms based on the conformation restriction phenomenon, other environment dependent mechanisms have been developed. The latter is based on the transfer of a proton within the excited state and is named “excited-state intramolecular proton transfer” (ESIPT).<sup>20</sup>

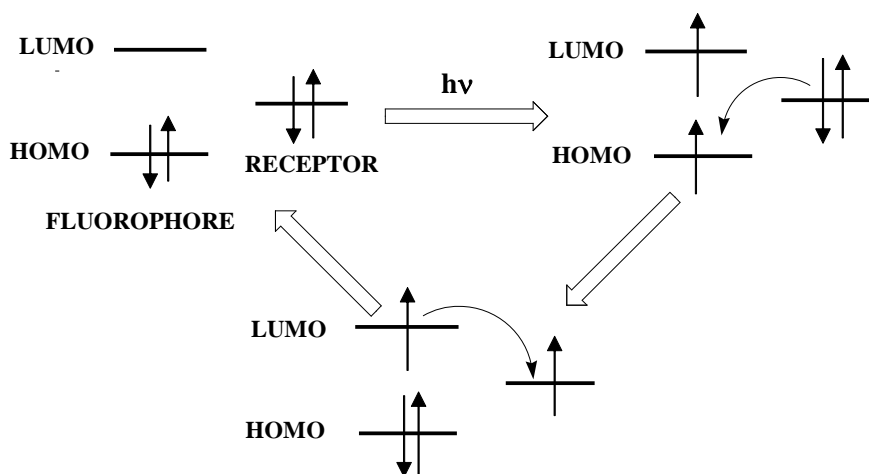
### 2.2.2.1 Photo-induced electron transfer (PET)

Photo-induced electron transfer (PET) is regarded as one of the most studied and widely applied mechanism in the development of luminescence-based chemosensors. The mechanism mimics the well-studied light-induced mechanisms occurring in some plants and bacteria during photosynthesis.<sup>21</sup> It derives its name from the fact that the process involves an electron transfer after absorption of light. In fact, when a fluorophore absorbs the light, an electron is promoted from the highest occupied molecular orbital (HOMO) to the lowest unoccupied

---

molecular orbital (LUMO). Depending on the chemical groups or receptors in the vicinity of fluorophore, the excited state relaxation to the ground state of fluorophore can occur in different ways than the usual relaxation process which results in fluorescence emission. This is because a fluorophore in its excited state can act as good electron donor or good electron acceptor. It can transfer a promoted electron to the other molecular orbital having energy between the HOMO and LUMO of the fluorophore or can accept electron from the same molecular orbital into its semi-vacant HOMO orbital. Those orbitals which donate electrons to, or accept electrons from, excited fluorophores are provided by the receptors which can be connected to a fluorophore *via* bonding (in the case of PET type chemosensors) or from another chemical system, usually known as a quencher.<sup>14c</sup>

In the instance where a full orbital is provided between the HOMO and LUMO of a fluorophore (in the case of a donor group), electron transfer from the full orbital to the semi-vacant HOMO of fluorophore can occur when the fluorophore is irradiated (**Figure 2.4**). A stable ground state is restored by a further electron transfer from the LUMO of fluorophore to the semi-vacancy of donor group. This process results in a decrease of emission intensity or absence of fluorescence (fluorescence quenching) because the usual transition from the excited state to the ground state, which results in fluorescence emission, is overtaken by non-radiative pathways.



**Figure 2.4:** PET mechanism showing the interaction between LUMO and HOMO of the fluorophore and the external molecular orbital of the receptor.

Similarly, when an empty orbital is introduced between the HOMO and LUMO of a fluorophore (in the case of an acceptor group), non-radiative de-excitation leading to fluorescence quenching occurs. In this case, an electron in the excited state is transferred to the

---

lower energy empty orbital of the receptor followed by further relaxation to the semi-vacant HOMO orbital of the fluorophore, regaining its original ground state. This alternative pathway results in the dissipation of the excitation energy in a non-radiative fashion.

Designers for PET-based chemosensors took advantage of the properties of the PET mechanism to target analytes which can cause the appearance or disappearance of molecular orbital energy levels between the HOMO and LUMO of fluorophores. As a result, fluorescent “turn-off” and “turn-on” PET based chemosensors were developed.<sup>22</sup>

In a fluorescent “turn-on” (off-on) chemosensor, the weak or non-fluorescing fluorophore becomes more fluorescent in the presence of an analyte. These types of chemosensors are characterized by receptors with high energy non-bonding electron pairs. When a chemosensor is in its unbound state, the PET process is active *via* rapid intra-molecular electron transfer (IET) from the HOMO of the donor group to the semi-vacant HOMO of the fluorophore (**Figure 2.5**). This leads to fluorescence quenching since the excited fluorophore is forced to follow the non-radiative pathway. However, when a chemosensor interacts with an electron deficient analyte, the energy of the donor group’s HOMO becomes lower than that of fluorophore’s HOMO and IET is disrupted. As a result, the usual relaxation pathway of the fluorophore which causes fluorescence emission is restored.

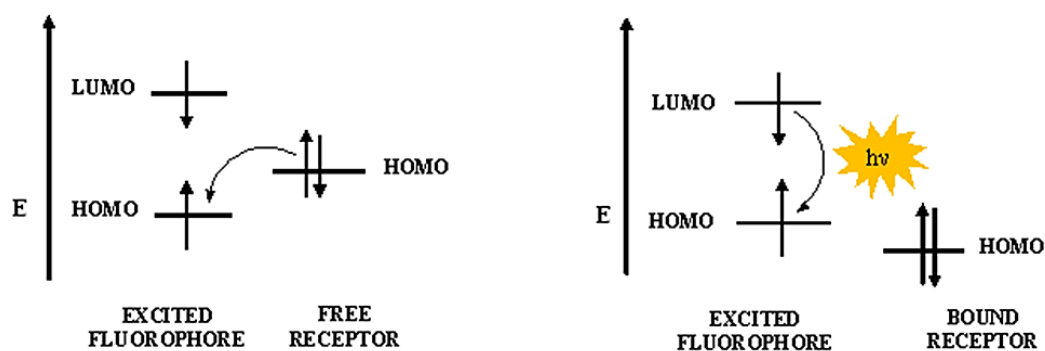


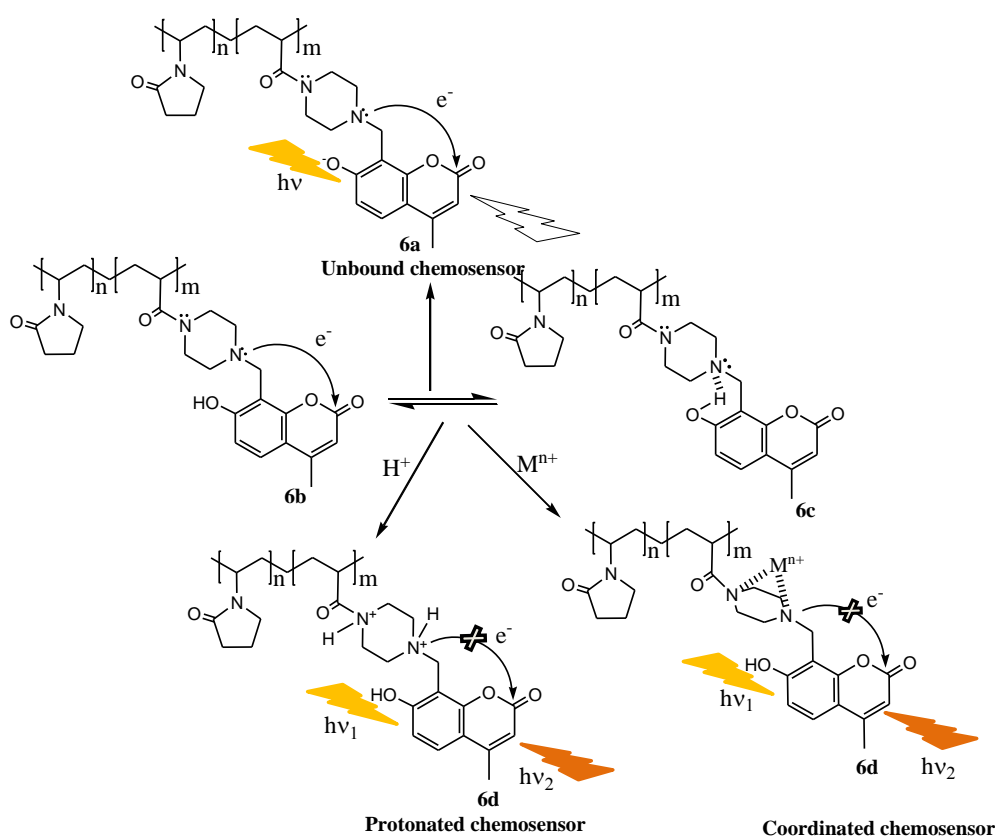
**Figure 2.5:** Fluorescent “turn-on” type PET chemosensor in terms of frontier molecular orbitals.

Fluorescent “turn-on” PET-based chemosensors are widely used as probes for various chemical entities in abiotic and biological systems.<sup>23</sup> Apart from small molecules which have been extensively studied and applied as fluorescent “turn-on” PET chemosensors, polymeric versions have emerged recently. An example is a proton and Ni<sup>2+</sup> polymeric chemosensor **6a** (**Scheme 2.1**) developed by Wang and co-workers.<sup>22</sup> The chemosensor was generated through



a radical copolymerization of an acrylic monomer bearing a coumarin moiety, with water soluble *N*-vinylpyrrolidone. The blue fluorescent copolymer displayed efficient fluorescent “off-on” in the pH range, 3.02 to 12.08. The same fluorescent enhancement was also observed in the presence of Ni<sup>2+</sup> ions.

This fluorescent enhancement in the polymer was attributed to a piperazine unit attached to a coumarin moiety which can perform the dual functions of binding the analyte (H<sup>+</sup>, Ni<sup>2+</sup>) and acting as a PET electron donor. Once piperazine binds the Ni<sup>2+</sup>/H<sup>+</sup> ions, the internal electron transfer to the excited coumarin fluorophore is disrupted, resulting in fluorescence enhancement.



**Scheme 2.1:** A fluorescent “turn-on” PET polymeric chemosensor for detection of proton and Ni<sup>2+</sup>.

In contrast to fluorescent “turn-on” PET chemosensors, the presence of the target analytes in fluorescent “turn-off” (on-off) PET chemosensors significantly decreases their emission intensity. In other words, when the target analyte coordinates with a receptor, the redox potential of the receptor is altered and the LUMO energy level of the receptor-analyte complex is lowered. This decrease in energy leaves the LUMO energy level of the receptor-analyte complex between the LUMO and HOMO energy level of the fluorophore, which favours a

non-radiative relaxation pathway. Since the excitation energy of the fluorophore is dissipated, fluorescence quenching is observed in these types of chemosensors. The mechanism for a fluorescent “turn-off” type PET chemosensor, in terms of frontier molecular orbitals, is illustrated in **Figure 2.6**.<sup>24</sup>

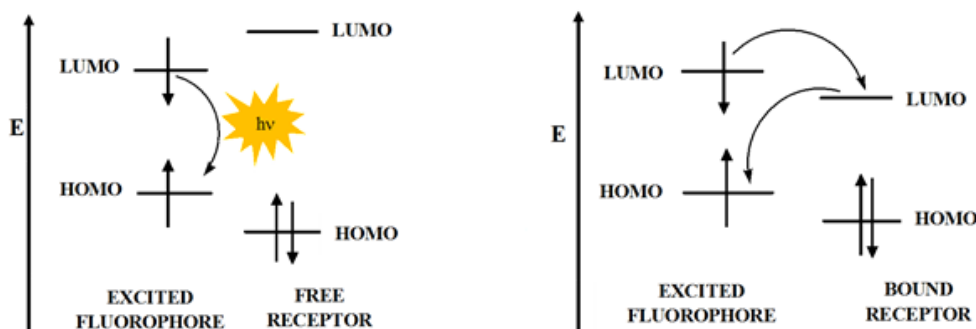
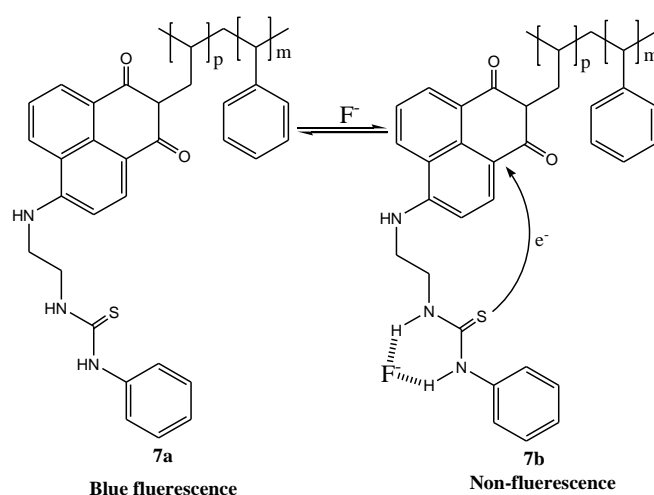


**Figure 2.6:** Fluorescent “turn-on” type PET chemosensor in terms of frontier molecular orbitals.

A naphthalimide-based polymer **7a** is a clear example of a sensor exhibiting “on-off” behaviour in the presence of  $F^-$  ions.<sup>25</sup> In a particular case depicted in **Scheme 2.2**, naphthalimide acts as a fluorophore subunit and urea as the receptor. The copolymer, which displays a green fluorescence in the absence of  $F^-$  ions, is completely quenched in the presence of  $F^-$  ions. The reason for this quenching is assigned to the formation of an anion-receptor hydrogen bonding complex which increases the reduction potential of the receptor and makes the IET process more feasible.



**Scheme 2.2:** A fluorescent “turn-on” PET polymeric chemosensors for  $F^-$  ions.

---

### 2.2.2.2 Intramolecular charge transfer (ICT)

An intramolecular charge transfer signalling mechanism (ICT) has been extensively used in cationic sensing, in which a ratiometric signal was often produced from the binding events.<sup>26</sup> In contrast to PET mechanism, ICT involves a fluorophore which is linked to the receptor *via* a conjugated system in such way that one end acts as an electron donor (electron rich group), while the other acts as an electron acceptor (electron deficient group). This results in a “push-pull”  $\pi$ -electron system when the fluorophore is in the excited state.

The presence of an analyte can either enhance or reduce the “push-pull” character resulting in a blue or red shift, in both absorption and emission spectra. In other words, if the electron-donating end (e.g. an amino group) interacts with the analyte, the electron-donating ability of the group decreases, resulting in perturbation of the conjugated system. This leads to a blue shift in both absorption and emission as shown in **Figure 2.7**. On the other hand, when an analyte binds an electron accepting end (e.g. a carbonyl group), the electron-accepting character of the group increases, resulting in improved ICT upon excitation. As a result a red shift in absorption and emission spectra is observed.<sup>3</sup> Furthermore, in some cases, changes in quantum yield and lifetime are also detected upon cation binding.<sup>27</sup> Charge dipole moments can be used to further explain how the photophysical properties change when an analyte interacts with either end of the probe (**Figure 2.7**).<sup>28</sup> Upon excitation, the electron donating end of the free probe becomes positively charged due to the ICT process. The interaction of an analyte with this end leads to a stronger destabilization of the excited state compared to the corresponding ground state. As a result, the energy gap between the ground and excited states becomes broad and a blue shift in both absorption and emission is observed. On the other hand, when interaction takes place between an analyte and the electron accepting end of the probe, the excited state becomes more stable than the ground state. This results in a decrease in the energy gap between the ground and excited states causing a red-shift in both absorption and emission.

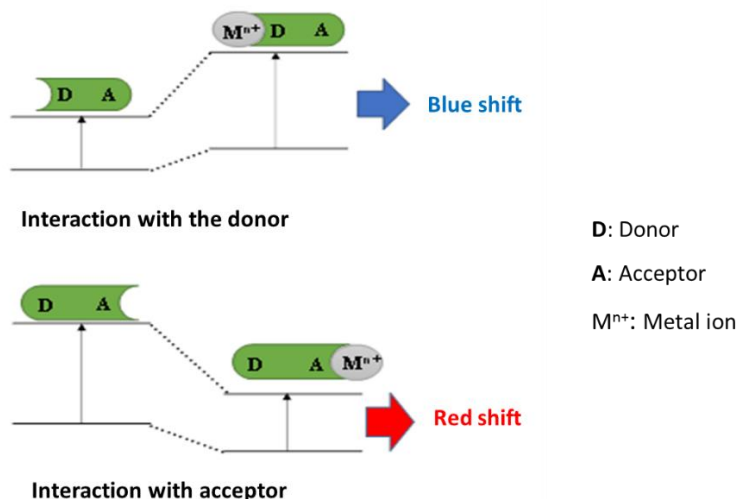
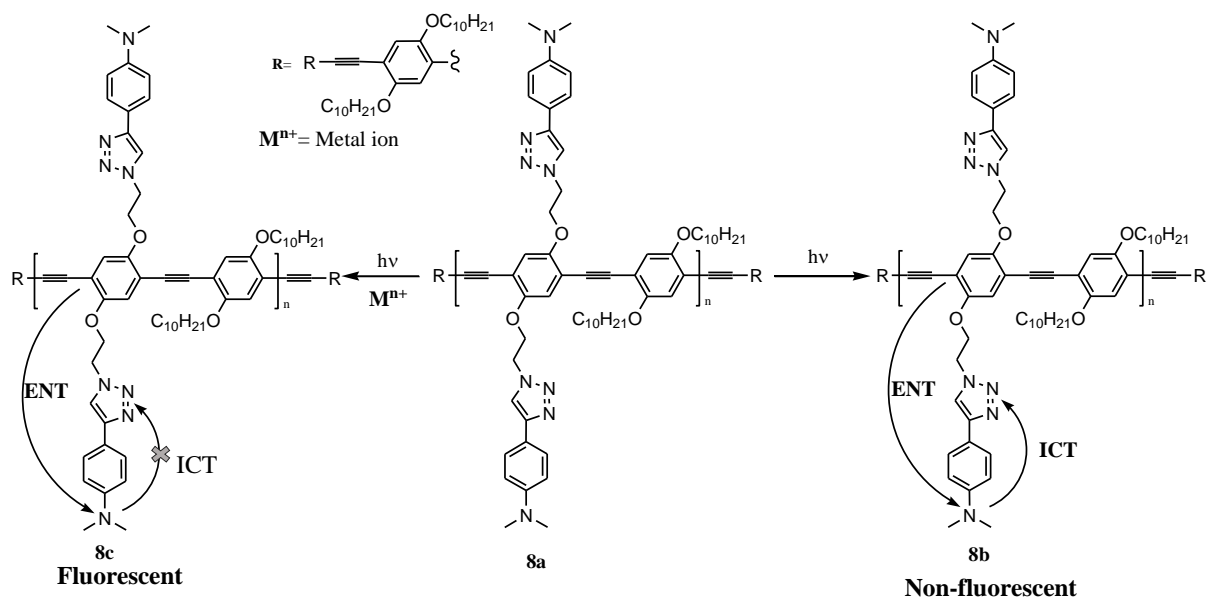


**Figure 2.7:** Shifts in ICT mechanism due to analyte binding.<sup>29</sup>

Due to a ratiometric detection offered by ICT mechanism, a number of ICT-based fluorescence chemosensors have been designed for quantitative determination of different target analytes in even more complex applications such as imaging in living cell and tissues. This is due to the fact that ratiometric detection eliminates most of the detection ambiguity by self-calibration using two emission bands. Examples of this type of fluorescent sensing include small molecule-based ratiometric fluorescence probes for cations, anions, and biomolecules.<sup>30</sup>

As mentioned earlier on, any alteration on ICT mechanism can lead to the changes in quantum yield. The triazole-containing polymer **8a** reported by Zhao and co-worker, is an example of a chemosensor which undergo such changes in the presence of target analytes.<sup>31</sup> The polymer which initially exhibited fluorescence quenching due to relay energy transfer (ENT), sensitization and charge transfer, has become more emissive in the presence of Cd<sup>2+</sup>, H<sup>+</sup> and Zn<sup>2+</sup>. This is due to the disruption of ICT mechanism between the triazole and aminophenyl group due to the presence of the analytes as depicted in **Scheme 2.3** below.



**Scheme 2.3:** ICT based polymeric chemosensor for  $\text{Cd}^{2+}$ ,  $\text{H}^+$  and  $\text{Zn}^{2+}$ .<sup>31</sup>

### 2.2.2.3 Energy transfer (ET)

Energy transfer (ET) sensing mechanism involves the energy transfer between a pair of chromophores where one acts as an energy donor (the excited-state), while other acts as energy acceptor. Depending on the interaction and distance between energy donor and energy acceptor, ET can be divided into two classes, which are fluorescence resonance energy transfer (FRET), also known as Förster energy transfer, and electronic energy transfer (EET), also known as Dexter energy transfer.<sup>32</sup>

Initially, when an acceptor is not a quencher type system, the energy of the excited donor chromophore which emits light at relatively a short wavelength, can be used to excite an acceptor chromophore emitting at a longer wavelength, as shown in **Figure 2.8**. The ratio of those two emissions can be affected by the analyte binding.

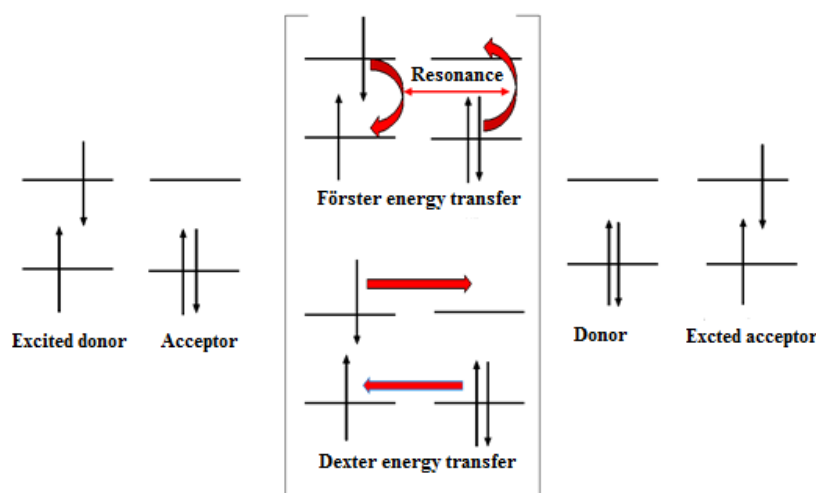


**Figure 2.8:** Förster type and Dexter energy transfer.

In order to get an efficient transfer of energy, several factors must be considered. In the case of FRET (Förster energy transfer) mechanism the efficiency of energy transfer is governed by:<sup>33</sup>

- i. The distance between the two fluorophores, which must be in the range 10-100Å.
- ii. Relative orientation of the transition dipoles of the donor and acceptor chromophores.
- iii. Spectral overlap between the emission spectrum of the donor chromophore.
- iv. The absorption spectrum of the acceptor chromophore.

On the other hand, efficient EET (Dexter) requires appropriate relative energy levels between donor and acceptor, specific characteristics of the spacer (conjugation) and a shorter distance between donor and acceptor (<10Å).<sup>34</sup>

### *i) Förster energy transfer*

Fluorescence resonance energy transfer or Förster energy transfer (FRET) is one of the widely used chemical strategies in ratiometric imaging. It was firstly introduced by Theodor Förster in 1948, and it involves the coupling of long range dipoles to allow an exchange of energy from an excited donor chromophore to the acceptor chromophore. The energy transfer occurs through space, *i.e.* with no direct overlap implication.<sup>32b</sup> The excited-state energy exchange results in a stable electronic ground state for the donor and emission then occurs at the centre of the acceptor fluorophore, as shown in **Figure 2.9**. In other words, an electron in the HOMO of the acceptor chromophore is promoted to the LUMO by the energy liberated during donor chromophore de-excitation (**Figure 2.8**). Since a strong correlation between energy absorbed by the acceptor chromophore and energy emitted by the donor chromophore is a requirement for efficient FRET to occur, a significant spectral overlap between emission spectrum of the

donor and absorption spectrum of the acceptor is necessary. Because of this requirement, FRET-based chromophore pairs are commonly connected *via* a non-conjugated spacer so that the energy transfer may occur through space.

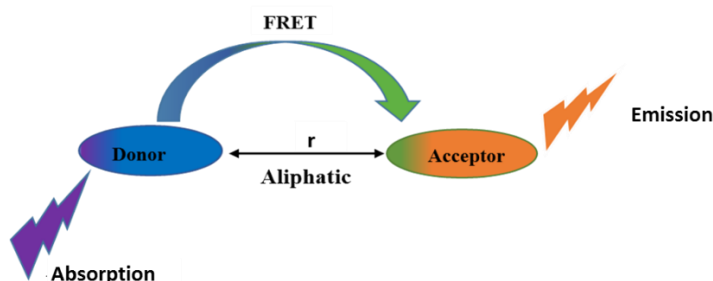


**Figure 2.9:** Schematic representation of FRET mechanism from a donor to an acceptor.

Upon excitation, an electron in the chromophore is promoted to a higher energy level and ground state is then restored through different de-excitation mechanisms such as emission processes, non-radiative processes or energy transfer processes. Representing the rate constant of donor emission and energy transfer process with  $k_f$  and  $k_T$ , respectively, the Förster equation can be described as follows:

$$k_T = \left\{ \frac{9000(\ln 10)k^2 J}{128\pi^5 n^4 N_A r^6} \right\} k_f$$

Where; n: Refractive index of the medium  $N_A$ : Avogadro's number;  $k^2$ : Orientation factor; J: Overlap integral; r: Distance between donor and acceptor.

From the equation, only three factors need to be modulated for a successful small molecule-based FRET chemosensor design. Those factors include; orientation factor ( $k^2$ ), overlap integral (J) and distance between donor and acceptor (r). Orientation factor ( $k^2$ ) indicates the relative orientation in space of transition dipoles of the donor and acceptor chromophore, it ranges from 0 to 4 and is usually applied to the synthetic small molecules based FRET sensors.<sup>35</sup> For perpendicularly orientated donors and acceptors,  $k^2$  is 0, where the donor and acceptor are in parallel orientation,  $k^2$  is 1 and for parallel transition dipoles,  $k^2$  is 4. Furthermore,  $k^2$  can be counted as 2/3 when both donor and acceptor are small molecule based fluorophores undergoing random motions. The overlap integral (J) indicates the spectral overlap between emission of the donor and absorption of the receptor (**Figure 2.10**). It is lineally proportional to  $k_T$  as shown in Förster equation. Distance between donor and acceptor

---

( $r$ ) is a highly used factor to control FRET efficiency. In the Förster equation  $k_T$  is inversely proportional to the sixth power of the distance between the donor and receptor and this has been confirmed from experimental work using different lengths of proline-based polypeptides.<sup>36</sup>

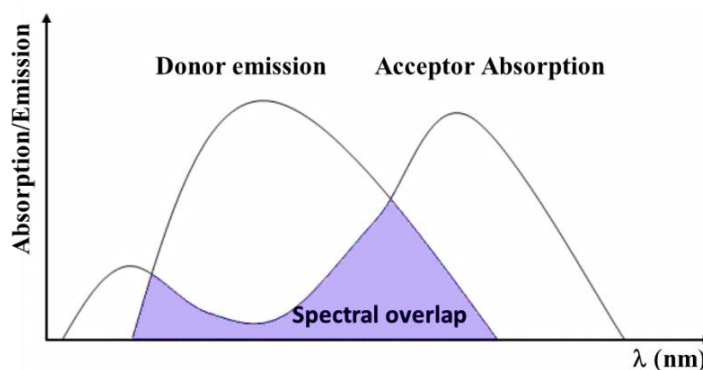


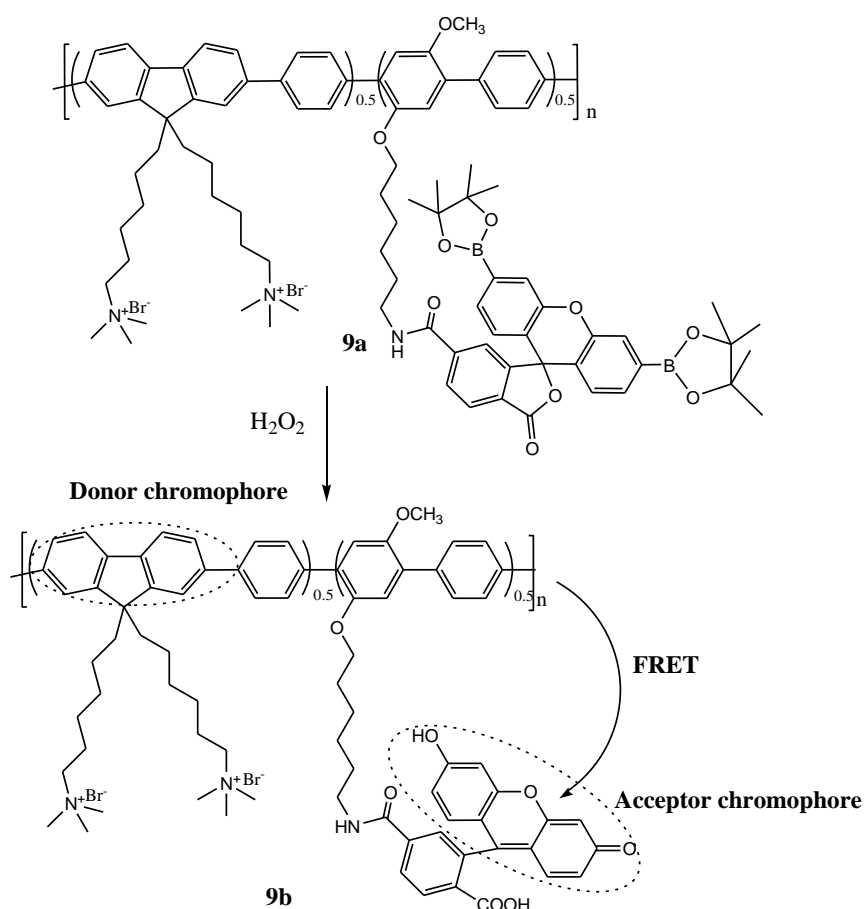
**Figure 2.10:** FRET spectral overlap.

As FRET mechanism involves transfer of excited-state energy from the donor to the acceptor chromophore, a decrease in donor emission and donor lifetime is observed, thus FRET can only be monitored using donor wavelength. However, most of FRET-based chemosensors utilize the photophysical characteristics of both chromophores to produce a ratiometric chemosensor by measuring the emission of the donor and sensitized emission of the acceptor chromophores. Consequently, a FRET ratio, which can be reported as either acceptor/donor or donor/acceptor, represents the ratio of sensitized acceptor emission and donor emission.

Generally, a FRET-based chemosensor consists of two chromophores (donor and acceptor) and an analyte binding unit (receptor) which interacts with the analyte and results in some structural modifications. The latter affects the distance between the two chromophores and/or dipolar orientations resulting in an enhanced or reduced FRET process. An example of a chemosensor system exhibiting the FRET mechanism, is a water soluble cationic polyfluorene **9a** bearing boronate-protected fluorescein for detection of hydrogen peroxide ( $H_2O_2$ ) and glucose in serum (**Scheme 2.4**).<sup>37</sup> In this polymer, fluorene units act as donors while fluorescein units act as acceptors. The fluorescein units are generated from the deprotection reaction of the boronate-protected non-fluorescent in the lactone form with  $H_2O_2$ . Consequently, the polymer, which initially displays a blue donor emission due to the absence of FRET process shows a green fluorescence in the presence of  $H_2O_2$  due to enhanced FRET process, from the fluorene unit to



the fluorescein unit. Since  $\text{H}_2\text{O}_2$  can be also generated from catalytic oxidation of  $\beta\text{-D-(+)-}$ glucose by glucose oxidases (GOx), glucose can also be detected using the same probe.



**Scheme 2.4:** Polyfluorene-bearing boronate protected fluorescein for the detection of ( $\text{H}_2\text{O}_2$ ) and glucose in serum.

### ii) Dexter energy transfer

Dexter type energy transfer, also known as through bond energy transfer (TBET), is another energy transfer-based sensing mechanism which mainly relies on the orbital interactions between the donor and acceptor chromophores. The orbital interactions can be attained directly or through a bridge.<sup>38</sup> This type of sensing mechanism is commonly observed from the systems in which donor and acceptor chromophores are linked *via* electronically conjugated bonds (**Figure 2.11**). The latter reduces the chances of donor and acceptor to adopt a planar conformation and allows the energy transfer to occur through connecting bond(s) without any need for spectral overlap, like in Förster type energy transfer.<sup>39</sup> Unlike the FRET mechanism, which involves exchange of excited state energy through space, Dexter energy transfer involves electron exchange between two HOMOs and two LUMOs from both donor and acceptor

---

chromophores (**Figure 2.8**) resulting in non-radiative decay. For this reason, a short distance (<10 Å) between donor and acceptor is required.

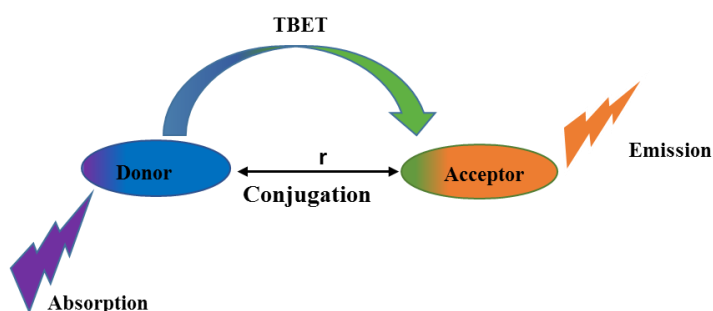


**Figure 2.11:** Dexter type energy transfer between a donor and an acceptor.

If  $k_{ET}$  represents energy transfer constant, the efficiency of energy transfer by Dexter energy transfer process can be summarized as;

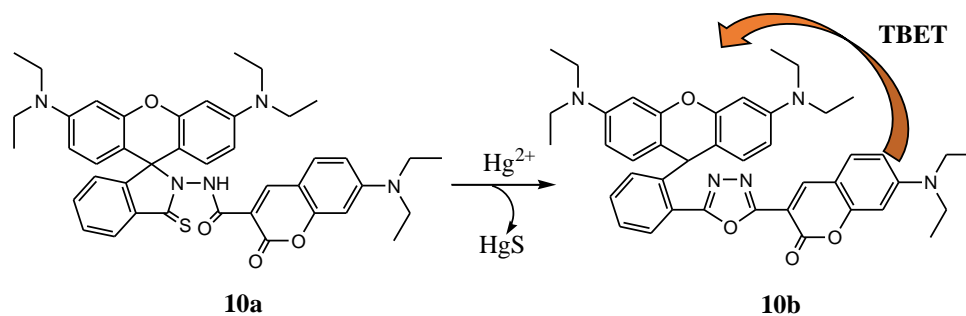
$$k_{ET} = K J \exp(-2R_{DA}/L)$$

Where; K: orbital interaction; J: overlap integral between donor emission and acceptor absorption;  $R_{DA}$ : donor acceptor separation; L: Van Del Waals radii.

From the equation, it is clear that the efficiency of energy transfer in a Dexter-based signalling system decreases exponentially as the distance between the donor and acceptor increases. Therefore, chemosensors based on this energy transfer mechanisms are highly dependent on distance.

As the spectral overlap between emission of the donor and absorption of the receptor is excluded among the requirements of Dexter-type energy transfer system, a large wavelength difference between emission peaks of the donor and acceptor can be obtained when energy is transferred to the acceptor chromophore. This can enhance the imaging resolution when appropriate chromophore pairs are connected.

An example of such a system is the coumarin-rhodamin **10a**, a ratiometric probe for  $Hg^{2+}$ , developed by Zhang and co-workers for bioimaging applications (**Scheme 2.5**).<sup>40</sup> Through TBET mechanism and dual-switch design, the probe resulted in two well separated emission peaks with a wavelength difference of 110 nm. A high energy transfer efficiency and a large signal-to-background ratio was also detected. These features allowed this probe to exhibit good sensitivity towards  $Hg^{2+}$  in biological systems, as well as in aqueous solutions.



**Scheme 2.5:** Coumarin-rhodamin TBET system for ratiometric detection of  $\text{Hg}^{2+}$ .

#### 2.2.2.4 Excimer and exciplex formation

During the excited state lifetime, fluorophores with flat and highly  $\pi$ -delocalized systems such as pyrene and anthracene can form an excited dimer when two fluorophores are in close proximity to each other. This results in two fluorescence bands from the monomer (free fluorophore) and the excited complex. Depending on the nature of interacting fluorophores, excited complexes can be divided into two categories; excimer and exciplex. The former results from the excited state interaction of two fluorophores with the same structure in their ground states, while the latter involves the interaction between different fluorophores.

Generally, the emission spectrum of an excimer/exciplex appears at a lower energy compared to the monomer emission spectrum. Their fluorescence intensity ratios depend on molecular mobility and microviscosity.<sup>41</sup> The presence of an analyte can encourage either the excimer/exciplex formation or disruption and the effect can be observed in the emission spectrum. Therefore, by monitoring monomer and excimer/exciplex fluorescence intensities ratio, analyte recognition can be achieved.

A typical chemosensor in this category is the novel fluorogenic calix[4]triazacrown-5 (**Figure 2.12**) bearing two pyrene amide groups and one coumarin amine group developed by Kim and co-worker for selective  $\text{F}^-$  ions detection.<sup>42</sup> The chemosensor **11** displayed exciplex fluorescence emission at 425 nm with significantly enhanced intensity due to H-bonding between the azacrown unit and two pyrene amide groups which enables the pyrene unit to get closer to the coumarin unit resulting in an overlap. The presence of  $\text{F}^-$  induces changes in conformation resulting in exciplex rupture. Fluorescence quenching and a decrease in exciplex emission intensity at 425 nm is observed due to this interaction.

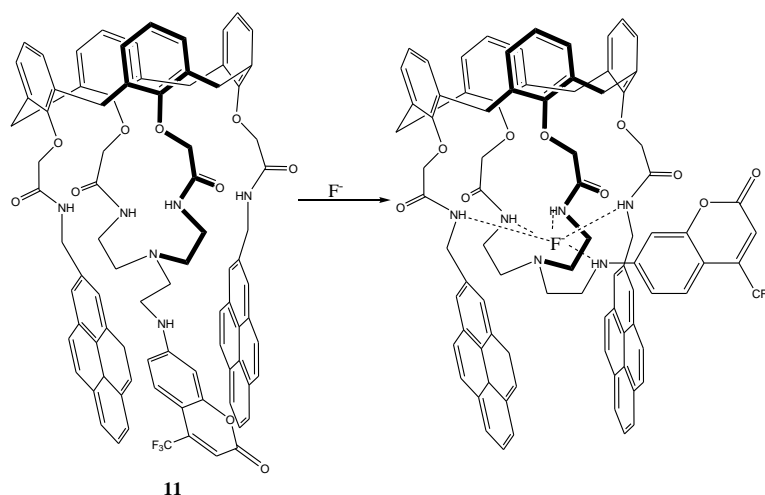


**Figure 2.12:** Pyrene-coumarin-based calix fluorophore emitting exciplex for  $F^-$  ions detection.

### 2.2.2.5 Aggregation-induced emission

Several highly fluorescent single molecule and polymeric organic materials exhibit fluorescence quenching in their highly concentrated solutions and also in their aggregated forms. The effect has been described as an aggregation-caused quenching mechanism (ACQ).<sup>43</sup> The mechanism has extensively limited the range of applications of several organic fluorophores as sensory materials (chemosensors and biosensor) and as organic light emitting diodes (OLEDs).<sup>44</sup> A number of structural modifications,<sup>44</sup> such as attachment of a branched chain, bulky cyclic species and dendritic wedges to the fluorophore *via* covalent linkage have been applied to avoid this nuisance effect.<sup>45</sup> Nevertheless, abnormal behaviour was noted from some organic molecules which are practically non-fluorescent in solution, but become strongly fluorescent in their aggregated states. This uncommon fluorescence incident was firstly observed from a solution of 1-methyl-1,2,3,4,5-pentaphenylsilole by Tang and co-worker in 2001 and was named as aggregation induced emission (AIE).<sup>46</sup> The molecule, which were approximately non-emissive in pure ethanol, displayed 333 times increment in quantum yield ( $\Phi_F$ ) when the water fraction was increased to 90%.

From experimental and theoretical investigations carried out by Tang and co-workers on various molecules, it was denoted that the intramolecular rotation in AIE molecules is the main cause of deactivating excited states, which results in non-emissive decay in certain solvents. However, when intramolecular rotation is restricted in the aggregated state, the AIE process is triggered and strong fluorescence emission is observed.<sup>47</sup>

Due to this uncommon fluorescence feature, efficient organic light emitting diodes (OLEDs), as well as sensitive and selective bio/chemosensors, have been developed using the AIE principle. In **Figure 2.13** are some examples of chemosensors which use AIE as their recognition mechanism. These sensors have been used in a number of applications including;

- i. Detection of volatile organic compounds (compound **12**).<sup>48</sup>
- ii. Fluorescent turn-on chemosensor for  $\text{Hg}^{2+}$  (compound **13**).<sup>49</sup>
- iii.  $\text{CN}^-$  ion detection in aqueous solution (compound **14**).<sup>50</sup>
- vi. Biomolecules detection (DNA and bicine serum albumin) (compound **15**).<sup>51</sup>

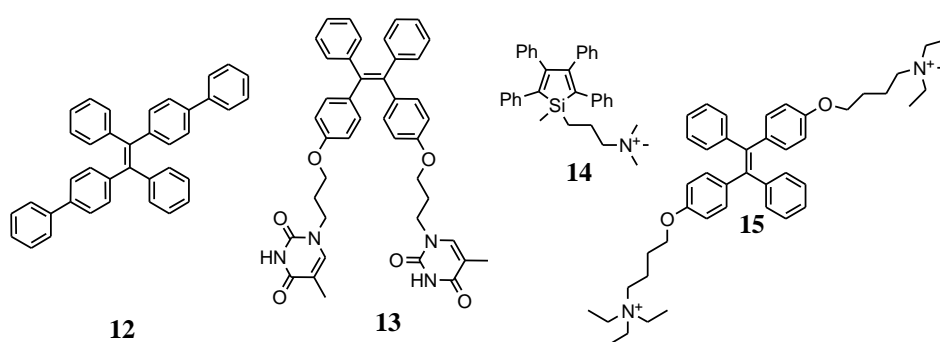


**Figure 2.13:** AIE based chemosensors.

#### 2.2.2.6 C=N isomerization

C=N isomerization features among recently developed fluorescence sensing techniques. It was firstly reported in 2007 based on the investigation of photophysical behaviors of conformationally restricted molecules.<sup>52</sup> From those studies, C=N isomerization was found to be an ultimate decay process of excited states in the systems with unbridged C=N bond, which usually results in non-emissive decay. However, an investigation conducted on their counterparts (covalently bridged C=N structures) showed opposite results with fluorescent enhancement. The latter was attributed to C=N isomerization restraint in the excited state. Further studies on the photophysical properties induced by C=N isomerization showed that the presence of appropriate guest analytes can inhibit C=N isomerization, making it a turn-on fluorescence chemosensor system for that analyte. Guest analytes interaction leading to the inhibition of C=N isomerization can occur in various ways including complexation,<sup>53</sup> removal,<sup>54</sup> and hydrogen bond formation (**Figure 2.14**).<sup>55</sup>

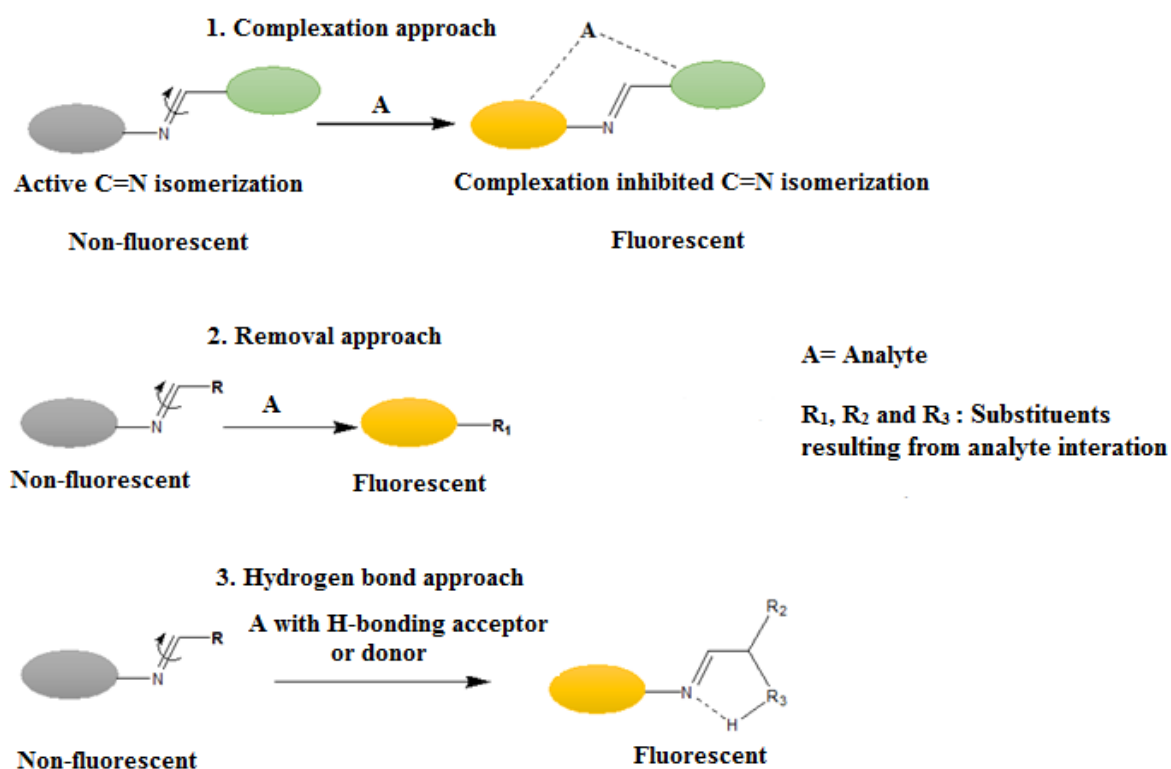
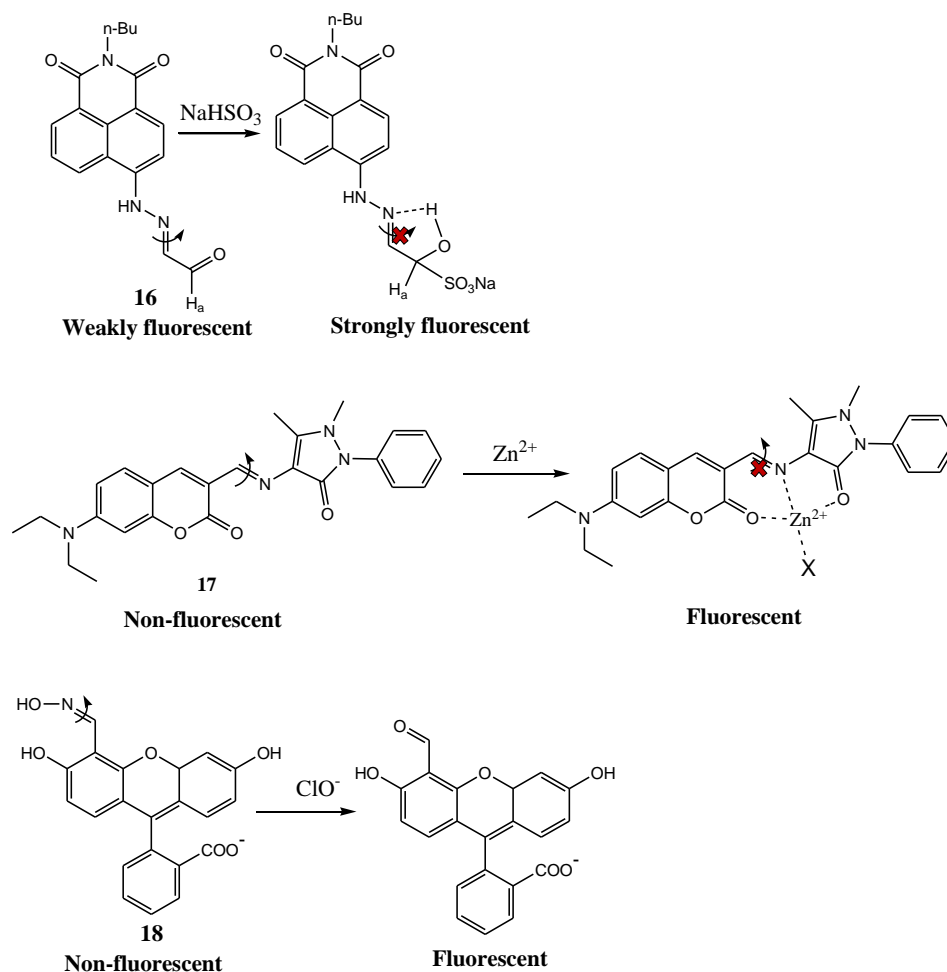


**Figure 2.14:** Mode of analyte interactions which lead to the inhibition of C=N isomerization.

Examples of chemosensors which use this fluorescent sensing mechanism include: a fluorescent turn-on probe for bisulfite ions which involves hydrogen bond formation to inhibit C=N isomerization (compound **16** in **Scheme 2.6**),<sup>56</sup> a coumarin-based probe for selective detection of Zn<sup>2+</sup> which uses a complexation approach to initiate fluorescent turn-on sensing in both aqueous as well as in biological system (compound **17** in **Scheme 2.6**)<sup>57</sup> and a xanthene-based probe for hypochlorous acid recognition which uses the removal approach to inhibit C=N isomerization (compound **18** in **Scheme 2.6**).<sup>54</sup>



**Scheme 2.6:** Different types of C=N isomerization-based chemosensors.

### 2.2.2.7 Excited state intramolecular proton transfer (ESIPT)

The excited state intramolecular proton transfer (ESIPT) signalling mechanism has contributed to the design of fluorogenic chemosensors over the past few decades.<sup>58</sup> The chemosensors that emerged from this mechanism displayed beneficial photophysical properties such as intense luminescence, large Stokes shifts and photostability.<sup>59</sup> Owing to the large Stokes shift, ESIPT fluorophores exhibit almost complete absence of spectral overlap between absorption and emission which makes them suitable for use in fluorescent probing.

The ESIPT mechanism requires a transfer of a proton from hydroxyl or amino group to a neighbouring hydrogen acceptor at a distance less than 2 Å. This transfer occurs *via* a six or five membered ring hydrogen bonding configuration.<sup>60</sup> Numerous studies describe ESIPT as a faster process than electron transfer (sub-picosecond timescale) and the rate of proton transfer is environment reliant.<sup>61</sup> For example, in nanocavities of cyclodextrin or in emulsion, it occurs at a very slower rate. Furthermore, investigation of ESIPT-based molecules showed a separate

---

dual fluorescence as a result of a three energy level system including a ground state, a normal excited state and a tautomer excited state. The dual fluorescence is as a result of tautomerism.

Due to the environmental dependence of ESIPT processes, which can lead to the changes in a dual fluorescence depending on the nature of surrounding environment, many ESIPT molecules and polymers have been investigated for their sensing capabilities in the presence of different analytes.<sup>62</sup> An example is the  $\pi$ -conjugated polymer with 2,5-bis(benzoxazol-2'-yl)benzene-1,4-diol fluorene units (**Figure 2.15**) developed by Pang and co-workers for anionic species detection.<sup>63</sup> The polymer exhibited large Stokes shift ( $\sim 200\text{nm}$ ) due to the ESIPT mechanism. In the presence of ionic species such as  $\text{OH}^-$ ,  $\text{AcO}^-$  and  $\text{F}^-$  a red shift in absorption from  $\approx 421\text{ nm}$  to  $510\text{-}540\text{ nm}$  and an increase of fluorescence quantum efficiency by the factor  $\sim 20$  was also detected.

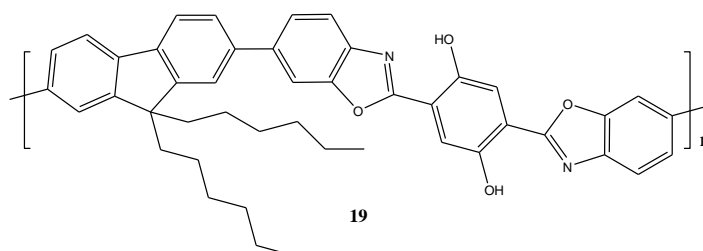


**Figure 2.15:** ESIPT-based polymeric chemosensor for anions.

## 2.3 Fluorescent polymers

Generally, when small molecule-based probes are produced, the next step is to incorporate them in/onto a solid support to improve their processability. Physical entrapment of those molecules into a polymer matrix is the most common method that has been applied so far to immobilize the sensitive probes.<sup>64</sup> However, this method generates inhomogeneity in the material which results in stability problems due to the leaching of the fluorescent sensitive probe molecules. The latter lowers the lifetime and reproducibility of the sensor and limits its application in commercial devices. As an alternative, a permanent immobilization of sensitive probes which leads to stable material has been achieved *via* incorporation of sensing components (receptor and fluorophore) into the polymer backbone.

Compared to the small organic molecules, fluorescent polymer-based chemosensors offer many crucial advantages. For instance, small molecule chemosensors are characterized by low sensing performance levels (sensitivity and selectivity), compared to their polymer counterparts. This is based on the fact that receptor-analyte interactions in small molecules



which rely on feeble interactions (*e.g.* hydrogen bonding), are greatly affected by solvents and usually result in impairment in aqueous environment due to the competitiveness of water molecules. On the other hand, polymeric chemosensors provide numerous options to combine analyte-receptor interactions with intra/interchain polymer interactions and solvent-polymer interactions in solution and solid states, as well as in their swelled and gel states. Furthermore, due to the intra/interchain polymer interactions and solvent-polymer interactions which can interfere with the sensing events, hydrophilic or hydrophobic environments can be created for pendant or main chain receptors units through structural modifications. Another important feature which is mainly noted in conjugated polymer-based chemosensors is an existence of collective properties due to electronic communication between receptors across the polymer chains. This allows those chemosensors to be sensitive to even minor perturbations as shown in **Figure 2.16**.

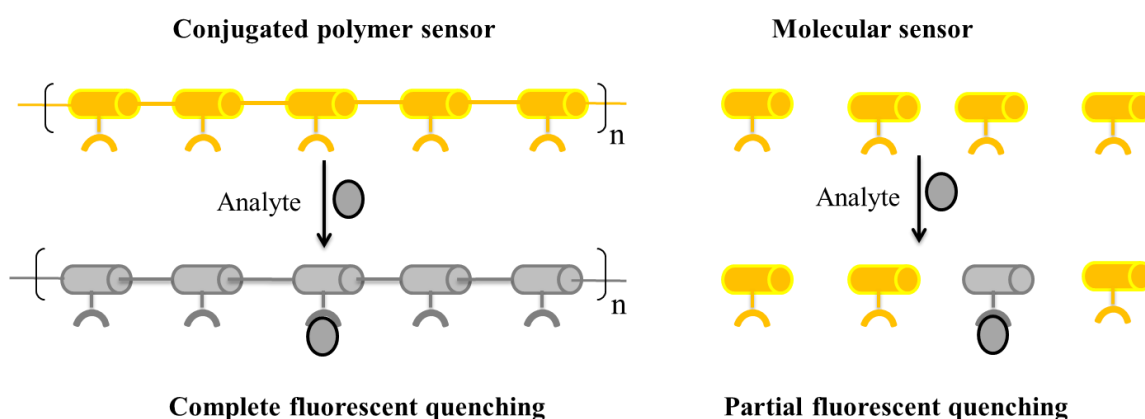


**Figure 2.16:** Comparison between small molecule-based chemosensors and conjugated polymer-based chemosensors in term of sensitivity.

Permanent immobilization of fluorescent components into polymeric materials can be achieved either after polymerization, when the synthesized polymer has reactive functional groups, or *via* polymerization of fluorescent monomers.<sup>65</sup> The former technique has been initially utilized for natural polymers such as cellulose to produce sensitive polymeric materials.<sup>66</sup> However, the technique has been extended to synthetic polymers with molecular and ionic sensing capabilities.<sup>67</sup> In polymeric chemosensors, target analyte recognition can be performed in different ways. Primarily, it can be performed through the interaction between target analytes and receptors situated in the polymer pendant chains or polymer backbone, or through conformation changes induced by the analyte in polymer-solvent system. In addition, due to

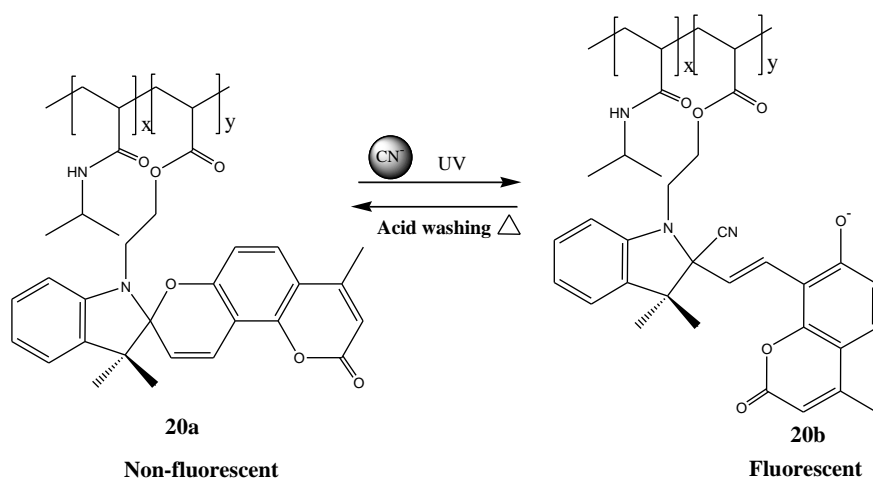
---

collective properties in the polymer chains, the two effects can merge to form another analyte recognition mode. Depending on structure and receptor types, polymeric chemosensors can be classified as side-chain polymers, conjugated polymers, imprinted polymers and dendrimers.

### 2.3.1 Side-chain polymer based chemosensors

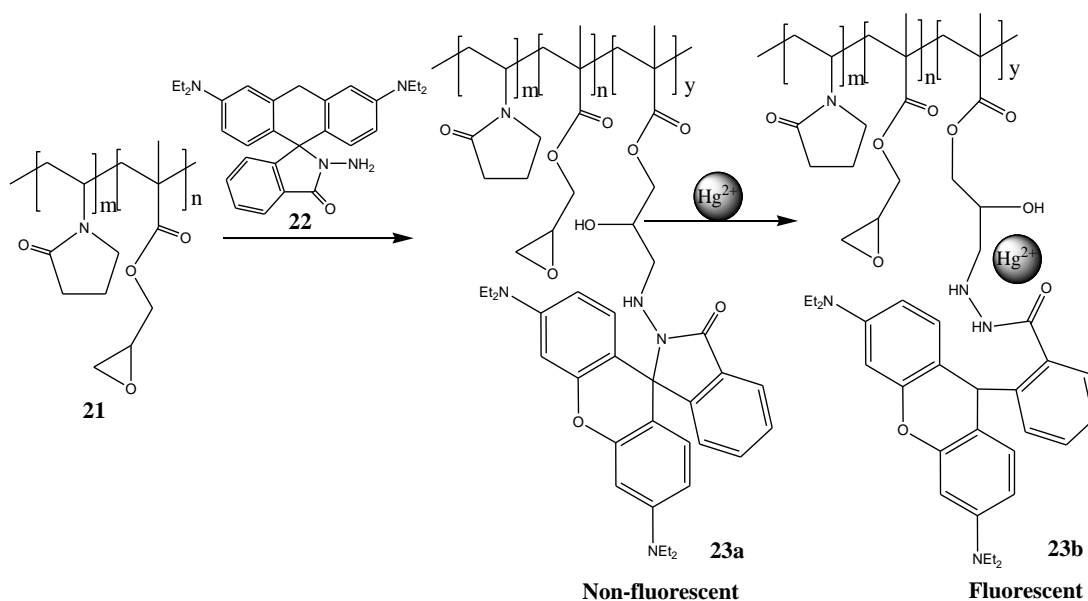
Most of the polymeric chemosensors of this type are produced mainly by conventional free radical polymerization techniques or post-polymerization labelling methods, in which highly efficient reactions (such as click reactions) are required to overcome the coiling nature of polymers in solution.<sup>68</sup> On these polymers, optoelectronic properties of the polymers with sensing components (receptor and fluorophore) on the side chains are mostly not dictated by the degree of polymerization or the number of repeating units.

Based on various potential properties such as permeability, solubility, mechanical strength, polarity and biocompatibility, a series of polymeric probes for molecular and ionic species with sensing components on the side-chain have been developed and applied in different environments. For example, a reusable thermoresponsive co-polymer **20a** with coumarin-spiropyran conjugate was developed by Shiraishi and co-workers for detection of cyanide ions in water.<sup>69</sup> The polymer utilizes coumarin conjugate spiropyran as a sensing component, while poly-N-isopropylacrylamide serves as a thermoresponsive unit. The co-polymer which is fully soluble in water at a temperature below 30°C, exhibited selective recognition of cyanide ions in water under UV-light irradiation with a fluorescence turn-on response. This results from a nucleophilic interaction between cyanide ions and the photoformed merocyanide form of the coumarin-spiropyran conjugate, which concentrate  $\pi$ -electrons on the coumarin units (**Scheme 2.7**). The co-polymer was successfully applied in the quantification of cyanide ions in water at very low concentrations ( $>0.5\mu\text{M}$ ). Its recovery was achieved through a high temperature ( $>40^\circ\text{C}$ ) centrifugation method.



**Scheme 2.7:** A reusable thermoresponsive co-polymer with coumarin-spiropyran conjugate for cyanide ion detection.

An example where post-polymerization labelling method has been utilized to introduce a sensing units into polymer structures is the water soluble co-polymer **23a**, developed by Liu and his teammates for the  $\text{Hg}^{2+}$  ions detection in water.<sup>70</sup> The reporting unit of this co-polymer includes rhodamine B which has been incorporated on the side chains *via* post-polymerization labelling method (**Scheme 2.8**). In the presence of  $\text{Hg}^{2+}$  ions, a notable fluorescence enhancement and visible colour change from colourless to pink was detected. These observations were attributed to fact that,  $\text{Hg}^{2+}$  ions induce a highly conjugated rhodamine system through spirolactam ring-opening.



**Scheme 2.8:** Highly sensitive and selective turn-on fluorescent polymeric chemosensor for  $\text{Hg}^{2+}$  in pure water.

---

Besides sensitive materials produced *via* conventional polymerization methods of fluorescent monomers, new techniques involving directionally confinement of sensing units in a physical space (surface or surfactant aggregate) have been recently developed. A number of receptor units have been combined with different materials including glass and gold surfaces,<sup>71</sup> silica particles,<sup>72</sup> and quantum dot,<sup>73</sup> to produce new sensing systems.

### 2.3.2 Conjugated polymers based-chemosensors

Conjugated polymers (CPs) are characterized by the presence of sp- or sp<sup>2</sup>-hybridized atoms in the main chain as single and multiple bonds alternate across the polymer backbone. This feature allows CPs to exhibit potential optical and optoelectronic properties due to inherent semi-conductive behaviour generated from the interactions between orbitals. The latter result in a semi-conductor band structure with a valence band (populated band) and a conduction band (vacant band). Owing to CPs electronic structures of extensive  $\pi$ -systems, described as molecular wire by Swager,<sup>74</sup> and their typical semi-conductive properties, CPs found application in various fields including; organic light emitting diodes (OLED),<sup>75</sup> field effect transistors,<sup>76</sup> photovoltaics,<sup>77</sup> batteries<sup>78</sup> and actuators.<sup>79</sup>

Recently, CPs applications have been extended to fluorescent sensing and many conjugated systems have been investigated for their chemosensory capabilities.<sup>80</sup> In comparison to non-polymeric sensor systems, CPs exhibit ultra-high sensitivity due to the efficient transfer of excitation energy between the receptors across the polymer backbone.<sup>74</sup> The functional characteristics of CPs can be expressed through conformational changes of the conjugated system induced by the interaction with the analytes or electron density changes within the polymer backbone.

Since CPs receptors are linked *via* conjugation, self-amplification of fluorescent signals can be obtained in CP-based chemosensors when the CP's electronic system is disrupted by the analyte. **Figure 2.17** describes CP signal amplification upon analyte binding, as a result of electron's delocalisation along the polymer backbone.

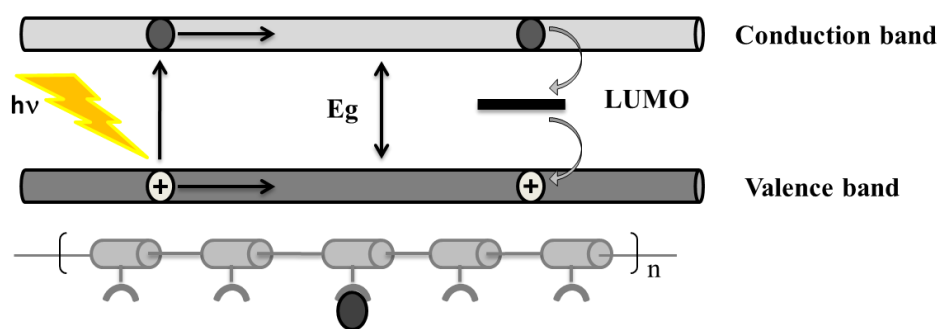


**Figure 2.17:** CP signal amplification upon analyte binding.

The above diagram represents a common PET fluorescent quenching mechanism in CP-based chemosensors. Upon photon irradiation, a CP electron is promoted to the higher energy conduction band and then migrates across the polymer chain due to conjugation. The presence of an analyte induces the formation of a trapping site in the system by introducing an empty orbital between valence and conduction bands. This leads to an excited state relaxation process, whereby a promoted electron is required to go through the LUMO of the quencher on its way to ground state. Since excitation energy is dissipated during this process, a non-radiative relaxation process is obtained and the CP can no longer fluoresce.

Owing to the outstanding sensitivity and availability of different transduction methods such as changes in wavelength (absorption and emission), intensity, lifetime and energy transfer, numerous CP based fluorogenic chemosensors have been investigated for different target analytes. These analytes include ions (cations and anions),<sup>81</sup> neutral compounds<sup>82</sup> and biological samples.<sup>83</sup> Additionally, CPs based on other transduction methods such as potentiometry, conductometry and colorimetry have also been investigated.<sup>84</sup> **Figure 2.18** illustrates some examples of CPs with chemosensing applications.

- i. Fluorogenic chemosensor for  $\text{Hg}^{2+}$  (compound **24**),<sup>85</sup>
- ii. Chromogenic chemosensor for  $\Gamma^-$  (compound **25**).<sup>86</sup>
- iii. Fluorogenic chemosensor for sugars and biological molecules (compound **26**).<sup>87</sup>
- iv. Fluorogenic chemosensor for explosive nitroaromatic compounds (compound **27**).<sup>88</sup>

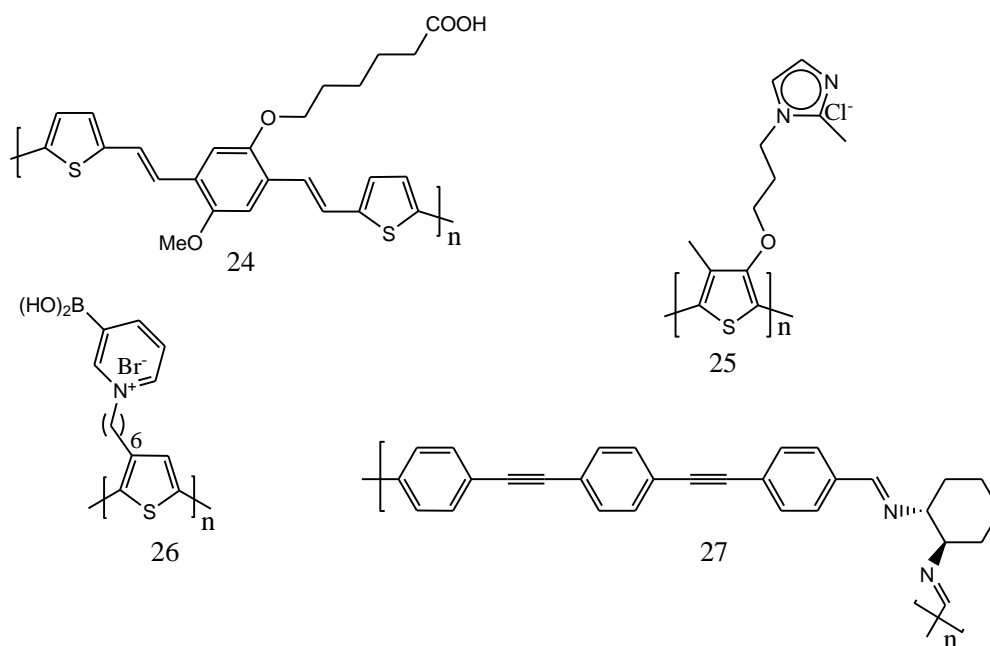


**Figure 2.18:** Examples of CPs with chemosensing applications.

### 2.3.3 Molecular imprinted polymer based-chemosensors

Fluorescent molecular imprinted polymers (MIP) are an important class of fluorescent polymers. These materials came as a supplement to the molecular imprinting method introduced by Dickey in 1945, and their performance is based on the “lock and key” model employed by enzymes for substrate recognition.<sup>89</sup> In comparison with other synthetic probes, MIPs offer an easy synthetic route since their synthetic method do not require a fore-understanding of the three dimensional structure of the target analyte, as well as the total synthesis of the probe.

Molecular imprinted polymers are generally produced *via* a template-directed synthesis. The method involves a template molecule (analyte) and functionalized monomers that assemble around the template molecule. In the presence of a cross-linking agent, the functional monomers undergo a copolymerization reaction with a cross-linker resulting in a polymer matrix around the template. In the early stage, the monomers and imprint molecule interact through their functional groups and are kept in the same position by a highly cross-linked polymer matrix generated from polymerization reaction. Removal of the template molecule from the binding sites leads to a vacant recognition site which is complementary in shape, size and functionality to the original template molecule, as shown in **Figure 2.19**. The created

vacant site enables the MIPs to have “molecular memory” which allows a selective recognition of template molecule or structurally chemical analogues.

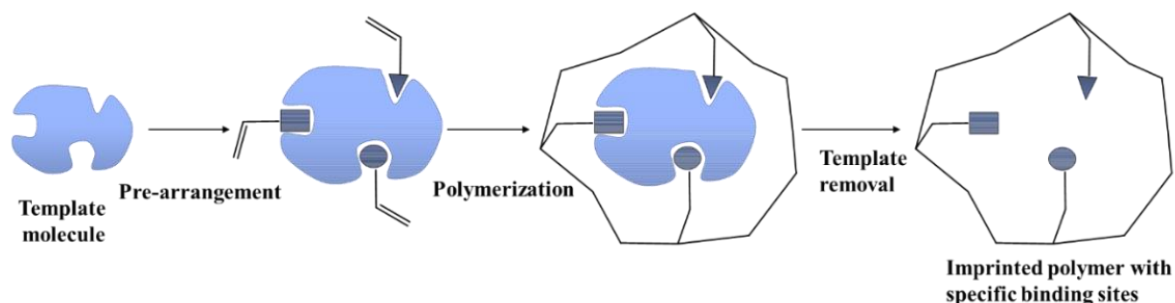
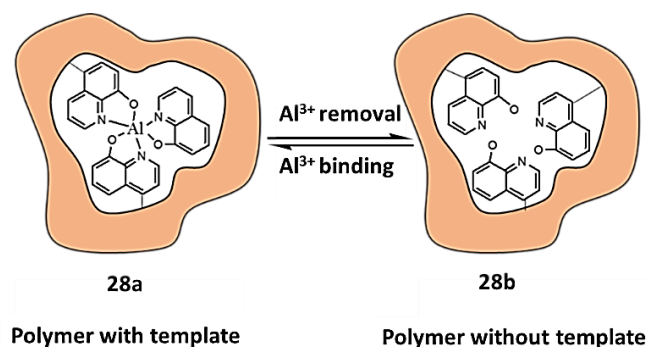


**Figure 2.19:** Summary of polymer imprinting process.

The first system where the recognition properties of MIP was coupled with fluorescent reporter groups was reported in 1998.<sup>90</sup> In this work, by Powell and co-workers, a polymer imprinted with cyclic adenosine monophosphate (cAMP) in the presence of *trans*-4-[*p*-(*N,N*-dimethylamino)styryl]-*N*-vinylbenzyl-pyridinium chloride as the fluorescent monomer was synthesized. The polymer, whose signalling unit was part of the created recognition sites, displayed a fluorescent quenching in presence of cAMP in aqueous medium.

For the past few years, many reports on the fluorescent imprinted polymers for the detection of amino acids,<sup>91</sup> saccharides,<sup>92</sup> and other analytes<sup>93</sup> have been reported. Although analyte recognition results in fluorescent quenching in most of the cases, fluorescent imprinted polymers exhibiting fluorescent intensity enhancement upon analyte binding have been recently reported. For example, the MIP reported by Ng and Narayanaswamy for the detection of  $\text{Al}^{3+}$  ions in aqueous medium (**Scheme 2.9**).<sup>94</sup> The polymer incorporates 8-hydroxyquinoline sulfonic acid as the fluorescent unit and displayed an “off-on” fluorescent response in the presence of  $\text{Al}^{3+}$  through flow cell analysis. The polymer also exhibited a linear response up to  $1.0 \times 10^{-4}$  M with a detection limit of 3.62  $\mu\text{M}$ .



**Scheme 2.9:** Representation of imprinted process for  $\text{Al}^{3+}$ -imprinted polymer.

---

### 2.3.4 Dendrimer-based chemosensors

Luminescent dendrimers form a special class of fluorescent polymers. These macromolecules exhibit well-defined morphology and unique characteristics, which allow the incorporation of specific chemical units for recognition of ions or neutral molecules. Topologically, dendrimers consist of three different sections: the core, branches and the surface. Fluorescent units can be integrated into any of those sections, uncovalently hosted in the dendrimers cavities, or connected to the dendrimers surface.

For the past few years, a number of systems in which dendritic structures are coupled with luminescence have been reported. These systems have found applications in various fields which include biological<sup>95</sup> and chemical sensing.<sup>96</sup> **Figure 2.20** depicts a poly(amine ester) dendrimer **29** which has been used as fluorogenic chemosensor for  $\text{Al}^{3+}$ ,  $\text{Cu}^{2+}$  and  $\text{Zn}^{2+}$  in acetonitrile.<sup>97</sup>

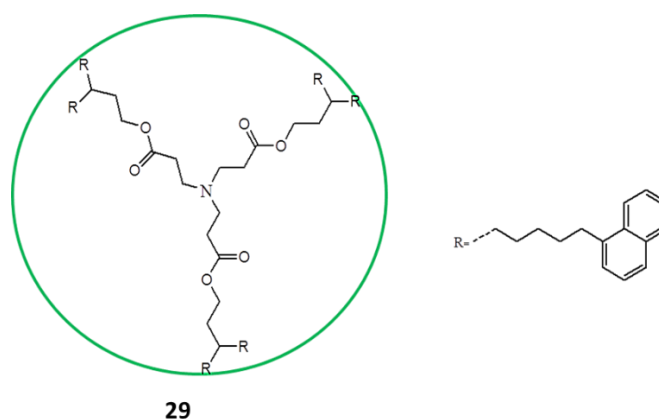


**Figure 2.20:** Poly(amine ester) dendrimer for  $\text{Al}^{3+}$ ,  $\text{Cu}^{2+}$  and  $\text{Zn}^{2+}$  detection.

### 2.4 Triazole-based chemosensors

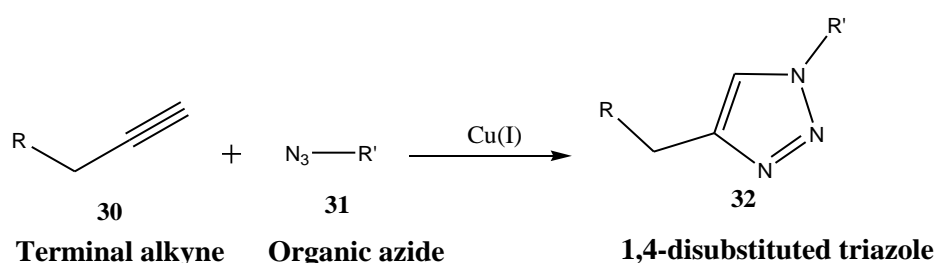
Since fluorescent chemical sensors depend on binding events or chemical reactions that induce changes in the photophysical properties of the fluorophore unit (reporter), a proper design for the receptors capable of interacting with the analytes to induce significant changes in the reporter, is highly desirable. Despite a significant growth in chemosensor design and synthesis, much more needs to be done in this field as some reported chemsensors exhibit poor sensitivity and are easily hampered by competing analytes. Therefore, a major effort in developing fluorogenic chemosensors with higher sensitivity and selectivity towards various target analytes is necessary.



---

To date, several receptor systems such as Schiff bases, crown ethers, bipyridines, di-2-picolylamines (DPA), urea *etc.*, have been incorporated into different chemosensor systems along with various fluorophores. The incorporation of receptor systems is meant to improve the sensitivity and selectivity of the chemosensor systems. However, further research work is needed to develop novel, reliable and highly selective chemosensors for biological, environmental and medicinal applications.

Recently, new sensing systems, which involve click-derived triazoles as receptors have emerged.<sup>98</sup> The highly yielding and regioselective Cu(I)-catalyzed azide-alkyne 1,3-dipolar cycloaddition (CuAAC), which is a typical click reaction, is usually used for the synthesis of triazole-containing systems (**Scheme 2.10**).<sup>99</sup>



**Scheme 2.10:** Cu(I) catalyzed 1,3-dipolar cycloaddition reaction of azide and alkyne.

In addition to the synthetic simplicity and modular nature of this reaction, the afforded 1,2,3-triazole (click triazole) structure can play an important role in chemosensing. This was supported through the investigations carried out on triazole-containing systems such as oligo-triazoles and macrocyclic triazophane.<sup>100</sup> In those reports, it was demonstrated that the click triazole motif possesses the ability to act as hydrogen bond acceptor through lone pair of the middle nitrogen atom or as a hydrogen bond donor through a polarized triazole C-H bond. This clearly indicates that the click-triazole ring has the ability to effectively bind to both cations and anions.

Recently, several researchers have been inspired by the features of the click triazole. A number of cation and anion chemosensors with the click triazole ring acting as the receptor unit have been developed.<sup>101</sup> These special features of the click triazole were also translated into triazole-containing polymeric materials to obtain an array of polymers with optoelectronic, pharmaceutical and biomedical applications.<sup>102</sup> However, in the field of macromolecules, there is a lack of exploration around these types of polymers in terms of sensing applications.

---

To date very few triazole-containing polymers with chemosensing capabilities have been reported. For instance; a highly conjugated polymer was reported by Zhu and co-workers (compound **33** in **Figure 2.21**).<sup>103</sup> The polymer showed a higher sensitivity and selectivity towards  $\text{Hg}^{2+}$  ions with “turn-off” fluorescent response when solutions of metal ions in acetonitrile were added to the polymer solution in chloroform. Furthermore, this report suggested the contribution of the triazole unit to binding of  $\text{Hg}^{2+}$ .

Recently, a chiral poly(imine-triazole) was reported as a fluorescent “turn-on” chemosensor for  $\text{Zn}^{2+}$  ions by Jiang and associates (compound **34** in **Figure 2.21**).<sup>104</sup> The polymer was synthesized using AB type clickable monomer (*S*)-2-[(2-azido-1-phenylethylimino)methyl]-5-propargyl-oxyphenol (AMPP) *via* a metal-free AB click reaction.<sup>105</sup> The possible interaction patterns between polymer and  $\text{Zn}^{2+}$  ions were investigated by comparing the emission spectra of the repeating unit with that of the triazole-containing *N*-salicylidene derivative, which is structurally close to the repeating unit. This triazole-containing model compound exhibited a high fluorescence enhancement response (12 folds) compared to the repeating unit (7 folds), suggesting the interaction of triazole ring with  $\text{Zn}^{2+}$ .

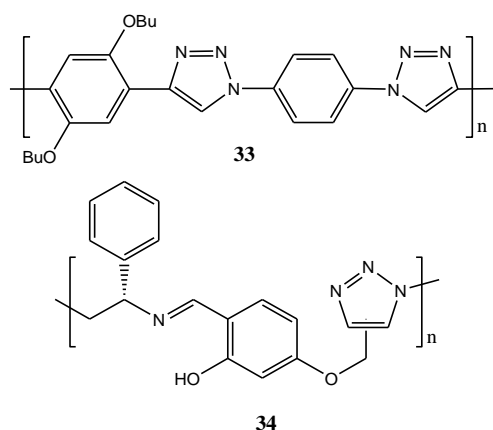


**Figure 1.21:** Triazole-containing polymer for  $\text{Hg}^{2+}$  and  $\text{Zn}^{2+}$  recognition.

Despite the hydrogen bond abilities of the 1,2,3-triazole ring, which can allow triazole-containing materials to interact with anions, not much has been done so far in the field of anion sensing. This can be attributed to the interferences from foreign analytes which tamper with the selective detection of anions. To date, most of the click triazole-containing chemosensors that have been reported for anion recognition are based on small molecules or oligomeric compounds.

A chromogenic chemosensor which utilises 1,2,3-triazole motif and amide functionality to create binding sites for halides have been reported by Haridas and co-workers (**Figure 2.22**).<sup>106</sup> The addition of F<sup>-</sup> ions to CHCl<sub>3</sub>: DMSO (98:2 v/v) solutions of the compound **35a** induced intense colour change from yellow to orange compared to other halides. This observable chromogenic response was attributed to the interaction between F<sup>-</sup> ions and the recognition subunit *via* hydrogen bonding formation between; F<sup>-</sup> ions and C-H of triazole ring, F<sup>-</sup> ions and N-H of amide and F<sup>-</sup> ions and C-H of 1,3-disubstituted benzene ring.

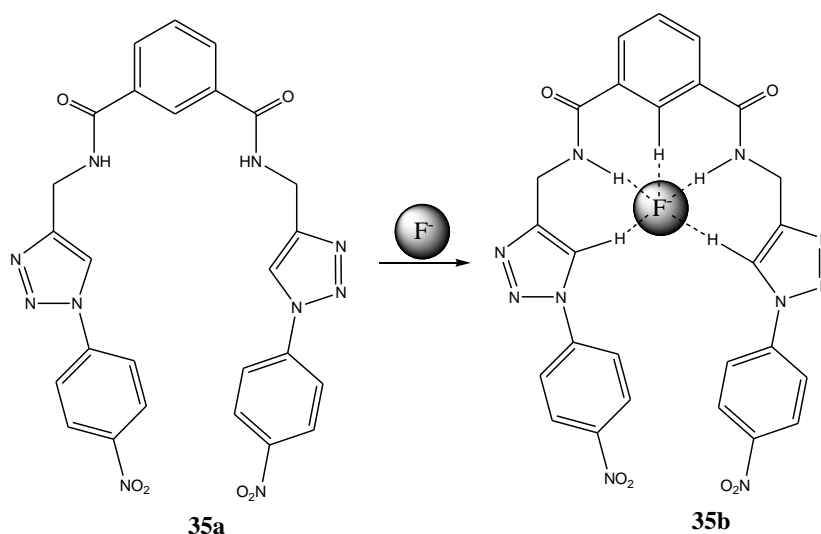


**Figure 2.22:** Triazole containing chromogenic chemosensor for F<sup>-</sup> ions.

Another example is the recently reported tris(triazole) tripodal receptor **36** which acts as a selective probe for citrate ions (**Figure 2.23**).<sup>107</sup> This probe contains 1,3,5-trisubstituted-2,4,6-triethylbenzene scaffold with a highly flexible arms incorporating 1,2,3-triazole motifs as recognition sites and pyrene as the reporter unit. Upon photon irradiation at  $\lambda = 345$  nm, the probe exhibited two emission bands at 386 nm and 405 nm which were assigned to monomeric pyrene emission. A structureless red-shift band at 486 nm was assigned to pyrene excimer emission. In the presence of citrate ions the probe displayed a slight quenching of pyrene excimer band intensity and enhancement of monomeric pyrene emission band with a quantum yield of 1.87 more than that of the free probe. This observations were only detected upon addition of citrate ions suggesting a selective recognition of the probe towards citrate ions.

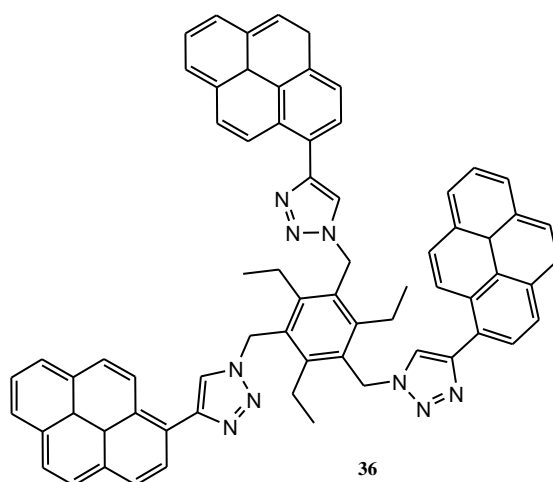
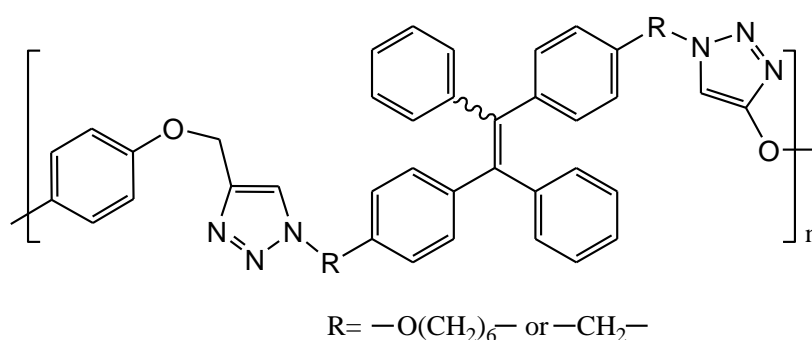


**Figure 2.23:** Triazole containing fluorogenic chemosensor for citrate ions.

Furthermore, 1,2,3 triazole-containing polymers were also reported to show molecular recognition properties. For example, polymer **37** with tetraphenylethene as the fluorescent unit was reported by Tang and co-workers for explosive compounds detection (**Figure 2.24**).<sup>108</sup> Usually polytriazole preparation from fluorogenic repeating units leads to the fluorescent quenching of the resulting polymer due to formation of aggregates. However, in this polymer, the emission of practically non-emissive tetraphenylethene units is boosted by an aggregation induced emission phenomenon (AIE) and it was quenched by picric acid during polymer recognition tests towards explosive compounds.



37

**Figure 2.24:** Triazole based polymer for the detection of explosive compounds.

---

## 2.5 Coumarin derivatives

Coumarin compounds, are a large and important group of organic compounds that have been widely investigated as an ideal component for various high-technological applications such as electronic and photonic applications,<sup>109</sup> fluorescent probes and sensors.<sup>110</sup> Coumarins are naturally occurring compounds, and the basic coumarin was first isolated and reported in the 1820's from Tonka beans (*Dipteryx odorata*).<sup>111</sup> The parent molecule known as 2*H*-chromen-2-one or 1-benzopyran-2-one consists of fused pyrone and benzene rings with a carbonyl group at position 2 as shown in **Figure 2.25**. Due to the extended  $\pi$ -conjugation of benzopyrone system, coumarins display excellent chromogenic and fluorogenic properties including a high degree of sensitivity to their local environments such as polarity and viscosity.<sup>112</sup> The synthesis of coumarins has been attained via several methods such as the Knoevenagel,<sup>113</sup> Perkin,<sup>114</sup> Pechmann,<sup>115</sup> Reformatsky,<sup>116</sup> and the Wittig<sup>117</sup> reaction.

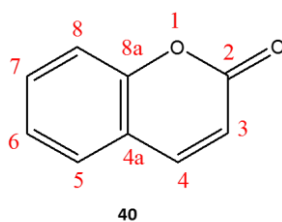


**Figure 2.25:** Coumarin structure showing the numbering of carbon.

Besides the inherent photochemical features of the coumarins, their commercial value and applicability in different disciplines have been enhanced by their biocompatibility, high fluorescence quantum yield, relative ease of synthesis, excellent light stability and solubility. Furthermore, it was demonstrated that the absorption and emission of the coumarins can be tuned *via* the manipulation of substituents on the coumarin structure.<sup>118</sup> For instance, the addition of electron donating groups to position 7 of the coumarin moiety results in a “push-pull” of the  $\pi$ -electron system as shown in **Figure 2.26**. This leads to the extended  $\pi$ -conjugated system between an electron-donating group of position 7 and the electron-accepting carbonyl group to produce a charge-transfer complex.<sup>110</sup> The ionization potential of the electron-donating group and the electron affinity of the electron-accepting group have a major effect on the specific charge-transfer transition energy of the system. Since the carbonyl group forms a part of the coumarin structure, the charge-transfer character of the coumarin system can be enhanced by optimizing the nature of the electron-donating group towards ionization potential.

---

Furthermore, from photophysical property studies of coumarin compounds conducted in the late 1950s by Wheelock, it was demonstrated that the addition of electron-donating group in the 4, 6, or 7 position or electron accepting group in the position 3 results in the fluorescence shift to longer wavelength.<sup>119</sup> Such properties of the coumarin motif have been the driving force in the exploitation of coumarins as powerful components in chromogenic and fluorogenic systems.

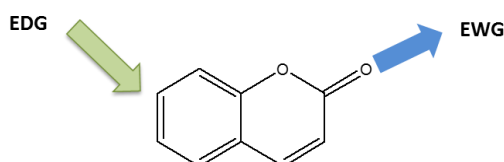


**Figure 2.26:** Coumarin “push-pull”  $\pi$ -electron system

## 2.6 References

1. T. W. Bell, and N. M. Hext, Artificial receptors for chemosensors, in: optical biosensors: present and future, F. S. Ligler, C. A. R. Taitt, Eds., **2002**, p 331.
2. a) T. W. Bell and N. M. Hext, *Chem. Soc. Rev.*, **2004**, 33, 589-598. b) J. Lippincott-Schwartz, *Annu. Rev. Biochem.*, **2011**, 80, 327-332. c) T. W. Bell, and N. M. Hext, *Artificial receptors for chemosensors, in: optical biosensors: present and future*, F. S. Ligler, C. A. R. Taitt, Eds., **2002**, p 331, Gulf Professional Publishing.
3. B. Valeur and I. Larrey, *Coord. Chem. Rev.*, **2000**, 205, 3-40.
4. a) L. Prodi, F. Bollta, M. Montalti and N. Zaccheroni, *Coord. Chem. Rev.*, **2000**, 205, 59-83. b) O. S. Wolfbeis, *Fibre Optic Chemical Sensors and Biosensors*; CRC Press: Boca Raton, **1991**, Vols. 1 and 2. c) G. Orellana and M. C. Moreno-Bondi, *Chapter 1: Organic Fluorescent Probes, in: Frontiers in Chemical Sensors: Novel Principles and Techniques*, Springer: New York, **2005**.
5. a) K. Kikuchi, *Chem. Soc. Rev.*, **2010**, 39, 2048–2053. b) C. Wang, C. Wu, J. Zhu, R. H. Miller and Y. Wang, *J. Med. Chem.*, **2011**, 54, 2331–2340. c) K. P. Carter, A. M. Young and A. E. Palmer, *Chem. Rev.*, **2014**, 114, 4564–4601.
6. J. Isaad, F. Malek and A. El Achari, *RSC Adv.*, **2013**, 3, 22168–22175.
7. B. Valeur, *Fluorescent molecular sensors of ions and molecules, in: Molecular fluorescence: principles and Applications*. Wiley-VCH Verlag GmbH, **2001**, p 273.

- 
8. A. Fernández-Gutierrez and A. M. de la Peña, Chapter 4: A. *Determination of inorganic substances by luminescence methods*, in: S.G. Schulman, Ed., *Molecular Luminescence Spectroscopy part 1*, Wiley, New York, **1985**, p. 371.
  9. A. P. de Silva, H. Q. N. Gunaratne, T. Gunnlaugsson, A. J. M. Huxley, C. P. McCoy, J. T. Rademacher and T. E. Rice, *Chem. Rev.*, **1997**, 97, 1515-1566.
  10. N. Saleh, Y. A. Al-Soud and W. M. Nau, *Spectrochim. Acta A*, **2008**, 71, 818-822.
  11. S. L. Wiskur, H. Aït-Haddou, J. J. Lavigne and E. V. Anslyn, *Acc. Chem. Res.*, **2001**, 34, 963-972.
  12. R. Martínez-Mañez, F. Sancenón, *Coord. Chem. Rev.*, **2006**, 250, 3081-3093.
  13. G.-J. Kim and H.-J. Kim, *Tetrahedron Lett.*, **2010**, 51, 185-187.
  14. a) T. Gunnlaugsson, H. D. P. Ali, M. Glynn, P. E. Kruger, G. M. Hussey, F. M. Pfeffer, C. M. D. Santos and J. Tierney, *J. Fluoresc.*, **2005**, 15, 287-299. b) Z. C. Xu, J. Yoon and D. R. Spring, *Chem. Soc. Rev.*, **2010**, 39, 1996-2006. c) J. S. Kim and D. T. Quang, *Chem. Rev.*, **2007**, 107, 3780-3799.
  15. a) Q. Zhao, F. Y. Li and C. H. Huang, *Chem. Soc. Rev.*, **2010**, 39, 3007-3030. b) W. Rettig and R. Lapouyade, *Fluorescence probes based on twisted intramolecular charge transfer (TICT) states and other adiabatic photoreactions*, in: J. R. Lakowicz, ed., *Fluorescence Spectroscopy, Probe Design and Chemical Sensing*, Plenum Press, New York, **1994**, vol. 4, p. 109.
  16. a) K. E. Sapsford, L. Berti and I. L. Medintz, *Angew. Chem. Int. Ed.*, **2006**, 45, 4562-4589. b) H. J. Carlson and R. E. Campbell, *Curr. Opin. Biotechnol.*, **2009**, 20, 19-27. c) J. Fan, M. Hu, P. Zhan and X. Peng, *Chem. Soc. Rev.*, **2013**, 42, 29-43.
  17. C. Lodeiro and F. Pina, *Coord. Chem. Rev.*, **2009**, 253, 1353-1383.
  18. a) Y. Hong, J. W. Y. Lam and B. Z. Tang, *Chem. Commun.*, **2009**, 4332-4353. b) M. Wang, G. X. Zhang, D. Q. Zhang, D. B. Zhu and B. Z. Tang, *J. Mater. Chem.*, **2010**, 20, 1858-1867.
  19. J. S. Wu, W. M. Liu, X. Q. Zhuang, F. Wang, P. F. Wang, S. L. Tao, X. H. Zhang, S. K. Wu and S. T. Lee, *Org. Lett.*, **2007**, 9, 33-36.
  20. a) J. Wu, W. Liu, J. Ge, H. Zhang and P. Wang, *Chem. Soc. Rev.*, **2011**, 40, 3483-3495. b) A. P. Demchenko, K.-C. Tang and P.-T. Chou, *Chem. Soc. Rev.*, **2013**, 42, 1379-1408.
  21. M. R. Wasielewski and J. M. Fenton, *Photosyn. Res.*, **1987**, 12, 181-189.
  22. a) Y. Lu, S. Huang, Y. Liu, S. He, L. Zhao and X. Zeng, *Org. Lett.*, **2011**, 13, 5274-5277. b) L. Zeng, E. W. Miller and C. J. Chang, *J. Am. Chem. Soc.*, **2006**, 128, 10-11.

- 
23. B. Wang, X. Liu, Y. Hu and Z. Su, *Polym. Int.*, **2009**, 58, 703-709.
  24. L. L. Fan, *J. Fluoresc.*, **2009**, 19, 555-559.
  25. P. Alaei, S. Rouhania, K. Gharanjig and J. Ghasemi, *Spectrochim. Acta A*, **2012**, 90, 85-92.
  26. J. F. Callan, A. P. de Silva and D. C. Margi, *Tetrahedron*, **2005**, 61, 8551-8588.
  27. H. Szmecinski and J.R. Lakowicz, *Sensor Actuat. B-Chem*, **1995**, 29, 16-24.
  28. H. -G. Löhr and F. Vögtle, *Acc. Chem. Res.*, **1985**, 18, 6-72.
  29. M. H. Lee, J. S. Kim and J. L. Sessler, *Chem. Soc. Rev.*, **2015**, 44, 4185-4191.
  30. a) R. Y. Tsien, *In optical methods in cell physiology*, P. de Weer and B. M. Salzberg, ed., Wiley, New York, **1986**, p. 327. b) M. Taki, M. Desaki, A. Ojida, S. Iyoshi, T. Hirayama, I. Hamachi and Y. Yamamoto, *J. Am. Chem. Soc.*, **2008**, 130, 12564-12565. c) M. H. Lee, H. M. Jeon, J. H. Han, N. Park, C. Kang, J. L. Sessler and J. S. Kim, *J. Am. Chem. Soc.*, **2014**, 136, 8430- 8437.
  31. Y. Pourghaz, P. Dongare, D. W. Thompson and Y. Zhao, *Chem. Commun.*, **2011**, 47, 11014–11016.
  32. a) Y. Feng, J. Cheng, L. Zhou, X. Zhou and H. Xiang, *Analyst*, **2012**, 137, 4885-4901. b) T. Forster, *Ann. Phys.* **1948**, 437, 55-75.
  33. a) M. A. Rizzo, G. H. Springer, B. Granada and D. W. Piston, *Nat. Biotechnol.*, **2004**, 22, 445-449. b) W. M. Shih, Z. Gryczynski, J. R. Lakowicz and J. A. Spudich, *Cell.*, **2000**, 102, 683-694.
  34. N. J. Turro, *Modern Molecular Photochemistry*, University Science Books, Sausalito, **1991**.
  35. J. R. Lakowicz, *Principles of Fluorescence Spectroscopy*, Kluwer Academic/Plenum Publishers, New York, USA, **1999**.
  36. L. Stryer and R. P Haugland, *Proc. Natl. Acad. Sci. U. S. A.*, **1967**, 58, 719–726.
  37. F. He, F. Feng, S. Wang, Y. Li and D. Zhu, *J. Mater. Chem.*, **2007**, 17, 3702-3707.
  38. D. L. Dexter, *J. Chem. Phys.*, **1953**, 21, 836-850.
  39. J. Fan, M. Hu, P. Zhan and X. Peng, *Chem. Soc. Rev.*, **2013**, 42, 29-83.
  40. Y. J. Gong, X. B. Zhang, C. C. Zhang, A. L. Luo, T. Fu, W. Tan, G. L. Shen and R. Q. Yu, *Anal. Chem.*, **2012**, 84, 10777–10784.



- 
41. B. Valeur, In *Molecular Luminescence Spectroscopy*, Part 3, Ed. S.G. Schulman, Wiley, New York, **1993**, p. 25.
  42. Y. O. Lee, J. Y. Lee, D. T. Quang, M.-H. Lee and J.-S. Kim, *Bull. Korean Chem. Soc.*, **2006**, 27, 1469.
  43. S. W. Thomas III, G. D. Joly and T. M. Swager, *Chem. Rev.*, **2007**, 107, 1339-1386.
  44. Y. N. Hong, J. W. Y. Lam and B. Z. Tang, *Chem. Commun.*, **2009**, 29, 4332-4353.
  45. a) A. Kraft, A. C. Grimsdale and A. B. Holmes, *Angew. Chem. Int. Ed.*, **1998**, 37, 402-428. b) S. Hecht and J. M. J. Frechet, *Angew. Chem. Int. Ed.*, **2001**, 40, 74-91. c) C. Fan, S. Wang, J. W. Hong, G. C. Bazan, K. W. Plaxco and A. J. Heeger, *Proc. Natl. Acad. Sci. U. S. A.*, **2003**, 100, 6297-6301.
  46. J. D. Luo, Z. L. Xie, J. W. Y. Lam, L. Cheng, H.-Y. Chen, C. F. Qiu, H. S. Kwok, X. W. Zhan, Y. Q. Liu, D. B. Zhu and B. Z. Tang, *Chem. Commun.*, **2001**, 18, 1740-1741.
  47. G. Yu, S. Yin, Y. Liu, J. Chen, X. Xu, X. Sun, D. Ma, X. Zhan, Q. Peng, Z. Shuai, B. Z. Tang, D. Zhu, W. Fang and Y. Luo, *J. Am. Chem. Soc.*, **2005**, 127, 6335-6346.
  48. Y. Dong, J. W. Y. Lam, A. Qin, J. Liu, Z. Li, B. Z. Tang, J. Sun and H. S. Kwok, *Appl. Phys. Lett.*, **2007**, 91, 011111.
  49. L. Liu, G. X. Zhang, J. F. Xiang, D. Q. Zhang and D. B. Zhu, *Org. Lett.*, **2008**, 10, 4581-4584.
  50. L. Peng, M. Wang, G. Zhang, D. Zhang and D. Zhu, *Org. Lett.*, **2009**, 11, 1943-1946.
  51. H. Tong, Y. N. Hong, Y. Q. Dong, M. Haussler, J. W. Y. Lam, Z. Li, Z. F. Guo, Z. H. Guo and B. Z. Tang, *Chem. Commun.*, **2006**, 3705-3707.
  52. J. S. Wu, W. M. Liu, X. Q. Zhuang, F. Wang, P. F. Wang, S. L. Tao, X. H. Zhang, S. K. Wu and S. T. Lee, *Org. Lett.*, **2007**, 9, 33-36.
  53. a) Z. M. Li and S. K. Wu, *J. Fluoresc.*, **1997**, 7, 237-242. b) P. F. Wang and S. K. Wu, *J. Photochem. Photobiol., A*, **1995**, 86, 109-113.
  54. X. Cheng, H. Jia, T. Long, J. Feng, J. Qin and Z. Li, *Chem. Commun.*, **2011**, 47, 11978-11980.
  55. M. Suresh, A. K. Mandal, S. Ssha, E. Suresh, A. Mandoli, R. D. Liddo, P. P. Parnigotto and A. Das, *Org. Lett.*, **2011**, 12, 5406.
  56. Y-Q. Sun, P. Wang, J. Liu, J. Zhang and W. Guo, *Analyst*, **2012**, 137, 3430-3433.
  57. J. Wu, R. Sheng, W. Liu, P. Wang, H. Zhang and J. Ma, *Tetrahedron*, **2012**, 68, 5458-5463.
  58. J. Zhao, S. Ji, Y. Chen, H. Guo and P. Yang, *Phys. Chem. Chem. Phys.*, **2012**, 14, 8803-8817.

- 
59. a) M. J. Paterson, M. A. Robb, L. Blancafort, A. D. DeBellis, *J. Phys. Chem. A*, **2005**, 109, 7527–7537. b) H. Yao and T. Funada, *Chem. Commun.*, **2014**, 50, 2748–2750. c) K. C. Tang, M. J. Chang, T. Y. Lin, H. A. Pan, T. C. Fang, K. Y. Chen, W. Y. Hung, Y. H. Hsu and P. T. Chou, *J. Am. Chem. Soc.*, **2011**, 133, 17738–17745.
60. M. M. Henary and C. J. Fahrni, *J. Phys. Chem. A*, **2002**, 106, 5210–5220.
61. a) J. Seo, S. Kim and S. Y. Park, *J. Am. Chem. Soc.*, **2004**, 126, 11154–11155. b) O. K. Abou-Zied, R. Jimenez, E. H. Z. Thompson, D. P. Millar and F. E. Romesberg, *J. Phys. Chem. A*, **2002**, 106, 3665–3672. c) K. Das, N. Sarkar, A. K. Ghosh, D. Majumdar, D. N. Nath and K. Bhattacharyya, *J. Phys. Chem.*, **1994**, 98, 9126–9132.
62. a) J.-Y. Li, X.-Q. Zhou, Y. Zhou, Y. Fang and C. Yao, *Spectrochim. Acta A*, **2013**, 102, 66–70. b) Y. Wu, X. Peng, J. Fan, S. Gao, M. Tian, J. Zhao, and S. Sun, *J. Org. Chem.*, **2007**, 72, 62–70.
63. Q. Chu, D. A. Medvetz and Y. Pang, *Chem. Mater.*, **2007**, 19, 6421–6429.
64. I. Yoshimura, Y. Miyahara, N. Kasagi, H. Yamane, A. Ojida and I. Hamachi, *J. Am. Chem. Soc.*, **2004**, 126, 12204–12205.
65. a) E. Brasola, F. Mancin, E. Rampazzo, P. Tecilla and U. Tonellato, *Chem. Commun.*, **2003**, 3026–3027. b) J. T. Suri, D. B. Cordes, F. E. Cappuccio, R. A. Wessling and B. Singaram, *Angew. Chem. Int. Ed.*, **2003**, 42, 5857–5859.
66. O. S. Wolfbeis, N. V. Rodriguez and T. Werner, *Mikrochim. Acta*, **1992**, 108, 133–141.
67. a) M. Malanga, M. Bálint, I. Puskás, K. Tuza, T. Sohajda, L. Jicsinszky, L. Szente and É. Fenyves, *Beilstein J. Org. Chem.*, **2014**, 10, 3007–3018. b) R. Nishiyabu, S. Ushikubo, Y. Kamiya and Y. Kubo, *J. Mater. Chem. A*, **2014**, 2, 15846–15852.
68. K. Kempe, A. Krieg, C. R. Becer and U. S. Schubert, *Chem. Soc. Rev.*, **2012**, 41, 176–191.
69. Y. Shiraishi, S. Sumiya, K. Manabe, and T. Hirai, *ACS Appl. Mater. Interfaces*, **2011**, 3, 4649–4656.
70. J. Luo, S. Jiang, S. Qin, H. Wu, Y. Wang, J. Jiang and X. Liu, *Sensor Actuat. B-Chem.*, **2011**, 160, 1191–1197.
71. a) M. Crego-Calama and D. N. Reinhoudt, *Adv. Mater.*, **2001**, 13, 1171–1174. b) B. Leng, L. Zou, J. Jiang and H. Tian, *Sensor Actuat. B-chem*, **2009**, 140, 162–169.
72. H. J. Kim, S. J. Lee, S.-Y. Park, J. H. Jung and J. S. Kim, *Adv. Mater.*, **2008**, 20, 3229–3234.
73. K. A. Gattas-Asfura and R. M. Leblanc, *Chem. Commun.*, **2003**, 2684–2685.
74. T. Swager, *Acc. Chem. Res.*, **1998**, 31, 201–207.
75. J. H. Alan, *Angew. Chem., Int. Ed.*, **2001**, 40, 2591–2611.

- 
76. C. D. Dimitrakopoulos and P. R. L. Malenfant, *Adv. Mater.*, **2002**, 14, 99-117.
77. S. A. McDonald, G. Konstantatos, S. G. Zhang, P. W. Cyr, E. J. D. Klem, L. Levina and E. H. Sargent, *Nat. Mater.*, **2005**, 4, 138-142.
78. R. Gangopadhyay and A. De, *Chem. Mater.*, **2000**, 12, 608-622.
79. E. W. H. Jager, O. Inganäs and I. Lundström, *Adv. Mater.*, **2001**, 13, 76-79.
80. S.W. Thomas, G.D. Joly and T.M. Swager, *Chem. Rev.*, **2007**, 107 1339-1386.
81. a) G. Xiang, W. Cui, S. Lin, L. Wang, H. Meier, L. Li and D. Cao, *Sens. Actuators B*, **2013**, 186, 741–749. b) W. Cui, L. Wang, G. Xiang, L. Zhou, X. An and D. Cao, *Sens. Actuators B*, **2015**, 207, 281–290. c) X. Wu, B. Xu, H. Tong and L. Wang, *Macromolecules*, **2011**, 44, 4241–4248. d) R. Sakai, *Polym. J.*, **2016**, 48, 59–65.
82. a) T. H. Kim, H. J. Kim, C. G. Kwak, W. H. Park and T. S. Lee, *J. Polym. Sci. Part A: Polym. Chem.*, **2006**, 44, 2059–2068. b) J. C. Sanchez, A. G. DiPasquale, A. L. Rheingold and W. C. Trogler, *Chem. Mater.*, **2007**, 19, 6459–6470.
83. a) P. K. Lo and H. F. Sleiman, *Macromolecules*, **2008**, 41, 5590–5603. b) B. Liu and G. C. Bazan, *J. Am. Chem. Soc.*, **2006**, 128, 1188–1196.
84. D. T. Mcquade, A. E. Pullen and T. M. Swager, *Chem. Rev.*, **2000**, 100, 2537–2574.
85. A. Balamurugan, M. L. P. Reddy and M. Jayakannan, *J. Polym. Sci. Part A: Polym. Chem.*, **2009**, 47, 5144–5157.
86. H. A. Ho and M. Leclerc, *J. Am. Chem. Soc.*, **2003**, 125, 4412–4413.
87. C. Xue, F. Cai and H. Liu, *Chem. Eur. J.*, **2008**, 14, 1648–1653.
88. S. Clavaguera, O. J. Dautel, L. Hairault, C. Méthivier, P. Montméat, E. Pasquinet, C. M. Pradier, F. Serein-Spirau, S. Wakim, F. Veignal, J. J. E. Moreau and J. P. Lère-Porte, *J. Polym. Sci. Part A: Polym. Chem.*, **2009**, 47, 4141–4149.
89. F. H. Dickey, *Proc. Natl. Acad. Sci. U. S. A.*, **1949**, 35, 227–229.
90. P. Turkewitsch, B. Wandelt, G. D. Darling and W. S. Powell, *Anal. Chem.*, **1998**, 70, 2025–2030.
91. a) Y. Liao, W. Wang and B. H. Wang, *Bioorg. Chem.*, **1999**, 27, 463–476. b) A. J. Tong, H. Dong and L. D. Li, *Anal. Chim. Acta*, **2002**, 466, 31–37.
92. W. Wang, S. H. Gao and B. H. Wang, *Org. Lett.*, **1999**, 1, 1209–1212.
93. a) T. H. Nguyen and R. J. Ansell, *Org. Biomol. Chem.*, **2009**, 7, 1211–1220. b) O Güney and F.C. Cebeci, *J. Appl. Polym. Sci.*, **2010**, 117, 2373-2379.
94. S. M. Ng and R. Narayanaswamy, *Anal. Bioanal. Chem.*, **2006**, 386, 1235-1244.
95. Y. Lee, J. Kim, S. Kim, W. Jang, S. Parka and W. Koh, *J. Mater. Chem.*, **2009**, 19, 5643-5647.

- 
96. a) J. S. Kim, S. Y. Lee, J. Yoon and J. Vicens, *Chem. Commun.*, **2009**, 4791-4802. b) J. Kawakami, T. Mizuguchi and S. Ito, *Anal. Sci.*, **2006**, 22, 1383-1384.
97. L. Pu, *J. Photochem. Photobiol. A*, **2003**, 155, 47-55.
98. Y. H. Lau, P. J. Rutledge, M. Watkinson and M. H. Todd, *Chem. Soc. Rev.*, **2011**, 40, 2848-2866.
99. a) V. V. Rostovtsev, L. G. Green, V. V. Fokin and K. B. Sharpless, *Angew. Chem. Int. Ed.*, **2002**, 41, 2596-2599. b) M. Meldal and C.W. Torne, *Chem. Rev.*, **2008**, 108, 2952-3015.
100. a) Y. Hua and A. H. Flood, *Chem. Soc. Rev.*, **2010**, 39, 1262-1271. b) H. F. Chow, K. N. Lau, Z. Ke, Y. Liang and C. M. Lo, *Chem. Commun.*, **2010**, 46, 3437-3453.
101. a) A. C. Fahrenbach and J. F. Stoddart, *Chem. Asian J.*, **2011**, 6, 2660-2669. b) H. Struthers, T. L. Mindt and R. Schibli, *Dalton Trans.*, **2010**, 39, 675-696.
102. a) Z. Chen, D. R. Dreyer, Z. Q. Wu, K. M. Wiggins, Z. Jiang and C. W. Bielawski, *J. Polym. Sci. Part A: Polym. Chem.*, **2011**, 49, 1421-1426. b) X. M. Liu, L. D. Quan, J. Tian, F. C. Laquer, P. Ciborowski and D. Wang, *Biomacromolecules*, **2010**, 11, 2621-2628. c) Y. Wang, R. Zhang, N. Xu, F. S. Du, Y. L. Wang, Y. X. Tan, S. P. Ji, D. H. Liang and Z. C. Li, *Biomacromolecules*, **2011**, 12, 66-74. d) J. Guo, Y. Wei, D. Zhou, P. Cai, X. Jing, X. S. Chen and Y. Huang, *Biomacromolecules*, **2011**, 12, 737-746. e) A. M. Eissa and E. Khosravi, *Eur. Polym. J.*, **2011**, 47, 61-69.
103. X. Huang, J. Meng, Y. Dong, Y. Cheng and C. Zhu, *Polymer*, **2010**, 51, 3064-3067.
104. J. Zhu, W. Lu, F. Hu, M. Zhang, L. Jiang and Z. Shen, *J. Polym. Sci. Part A: Polym. Chem.*, **2014**, 52, 2248-2257.
105. A. J. Qin, J. W. Y. Lam and B. Z. Tang, *Chem. Soc. Rev.*, **2010**, 39, 2522-2544.
106. V. Haridas, S. Sahu and P. P. Praveen Kumar, *Tetrahedron Lett.*, **2011**, 52, 6930-6934.
107. M. C. González, F. Otón, A. Espinosa, A. Tárraga and P. Molina, *Org. Biomol. Chem.*, **2015**, 13, 1429-1438.
108. A. Qin, J. W. Y. Lam, L. Tang, C. K. W. Jim, H. Zhao, J. Sun, and B. Z. Tang, *Macromolecules*, **2009**, 42, 1421-1424.
109. a) R. M. Christie and C. H. Lui, *Dyes and Pigments*, **2000**, 47, 79-89. b) Moylan and R. Christopher, *J. Phys. Chem.*, **1994**, 98, 13513-13516. c) A. Fischer, C. S. Cremer, and E. H. K. Stelzer, *Appl. Optics*, **1995**, 34, 1989-2003.
110. D. J. Yee, V. Balsanek and D. Sames, *J. Am. Chem. Soc.*, **2004**, 126, 2282-2283.
111. R. D. H. Murray, J. Mendez and S. A. Brown, *The Natural Coumarins: Occurrence, Chemistry and Biochemistry*, John Wiley & Sons, New York, **1982**.

- 
112. G. Jones, W. R. Jackson, C. Y. Choi and W. R. Bergmark, *J. Phys. Chem.*, **1985**, 89, 294-300.
  113. G. Jones, *Org. React.*, **1967**, 15, 204-699.
  114. J. R. Jonson, *Org. React.*, **1942**, 1, 210-266.
  115. H. Pechmann and C. Duisberg, *Chem. Ber.*, **1884**, 17, 229-236.
  116. R. L. Shriner, *Org. React.*, **1942**, 1, 1-37.
  117. I. Yavari, R. Hekmat-Shoar and A. Zonouzi, *Tetrahedron Lett.*, **1998**, 39, 2391-2392.
  118. J. S. de Melo and P. F. J. Fernandes, *Mol. Struct.*, **2001**, 565, 69-78.
  119. C. J. Wheelock, *J. Am. Chem. Soc.*, **1959**, 81, 1348-1352.

---

## Chapter 3     Polymers with conjugated triazolyl coumarin units as pendant group

### 3.1 Introduction

As fluorescence remains one of the most powerful transduction processes to signal a chemical recognition event, numerous fluorescent compounds with different receptor units are currently being investigated for their sensing capabilities. These include fluorescent compounds with the coumarin units adjacent to the 1,2,3-triazole ring (conjugated triazolyl coumarin) which showed applications in different fields such as fluorescent imaging and ions chemosensing.<sup>1,2</sup> Due to the simplicity of the Cu(I)-catalyzed alkyne-azide 1,3-dipolar cycloaddition reaction (CuAAC) (click reaction), which is mainly used in the synthesis of these compounds, their applications have been extended to DNA labelling where the coumarin-triazole system acts as a fluorescent dye.<sup>3</sup> Generally, the synthesis of these compounds involves a non-fluorescent azide substituted coumarin system which becomes strongly fluorescent after reacting with an alkyne containing substrate *via* the CuAAC reaction.<sup>4</sup> The fluorescent changes accompanying triazole ring formation are the basis for bioimaging applications in this reaction as a fluorescent signal is triggered once the coumarin-triazole unit is formed.

Since the nature of substituents at positions 3 and 7 are well known to alter the fluorescence properties of the coumarin motif, a number of substituted coumarins with a triazole ring in position 3 were synthesized and investigated for their chemosensing capabilities. For instance, a water-soluble coumarin-based fluorescent probe **1** for hydrogen peroxide in water was developed by Wang and co-workers (**Figure 3.1**).<sup>5</sup> The probe incorporates a 1,2,3-triazole ring in position 3 and a pinacol-protected borane in position 7 of the coumarin backbone. The addition of H<sub>2</sub>O<sub>2</sub> induces the oxidation of boronate resulting in the enhancement of the triazolyl coumarin's system fluorescence. This effect was less noticeable in the presence of other oxygen reactive species such as O<sup>2-</sup>, OH<sup>-</sup> and <sup>-</sup>OCl.

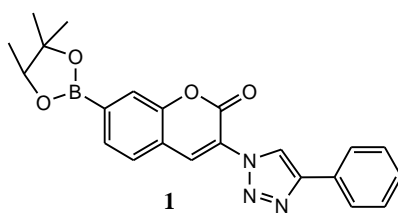


**Figure 3.1:** 1,2,3-Triazole-coumarin based fluorescent probe for hydrogen peroxide detection.

The conjugated triazolyl coumarin system has been also coupled with other chemical structures such as sugars in order to exploit the triazole ring and has found applications in the chemosensing field. Examples include coumarin glycoligands **2**, **3** and **4**, that act as selective turn-on and turn-off probes for  $\text{Ag}^+$  ions in both aqueous and buffer media.<sup>6</sup> These types of chemosensors involve two 7-hydroxycoumarins connected to the glucoside moiety by means of 1,2,3-triazole rings which also play a role as receptors for  $\text{Ag}^+$  ions. By varying the positions of the triazolyl coumarin system around the glucosyl nucleus three triazolyl coumarin-substituted glycoligands were obtained as shown in the **Figure 3.2**. Though all three exhibited a selective response towards  $\text{Ag}^+$ , their fluorescence responses were reversed depending on the position of the triazolyl coumarin system. The addition of  $\text{Ag}^+$  ions quenched the fluorescence of glycoligand **2** whereas the fluorescence of glycoligands **3** and **4** were greatly enhanced by the presence of  $\text{Ag}^+$  ions. From fluorescence and NMR titrimetric studies, it was concluded that the divergence was caused by the distinct coordination modes of conformationally constrained glycoligands with  $\text{Ag}^+$  ions.

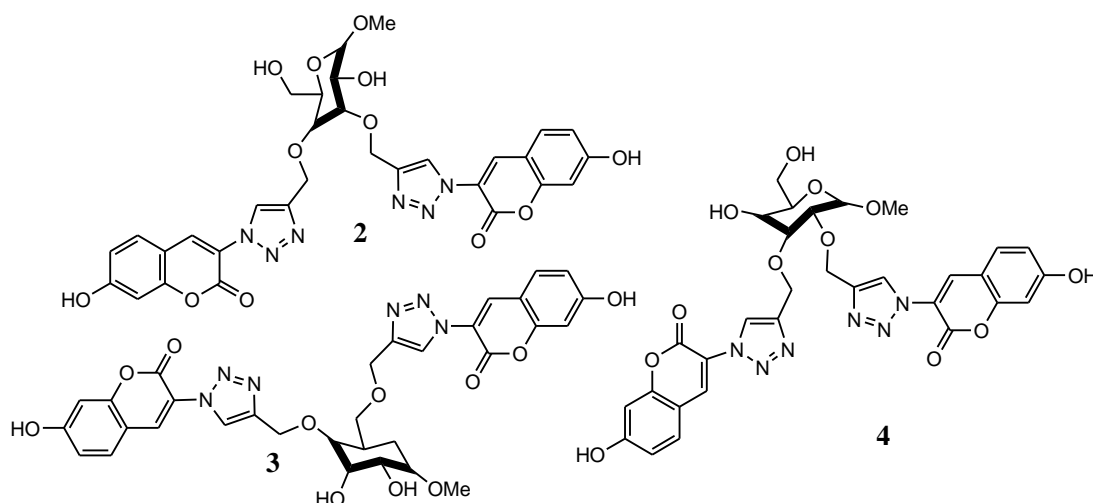
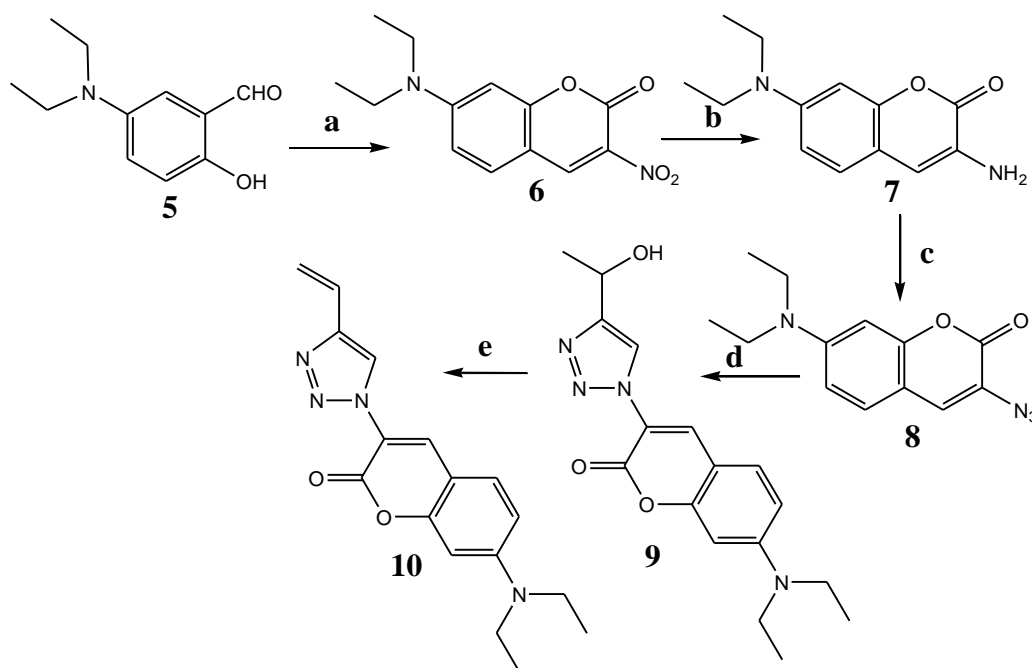


**Figure 3.2:** Triazolyl coumarin substituted glycoligands for selective recognition of  $\text{Ag}^+$  ions in aqueous solution.

Although almost all chemosensors involving the triazolyl coumarin system are small molecules, specific functionalization of the coumarin motif can allow incorporation of the triazolyl coumarin system into polymeric materials. Here, we describe the incorporation of conjugated triazolyl coumarin units as a pendant group for polymeric materials and we investigate the chemosensing capabilities of the resulting polymers.

## 3.2 Monomer synthesis

In order to incorporate a conjugated triazolyl coumarin unit into a polymer chain, monomers containing both the triazolyl coumarin unit and the functionality which allows polymerization of the monomers had to be synthesized. Coumarin-based vinyl monomers **10** with a 1,2,3-triazole ring at position 3 were designed and synthesized. For a better understanding on how the 1,2,3-triazole ring interacts with various ions, a coumarin-based monomer **16** with a free 1,2,3-triazole ring (away from other binding sites) at position **7** was also synthesized. Both monomers **10** and **16** were prepared *via* a multiple step synthesis. Vinyl monomer **10** was prepared from 4-(diethylamino)-2-hydroxybenzaldehyde as shown in **Scheme 3.1**.

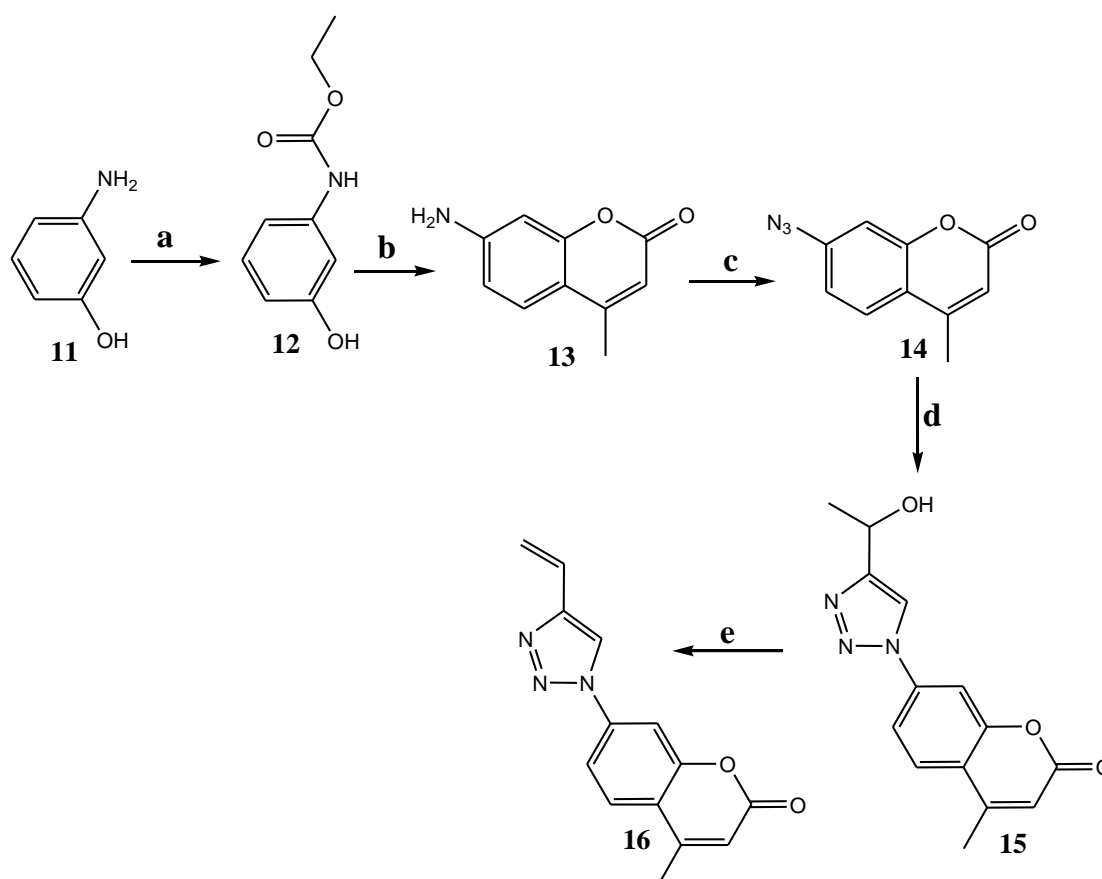


**Scheme 3.1:** Synthesis of vinyl monomer **10**; **a**) Ethyl 2-nitroacetate, AcOH, piperidine, Butanol, reflux; **b**) SnCl<sub>2</sub>, HCl<sub>aq</sub>, rt; **c**) NaNO<sub>2</sub>, KOAc, NaN<sub>3</sub>, HCl<sub>aq</sub>; **d**) 3-Butyn-2-ol, CuSO<sub>4</sub>·5H<sub>2</sub>O, PMDETA, NaAsc, THF, rt; **e**) PTSA, Toluene, 110°C.



The monomer precursor **9** was synthesized according to literature procedures.<sup>7</sup> The click reaction of the azide-functionalized coumarin derivative **8** with 3-butyn-2-ol was done in THF as solvent. The reaction was carried out in the presence of a catalytic amount of  $\text{CuSO}_4 \cdot 5\text{H}_2\text{O}$ , sodium ascorbate to reduce  $\text{Cu(II)}$  to  $\text{Cu(I)}$  and  $N,N,N',N'',N'''$ -pentamethyldiethylenetriamine (PMDTA) ligand for stabilizing the *in situ*-generated catalyst  $\text{Cu(I)}$ .<sup>4b</sup> Monomer precursor **9** was subjected to dehydration reaction in toluene using *p*-toluenesulfonic acid (PTSA) as the dehydrating agent to yield desired vinyl monomers in good yield.

The second vinyl monomer **16** was prepared from 3-aminophenol as shown in **Scheme 3.2**. The synthesis of 7-azido-4-methylcoumarin **14** was achieved in a good yield under acidic conditions through diazotization-azidation of 7-amino-4-methylcoumarin which was synthesized according to the reported procedure.<sup>8</sup> Monomer precursor **15** and vinyl monomer **16** were synthesized following the same procedures used for **9** and **10**.



**Scheme 3.2:** Synthesis of vinyl monomer **16** a)  $\text{C}_2\text{H}_5\text{OCOC}_2\text{H}_5$ ,  $\text{Et}_2\text{O}$ , rt b)  $\text{CH}_3\text{COCH}_2\text{COOC}_2\text{H}_5$ ,  $\text{H}_2\text{SO}_4:\text{C}_2\text{H}_5\text{OH}$  (7:3), rt c)  $\text{HCl}_{\text{aq}}$ ,  $\text{NaNO}_2$ ,  $\text{NaN}_3$  d) 3-Butyn-2-ol,  $\text{CuSO}_4 \cdot 5\text{H}_2\text{O}$ , NaAsc, PMDTA, THF, rt e) PTSA, Toluene,  $110^\circ\text{C}$ .

The structures of the two vinyl monomers **10** and **16** were confirmed by NMR and mass spectroscopy. The  $^1\text{H}$  NMR spectra of both monomers showed splitting patterns characteristic for vinyl functionality between 5.2 and 6.1 ppm along with the coumarin-triazole unit as shown in **Figures 3.3** and **3.4**. (For the  $^{13}\text{C}$  NMR spectra of monomers **10** and **16** and  $^1\text{H}$  NMR spectra of coumarins **6**, **7**, **8**, **13**, **14** and **15** see appendices **Figure A.1-A.9**)

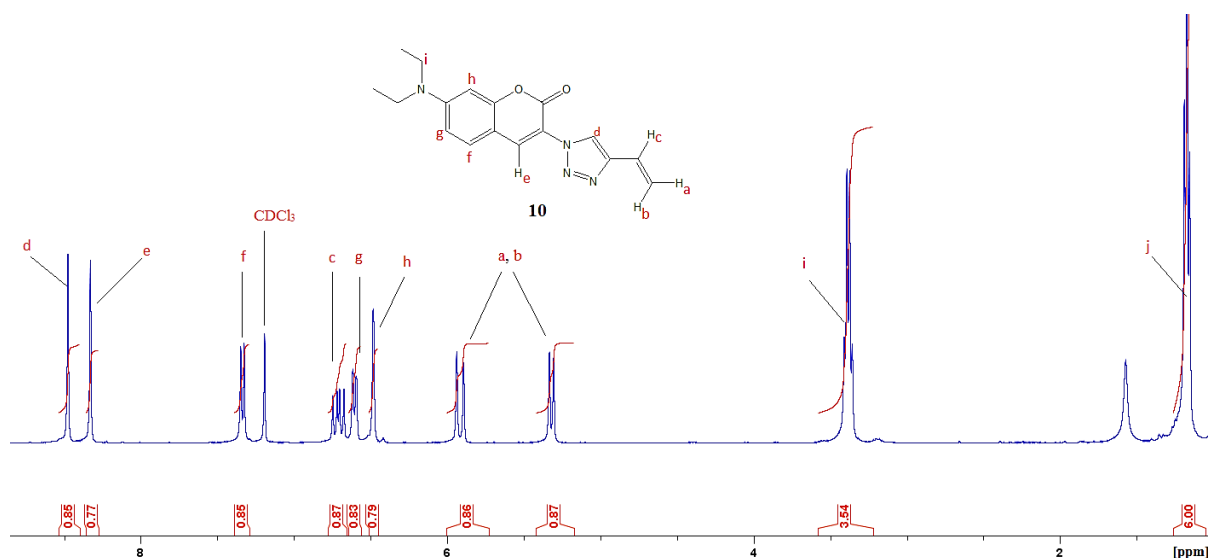


**Figure 3.3:**  $^1\text{H}$  NMR of the monomer **10** in  $\text{CDCl}_3$ .

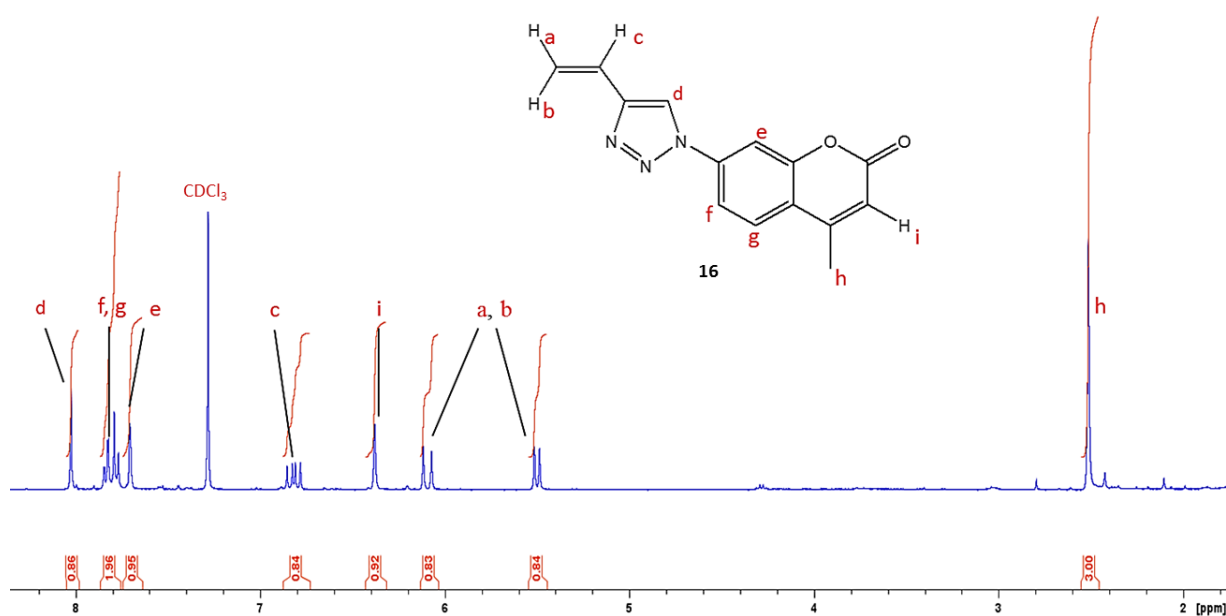
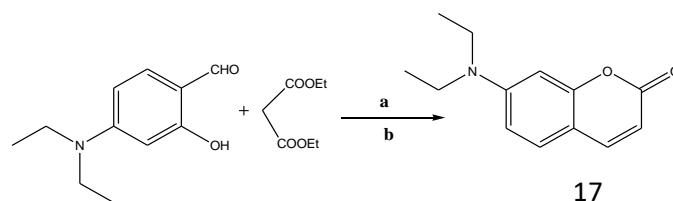


**Figure 3.4:**  $^1\text{H}$  NMR of the monomer **16** in  $\text{CDCl}_3$ .

### 3.2.1 Absorption and fluorescence properties of the monomers

In order to understand the impact of the triazole ring on the absorption and emission properties of the coumarin system in monomers **10** and **16**, 7-diethylaminocoumarin **17** without the triazole ring was synthesized. Compound **17** was synthesized according to a reported procedure from 4-(diethylamino)-2-hydroxybenzaldehyde as shown in **Scheme 3.3**.<sup>9</sup> The structure of the 7-diethylaminocoumarin **17** was confirmed by <sup>1</sup>H NMR spectroscopy (**Appendix Figure A.10**) and its absorption and emission properties were compared with that of monomers **10** and **16**.



**Scheme 3.3:** Synthesis of the 7-diethylaminocoumarin; a) Piperidine and ethanol, b) HCl and AcOH.

**Figure 3.5** shows the absorption and emission spectra of monomers **10** and **16**, and the 7-diethylaminocoumarin **17** in DMF. Notable from the absorption and emission properties of these compounds is the impact of the triazole ring on the coumarin-conjugated systems and its involvement in the photoinduced electron transfer mechanism (PET) which leads to fluorescence quenching. Monomer **10** and 7-diethylaminocoumarin **17** have similar coumarin systems. However, when a triazole ring was incorporated at position 3 in the coumarin system of monomer **10**, a bathochromic shift in both absorption and emission spectra was observed. This suggests that the incorporation of the triazole ring into the conjugated system extends the conjugation. The shift was also accompanied by an increase in the absorption intensity in monomer **10** compared to 7-diethylaminocoumarin **17**. Contrary to the increase in absorption intensity in monomer **10** after the addition of the triazole ring, its emission intensity decreased compared to that of 7-diethylaminocoumarin **17**. This suggests that the triazole ring is involved in the PET mechanism by transferring the lone pair of electrons from the nitrogen to the excited coumarin fluorophore.<sup>10</sup> This transfer leads to the decrease in the emission intensity since the usual relaxation process which results in fluorescence emission is disrupted.

In the case of monomer **16** where the triazole ring is placed at position 7 of the coumarin system, a bathochromic shift and a decrease in intensity in both the absorption and emission spectra were observed compared to 7-diethylaminocoumarin **17**. Due to the electron deficiency

of the triazole ring and the lone pair of electrons on the nitrogen which can participate in the PET process, the incorporation of a triazole ring in position 7 of coumarin system has a negative impact on the conjugation of the coumarin system as well as on the relaxation process of the coumarin fluorophore. This effect leads to a blue shift and a decrease in intensity in both absorption and emission spectra of monomer **16** compared to 7-diethylamionocoumarin **17** which has an electron donating diethylamiono group at position 7 of the coumarin system. These observations are in agreement with Wheelock's findings in the 1950s.<sup>11</sup>

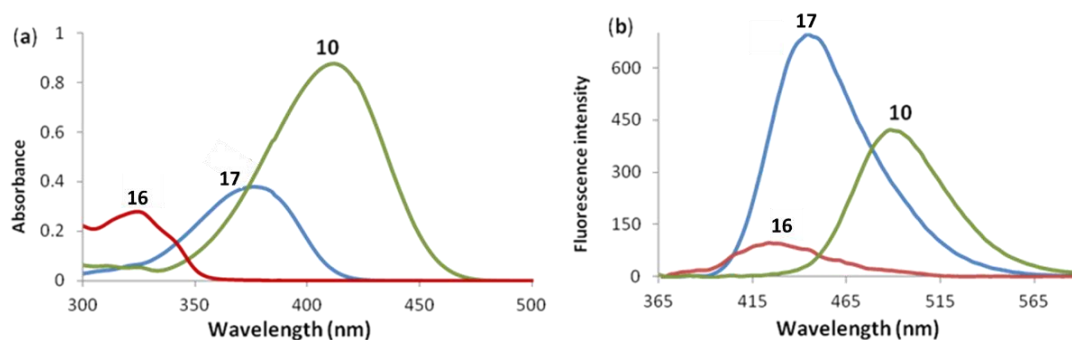
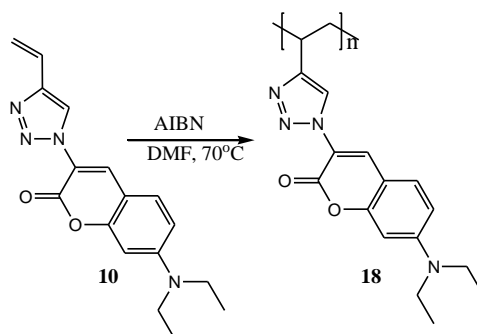


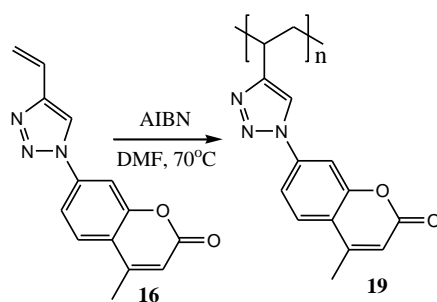
**Figure 3.5:** a) Absorption and b) Emission spectra of monomers **10** and **16**, and 7-diethylamionocoumarin **17**. The experiments were performed in DMF at 350 nm with a concentration of  $1.7 \times 10^{-5}$  M for absorption and  $10^{-7}$  M for emission analysis.

### 3.3 Polymer synthesis

Polymerization of the vinyl monomers **10** and **16** was accomplished *via* radical polymerization in which a degassed system was required to avoid interference of oxygen with the free radical species (**Scheme 3.4** and **3.5**).<sup>12</sup> Azobisisobutyronitrile (AIBN) was used as an initiator, and polymerization process was completed in 48 hrs in DMF at 70°C. The reaction mixtures were diluted with ethanol, and polymers were precipitated by dropwise addition of a minimum amount of water.



**Scheme 3.4:** Free radical polymerization of monomer **10** and **16**.



**Scheme 3.5:** RAFT polymerization of monomer **10** and **16**.

The structures of polymers **18** and **19** were confirmed by  $^1\text{H}$  NMR and FT-IR spectroscopy. **Figures 3.6** and **3.7** illustrate the assignment of proton signals in the  $^1\text{H}$  NMR spectra of polymers **18** and **19** respectively. Notable in both spectra is the disappearance of the proton signal between 5.2 and 6.1 ppm in the monomer (characteristic for the vinyl functional group) and the appearance of proton signals in the alkyl resonance range. These observations confirm the conversion of the terminal alkene functionality in monomers **10** and **16** to alkyl chains during polymerization. Due to the low solubility of polymer **19**, the average molecular weight and polydispersity index could not be determined from size exclusion chromatography experiments. On the other hand, average molecular weight and polydispersity index of polymer **18**, were determined to be  $2.17 \times 10^3$  and 1.92 respectively.

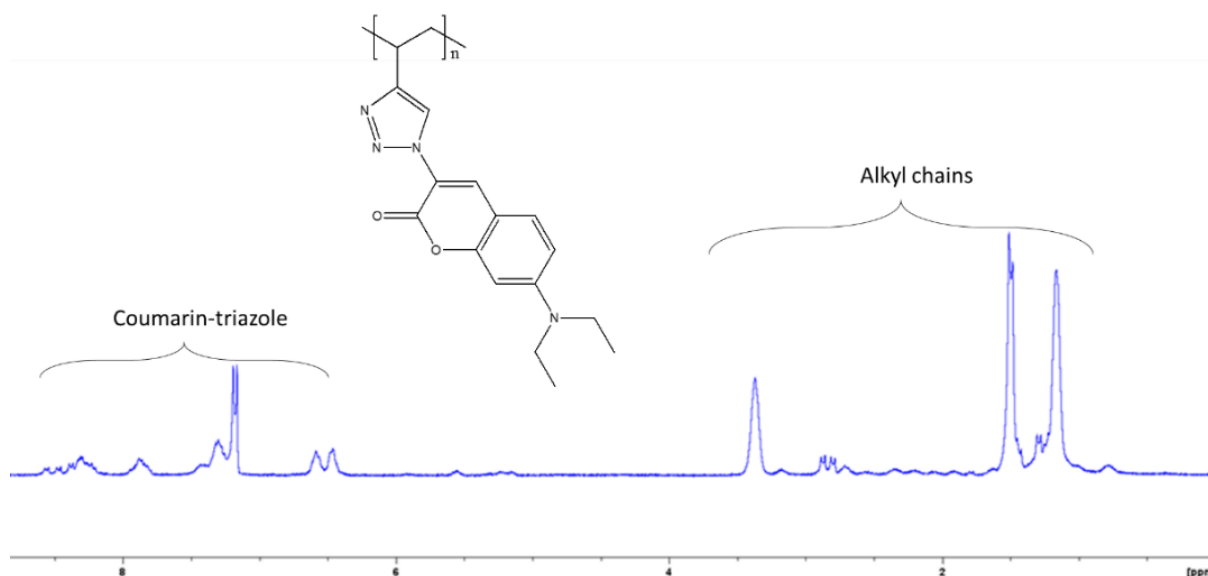


**Figure 3.6:**  $^1\text{H}$  NMR spectrum for polymer **18** in  $\text{CDCl}_3$ .

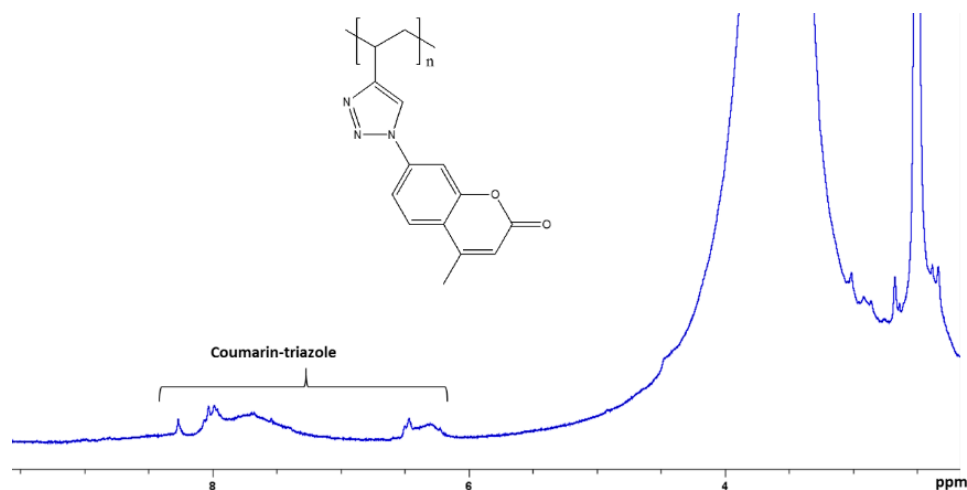


**Figure 3.7:**  $^1\text{H}$  NMR spectrum for polymer **19** in  $\text{DMSO-d}_6$ .

The structures of polymers **18** and **19** were further confirmed using FT-IR spectroscopy. **Figure 3.8** shows the comparative FT-IR spectra of the monomer **10** and **16** and their polymers. Notable in the spectra of the polymers is the disappearance of the terminal alkene stretchings at  $3145\text{ cm}^{-1}$  and  $3148\text{ cm}^{-1}$  in polymers **18** (**Figure 3.8 a**) and **19** (**Figure 3.8 b**) respectively. This confirms once again a successful conversion of terminal alkene groups in the monomers into alkyl chains in the polymers.

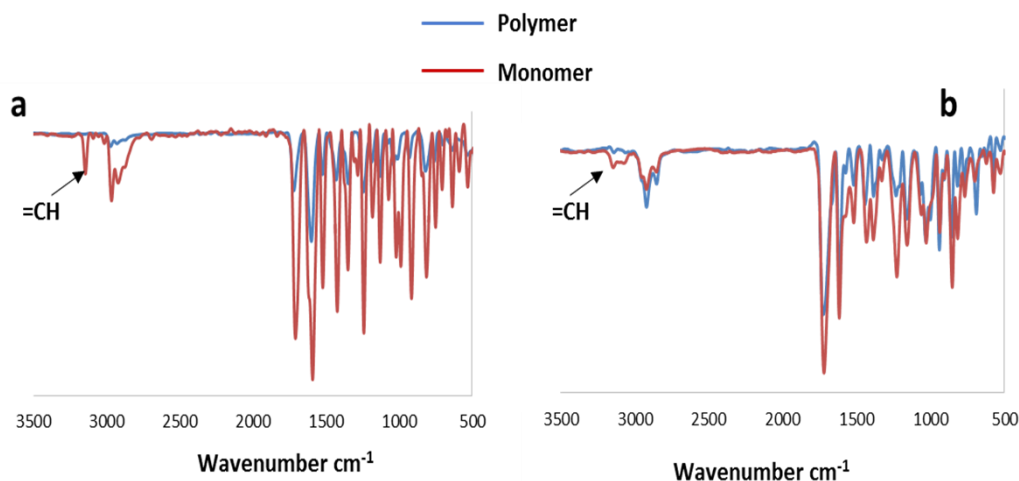


**Figure 3.8:** Comparative FT-IR spectra of **a**) Monomer **10** and polymer **18** and **b**) Monomer **16** and polymer **19**.

### 3.4 Absorption and fluorescence properties of the polymers

The effect of polymerization on the photophysical properties of the monomers was investigated. This was achieved by comparing the absorption and emission properties of DMF

solutions containing specific quantities of the monomers, and DMF solutions containing the respective polymer **18** or **19** with an equivalent number of repeating monomer units. In both cases (**Figure 3.9**), the polymers and their respective monomers showed the same absorption and emission behaviour. However, the polymers absorbed and emitted more than their respective monomer units. This could be attributed to the cooperative effect of chromophores from the pendant chains.<sup>13</sup> Furthermore, the removal of the alkene functionality during polymerization increases the electron-withdrawing effect of the triazole ring which can decrease the ability of the triazole nitrogen to quench the fluorescence of the coumarin *via* the PET mechanism. When polymer **18** was compared to its monomer **10**, up to an 8 fold increase in absorption and a 7 fold increase in emission were observed (**Figure 3.9 a and b**). In polymer **19** compared to its monomer **16**, a 22 fold increase in absorption and a 5 fold increase in emission were observed (**Figure 3.9 c and d**).

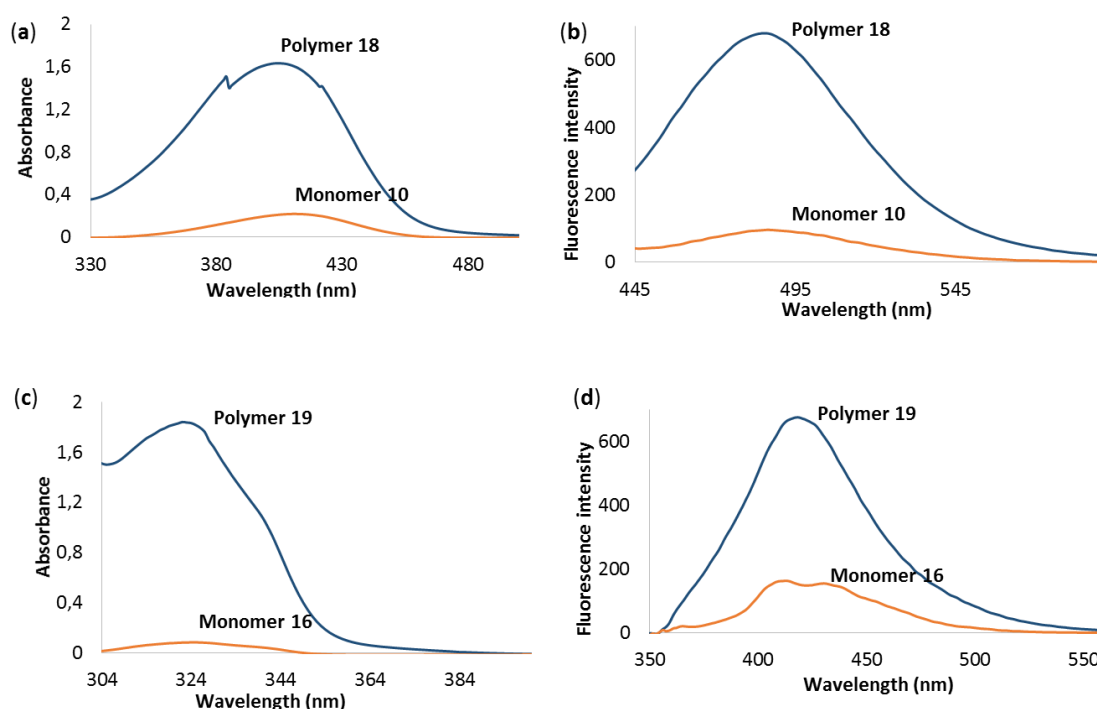


**Figure 3.9:** a) Absorption and b) Emission spectra of monomer **10** and polymer **18** (Repeating units concentration:  $3 \times 10^{-6}$  M for absorption and  $3 \times 10^{-9}$  M for emission); and c) Absorption and d) Emission spectra of monomer **16** and polymer **19** (Repeating units concentration:  $6 \times 10^{-6}$  M for absorption and  $9.5 \times 10^{-7}$  M for emission. Emission was performed at 350 nm.

In order to establish the chemosensing capabilities of polymers **18** and **19**, differences in the photophysical properties of the two polymers were investigated. **Figure 3.10** shows the absorption and emission spectra of polymers **18** and **19** in DMF. Both polymers exhibited

---

single absorption bands which are attributed to the  $n$  to  $\pi^*$  transition from the carbonyl group and a  $\pi$  to  $\pi^*$  transition in the coumarin system. Polymer **18** showed a maximum absorption at 407 nm while the maximum absorption of polymer **19** was at 324 nm. The differences in the absorption spectra of the polymers suggests different electronic arrangements in the coumarin chromophores from the two polymers.

Same as in the absorption spectra, the emission spectra of both polymers **18** and **19** showed single emission bands at 486 and 433 nm respectively. In both absorption and emission spectra of the two polymers, it was noted that polymer **18** absorbs and emits light at longer wavelengths compared to polymer **19**. These observations could be attributed to the increased charge-transfer character of the coumarin system in polymer **18** compared with polymer **19**. In polymer **18**, the tertiary amine, which is a strong electron-donor is in position 7 of the coumarin system and the electron-withdrawing carbonyl and triazole groups, are in positions 2 and 3 respectively. This structural arrangement results in an enhanced “push-pull” electronic system when the coumarin chromophore is excited and the effect is translated into a red shift in both absorption and emission spectra.

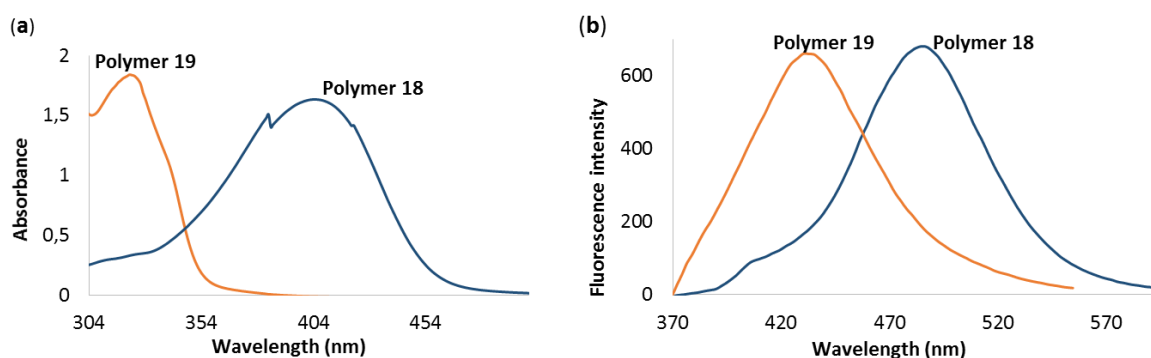


**Figure 3.10:** a) Absorption and b) Emission spectra of polymers **18** and **19** in DMF. Excitation was performed at 350 nm. Concentrations used in terms of the repeating units: Emission ( $1.4 \times 10^{-8}$  M and  $1.4 \times 10^{-7}$  M for polymers **18** and **19** respectively), and Absorption ( $3 \times 10^{-6}$  M and  $6 \times 10^{-6}$  M for polymers **18** and **19** respectively).

### 3.4 Chemosensing studies of polymer **18** and **19**

Since the triazole ring can act as a Lewis base through the middle nitrogen atom,<sup>14</sup> its presence along with the carbonyl group in polymers **18** and **19** makes them potential metal ion chemosensors, prompting further investigation. Binding of the polymers with different metal ions including monovalent, divalent and trivalent ions such as  $\text{Na}^+$ ,  $\text{Ca}^{2+}$ ,  $\text{Ag}^+$ ,  $\text{Al}^{3+}$ ,  $\text{Ba}^{2+}$ ,  $\text{Cr}^{3+}$ ,



---

$\text{Cu}^{2+}$ ,  $\text{Fe}^{3+}$ ,  $\text{Hg}^{2+}$ ,  $\text{Mn}^{2+}$ ,  $\text{Co}^{2+}$ ,  $\text{Zn}^{2+}$ ,  $\text{Cd}^{2+}$ ,  $\text{Ni}^{2+}$  and  $\text{Pb}^{2+}$  were investigated through absorption and emission spectral analysis under similar experimental conditions. Furthermore, the 1,2,3-triazole ring possesses the ability to be involved in hydrogen bonding with anions through its polarized triazole C-H bond; therefore chemosensing capabilities of polymers **17** and **18** were also investigated in the presence of anions which included  $\text{H}_2\text{PO}_4^-$ ,  $\text{F}^-$ ,  $\text{Cl}^-$ ,  $\text{Br}^-$ ,  $\text{HSO}_4^-$ ,  $\text{ClO}_4^-$ ,  $\text{OH}^-$ ,  $\text{I}^-$ ,  $\text{NO}_3^-$ ,  $\text{AcO}^-$  and  $\text{CN}^-$ . Due to the limited solubility of the polymeric materials, all the studies were performed in DMF, which is a more polar solvent. In all chemosensing studies, solutions of nitrate and tetrabutylammonium salts were used as cation and anion source respectively.

### 3.4.1 UV-Vis analysis

The chemosensing capabilities of polymers **18** and **19** towards metal ions were initially investigated by UV-Vis spectral analysis. This was achieved at room temperature by mixing the DMF solutions of polymers **18** and **19** with the aliquots of listed metal ions and anions. As shown in **Figure 3.11**, all the metal ions and anions tested, except  $\text{Fe}^{3+}$ , did not show any significant changes in the absorption band at 407 nm for polymer **18**.  $\text{Fe}^{3+}$  induced a small increase in the intensity of the absorption band. On the contrary, the addition of the same concentration of both metal ions and anions to the DMF solution of polymer **19** showed some variations in the responses as shown in **Figure 3.12**. As noted for polymer **18**, no significant change in the absorption band at 324 nm was observed for polymer **19** in the presence of the metal ions under investigation, except for  $\text{Fe}^{3+}$  (**Figure 3.12 a**).  $\text{Fe}^{3+}$  induced an increase in absorption in polymer **19**, much higher compared to polymer **18**. This suggests that polymer **19** efficiently interacts with  $\text{Fe}^{3+}$ , more so than polymer **18**. Additionally, polymer **19** showed some interaction with  $\text{Cu}^{2+}$  which resulted in an increase in absorption. In the presence of anions (**Figure 3.12 b**), weak variations in the intensities of the absorption bands were observed but no conclusive selective response was noted from any of the tested anions.

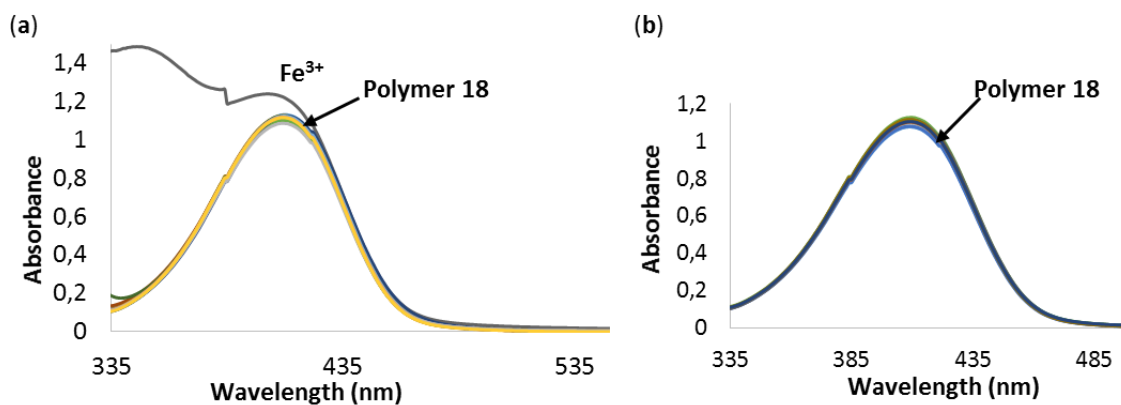


**Figure 3.11:** Absorption spectra of polymer **18** ( $1.5 \times 10^{-2}$  g/L) in the presence of the aliquot ( $6.5 \times 10^{-5}$ M) of **a**) metal ions ( $\text{Na}^+$ ,  $\text{Ca}^{2+}$ ,  $\text{Ag}^+$ ,  $\text{Al}^{3+}$ ,  $\text{Ba}^{2+}$ ,  $\text{Cr}^{3+}$ ,  $\text{Cu}^{2+}$ ,  $\text{Fe}^{3+}$ ,  $\text{Hg}^{2+}$ ,  $\text{Mn}^{2+}$ ,  $\text{Co}^{2+}$ ,  $\text{Zn}^{2+}$ ,  $\text{Cd}^{2+}$ ,  $\text{Ni}^{2+}$  and  $\text{Pb}^{2+}$ ), and **b**) anions ( $\text{H}_2\text{PO}_4^{2-}$ ,  $\text{F}^-$ ,  $\text{Cl}^-$ ,  $\text{Br}^-$ ,  $\text{HSO}_4^-$ ,  $\text{ClO}_4^-$ ,  $\text{OH}^-$ ,  $\text{I}^-$ ,  $\text{NO}_3^-$ ,  $\text{AcO}^-$  and  $\text{CN}^-$ ).

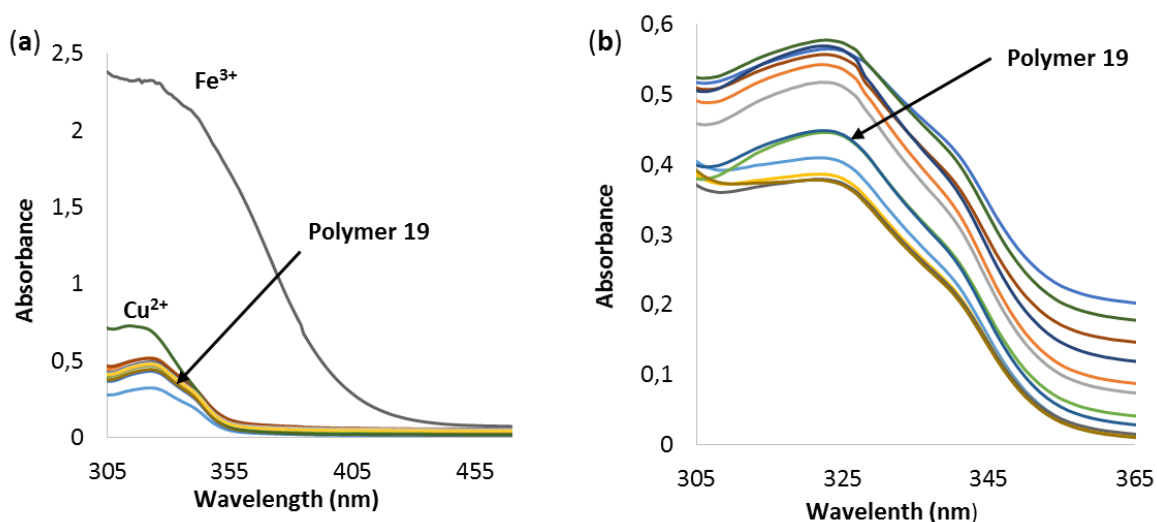


**Figure 3.12:** Absorption spectra of polymer **19** ( $5 \times 10^{-3}$  g/L) in the presence of the aliquot ( $6.5 \times 10^{-5}$ M) of **a**) metal ions ( $\text{Na}^+$ ,  $\text{Ca}^{2+}$ ,  $\text{Ag}^+$ ,  $\text{Al}^{3+}$ ,  $\text{Ba}^{2+}$ ,  $\text{Cr}^{3+}$ ,  $\text{Cu}^{2+}$ ,  $\text{Fe}^{3+}$ ,  $\text{Hg}^{2+}$ ,  $\text{Mn}^{2+}$ ,  $\text{Co}^{2+}$ ,  $\text{Zn}^{2+}$ ,  $\text{Cd}^{2+}$ ,  $\text{Ni}^{2+}$  and  $\text{Pb}^{2+}$ ), and **b**) anions ( $\text{H}_2\text{PO}_4^{2-}$ ,  $\text{F}^-$ ,  $\text{Cl}^-$ ,  $\text{Br}^-$ ,  $\text{HSO}_4^-$ ,  $\text{ClO}_4^-$ ,  $\text{OH}^-$ ,  $\text{I}^-$ ,  $\text{NO}_3^-$ ,  $\text{AcO}^-$  and  $\text{CN}^-$ ).

### 3.4.2 Fluorescence analysis

The chemosensing capability of polymers **18** and **19** were also investigated using emission spectral analysis in the same way and using the same ionic species as applied in the UV-Vis spectral analysis. An excitation wavelength of 350 nm was used for both polymers. For polymer **18**, most of the metal ions generally showed some interaction resulted in alteration of

emission spectrum. Exceptional changes in the emission band at 486 nm were observed in the presence of  $\text{Fe}^{3+}$  and  $\text{Cu}^{2+}$  and could be attributed to the transfer of excitation energy from the fluorophores to the metal *d*-orbital and/or charge transfer from the fluorophores to the metal ion which resulted in a fluorescence quenching response (**Figure 3.13 a**).<sup>15</sup> The presence of  $\text{Fe}^{3+}$  induced up to a 78 % quenching effect in the emission band while  $\text{Cu}^{2+}$  induced up to 50% quenching. On the other hand, the presence of anions did not significantly affect the fluorescence band of polymer **18** (**Figure 3.13 b**).

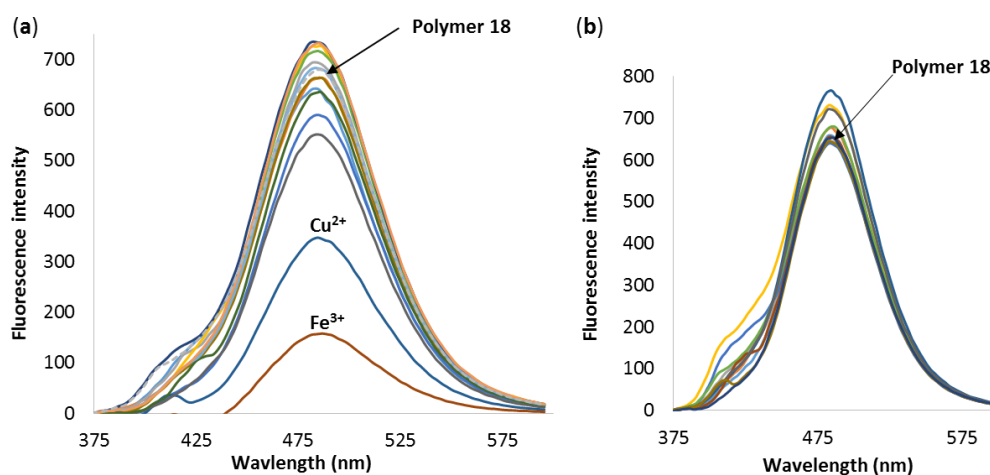


**Figure 3.13:** Emission spectra of polymer **18** ( $1.9 \times 10^{-4}$  g/L) in the presence of the aliquot (0.5  $\mu\text{M}$ ) of **a**) metal ions ( $\text{Na}^+$ ,  $\text{Ca}^{2+}$ ,  $\text{Ag}^+$ ,  $\text{Al}^{3+}$ ,  $\text{Ba}^{2+}$ ,  $\text{Cr}^{3+}$ ,  $\text{Cu}^{2+}$ ,  $\text{Fe}^{3+}$ ,  $\text{Hg}^{2+}$ ,  $\text{Mn}^{2+}$ ,  $\text{Co}^{2+}$ ,  $\text{Zn}^{2+}$ ,  $\text{Cd}^{2+}$ ,  $\text{Ni}^{2+}$  and  $\text{Pb}^{2+}$ ) and **b**) anions ( $\text{F}^-$ ,  $\text{Cl}^-$ ,  $\text{Br}^-$ ,  $\text{HSO}_4^-$ ,  $\text{ClO}_4^-$ ,  $\text{OH}^-$ ,  $\text{I}^-$ ,  $\text{NO}_3^-$ ,  $\text{AcO}^-$  and  $\text{CN}^-$ ). Excitation was performed at 350 nm.

The presence of metal ions, except  $\text{Fe}^{3+}$ , showed negligible changes in the emission band at 433 nm for polymer **19** implying that the interactions were negligible (**Figure 3.14 a**). The presence of  $\text{Fe}^{3+}$  induced a fluorescence quenching response up to 80% in the emission band of polymer **19**. As for polymer **18**, the presence of anions induced negligible changes in the fluorescence spectra of polymer **19** (**Figure 3.14 b**).

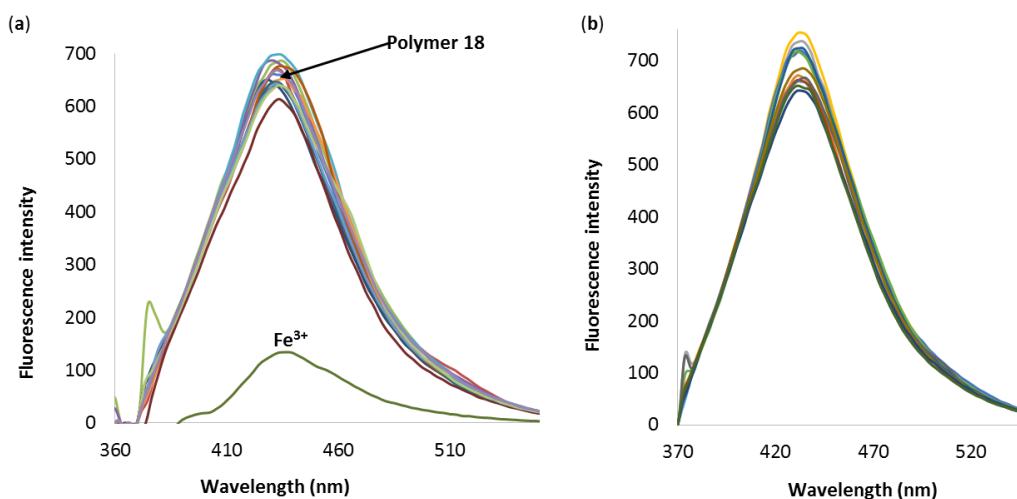


**Figure 3.14:** Emission spectra of polymer **19** ( $1.5 \times 10^{-3}$  g/L) in the presence of the aliquot (0.4  $\mu$ M) of **a**) metal ions ( $\text{Na}^+$ ,  $\text{Ca}^{2+}$ ,  $\text{Ag}^+$ ,  $\text{Al}^{3+}$ ,  $\text{Ba}^{2+}$ ,  $\text{Cr}^{3+}$ ,  $\text{Cu}^{2+}$ ,  $\text{Fe}^{3+}$ ,  $\text{Hg}^{2+}$ ,  $\text{Mn}^{2+}$ ,  $\text{Co}^{2+}$ ,  $\text{Zn}^{2+}$ ,  $\text{Cd}^{2+}$ ,  $\text{Ni}^{2+}$  and  $\text{Pb}^{2+}$ ) and **b**) anions ( $\text{F}^-$ ,  $\text{Cl}^-$ ,  $\text{Br}^-$ ,  $\text{HSO}_4^-$ ,  $\text{ClO}_4^-$ ,  $\text{OH}^-$ ,  $\text{I}^-$ ,  $\text{NO}_3^-$ ,  $\text{AcO}^-$  and  $\text{CN}^-$ ). Excitation was performed at 350 nm.

Despite the observed higher sensitivity towards  $\text{Fe}^{3+}$  ions by both polymers, their sensitivities towards other metal ions were different. In polymer **19**, all the metal ions except  $\text{Fe}^{3+}$  showed a negligible interaction with polymer **19** while in polymer **18**, some metal ions such as  $\text{Hg}^{2+}$ ,  $\text{Co}^{2+}$  and  $\text{Cu}^{2+}$  exhibited levels of interaction which led to visible quenching of the emission band. These observations suggest different binding modes of the two polymers towards the metal ions.

### 3.4.3 Titration experiments of polymer **18** and **19** with $\text{Fe}^{3+}$ ions

To further investigate the sensitivity of polymers **18** and **19** towards  $\text{Fe}^{3+}$ , UV-Vis and fluorescence titration experiments were performed. Variations in the absorption spectra of polymers **18** (**Figure 3.15 a**) and **19** (**Figure 3.15 b**) with increasing amounts of  $\text{Fe}^{3+}$  ions were observed. Notable was that the addition of  $\text{Fe}^{3+}$  aliquots to the DMF solution of both polymers resulted in a gradual increase in the intensities of the absorption bands of the two polymers. The response was greater in polymer **19** than in polymer **18**. This confirms that both polymers interact with  $\text{Fe}^{3+}$  with different levels of sensitivity.

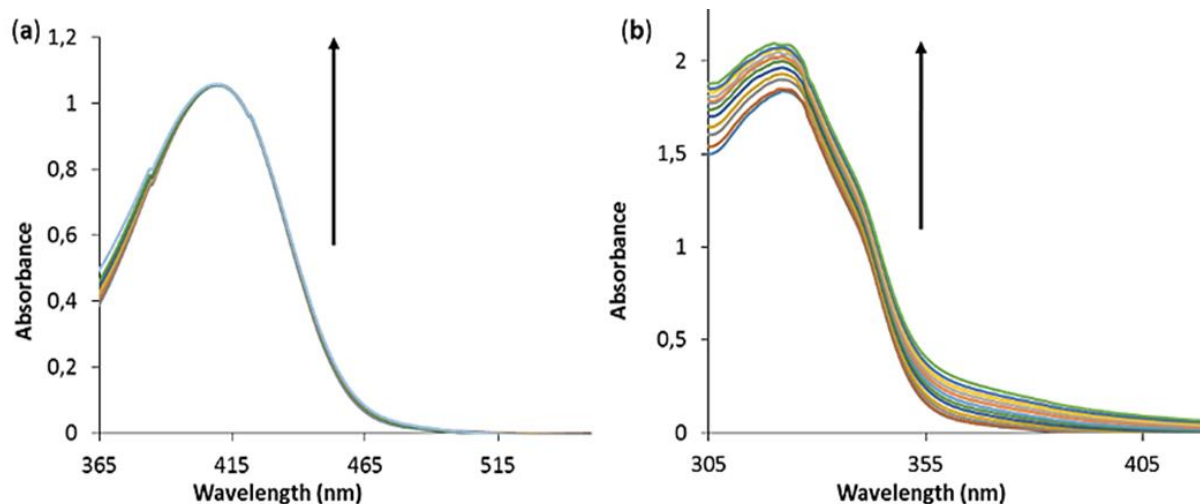


**Figure 3.15:** Changes in the absorption spectra of **a)** polymer **18** and **b)** polymer **19** in DMF upon addition of  $\text{Fe}^{3+}$  aliquots ( $0.02 \mu\text{M}$ ). Concentrations of  $1.5 \times 10^{-2} \text{ g/L}$  and  $5 \times 10^{-2} \text{ g/L}$  were used for polymer **18** and **19** respectively.

Fluorescence titrations of polymers **18** and **19** using  $\text{Fe}^{3+}$  were performed in DMF solutions. As shown in the **Figure 3.16**, the addition of  $\text{Fe}^{3+}$  aliquots induced a gradual decrease in the emission bands of both polymers. When  $3.24 \times 10^{-4} \text{ M}$  of  $\text{Fe}^{3+}$  was added to the DMF solution of polymer **19** (**Figure 3.16 b**), the fluorescence at  $433 \text{ nm}$  was almost completely quenched. In contrast to the polymer **19**, the addition of  $\text{Fe}^{3+}$  ions to the DMF solution of polymer **18** reached a saturation point with 78% quenching when  $8 \times 10^{-7} \text{ M}$  of  $\text{Fe}^{3+}$  had been added.

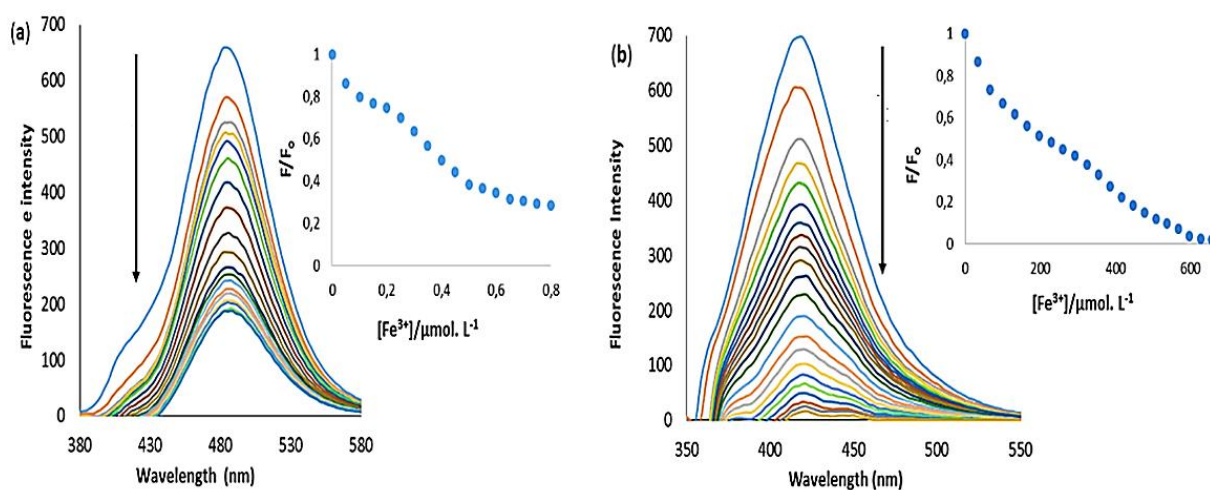


**Figure 3.16:** Emission spectra of **a)** polymer **18** ( $1.9 \times 10^{-4} \text{ g/L}$ ) and **b)** polymer **19** ( $1.5 \times 10^{-3} \text{ g/L}$ ) in DMF in the presence of increasing amounts of  $\text{Fe}^{3+}$  ( $0$ - $0.8 \mu\text{M}$  for polymer **18** and  $0$ - $324 \mu\text{M}$  for polymer **19**). An excitation wavelength of  $350 \text{ nm}$  was used.

Using titration information data of polymers **18** and **19**, plots of  $F/F_0$  (where  $F_0$  and  $F$  are fluorescence intensities in the absence and in the presence of  $\text{Fe}^{3+}$ ) against concentration of  $\text{Fe}^{3+}$  were plotted (insets in **Figure 3.16**). In polymer **18**, linearity between  $F/F_0$  and  $[\text{Fe}^{3+}]$  was found in the 0.2-0.5  $\mu\text{mol/L}$  range with a correlation coefficient of  $R^2=0.9978$ , while in polymer **19** this was observed between 33 and 98  $\mu\text{mol/L}$  with a correlation coefficient of  $R^2=0.9981$ . The detection limit of each polymer was calculated according to the IUPAC definition ( $C_{\text{DL}}=3S_b/m$ ), where  $S_b$  represents the standard deviation of a blank solution and  $m$  the slope.<sup>16</sup> The detection limits were found to be  $1.7 \times 10^{-7}$  M and  $4 \times 10^{-6}$  M for polymers **18** and **19** respectively (For detection limit calculation see **Appendices**). The differences in the detection limits could be attributed to the higher fluorescence intensity associated with polymer **18** (approximately 10 times more fluorescent than polymer **19**).

### 3.4.4 Competitive studies

To investigate the effect of other metal ions on the interaction between the polymers and  $\text{Fe}^{3+}$ , competitive studies were performed. This was achieved by using  $\text{Fe}^{3+}$  ions mixed with two equivalents of other metal ions. The emission spectra were recorded in DMF at 350 nm for polymer **18** and **19**. As shown in **Figure 3.17**, the fluorescence quenching responses induced by the presence of  $\text{Fe}^{3+}$  ions in polymer **18** (**Figure 3.17 a**) and polymer **19** (**Figure 3.17 b**) were not significantly affected by the presence of two equivalents of other metal ions. The higher sensitivities of polymers **18** and **19** towards  $\text{Fe}^{3+}$  and the formation of stable complexes with minimal interference from the presence of other metal ions makes these types of polymers potential “on-off” selective chemosensors for  $\text{Fe}^{3+}$  ions.

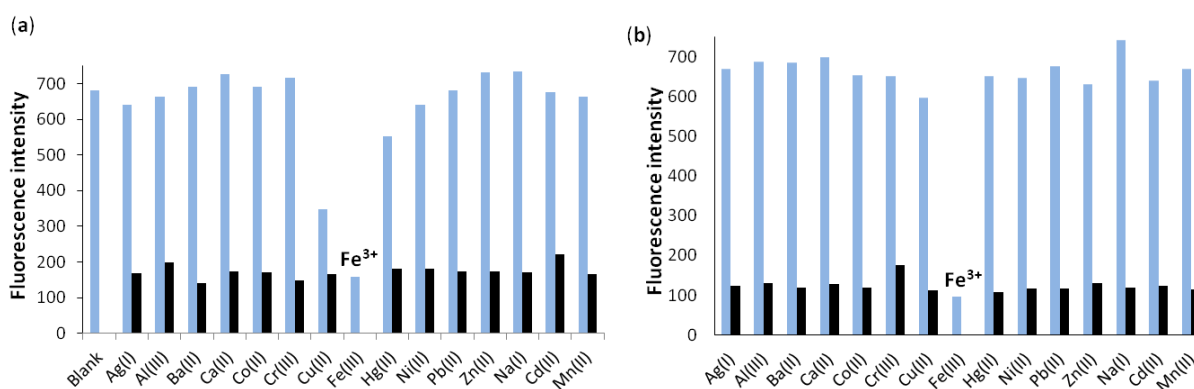


**Figure 3.17:** Fluorescence responses of **a**) polymer **18** ( $1.9 \times 10^{-4}$  g/L) and **b**) polymer **19** ( $1.5 \times 10^{-3}$  g/L) in the presence of metal ions ( $0.5 \mu\text{M}$  for polymer **18** and  $0.4 \mu\text{M}$  for polymer **19**)  $\text{Na}^+$ ,  $\text{Ca}^{2+}$ ,  $\text{Ag}^+$ ,  $\text{Al}^{3+}$ ,  $\text{Ba}^{2+}$ ,  $\text{Cr}^{3+}$ ,  $\text{Cu}^{2+}$ ,  $\text{Fe}^{3+}$ ,  $\text{Hg}^{2+}$ ,  $\text{Mn}^{2+}$ ,  $\text{Co}^{2+}$ ,  $\text{Zn}^{2+}$ ,  $\text{Cd}^{2+}$ ,  $\text{Ni}^{2+}$  and  $\text{Pb}^{2+}$

---

(blue bars) and in the presence of a mixture of  $\text{Fe}^{3+}$  (0.5  $\mu\text{M}$  for polymer **18** and 0.4  $\mu\text{M}$  for polymer **19**) with two equivalents (1  $\mu\text{M}$  for polymer **18** and 0.8  $\mu\text{M}$  for polymer **19**) of other metal ions (black bars). Excitation was performed at 350 nm.

#### 2.4.5 Sensing mechanism of polymers **18** and **19** toward metal ions

Since both polymers **18** and **19** showed higher sensitivity towards  $\text{Fe}^{3+}$  and also considering that more than one binding site is present in each polymer, the task was to find the binding sites from the polymers which are involved in binding the  $\text{Fe}^{3+}$ . Although the presence of  $\text{Fe}^{3+}$  induced fluorescence quenching in both polymers, the presence of some metal ions such as  $\text{Cu}^{2+}$ ,  $\text{Hg}^{2+}$  and  $\text{Co}^{2+}$  showed some level of interaction which leads to visible fluorescence quenching in polymer **18** compared to polymer **19**. This suggested different affinities in the two polymers towards metal ions. In order to analyse these different affinities and gain an insight on the interaction between the polymers and  $\text{Fe}^{3+}$ , fluorescence responses of 7-diethylaminocoumarin **17**, monomer **10** and monomer **16** were investigated in the presence of those metal ions that induced visible fluorescence quenching responses in polymer **18**.

The choice of 7-diethylaminocoumarin was based on the fact that the molecule possesses all the binding sites present in polymer **18** and in its starting monomer **10** except for the triazole ring. Furthermore, 7-diethylaminocoumarin also has a carbonyl group which is in the same chemical environment as the carbonyl group in polymer **19** and its starting monomer **16**. Therefore the comparison of the fluorescence responses of the 7-diethylaminocoumarin **17**, monomer **10** and **16** can provide an insight into how polymers **18** and **19** interact with the metal ions as well as the effect of the interchain interactions on the binding of the metal ions.

The emission spectra of the three compounds were recorded under the same conditions as their corresponding polymers and using the same excitation energy. As shown in **Figure 3.18**, the presence of the four metal ions ( $\text{Fe}^{3+}$ ,  $\text{Cu}^{2+}$ ,  $\text{Hg}^{2+}$  and  $\text{Co}^{2+}$ ) induced almost the same responses in 7-diethylaminocoumarin **17**, monomer **10** and **16** emission bands. As observed for their corresponding polymers, higher responses were also observed in the presence of  $\text{Fe}^{3+}$  for the monomers.

Since all the three compounds exhibited strong fluorescence quenching in the presence of  $\text{Fe}^{3+}$  as observed in their corresponding polymers, it is likely that the same binding mode is used when  $\text{Fe}^{3+}$  interacts with each one of the three compounds as well as their corresponding polymers. To achieve the same binding mode, the same binding sites must be involved in metal

ion coordination. Hence it can be concluded that the common binding site in compound **10**, **16** and **17**, as well as in their corresponding polymers is the carbonyl group, and the contribution from the triazole ring is minimized. Since the quenching induced by the presence of  $\text{Cu}^{2+}$ ,  $\text{Hg}^{2+}$  and  $\text{Co}^{2+}$  in the polymer **18** could not be observed in its repeating unit **10**, the quenching in the polymer **18** can be attributed to the interchain aggregation induced by the presence of those metal ions.<sup>17,18</sup> As the same effect was not observed in polymer **19**, it can be concluded that the triazole ring environment in polymer **18** played a role in the sensitivity towards those metal ions ( $\text{Cu}^{2+}$ ,  $\text{Hg}^{2+}$  and  $\text{Co}^{2+}$ ).

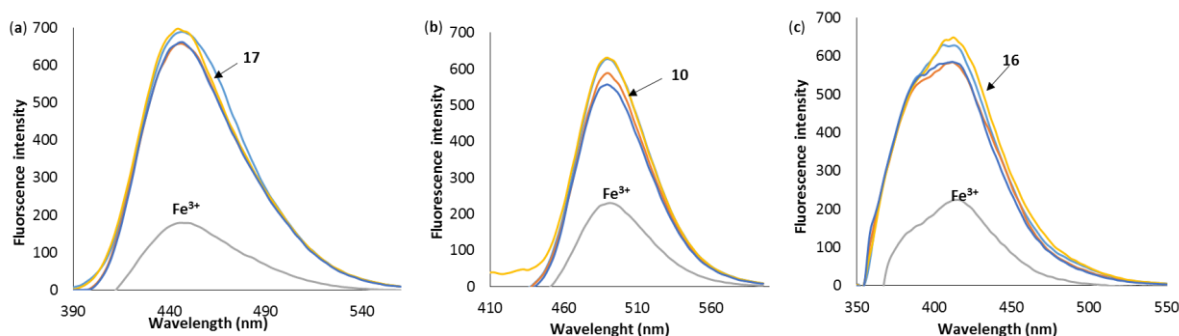


**Figure 3.18:** Emission spectra of **a)** 7-diethylamionocoumarin **17** (0.033  $\mu\text{M}$ ), **b)** monomer **10** (0.67  $\mu\text{M}$ ), **c)** monomer **16** (0.083  $\mu\text{M}$ ) in the presence of  $\text{Fe}^{3+}$ ,  $\text{Cu}^{2+}$ ,  $\text{Hg}^{2+}$  and  $\text{Co}^{2+}$  (0.01 M). Excitation was performed at 350 nm.

The interaction between  $\text{Fe}^{3+}$  with the carbonyl functional group was confirmed using FT-IR titration experiments and the results are presented in **Figure 3.19**. This was conducted by adding aliquots of  $\text{Fe}^{3+}$  to dimethylsulfoxide solutions of polymers **18** and **19** and an aliquot was collected for FT-IR analysis from the mixture after each addition. Notable from both polymers is that the intensity of the FT-IR peak at  $1690\text{ cm}^{-1}$  gradually increases with addition of  $\text{Fe}^{3+}$  while the other peaks are not significantly affected. Since this peak was assigned to the carbonyl group, it is clear that the carbonyl group is involved in binding  $\text{Fe}^{3+}$ .



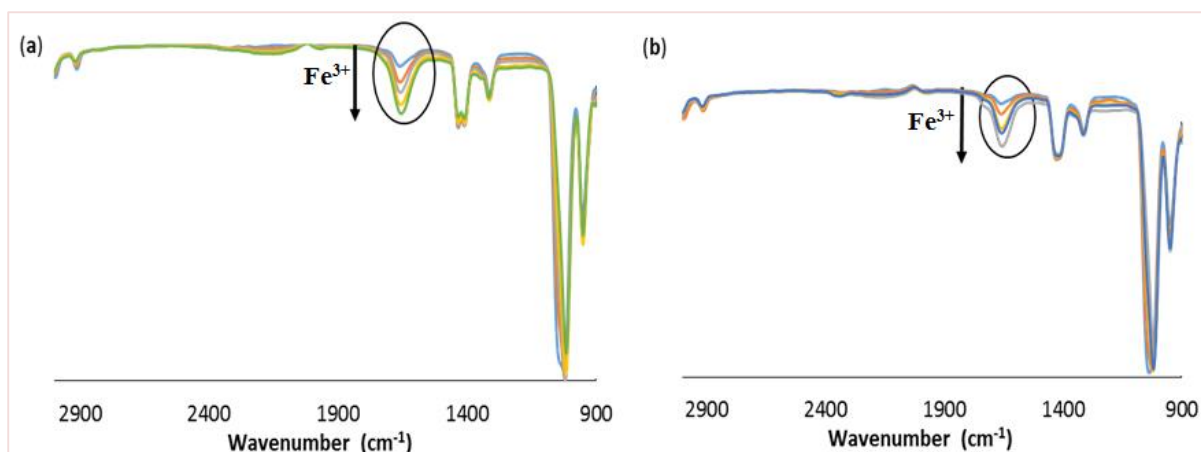


**Figure 3.19:** Changes in the FT-IR spectra of polymers **18** and **19** ( $10^{-4}$  g/L) with addition of 1  $\mu$ L aliquots of  $\text{Fe}^{3+}$  (0.1 M).

### 3.4 Conclusion

Two polymers with conjugated triazolyl coumarin units as pendant groups have been synthesized through multiple step syntheses. Their chemosensing capabilities for metal ions and anions were investigated in DMF solvent and both polymers showed higher sensitivity towards  $\text{Fe}^{3+}$  ions. An investigation that was carried out on their starting monomers and a reference molecule (7-diethylaminocoumarin **17**) indicated the carbonyl functionality as the possible main binding site for the  $\text{Fe}^{3+}$  ions. This observation was further confirmed through FT-IR titration experiments. The fluorescence quenching in the presence of  $\text{Fe}^{3+}$  was attributed to the transfer of excitation energy from the coumarin fluorophore in the polymers to the metal *d*-orbital and/or charge transfer from polymer to metal ion.

### 3.5 Experimental

#### 3.5.1 General information

All chemicals and solvents were purchased from Sigma Aldrich or Merck and were used as received without further purification. Reactions were monitored by thin layer chromatography (TLC) on pre-coated silica gel 60 F<sub>254</sub> aluminum sheets (0.063 - 0.2 mm/70 - 230 mesh) and column chromatography was performed using silica gel (particle size 0.040-0.063 mm).

$^1\text{H}$  NMR and  $^{13}\text{C}$  NMR spectra were measured on a Bruker Advance DPX 400 (400 MHz) using TMS as an internal standard. NMR samples were prepared in deuterated solvents

---

(CDCl<sub>3</sub> or DMSO-d<sub>6</sub>) and all samples were run at 300 K. Coupling constants (*J*) and chemical shifts ( $\delta$ ) are expressed in Hz and parts per million (ppm) respectively.

FT-IR spectra were recorded in the range 4000-500 cm<sup>-1</sup> using Opus software (version 6.5.6) on a Bruker Platinum Tensor 27 ATR-IR spectrophotometer. The elemental analysis for carbon, hydrogen and nitrogen was performed using a Vario EL (Elementar Analysen System GmbH) instrument.

The melting point data were determined using a Lasec Hot Stage apparatus. The UV-Vis absorption spectra were recorded on a Perkin Elmer Lambda 35 UV-Vis spectrometer using a 1 cm quartz cell while emission spectra were recorded on a Perkin Elmer LS 45 fluorescence spectrometer. Stock solution of the polymer and starting monomers were prepared by dissolving the samples in DMF, and the solutions were diluted to the desired concentrations. For the polymers mass/vol concentration was used, while for starting monomer molarity was used. The solution was further diluted to 7 x 10<sup>-5</sup>. Stock solutions of various cations and anions were prepared using nitrate and tetrabutylammonium salts.

### 3.5.1 Synthesis of vinyl monomer (10)

Compounds **6** to **8** were synthesized according to procedures available in the literature.<sup>7</sup>

#### 3.5.1.1 7-(Diethylamino)-3-nitro-2*H*-chromen-2-one (6)

Yield: 75%. <sup>1</sup>H NMR (CDCl<sub>3</sub>, 400 MHz):  $\delta$  = 8.73 (s, 1H), 7.45 (d, *J* = 8.24 Hz, 1H), 6.72 (d, *J* = 9.08 Hz, 1H), 6.51 (s, 1H), 3.41 (q, *J* = 6.04 Hz, 4H), 1.20 (t, *J* = 6.04, 6H). <sup>13</sup>C NMR (CDCl<sub>3</sub>, 400 MHz):  $\delta$  = 162.31, 151.56, 149.45, 145.68, 137.21, 129.01, 111.57, 105.03, 45.81, 12.90.

#### 3.5.1.2 3-Amino-7-(diethylamino)-2*H*-chromen-2-one (7)

Yield: 61%. <sup>1</sup>H NMR (CDCl<sub>3</sub>, 400 MHz):  $\delta$  = 7.14 (d, *J* = 8.56 Hz, 1H), 6.72 (s, 1H), 6.57 (m, 2H), 3.89 (s, 2H), 3.39 (q, *J* = 6.84 Hz, 4H), 1.20 (t, *J* = 6.84 Hz, 6H). <sup>13</sup>C NMR (CDCl<sub>3</sub>, 400 MHz):  $\delta$  = 160.43, 156.89, 154.35, 139.37, 129.64, 113.67, 112.14, 111.08, 105.69, 45.41, 12.63.

#### 3.5.1.3 3-Azido-7-(diethylamino)-2*H*-chromen-2-one (8)

Yield: 64%. <sup>1</sup>H NMR (CDCl<sub>3</sub>, 400 MHz):  $\delta$  = 7.20 (d, *J* = 9.04 Hz, 1H), 7.11 (s, 1H), 6.60 (d, *J* = 8.96 Hz, 1H), 6.52 (s, 1H), 3.41 (q, *J* = 6.04 Hz, 4H), 1.22 (t, *J* = 6.04 Hz, 6H). <sup>13</sup>C NMR

---

(CDCl<sub>3</sub>, 400 MHz):  $\delta$  = 158.34, 152.78, 151.89, 149.98, 149.34, 128.47, 118.18, 112.95, 111.02, 45.67, 12.70.

#### 3.5.1.4 7-(Diethylamino)-3-(4-(1-hydroxyethyl)-1H-1,2,3-triazol-1-yl)-2H-chromen-2-one (9)

A mixture of 3-azido-7-(diethylamino)-2H-chromen-2-one (**8**) (2.10 g, 8.10 mmol), 3-butyn-2-ol (0.90 mL, 12 mmol), CuSO<sub>4</sub>·5H<sub>2</sub>O (0.39 g, 1.6 mmol) and sodium ascorbate (0.39 g, 1.9 mol) in THF (100 mL) were stirred at RT for 72 h. THF was removed under reduced pressure and the crude product was dissolved in EtOAc. The mixture was washed with water and then concentrated to give a product which was purified by column chromatography over silica gel (EtOAc: Hexane, 70:30) to afford a yellow solid in 71 % yield. m.p. 142-145°C. IR  $\nu_{\max}$  (cm<sup>-1</sup>): 3313 (OH), 2969 (N-Et<sub>2</sub>). <sup>1</sup>H NMR (CDCl<sub>3</sub>, 400 MHz):  $\delta$  = 8.40 (s, 1 H), 8.30 (s, 1H), 7.34 (d,  $J$  = 8.72 Hz, 1H), 6.61 (d,  $J$  = 8.72 Hz, 1H), 6.49 (s, 1 H), 5.09 (s, 1H), 3.39 (q,  $J$  = 7.04 Hz, 4H), 1.58 (d,  $J$  = 6.44 Hz, 3H), 1.17 (t,  $J$  = 6.75 Hz, 6H). <sup>13</sup>C NMR (CDCl<sub>3</sub>, 400 MHz):  $\delta$  = 156.97, 155.82, 151.99, 151.58, 134.79, 129.99, 121.06, 116.91, 110.06, 107.08, 97.06, 63.17, 45.00, 22.97, 12.41. Anal. Calc. for C<sub>17</sub>H<sub>20</sub>N<sub>4</sub>O<sub>3</sub>: C: 62.18, H: 6.14, N: 17.06. Found: C: 62.17, H: 6.30, N: 17.59.

#### 3.5.1.5 7-(Diethylamino)-3-(4-vinyl-1H-1,2,3-triazol-1-yl)-2H-chromen-2-one (10)

In a two-necked round-bottomed flask equipped with a Dean Stark apparatus, 7-(diethylamino)-3-(4-(1-hydroxyethyl)-1H-1,2,3-triazol-1-yl)-2H-chromen-2-one (**9**) (0.51 g, 1.54 mmol) and 20% *para*-toluenesulfonic acid (0.05 g, 0.31 mmol) in toluene (100 ml) were refluxed at 130°C for 24 h. The reaction mixture was cooled to room temperature and then neutralized with sodium hydroxide solution (30 mL, 3 M). The organic layer was collected, washed with water (3 X 30 mL) and dried over anhydrous Na<sub>2</sub>SO<sub>4</sub>. The solvent was removed under reduced pressure and the crude product was purified by column chromatography over silica gel (Hexane: EtOAc, 70:30) to afford a yellow solid product in 50% yield. m.p. 149-151°C. <sup>1</sup>H NMR (CDCl<sub>3</sub>, 400 MHz):  $\delta$  = 8.48 (s, 1H), 8.33 (s, 1H), 7.33 (d,  $J$  = 8.52 Hz, 1H), 6.67 (dd,  $J$  = 11.20 Hz, 1H), 6.61 (d,  $J$  = 8.48 Hz, 1H), 6.48 (s, 1H), 5.92 (d,  $J$  = 17.6 Hz 1H), 5.32 (d,  $J$  = 11.16 Hz, 1H), 3.38 (q,  $J$  = 6.36 Hz, 4H), 1.17 (t,  $J$  = 6.36 Hz, 6H). <sup>13</sup>C NMR (CDCl<sub>3</sub>, 400 MHz):  $\delta$  = 156.92, 155.79, 151.56, 146.19, 134.48, 129.98, 125.45, 121.00, 116.84, 116.39, 110.08, 107.10, 97.03, 45.00, 12.42.

---

## 3.5.2 Synthesis of vinyl monomer (16)

**3.5.2.1 7-Amino-4-methyl-2H-chromen-2-one (13):**<sup>8</sup> <sup>1</sup>H NMR (CDCl<sub>3</sub>, 400 MHz):  $\delta$  = 7.29 (d,  $J$  = 8.44 Hz, 1H), 6.50 (s, 2H), 5.94 (s, 1H), 4.09 (s, 2H), 2.27 (s, 3H). <sup>13</sup>C NMR (CDCl<sub>3</sub>, 400 MHz):  $\delta$  = 160.0, 154.68, 151.88, 143.93, 126.01, 117.10, 115.32, 114.03, 107.18, 18.64.

### 3.5.2.2 7-Azido-4-methyl-2H-chromen-2-one (14)

7-Amino-4-methyl-2H-chromen-2-one (**13**) (1.00 g, 5.70 mmol) was dissolved in 30 mL HCl solution (1M) and the mixture was kept in ice until its temperature was below 5°C. To the cooled mixture, NaNO<sub>2</sub> (2.00 g, 28.50 mmol) was added and the mixture stirred for 30 minutes. Then NaN<sub>3</sub> (1.86 g, 28.50 mmol) was slowly added to allow the azidation reaction to take place. After 30 min of stirring, the resulted precipitate were filtered off, washed with water and dried under reduced pressure to afford the azide-functionalized product **14** in 64% yield. m.p. 103-107°C. IR  $\nu_{\max}$  (cm<sup>-1</sup>): 2124.79 (N<sub>3</sub>), 1697.50 (C=O). <sup>1</sup>H NMR (CDCl<sub>3</sub>, 400 MHz):  $\delta$  = 7.50 (d,  $J$  = 8.04 Hz, 1H), 6.90 (s, 1H), 6.89 (d,  $J$  = 8.04 Hz, 1H), 6.16 (s, 1H), 2.35 (s, 3H). <sup>13</sup>C NMR (CDCl<sub>3</sub>, 400 MHz):  $\delta$  = 160.0, 154.68, 151.88, 143.93, 126.01, 117.10, 115.32, 114.03, 107.18, 18.64.

### 3.5.2.3 7-(4-(1-Hydroxyethyl)-1H-1,2,3-triazol-1-yl)-4-methyl-2H-chromen-2-one (15)

A mixture of 7-azido-4-methyl-2H-chromen-2-one (**14**) (0.1 g, 0.5 mmol), 3-butyn-2-ol (0.06 g, 0.5 mmol), CuSO<sub>4</sub>·5H<sub>2</sub>O (0.02 g, 0.05 mmol), sodium ascorbate (0.03 g, 0.15 mmol) and PMDETA (0.03 g, 0.15 mmol) in THF (100 mL) was stirred at room temperature for 72 h. THF was removed under reduced pressure and the crude product dissolved in chloroform. The mixture was washed with water and then concentrated to afford a yellow solid product in 80 % yield. m.p. 170-175 °C. IR  $\nu_{\max}$  (cm<sup>-1</sup>): 3152 (C=C-H), 1719.73 (C=O), 1618 (C=C). <sup>1</sup>H NMR (CDCl<sub>3</sub>, 400 MHz):  $\delta$  = 8.83 (s, 1H), 8.00-7.98 (m, 2H), 6.47 (s, 1H), 5.46 (d,  $J$  = 4.72 Hz, 1H), 4.82 (q,  $J$  = 5.92, Hz, 1H), 2.48 (s, 3H), 1.49 (d,  $J$  = 6.48 Hz, 1H). <sup>13</sup>C NMR (CDCl<sub>3</sub>, 400 MHz):  $\delta$  = 159.95, 154.60, 154.13, 153.24, 139.18, 127.68, 120.39, 119.73, 115.79, 115.03, 107.66, 61.98, 24.05, 18.56. Anal. Calc. for C<sub>14</sub>H<sub>13</sub>N<sub>3</sub>O<sub>3</sub>: C: 61.99, H: 4.83, N: 15.49. Found: C: 61.94, H: 4.82, N: 11.46.

### 3.5.2.4 4-Methyl-7-(4-vinyl-1H-1,2,3-triazol-1-yl)-2H-chromen-2-one (16)

In a two-necked round-bottomed flask equipped with a Dean-Stark apparatus, 7-(4-(1-hydroxyethyl)-1H-1,2,3-triazol-1-yl)-4-methyl-2H-chromen-2-one (**15**) (0.5 g, 1.84 mmol) and *para*-toluenesulfonic acid (0.35 g, 2.03 mmol) in toluene (100 mL) were refluxed at 130°C

---

for 24 h. The reaction mixture was cooled to room temperature and then neutralized with sodium hydroxide solution (30 mL, 3 M). The organic layer was collected, washed with water (3 X 30 mL) and dried over anhydrous Na<sub>2</sub>SO<sub>4</sub>. The solvent was removed under reduced pressure and the crude product purified by column chromatography over silica gel (Hexane: EtOAc, 50:50) to afford yellow solid in 56% yield. m.p. 203-207 °C. IR  $\nu_{\max}$  (cm<sup>-1</sup>): 3152 (C=C-H), 1719 (C=O), 1618 (C=C). <sup>1</sup>H NMR (CDCl<sub>3</sub>, 400 MHz):  $\delta$  = 8.02 (s, 1H), 7.84-7.76 (m, 2H), 7.70 (s, 1H), 6.81 (dd, *J* = 11.24 Hz, 1H), 6.38 (s, 1H), 6.09 (d, *J* = 16.92 Hz, 1H), 5.50 (d, *J* = 12.04 Hz, 1H), 2.51 (s, 3H), <sup>13</sup>C NMR (CDCl<sub>3</sub>, 400 MHz):  $\delta$  = 159.93, 154.24, 151.50, 147.42, 138.93, 126.26, 124.81, 119.89, 117.85, 117.67, 115.84, 115.66, 108.18, 18.69.

### 3.5.3 7-(Diethylamino)-2H-chromen-2-one (17)

Compound (17) was synthesized according to procedures available in the literature.<sup>9</sup> <sup>1</sup>H NMR (CDCl<sub>3</sub>, 400 MHz):  $\delta$  = 7.54 (d, *J* = 9.28 Hz, 1H), 7.26 (d, *J* = 8.76, 1H), 6.57 (d, *J* = 8.80 Hz, 1H), 6.50 (s, 1H), 6.04 (d, *J* = 9.28 Hz, 1H), 3.42 (q, *J* = 7.08 Hz, 4H), 1.22 (t, *J* = 7.08 Hz, 6H). <sup>13</sup>C NMR (CDCl<sub>3</sub>, 400 MHz):  $\delta$  = 162.26, 156.75, 150.69, 143.66, 128.74, 109.21, 108.64, 108.29, 97.56, 44.78, 12.43.

### 3.5.4 Radical polymerization of monomer 10 and 16

To a Schlenk, flask a mixture of vinyl monomer **10** or **16** (0.21 mmol) and azobisisobutyronitrile (AIBN) (4.29 x 10<sup>-3</sup> mmol) in DMF (4 mL) was added. The mixture was degassed using a freeze-thaw method (5 cycles) then flushed with argon, heated for 48 h at 70°C and then poured to ethanol (50 ml). The polymers were precipitated by a dropwise addition of a minimum amount of water to afford branched polymers **18** and **19** in 46% and 39% yield respectively.

## 3.6 References

1. K. Varazo, C. L. Droumaguet, K. Fullard and Q. Wang, *Tetrahedron Lett.*, **2009**, 50, 7032–7034.
2. Y. Zhou, K. Liu, J. Y. Li, Y. Fang, T. C. Zhao and C. Yao, *Org. Lett.*, **2011**, 13, 1290-1293.
3. F. Seela, V. R. Sirivolu and P. Chitpepu, *Bioconjugate Chem.*, **2007**, 19, 211-224.
4. a) V. V. Rostovtsev, L. G. Green, V. V. Fokin and K. B. Sharpless, *Angew. Chem. Int. Ed.*, **2002**, 41, 2596–2599. b) M. Meldal and C.W. Torne, *Chem. Rev.*, **2008**, 108, 2952–3015.
5. L. Du, N. Ni, M. Li and B. Wang, *Tetrahedron Lett.*, **2010**, 51, 1152–1154.

- 
6. D. T. Shi, X. L. Wei, Y. Sheng, Y. Zang, X. P. He, J. Xie, G. Liu, Y. Tang, J. Li and G. R. Chen, *Sci. Rep.*, **2014**, 4, 4252-4257.
  7. K. Sivakumar, F. Xie, B. M. Cash, S. Long, H. N. Barnhill and Q. Wang *Org. Lett*, **2004**, 6, 4603-4606.
  8. A. Kathuria, S. Jalal, R. Tiwari, A. N. Shirazi, S. Gupta, S. Kumar, K. Parang and S. K. Sharma, *Chem. Biol. Interface*, **2011**, 1, 279-296.
  9. J. Wu, W. Liu, X. Zhuang, F. Wang, P. Wang, S. Tao, X. Zhang, S. Wu and S. Lee, *Org. Lett.*, **2007**, 9, 33.
  10. S. Sarkar and R. Shunmugam, *Chem. Commun.*, **2014**, 50, 8511-8513.
  11. C. J. Wheelock, *J. Am. Chem. Soc.* **1959**, 81, 1348.
  12. V. Hasirci, P. Yilgor, T. Endogan, G. Eke and N. Hasirci, Polymer fundamentals: polymer synthesis, *Comprehensive Biomaterials*, **2011**, 1, 349-371.
  13. a) D. Chen, W. Lu, G. Du, L. Jiang, J. Ling, Z. Shen, *J. Polym. Sci. Part A: Polym. Chem.* **2012**, 50, 4191-4197. b) J. Zhou, W. Lu, F. Hu, M. Zhang, L. Jiang and Z. Shen, *J. Polym. Sci. Part A: Polym. Chem.*, **2014**, 52, 16, 2248-2257.
  14. Y. Hua and A. H. Flood, *Chem. Soc. Rev.*, **2010**, 39, 1262-1271.
  15. R. Wang, Q. Wan, F. Feng and Y. Bai, *Chem. Res. Chin. Univ.*, **2014**, 30, 560-565.
  16. S. Goswami, A.K. Das and S. Maity, *Dalton Trans.*, **2013**, 42, 16259-16263.
  17. Y. Chen, K. Y. Pu, Q. L. Fan, X. Y. Qi, Y. Q. Huang, X. M. Lu and W. Huang, *J. Polym. Sci. Part A: Polym. Chem.*, **2009**, 47, 5057-5067.
  18. H. Tong, L. Wang, X. Jing and F. Wang, *Macromolecules*, **2002**, 35, 7169-7171.

---

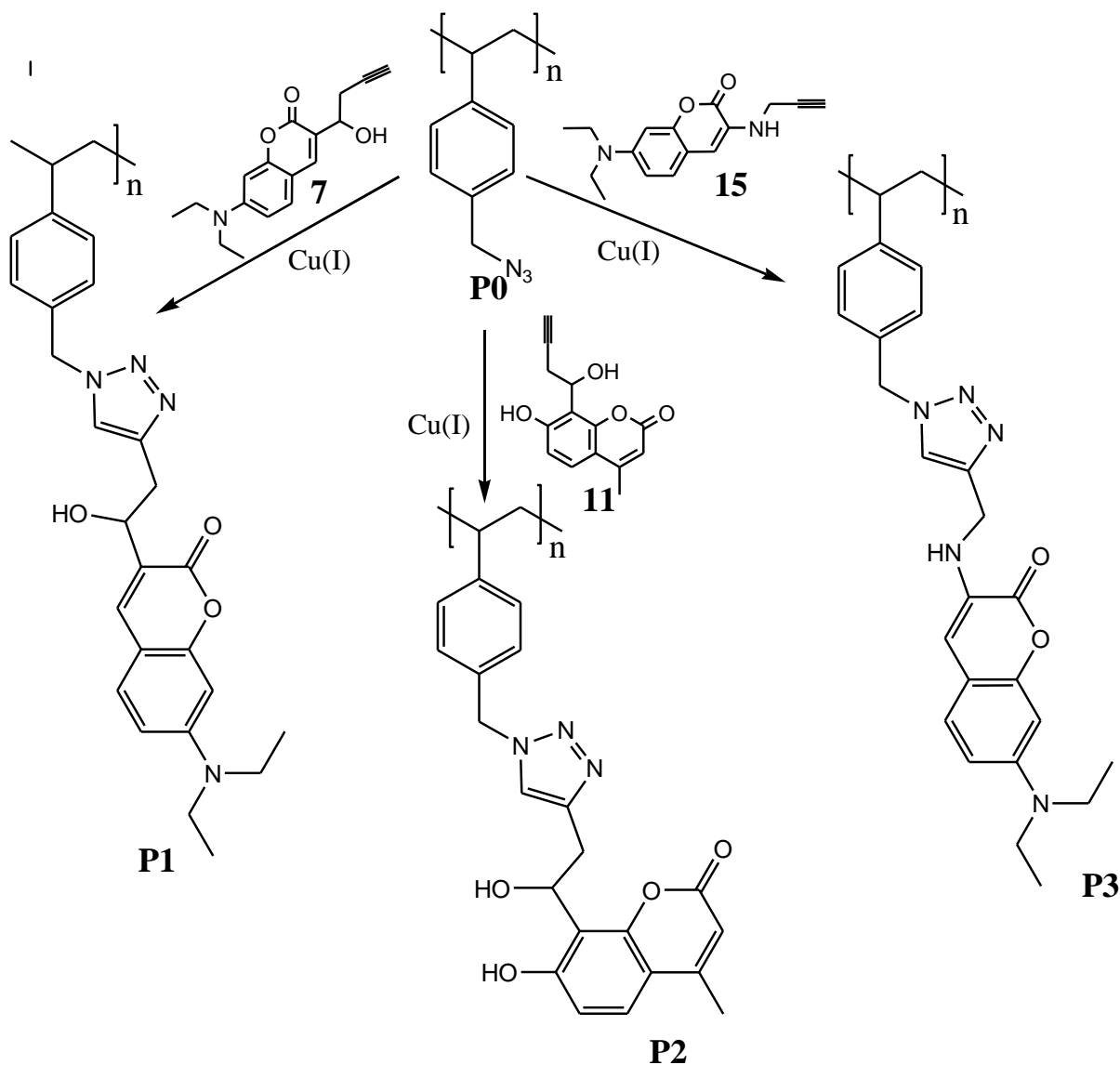
## Chapter 4 Polymers with bridged triazolyl coumarin units as pendant group

### 4.1 Introduction

In the previous Chapter (Chapter 3), it was shown that when the triazole ring is in direct conjugation with coumarin backbone could not efficiently interact with either cations or anions. Furthermore, it was also noted in most literature reports that whenever the 1,2,3-triazole ring was used as a receptor for chemosensors, more than one supporting groups were also involved.<sup>1</sup> Those auxiliary groups help 1,2,3-triazole to interact efficiently with the guest substrate and induce detectable changes in the signalling unit. Widely used auxiliary groups for the 1,2,3-triazole complexation include, hydroxyl,<sup>2</sup> cyclam,<sup>3</sup> carbonyl,<sup>4</sup> pyridinyl<sup>5</sup> or an additional 1,2,3-triazole unit in the system.<sup>6</sup> These auxiliary groups can be in direct conjugation or can be separated from the triazole through a spacer.

With the aim of improving the binding ability of the triazole ring towards ions, a novel set of branched polymers with functional linkages between the coumarin and the 1,2,3-triazole ring were designed and synthesized. Firstly, functional linkages were formed between the alkyne functional group and the coumarin system upon reaction with the alkyne containing precursor. Secondly, the alkyne functionalized coumarin systems were then incorporated into azide functionalized pendant chains of the optically inactive polymer *via* a Cu(I)-catalysed alkyne-azide cycloaddition reaction (CuAAC) to yield the desired functionalized polymer.

Due to their easy preparation, derivatization and strong luminescence as noted in Chapter 3, 7-(diethylamino)coumarin and 7-hydroxy-4-methylcoumarin were used as fluorophore units in these studies. From the two fluorophores, three coumarin derivatives **7**, **11** and **15** with functionalized linkages in positions 3 and 8 were synthesized. These compounds were incorporated into poly(4-vinylbenzyl azide) **P0** under click conditions<sup>7</sup> to a yield triazole-functionalized polymers with coumarin fluorophores linked to 1,2,3-triazole ring *via* functionalized linkages (**Scheme 4.1**). Functionalized linkages which have been investigated in these studies are hydroxyethylene (in **P1** and **P2**) and amino-methylene (in **P3**).



**Scheme 4.1:** A summary for the synthesis of triazolyl coumarin based polymers with functionalized linkages between coumarin and 1,2,3-triazole units.

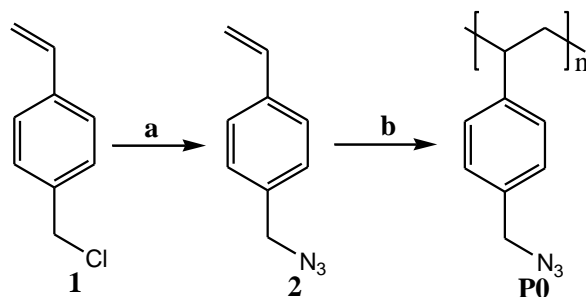
Post-polymerization functionalization was preferred over radical polymerization of triazole functionalized vinyl monomer which can be obtained from 4-vinylbenzyl azide and alkyne functionalized coumarin under click conditions. The reason for this is the size of starting monomer which can lead to the increase in steric hindrance in the growing polymer and result in decreased polymerization efficiency as reported in the literature.<sup>8</sup>

## 4.2 Synthesis of the poly(4-vinylbenzyl azide) polymer (P0)

Azide functionalized polymer **P0** which was the main polymer for post-polymerization functionalization by fluorescent alkyne functionalized coumarin derivatives was synthesized



in 2 steps from 4-vinylbenzyl chloride as shown in the **Scheme 4.2**. An azide functionalized vinyl monomer **2** which was synthesized in a good yield according to the reported literature,<sup>9</sup> was polymerized into the desired polymer **P0** via radical polymerization in DMF using AIBN as the initiator. After 48 hrs, the polymer was precipitated in ethanol and dried under vacuum. To avoid azide decomposition, the dry polymer was kept in the fridge for future use.<sup>10</sup>



**Scheme 4.2:** Synthesis of poly(4-vinylbenzyl azide) **P0**; a)  $\text{NaN}_3$ , DMF, rt, overnight; b) AIBN, DMF, under Argon.

The structure of monomer **2** was confirmed by  $^1\text{H}$  NMR and FT-IR spectroscopies. **Figure 4.1** below shows the assignment of proton signals in the  $^1\text{H}$  NMR spectrum of monomer **2**. Notable, is the presence of splitting patterns of vinylic protons between 5-6 ppm and at 6.7 ppm, confirming the presence of terminal alkene in compound **2**. The average molecular weight and polydispersity index of **P0** were determined to be  $1.26 \times 10^4$  g/mol and 2.24 respectively.

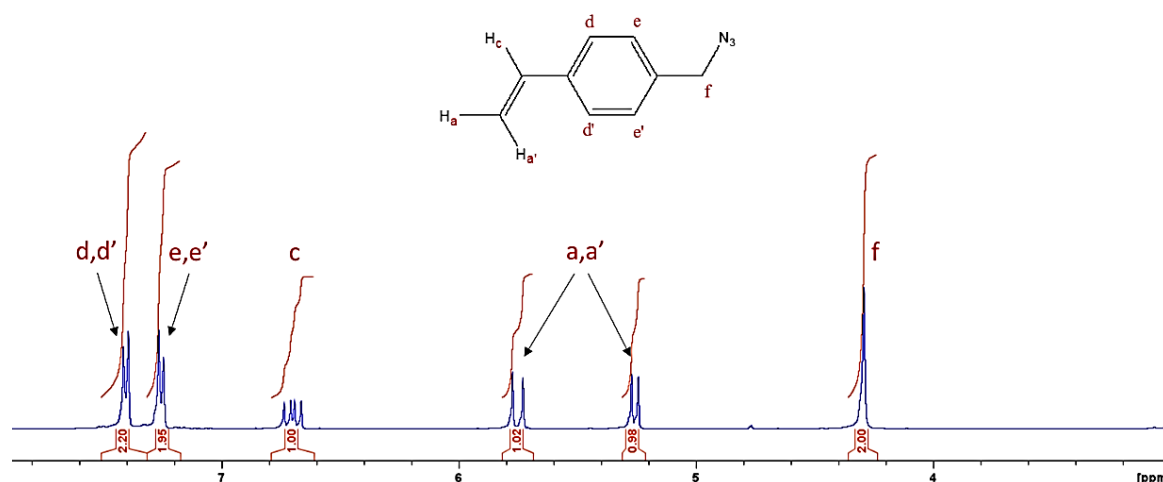


**Figure 4.1:**  $^1\text{H}$  NMR spectrum of monomer **2** in  $\text{CDCl}_3$ .

The presence of azide functionality in the monomer **2** was confirmed by comparing the FT-IR spectra of the starting material 4-vinylbenzyl chloride and the monomer **2** as shown in the **Figure 4.2**. The appearance of a stretching at  $2090\text{ cm}^{-1}$  in the spectrum of monomer **2** which

is in the absorption range of azide functionality, confirms a successful nucleophilic substitution reaction of the chloride by the azide group.

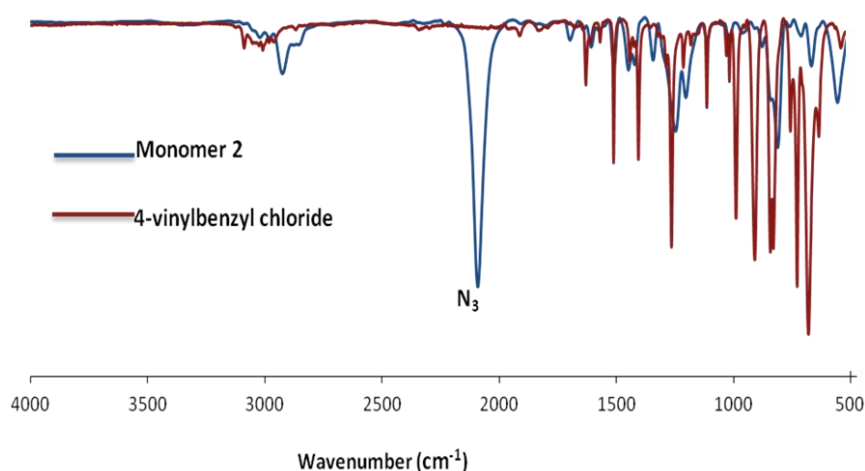


**Figure 4.2:** FT-IR spectra of 4-vinylbenzyl chloride and monomer **2**.

The structure of polymer **P0** was also confirmed by <sup>1</sup>H NMR and FT-IR spectroscopies. As shown in <sup>1</sup>H NMR spectrum of polymer **P0** (**Figure 4.3**) the disappearance of splitting patterns of vinylic protons between 5-6 ppm and at 6.7 ppm in <sup>1</sup>H NMR of the monomer **2** was compensated by the appearance of broad alkyl signals at 0.75-2 ppm, confirming a successful conversion of alkene functionality to alkyl units.

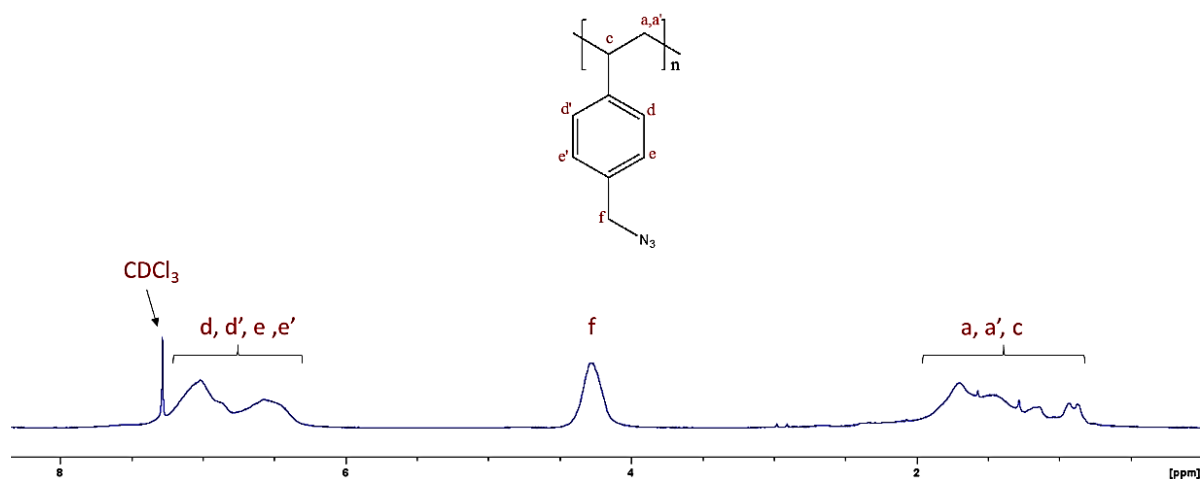


**Figure 4.3:** <sup>1</sup>H NMR spectrum of the polymer **P0** in CDCl<sub>3</sub>.

Due to the instability of the azide functional group at high temperatures, its retention throughout radical polymerization process was confirmed through comparison of FT-IR spectra of monomer **2** and polymer **P0**. Stretches typical for the azide functional group were observed at 2090 cm<sup>-1</sup> in both monomer **2** and polymer **P0** spectra (**Figure 4.4**).

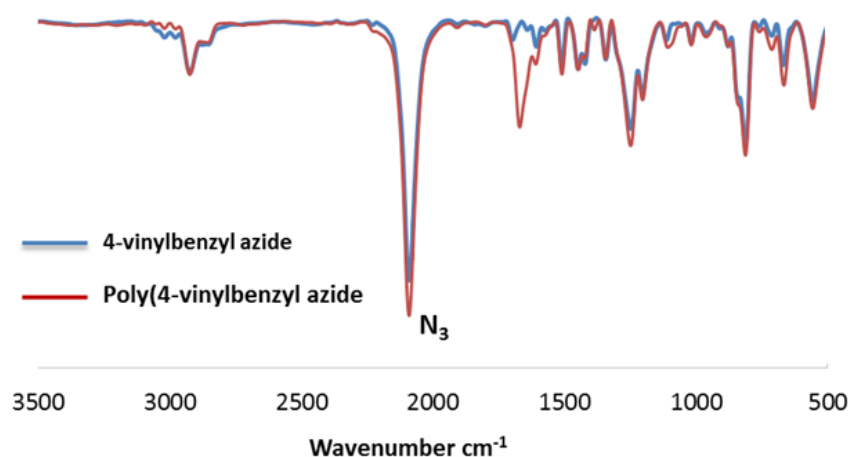


**Figure 4.4:** FT-IR spectra of monomer **2** and polymer **P0**.

### 4.3 Triazolyl coumarin based polymers with hydroxyethylene linkages between triazole and coumarin units

The synthesis of the polymers involved two alkynylated based coumarin molecules **7**, **11** with hydroxyethylene linkage between the terminal alkyne and the coumarin (**Figure 4.5**). For compound **7**, 7-diethylaminocoumarin was used as a fluorophore unit and the hydroxyethylene linkage was incorporated at 3-position of the coumarin motif while in compound **11**, 7-hydroxy-4-methylcoumarin was used as a fluorophore unit and the hydroxyethylene linkage was attached at position 8 of the coumarin motif. After the post-polymerization reaction under click conditions, all the polymers and alkyne functionalized molecules were tested for their chemosensing capabilities towards cations and anions. In all chemosensing studies, solutions of nitrates salts and tetrabutylammonium salts were used as cations and anions source respectively.

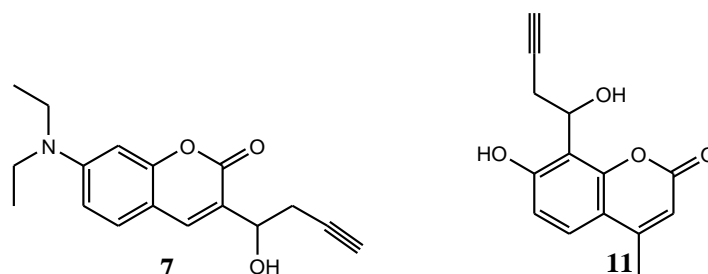


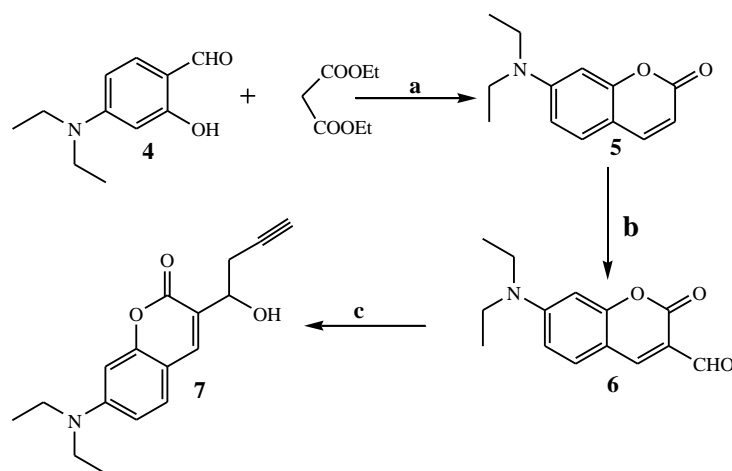
**Figure 4.5:** Structures of alkynylated coumarin derivatives **7**, **11**.

### 4.3.1 Triazolyl coumarin based polymers with the hydroxyethylene linkage at position 3 of the coumarin motif (P1)

Synthesis of polymer **P1** was accomplished in two stages. The first stage included a synthesis of alkynylated coumarin derivative **7**. The second stage involved a Cu(I) catalysed functionalization of polymer **P0** with alkynylated coumarin derivative **7** to yield polymer **P1** containing pendant chains with a triazole ring attached at position 3 of the coumarin motif *via* a hydroxyethylene linkage (**Scheme 4.1**).

#### 4.3.1.1 Synthesis of alkynylated coumarin derivative **7**

The synthesis of 7-(diethylamino)-3-(1-hydroxybut-3-ynyl)-2H-chromen-2-one (alkynylated coumarin derivative **7**) was accomplished in three steps from 4-(diethylamino)-2-hydroxybenzaldehyde as shown in the **Scheme 4.3**. Coumarins **5** and **6** were synthesized according to the reported literature.<sup>11</sup> In the presence of propargyl bromide, coumarin **6** was converted into an alkyne functionalized coumarin derivative **7** in a good yield using the reported procedure of zinc mediated regioselective Barbier reaction of propargylic bromide.<sup>12</sup>



**Scheme 4.3:** Synthesis of alkynylated coumarin **7** a) Piperidine, ethanol, HCl, AcOH, reflux; b) DMF, POCl<sub>3</sub>; c) Zn, THF, propargyl bromide, NH<sub>4</sub>Cl(aq).

The structures of coumarins **5**, **6** and **7** were characterized by NMR and mass spectrometry (for the <sup>13</sup>C NMR of coumarin **7** and <sup>1</sup>H NMRs of **5**, **6** and **7** see **Appendices** Figure A.10-A.12). **Figure 4.6** illustrates the assignment of proton signals in <sup>1</sup>H NMR spectrum of the coumarin derivative **7**. The appearance of the terminal alkyne proton (j) at 1.97 ppm, the hydroxyl proton (g) at 3.31 ppm and other three butynylic protons (h and i,i') at 4.75 ppm and 2.64-2.78 ppm respectively, confirms the structure of coumarin **7**.

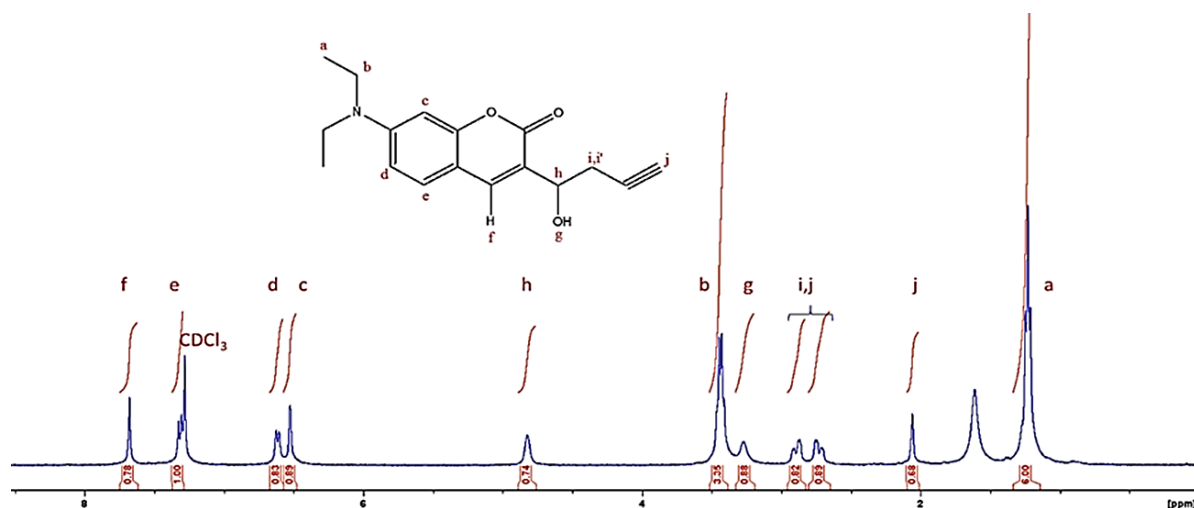
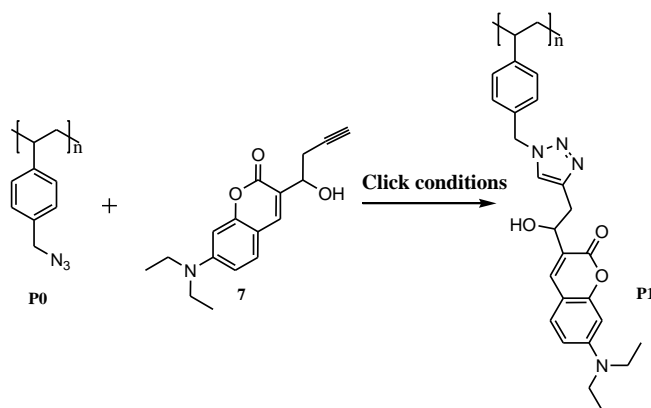


**Figure 4.6:**  $^1\text{H}$  NMR spectrum of alkylnated coumarin derivative **7** in  $\text{CDCl}_3$ .

#### 4.3.1.3 Functionalization of polymer **P0** using alkylnated coumarin derivative **7**

Polymer **P0** was functionalized with alkylnated coumarin **7** under a Cu(I)-mediated click reaction conditions as shown in **Scheme 4.4**. The reaction was performed at room temperature in THF in the presence of minimum amount of water. On completion of the reaction, the precipitated polymer was filtered and washed with water to afford polymer **P1** as yellow solid in 83% yield.



**Scheme 4.4:** Functionalization of Polymer **P0** with alkylnated coumarin **7**. Click conditions ( $\text{CuSO}_4 \cdot 5\text{H}_2\text{O}$ , NaAsc and PMDTA)

The structure of polymer **P1** was confirmed using  $^1\text{H}$  NMR and FT-IR spectroscopies. **Figure 4.7** below shows comparative  $^1\text{H}$  NMR spectra between polymer **P0**, alkylnated coumarin derivative **7** and the resulting polymer **P1**. Of interest, the proton signals from the starting materials were prominent as broad signals in the spectrum for polymer **P1**, confirming

successful synthesis. The average molecular weight and polydispersity index of **P1** were determined to be  $2.59 \times 10^4$  g/mol and 1.85 respectively.

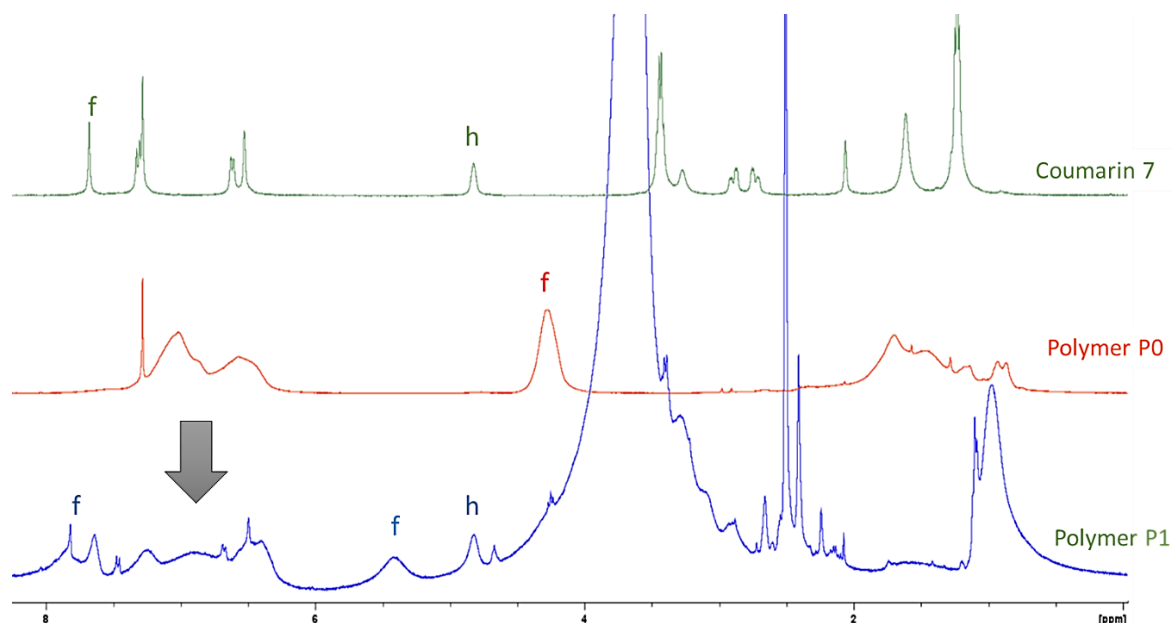


**Figure 4.7:**  $^1\text{H}$  NMR spectra of **P0**, the alkynylated coumarin derivative **7** and the polymer **P1**. For coumarin **7** and polymer **P0**  $\text{CDCl}_3$  solvent was used and  $\text{DMSO-d}_6$  was used for polymer **P1**.

**Figure 4.8** shows comparative FT-IR spectra of the starting polymer **P0** and the functionalized polymer **P1**. Noteworthy is a stretch at  $2090\text{ cm}^{-1}$  characteristic of the azide group which significantly decreased in polymer **P1** compared to the starting polymer **P0**. In addition, a peak for the hydroxyl group attached to the coumarin-triazole linkage also appeared in FT-IR spectrum of polymer **P1** at  $3385\text{ cm}^{-1}$ . These observations further confirmed the success of post-polymerization functionalization of polymer **P0** with alkynylated coumarin derivative **7**. The presence of the azide peak in polymer **P1** at  $2090\text{ cm}^{-1}$  suggested a partially functionalization of polymer **P0** *via* a triazole ring formation. This can be attributed to steric inaccessibility of the azide group in polymer **P0**. The degree of functionalization was determined to be 98% using the peak height method from FT-IR.<sup>13</sup>

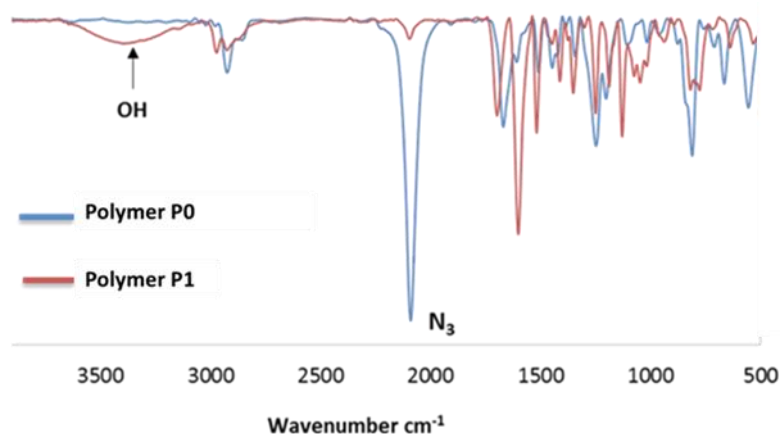


**Figure 4.8:** Comparison of FT-IR spectra of polymer **P0** and functionalized polymer **P1**.

#### 4.3.1.3 Absorption and emission studies of functionalized polymer **P0**

To further confirm the functionalization of polymer **P0** with alkynylated coumarin derivative **7**, the photophysical properties of polymer **P0** were compared with the photophysical properties of polymer **P1** and alkynylated coumarin derivative **7**. To verify if the isolated polymer is not one of the starting materials, DMF solutions containing the same amount (in grams) was used. As expected, polymer **P2** showed absorption and emission intensities with magnitude between the intensities of its starting materials (**Figure 4.9**). The Alkynylated coumarin derivative **7** with high content in coumarin chromophore showed higher absorption and emission intensities while polymer **P0** with a quenching azide group showed no UV-Vis absorption and weak emission band.

Furthermore, it was noted that both alkynylated coumarin derivative **7** and polymer **P1** exhibit same absorption and emission behaviours. They both exhibited two absorption peaks with different intensities (**Figure 4.9 a**). The strongest absorption wavelength ( $\lambda_{\max}$ ) was observed at 378 nm while the weak absorption appeared at 456 nm. In their emission spectra (**Figure 4.9 b**), the maximum emission wavelength ( $\lambda_{\max}$ ) was observed at 450 nm. This suggested that the changes in the functional group from alkyne to triazole ring during functionalization of polymer **P0** with alkynylated coumarin derivative **7** did not affect the emission coumarin fluorophore.

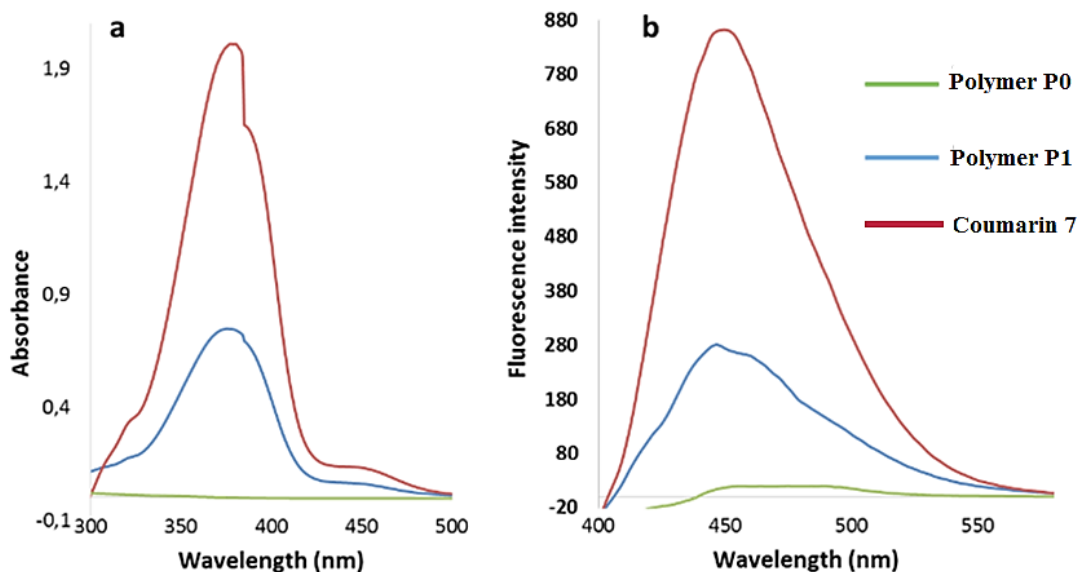


**Figure 4.9:** a) Absorption and b) emission spectra of alkynylated coumarin derivative **7** ( $10^{-6}$  g/L), polymer **P0** ( $10^{-6}$  g/L) and polymer **P1** ( $10^{-6}$  g/L) in DMF. The excitation was performed at 385 nm.

As the incorporation of alkynylated coumarin derivative **7** into polymer **P0** resulted in a polymer with improved optical properties which is in between the optical properties of the two starting materials, it can be concluded that the functionalization of polymer **P0** was successful. Furthermore, the similarities in the photophysical properties of alkynylated coumarin derivative **7** and polymer **P1** suggested that the photophysical properties of polymer **P1** depends on coumarin units from alkynylated coumarin derivative **7**.

#### 4.3.1.4 Chemosensing studies

As polymer **P1** formation involves a change in the functionality from alkyne functional group in alkynylated coumarin derivative **7** to triazole in polymer **P1**, the chemosensing capabilities of both coumarin **7** and polymer **P1** in the presence of various ions have been investigated and compared in order to understand the sensing mechanism in polymer **P1**. In all chemosensing studies, solutions of nitrates salts and tetrabutylammonium salts were used as cations and anions source respectively.



---

(i) Chemosensing studies of alkynylated coumarin derivative **7**

a) Absorption

The chemosensing capabilities of alkynylated coumarin **7** for cationic and anionic species were initially investigated by UV-Vis spectral analysis. The studies were carried out in DMF at room temperature in the presence of different metal ions including monovalent, divalent and trivalent ( $\text{Na}^+$ ,  $\text{Ca}^{2+}$ ,  $\text{Ag}^+$ ,  $\text{Al}^{3+}$ ,  $\text{Ba}^{2+}$ ,  $\text{Cr}^{3+}$ ,  $\text{Cu}^{2+}$ ,  $\text{Fe}^{3+}$ ,  $\text{Hg}^{2+}$ ,  $\text{Mn}^{2+}$ ,  $\text{Co}^{2+}$ ,  $\text{Zn}^{2+}$ ,  $\text{Cd}^{2+}$ ,  $\text{Ni}^{2+}$  and  $\text{Pb}^{2+}$ ) and different anionic species ( $\text{H}_2\text{PO}_4^-$ ,  $\text{F}^-$ ,  $\text{Cl}^-$ ,  $\text{Br}^-$ ,  $\text{HSO}_4^-$ ,  $\text{ClO}_4^-$ ,  $\text{OH}^-$ ,  $\text{I}^-$ ,  $\text{NO}_3^-$ ,  $\text{AcO}^-$  and  $\text{CN}^-$ ). As shown in the **Figure 4.10 a**, all the tested metal ions, except  $\text{Fe}^{3+}$  and  $\text{Hg}^{2+}$  did not show any detectable changes in the alkynylated coumarin derivative **7** absorption bands. The presence of  $\text{Hg}^{2+}$  resulted to a decrease in the intensity of the maximum absorption band at 378 nm and an increase in the intensity of the small absorption band at 456 nm. This can be attributed to the change in the push-pull character of 7-diethylaminocoumarin moiety due to metal binding.<sup>14</sup> The presence of  $\text{Fe}^{3+}$  greatly enhanced alkynylated coumarin **7** absorption and this higher intensity can be attributed to  $\text{Fe}^{3+}$  ions self-absorption as almost the same absorption was obtained in the absence of coumarin **7**.

In the case of anions as shown in the **Figure 4.10 b**, none of the tested anions resulted in an obvious change in the absorption bands of alkynylated coumarin **7**.

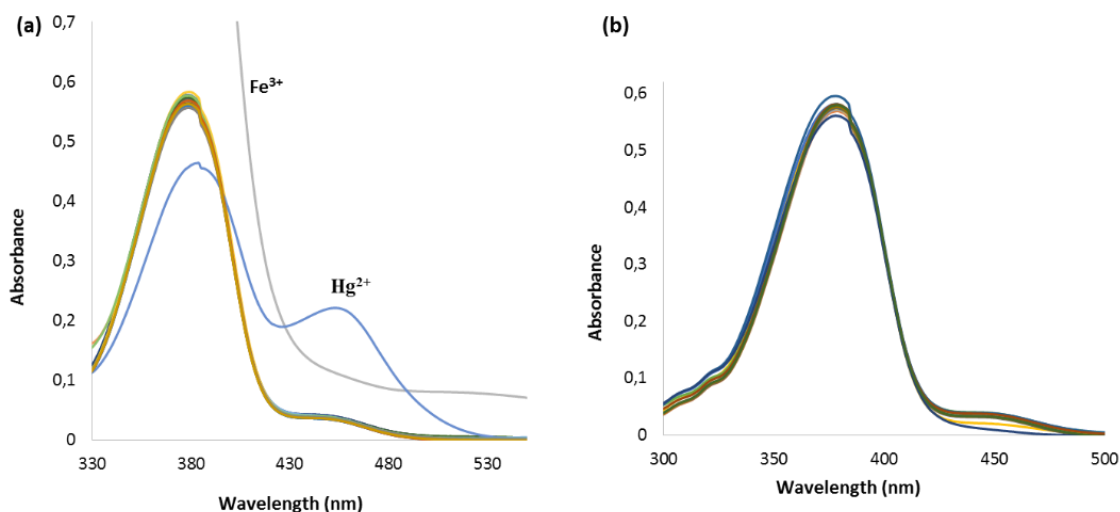


**Figure 4.10:** Absorption spectra of alkynylated coumarin **7** ( $1.7 \times 10^{-5}$  M) in the presence of the aliquot ( $3 \times 10^{-4}$  M) of **a**) different metal ions ( $\text{Na}^+$ ,  $\text{Ca}^{2+}$ ,  $\text{Ag}^+$ ,  $\text{Al}^{3+}$ ,  $\text{Ba}^{2+}$ ,  $\text{Cr}^{3+}$ ,  $\text{Cu}^{2+}$ ,  $\text{Fe}^{3+}$ ,  $\text{Hg}^{2+}$ ,  $\text{Mn}^{2+}$ ,  $\text{Co}^{2+}$ ,  $\text{Zn}^{2+}$ ,  $\text{Cd}^{2+}$ ,  $\text{Ni}^{2+}$  and  $\text{Pb}^{2+}$ ); **b**) different anions ( $\text{H}_2\text{PO}_4^-$ ,  $\text{F}^-$ ,  $\text{Cl}^-$ ,  $\text{Br}^-$ ,  $\text{HSO}_4^-$ ,  $\text{ClO}_4^-$ ,  $\text{OH}^-$ ,  $\text{I}^-$ ,  $\text{NO}_3^-$ ,  $\text{AcO}^-$  and  $\text{CN}^-$ ).

As UV-Vis chemosensing studies of alkynylated coumarin derivative **7** showed a selective interaction with  $\text{Hg}^{2+}$ , titration experiments under the same conditions were conducted in order to understand the interaction between alkynylated coumarin derivative **7** and  $\text{Hg}^{2+}$  ions. Upon addition of aliquots of  $\text{Hg}^{2+}$  to the DMF solution of coumarin derivative **7** (**Figure 4.11**) a gradual increase in maximum absorption band at 456 nm and a gradual decrease in absorption band at 378 nm with a weak red shift were detected. This suggests that push-pull character of 7-diethylaminocoumarin moieties is further affected by the presence of  $\text{Hg}^{2+}$  ions. Furthermore, a clear isosbestic point was observed at 410 nm suggesting formation of complex between alkynylated coumarin derivative **7** and  $\text{Hg}^{2+}$ .

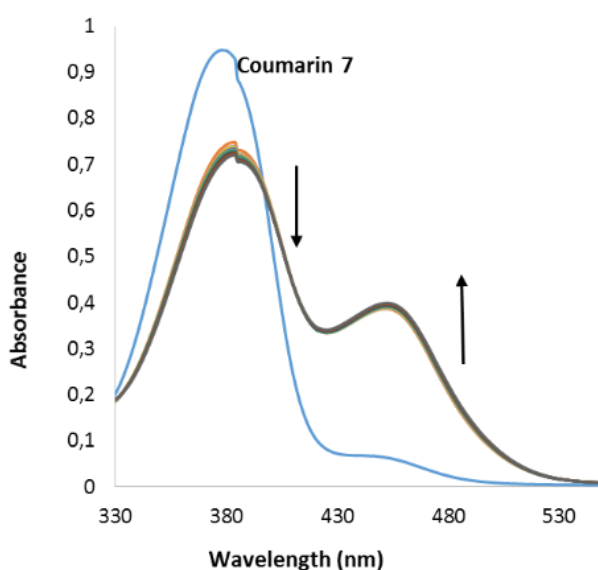


**Figure 4.11:** The absorption spectra of alkynylated coumarin derivative **7** ( $3.4 \times 10^{-5}$  M) in DMF upon addition of increasing amount of  $\text{Hg}^{2+}$  ( $3 \times 10^{-4}$  M).

#### *b) Emission studies*

The chemosensing capability of alkynylated coumarin derivative **7** was also investigated using the emission spectra in the presence of the same metal ions and anions applied in the UV-Vis analysis. The studies were carried out at room temperature in DMF at the excitation wavelength of 385 nm. Once again the presence of metal ions except  $\text{Fe}^{3+}$  and  $\text{Hg}^{2+}$  showed minimal changes in alkynylated coumarin derivative **7** emission band at 452 nm (**Figure 4.12 a**). The presence of  $\text{Fe}^{3+}$  induced a weak fluorescence quenching response of up to 31% of original fluorescence intensity while  $\text{Hg}^{2+}$  induced strong fluorescence quenching responses of up to 87%. This quenching response was due to the heavy atom effect which decreases the lifetime

of the singlet state of the fluorophore<sup>15</sup> and  $\pi$ -philic nature of  $\text{Hg}^{2+}$ .<sup>16</sup> This selective sensitivity of coumarin derivative **7** towards  $\text{Hg}^{2+}$  suggests its potential application as an “ON-OFF” chemosensor for  $\text{Hg}^{2+}$  ions.

Similarly to the corresponding UV-Vis studies, the emission band of alkynylated coumarin **7** was not affected by any of the tested anions (**Figure 4.12 b**).

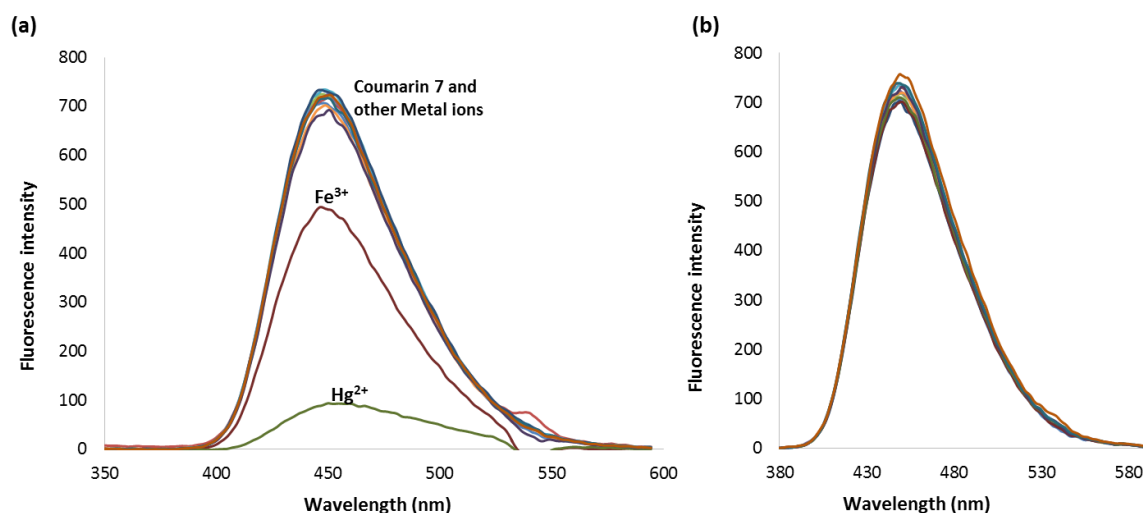


**Figure 4.12:** Emission spectra of alkynylated coumarin **7** ( $2 \times 10^{-6}$  M) **a**) in the presence of the aliquot ( $6.5 \times 10^{-5}$  M) of different metal ions ( $\text{Na}^+$ ,  $\text{Ca}^{2+}$ ,  $\text{Ag}^+$ ,  $\text{Al}^{3+}$ ,  $\text{Ba}^{2+}$ ,  $\text{Cr}^{3+}$ ,  $\text{Cu}^{2+}$ ,  $\text{Fe}^{3+}$ ,  $\text{Hg}^{2+}$ ,  $\text{Mn}^{2+}$ ,  $\text{Co}^{2+}$ ,  $\text{Zn}^{2+}$ ,  $\text{Cd}^{2+}$ ,  $\text{Ni}^{2+}$  and  $\text{Pb}^{2+}$ ); **b**) in the presence of the aliquot ( $6.5 \times 10^{-5}$  M) of various anions ( $\text{H}_2\text{PO}_4^-$ ,  $\text{F}^-$ ,  $\text{Cl}^-$ ,  $\text{Br}^-$ ,  $\text{HSO}_4^-$ ,  $\text{ClO}_4^-$ ,  $\text{OH}^-$ ,  $\text{I}^-$ ,  $\text{NO}_3^-$ ,  $\text{AcO}^-$  and  $\text{CN}^-$ ). Excitation was performed at 385 nm.

The sensitivity of alkynylated coumarin **7** towards  $\text{Hg}^{2+}$  was further investigated using fluorescence titration experiments (**Figure 4.13**). Upon addition of aliquots of  $\text{Hg}^{2+}$  ( $0.15 \mu\text{M}$ ) to a DMF solution of alkynylated coumarin **7** a gradual decrease in the emission band at 452 nm was detected. The inset of **Figure 4.13** shows the plot of emission intensity of alkynylated coumarin **7** at 385 nm against the concentration of added  $\text{Hg}^{2+}$  and a linear relationship with a correlation coefficient of  $R^2=0.9834$  was obtained in the range of 0-0.6  $\mu\text{M}$ . The detection limit of **7** towards  $\text{Hg}^{2+}$  was determined according to the IUPAC definition ( $C_{\text{DL}}=3S_b/m$ ), where  $S_b$  stands for the standard deviation of blank solutions while  $m$  is a slope. The detection limit was calculated within a linear range of 0-0.6  $\mu\text{M}$  and was found to be 0.1  $\mu\text{M}$  indicating the high sensitivity of alkynylated coumarin **7** towards  $\text{Hg}^{2+}$  ions.

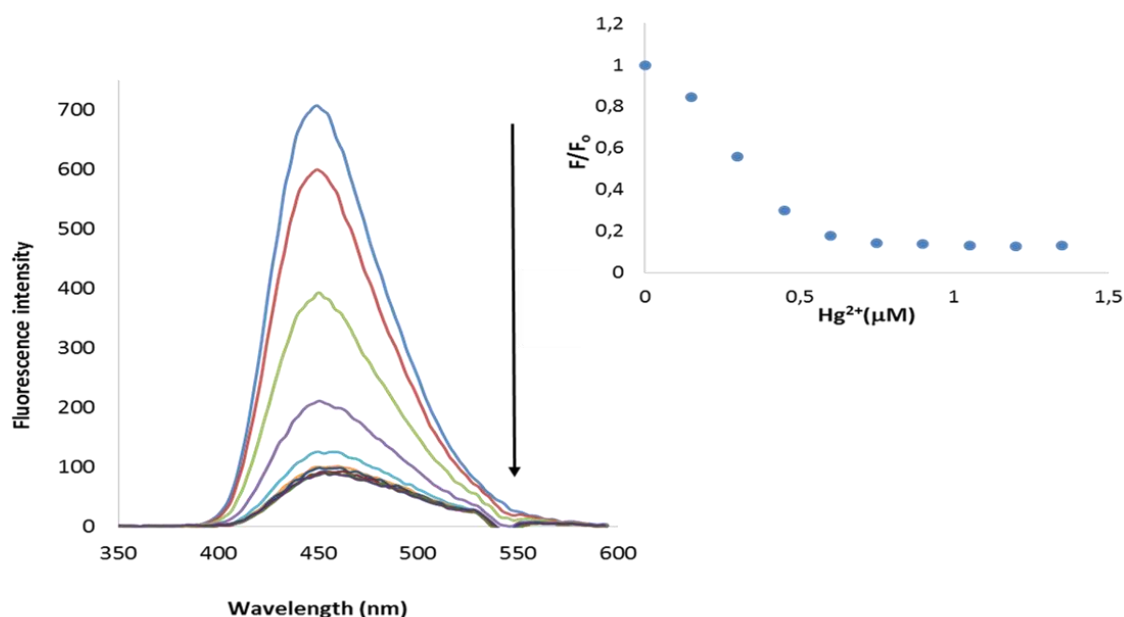


**Figure 4.13:** Emission spectra of alkynylated coumarin derivative **7** ( $2 \times 10^{-6}$  M) in DMF upon addition of  $\text{Hg}^{2+}$  (0-1.35  $\mu\text{M}$ ) aliquots. The excitation was performed at 385 nm. ( $F_0$ : Emission intensity of the alkynylated coumarin derivative **7** in absence  $\text{Hg}^{2+}$  and  $F$ : Emission intensity of the alkynylated coumarin derivative **7** in presence of  $\text{Hg}^{2+}$ ).

*c) Competitive studies*

The influence of other metal ions on the selective sensitivity of alkynylated coumarin derivative **7** towards  $\text{Hg}^{2+}$  was also investigated through competitive experiments. These involved emission spectra analysis of alkynylated coumarin derivative **7** in the presence of  $\text{Hg}^{2+}$  and 2.0 equivalents of other metal ions ( $\text{Na}^+$ ,  $\text{Ca}^{2+}$ ,  $\text{Ag}^+$ ,  $\text{Ba}^{2+}$ ,  $\text{Cr}^{3+}$ ,  $\text{Cu}^{2+}$ ,  $\text{Fe}^{3+}$ ,  $\text{Mn}^{2+}$ ,  $\text{Co}^{2+}$ ,  $\text{Zn}^{2+}$ ,  $\text{Cd}^{2+}$ ,  $\text{Ni}^{2+}$  and  $\text{Pb}^{2+}$ ). The emission spectra were recorded in DMF at room temperature using the same excitation wavelength as in the previous experiments. As shown in **Figure 4.14**, the fluorescence quenching response induced by the presence of  $\text{Hg}^{2+}$  ions was not significantly affected by the presence of other metal ions. This indicates that alkynylated coumarin derivative **7** and  $\text{Hg}^{2+}$  forms a stable complex, which cannot be interfered by the presence of other metal ions.

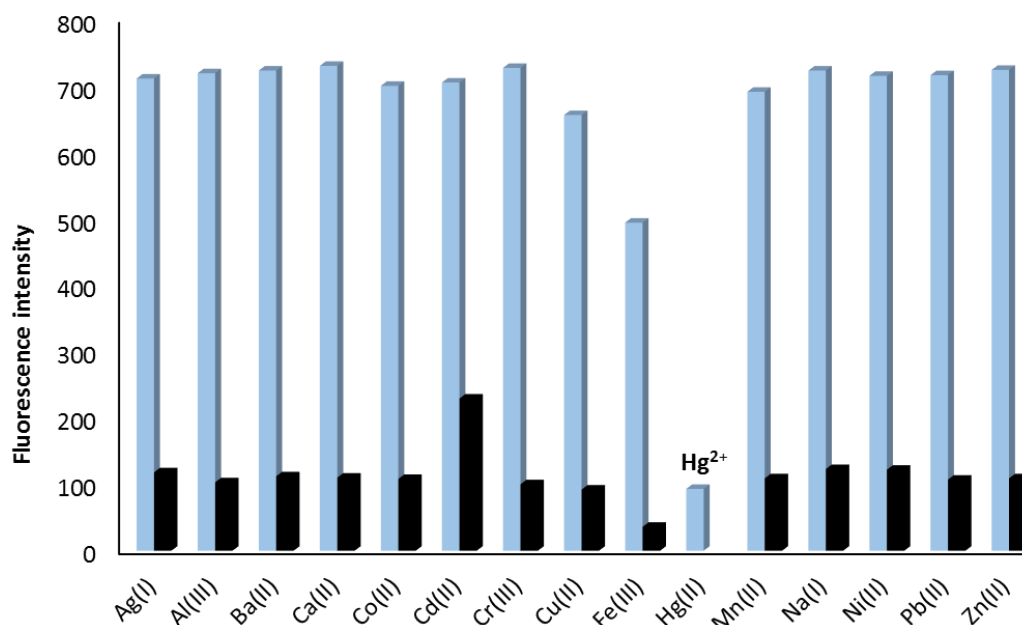


**Figure 4.14:** Fluorescence response of alkynylated coumarin derivative **7** ( $2 \times 10^{-6}$  M) in the presence of metal ions ( $2 \mu\text{M}$ )  $\text{Na}^+$ ,  $\text{Ca}^{2+}$ ,  $\text{Ag}^+$ ,  $\text{Al}^{3+}$ ,  $\text{Ba}^{2+}$ ,  $\text{Cr}^{3+}$ ,  $\text{Cu}^{2+}$ ,  $\text{Fe}^{3+}$ ,  $\text{Hg}^{2+}$ ,  $\text{Mn}^{2+}$ ,  $\text{Co}^{2+}$ ,  $\text{Zn}^{2+}$ ,  $\text{Cd}^{2+}$ ,  $\text{Ni}^{2+}$  and  $\text{Pb}^{2+}$  (blue bars) and in the presence of mixture of  $\text{Hg}^{2+}$  ( $2 \mu\text{M}$ ) with two equivalents ( $4 \mu\text{M}$ ) of other metal ions (black bars). Excitation was performed at 385 nm.

*d) The proposed binding modes of alkynylated coumarin derivative 7 with  $\text{Hg}^{2+}$*

To get an insight into the binding stoichiometry of alkynylated coumarin derivative **7**- $\text{Hg}^{2+}$  complexes, a Job plot analysis was conducted. This was achieved using the continuous variation method in which the total concentration of added  $\text{Hg}^{2+}$  and alkynylated coumarin derivative **7** were kept constant ( $7 \times 10^{-11}$  M) and with a variation of their relative proportions.<sup>17</sup> The plot of emission intensity versus the molar fraction of  $\text{Hg}^{2+}$  at 385 nm is shown **Figure 4.15 a**. Notable, the maximum was reached when the molar fraction was 0.5 suggesting a 1:1 stoichiometry of  $\text{Hg}^{2+}$ -alkynylated coumarin derivative **7** complexation.

The binding constant ( $K_a$ ) of the alkynylated coumarin **7** towards  $\text{Hg}^{2+}$  was evaluated graphically using the Benesi-Hildebrand method.<sup>18</sup> As shown in **Figure 4.15 b**,  $1/F_0 - F$  was plotted versus  $1/[\text{Hg}^{2+}]$  and the data were linearly fitted. The calculated value of  $K_a$  from the slope and intercept of the line was  $7 \times 10^5$  M.

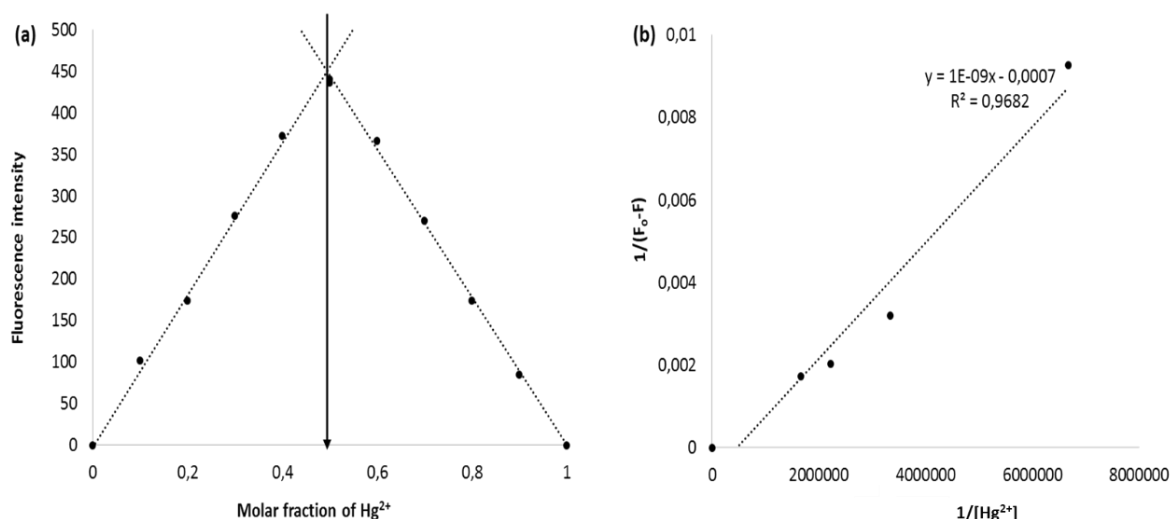


**Figure 4.15:** a) A Job plot for alkynylated coumarin derivative **7**- $\text{Hg}^{2+}$  complexation with a constant total concentration of  $7 \times 10^{-11}$  M; b) Benesi-Hildebrand plot of alkynylated coumarin derivative **7** with  $\text{Hg}^{2+}$ . The spectra were recorded in DMF at 385 nm.

In order to understand the binding behaviours of alkynylated coumarin derivative **7** with  $\text{Hg}^{2+}$ ,  $^1\text{H}$  NMR titration experiments of coumarin derivative **7** in the presence of increasing amounts of  $\text{Hg}^{2+}$  were conducted. The experiments were conducted in  $\text{DMSO-d}_6$  as shown in **Figure 4.16**. Upon addition of  $\text{Hg}^{2+}$ , the proton signal at 5.55 ppm which was assigned to the hydroxyl group of the functional linkage shifted downfield and simultaneously the terminal alkyne proton signal slightly shifted upfield with no other signal affected by  $\text{Hg}^{2+}$ .

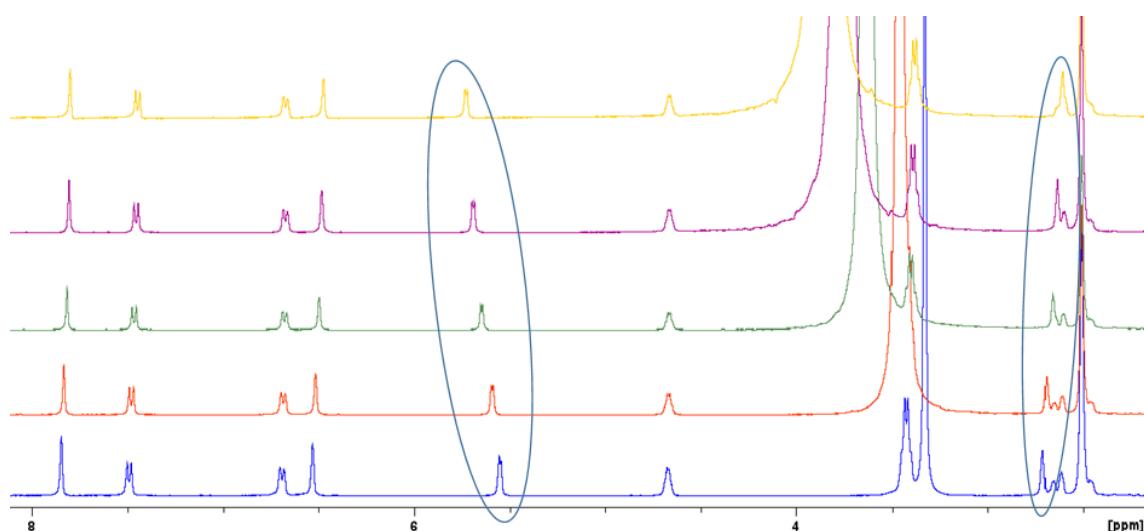
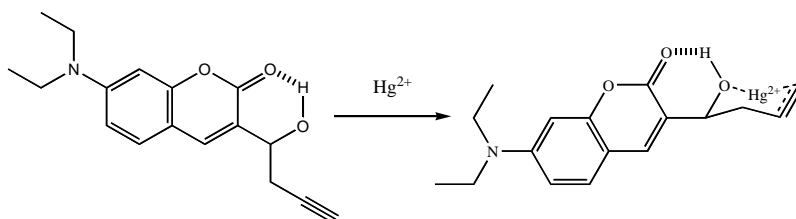


**Figure 4.16:** Changes in the  $^1\text{H}$  NMR signal of the alkynylated coumarin **7** with increasing amounts of  $\text{Hg}^{2+}$  in  $\text{DMSO-d}_6$ .

Since the Job plot analysis indicated 1:1 stoichiometry of  $\text{Hg}^{2+}$ -alkynylated coumarin derivative **7** complex, and from NMR data only protons from the hydroxyl group of the functional linkage and terminal alkyne were affected, it was then proposed that the complexation of  $\text{Hg}^{2+}$  involves three functional groups; carbonyl, hydroxyl and alkyne *via* 2 six membered rings. The  $\text{Hg}^{2+}$  forms a bidentate interaction with hydroxyl oxygen of functional linkage and terminal alkyne while the hydroxyl proton interacts with carbonyl oxygen *via* hydrogen bonding. This results in two six membered rings as shown in the **Scheme 4.5**.



**Scheme 4.5:** A proposed binding mode of alkynylated coumarin derivative **7** with  $\text{Hg}^{2+}$ .

(ii) *Chemosensing studies of polymer P1*

a) *Cations chemosensing*

❖ *Absorption studies*

Using the same principle as in alkynylated coumarin derivative **7**, chemosensing capabilities of polymer **P1** towards metal ions were initially investigated using UV-Visible spectral analysis. Same conditions and the same set of metal ions as in alkynylated coumarin derivative **7** were used in the studies. As shown in the **Figure 4.17 a** All the tested metal ions, except  $\text{Fe}^{3+}$  and  $\text{Hg}^{2+}$  did not show detectable changes in the absorption band of polymer **P1** at 381 nm. Similar to alkynylated coumarin derivative **7**,  $\text{Fe}^{3+}$  self-absorption caused a strong increase in absorption while the presence of  $\text{Hg}^{2+}$  showed a slight bathochromic shift in absorption from 378 to 381 nm (**Figure 4.17 b**).

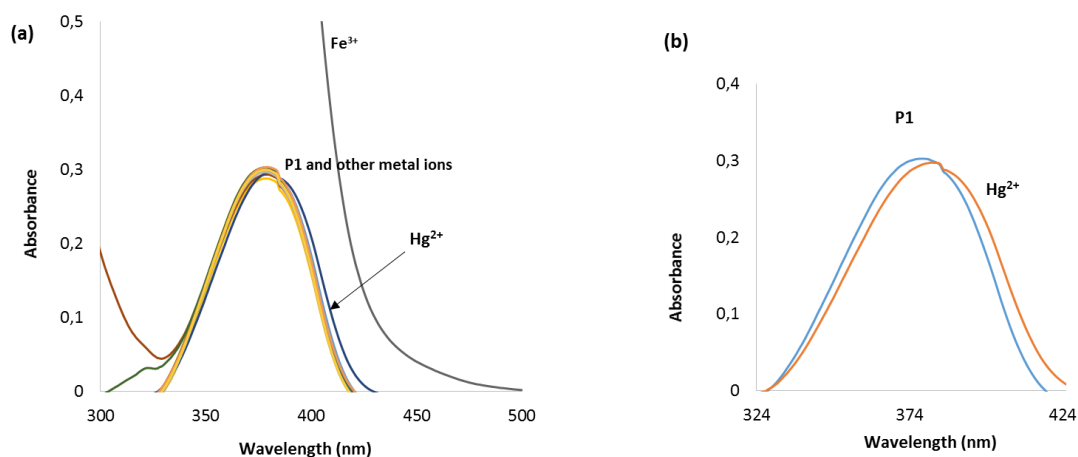


**Figure 4.17:** a) Absorption spectra of polymer **P1** (0.096 g/L) in the presence of various metal ions (1  $\mu\text{M}$ ) ( $\text{Na}^+$ ,  $\text{Ca}^{2+}$ ,  $\text{Ag}^+$ ,  $\text{Al}^{3+}$ ,  $\text{Ba}^{2+}$ ,  $\text{Cr}^{3+}$ ,  $\text{Cu}^{2+}$ ,  $\text{Fe}^{3+}$ ,  $\text{Hg}^{2+}$ ,  $\text{Mn}^{2+}$ ,  $\text{Co}^{2+}$ ,  $\text{Zn}^{2+}$ ,  $\text{Cd}^{2+}$ ,  $\text{Ni}^{2+}$  and  $\text{Pb}^{2+}$ ); b) Absorption spectra of polymer **P1** and polymer **P1** in the presence of  $\text{Hg}^{2+}$ .

❖ *Emission studies*

The chemosensing capability of polymer **P1** towards different metal ions was also investigated through emission spectra in the presence of same metal ions used in UV-Vis analysis. As shown in the **Figure 4.18**, all the tested metal ions except  $\text{Fe}^{3+}$  and  $\text{Hg}^{2+}$  showed very small influence on the emission band of polymer **P1** at 452 nm.

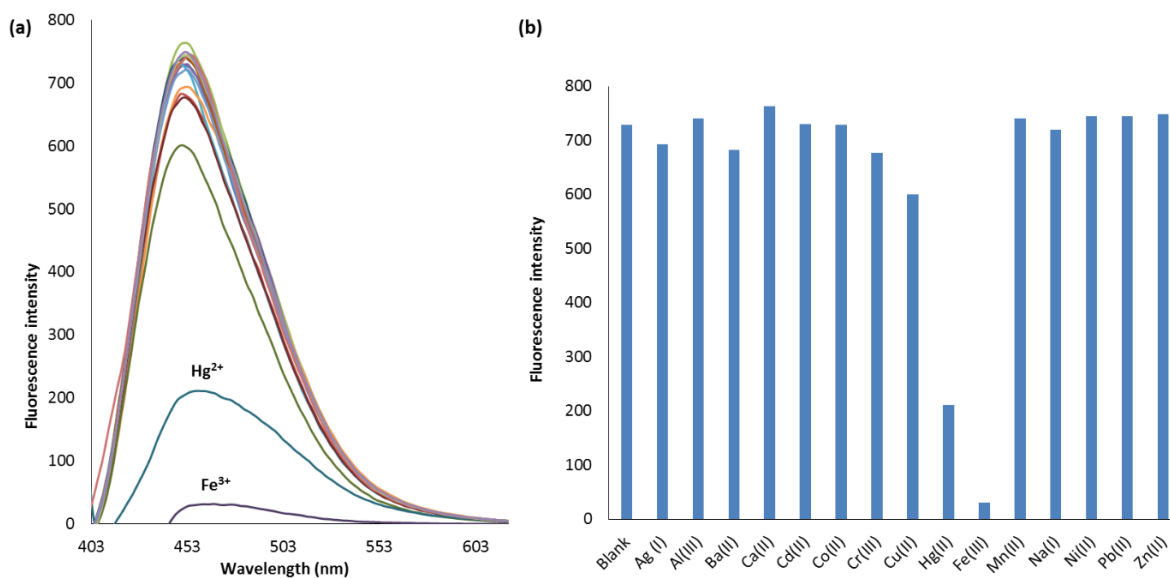


**Figure 4.18:** a) Emission spectra and b) Emission response of polymer **P1** ( $4 \times 10^{-5}$  g/L) in the presence of (1.5  $\mu\text{M}$ ) of  $\text{Na}^+$ ,  $\text{Ca}^{2+}$ ,  $\text{Ag}^+$ ,  $\text{Al}^{3+}$ ,  $\text{Ba}^{2+}$ ,  $\text{Cr}^{3+}$ ,  $\text{Cu}^{2+}$ ,  $\text{Fe}^{3+}$ ,  $\text{Hg}^{2+}$ ,  $\text{Mn}^{2+}$ ,  $\text{Co}^{2+}$ ,  $\text{Zn}^{2+}$ ,  $\text{Cd}^{2+}$ ,  $\text{Ni}^{2+}$  and  $\text{Pb}^{2+}$ . Excitation was performed at 385 nm.



The presence of either  $\text{Fe}^{3+}$  or  $\text{Hg}^{2+}$  greatly affected the emission band of polymer **P1** with fluorescence quenching response.  $\text{Fe}^{3+}$  showed a strongest response of up to 96 % quenching of the original fluorescence intensity while 71 % quenching was observed in presence of  $\text{Hg}^{2+}$ .

❖ *Titration experiments for  $\text{Fe}^{3+}$  and  $\text{Hg}^{2+}$*

The UV-Vis titrations were conducted by the gradual addition of  $\text{Fe}^{3+}$  or  $\text{Hg}^{2+}$  to the DMF solution of polymer **P1**. As shown in **Figure 4.19 a** the addition of  $\text{Fe}^{3+}$  (0.1  $\mu\text{M}$ ) resulted in gradual increase in absorption band at 378 nm with a weak hypsochromic shift from 378 to 372 nm while a gradual decrease in absorption band at 378 nm accompanied with a weak bathochromic shift from 378 to 383 nm was observed when  $\text{Hg}^{2+}$  (0.1  $\mu\text{M}$ ) was added (**Figure 4.19 b**). Furthermore, the addition of  $\text{Hg}^{2+}$  caused an increase in the absorption peak at 456 nm for polymer **P1** but not to the same extent as in the alkynylated coumarin derivative **7**. These observations suggested a different binding mode between  $\text{Hg}^{2+}$  and polymer **P1**.

In the same way as in the case of alkynylated coumarin derivative **7**, a clear isosbestic point was detected in the polymer **P1** absorption spectra at 397 nm indicating complex formation between polymer **P1** and  $\text{Hg}^{2+}$ . The difference in absorption behaviours of polymer **P1** towards  $\text{Fe}^{3+}$  and  $\text{Hg}^{2+}$  could be attributed to different coordination modes of polymer **P1** with  $\text{Fe}^{3+}$  or  $\text{Hg}^{2+}$  which can be used to distinguish between the two ions even if they both lead to the quenching of fluorescence of the polymer.

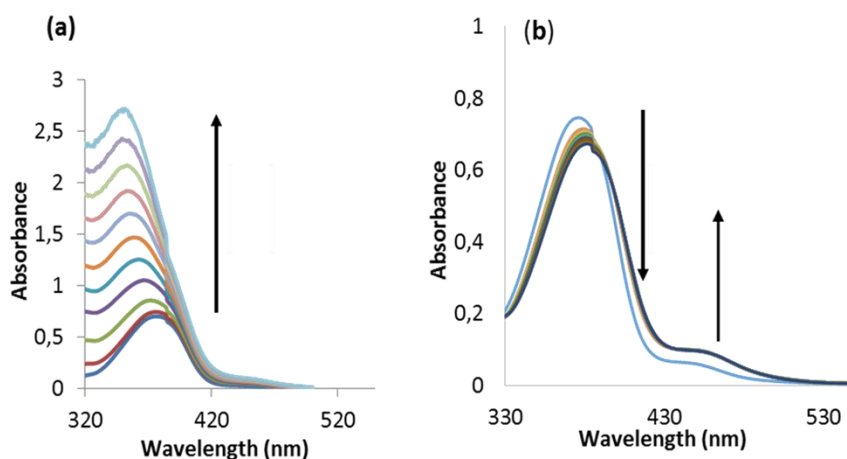


**Figure 4.19:** The absorption spectra of polymer **P1** (0.02 g/L) in DMF upon addition of increasing amount of **a**)  $\text{Fe}^{3+}$  (0.1  $\mu\text{M}$ ) and **b**)  $\text{Hg}^{2+}$  (1  $\mu\text{M}$ ).

In the fluorescence titration experiments (**Figure 4.20**), the addition of either  $\text{Fe}^{3+}$  or  $\text{Hg}^{2+}$  ( $0.025 \mu\text{M}$ ) to a solution of polymer **P1** induced a gradual decrease in the emission intensity at 452 nm. The plot of emission intensity of polymer **P1** at 385 nm against the concentration of added  $\text{Fe}^{3+}$  (Inset **Figure 4.20 a**) or  $\text{Hg}^{2+}$  (Inset **Figure 4.20 b**) showed a linear relationship with a correlation coefficient of  $R^2=0.9495$  and  $R^2=0.9906$  respectively. The detection limits of polymer **P1** towards  $\text{Fe}^{3+}$  and  $\text{Hg}^{2+}$  were determined according to the IUPAC definition ( $C_{\text{DL}}=3S_b/m$ ), where  $S_b$  stands for the standard deviation of blank solutions and  $m$  for slope. The detection limit was found to be  $0.0153 \mu\text{M}$  for  $\text{Hg}^{2+}$  within a linear response range of ( $0-0.125 \mu\text{M}$ ) and  $0.0244 \mu\text{M}$  for  $\text{Fe}^{3+}$  within a linear response range of  $0.025-0.377 \mu\text{M}$ . These low detection limits indicate that polymer **P1** has a higher sensitivity towards  $\text{Fe}^{3+}$  and  $\text{Hg}^{2+}$  ions.

Furthermore, by comparing the detection limit of alkynylated coumarin derivative **7** ( $0.1 \mu\text{M}$ ) and its corresponding polymer **P1** ( $0.0153 \mu\text{M}$ ) towards  $\text{Hg}^{2+}$ , it was found that polymer **P1** is ten times more sensitive than alkynylated coumarin derivative **7**. This confirms the higher sensitivity associated with polymeric materials due to collective properties of fluorophores in a polymer backbone.

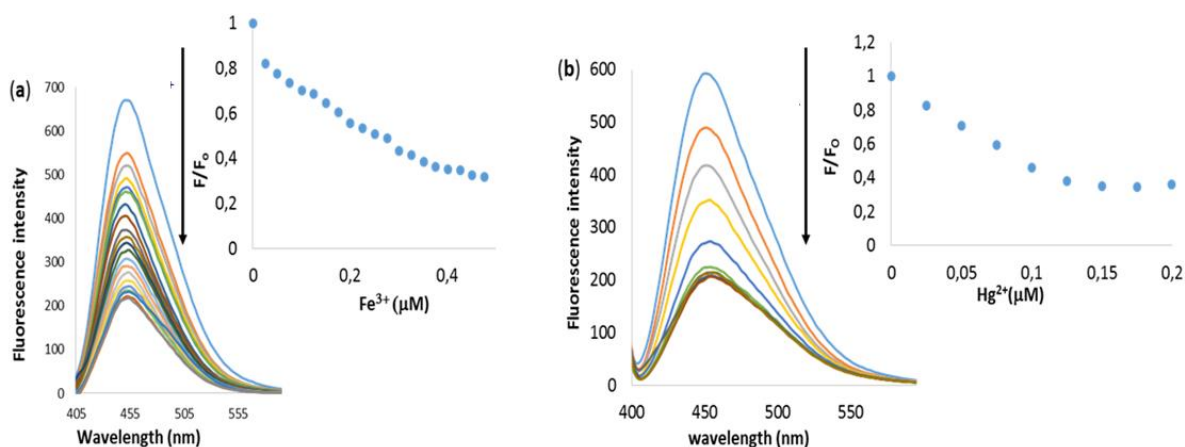


**Figure 4.20:** Emission spectra of polymer **P1** ( $4 \times 10^{-5} \text{ g/L}$ ) in DMF upon addition of increasing amounts of **a**)  $\text{Fe}^{3+}$  ( $0-0.376 \mu\text{M}$ ) and **b**)  $\text{Hg}^{2+}$  from ( $0-0.225 \mu\text{M}$ ). The excitation was performed at 385 nm.

#### ❖ *Competitive studies*

To investigate the influence of other metal ions on the **P1-Fe<sup>3+</sup>** and **P1-Hg<sup>2+</sup>** interactions, competitive experiments were conducted. These experiments were performed in the presence

of  $\text{Fe}^{3+}$  or  $\text{Hg}^{2+}$  mixed with 2.0 equivalents of other metal ions such as  $\text{Na}^+$ ,  $\text{Ca}^{2+}$ ,  $\text{Ag}^+$ ,  $\text{Ba}^{2+}$ ,  $\text{Cr}^{3+}$ ,  $\text{Cu}^{2+}$ ,  $\text{Fe}^{3+}$ ,  $\text{Mn}^{2+}$ ,  $\text{Co}^{2+}$ ,  $\text{Zn}^{2+}$ ,  $\text{Cd}^{2+}$ ,  $\text{Ni}^{2+}$  and  $\text{Pb}^{2+}$ . The emission spectra were recorded in DMF at room temperature using an excitation wavelength of 385 nm. As shown in **Figure 4.21**, the fluorescence quenching response induced by the presence of  $\text{Hg}^{2+}$  or  $\text{Fe}^{3+}$  ions was not significantly affected by the presence of 2.0 equivalents of other metal ions. However, the quenching response caused by the presence of  $\text{Hg}^{2+}$  ions was affected by the presence of  $\text{Fe}^{3+}$  and enhanced fluorescence quenching was detected. Overall, these shows that the presence of competing metal ions do not significantly affect **P1**- $\text{Fe}^{3+}$  and **P1**- $\text{Hg}^{2+}$  bindings.

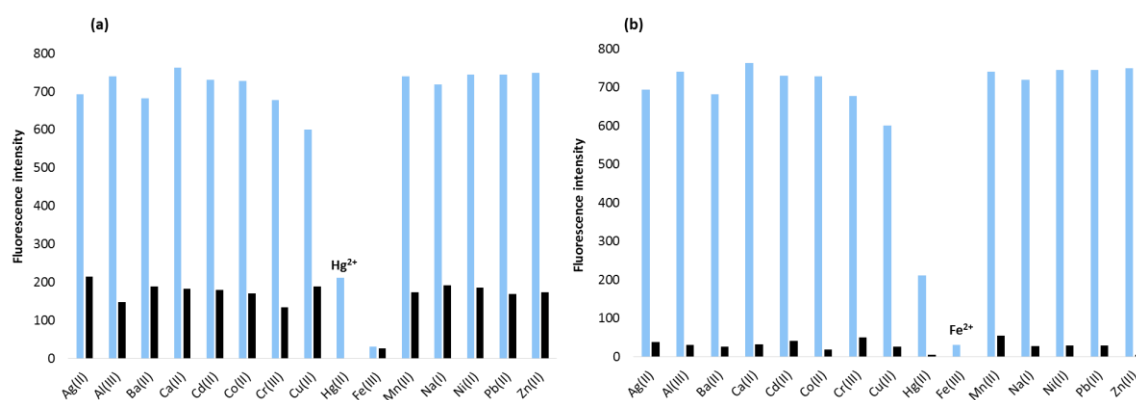


**Figure 4.21:** Fluorescence response of **P1** ( $4 \times 10^{-5}$  g/L) in the presence of metal ions ( $1.5 \mu\text{M}$ )  $\text{Na}^+$ ,  $\text{Ca}^{2+}$ ,  $\text{Ag}^+$ ,  $\text{Al}^{3+}$ ,  $\text{Ba}^{2+}$ ,  $\text{Cr}^{3+}$ ,  $\text{Cu}^{2+}$ ,  $\text{Fe}^{3+}$ ,  $\text{Hg}^{2+}$ ,  $\text{Mn}^{2+}$ ,  $\text{Co}^{2+}$ ,  $\text{Zn}^{2+}$ ,  $\text{Cd}^{2+}$ ,  $\text{Ni}^{2+}$  and  $\text{Pb}^{2+}$  (blue bars) and in the presence of mixture of **a)**  $\text{Hg}^{2+}$  ( $1.5 \mu\text{M}$ ) or **b)**  $\text{Fe}^{3+}$  ( $1.5 \mu\text{M}$ ) with two equivalents ( $3 \mu\text{M}$ ) of other metal ions (black bars). Excitation was performed at 385 nm.

#### b) Anions sensing

##### ❖ Absorption studies

The selectivity of polymer **P1** towards anions was also investigated by absorption spectral analysis. The absorption spectra from the mixture of polymer **P1** with various anionic species, including  $\text{H}_2\text{PO}_4^-$ ,  $\text{F}^-$ ,  $\text{Cl}^-$ ,  $\text{Br}^-$ ,  $\text{HSO}_4^-$ ,  $\text{ClO}_4^-$ ,  $\text{OH}^-$ ,  $\text{I}^-$ ,  $\text{NO}_3^-$ ,  $\text{AcO}^-$  and  $\text{CN}^-$  were recorded in DMF at room temperature. As shown in **Figure 4.22**, all the tested anions did not show significant spectral changes in the absorption band of polymer **P1**.

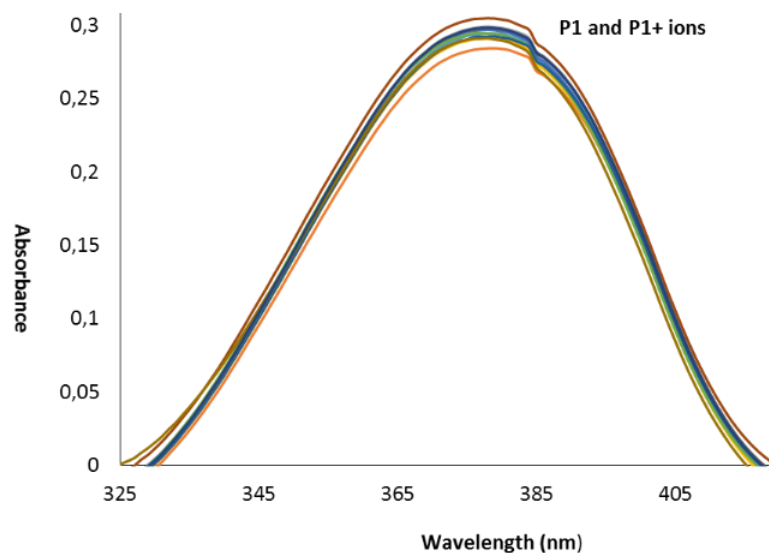


**Figure 4.22:** Absorption spectra of polymer **P1** ( $4.8 \times 10^{-3}$  g/L) in the presence of various anions ( $1 \mu\text{M}$ ) ( $\text{H}_2\text{PO}_4^-$ ,  $\text{F}^-$ ,  $\text{Cl}^-$ ,  $\text{Br}^-$ ,  $\text{HSO}_4^-$ ,  $\text{ClO}_4^-$ ,  $\text{OH}^-$ ,  $\text{I}^-$ ,  $\text{NO}_3^-$ ,  $\text{AcO}^-$  and  $\text{CN}^-$ ).

❖ *Emission studies*

The selectivity of polymer **P1** towards anions was further investigated using emission spectral analysis. As shown in **Figure 4.23**, all the tested anions except  $\text{OH}^-$  did not significantly affect the emission band of polymer **P1** at 452 nm. The presence of  $\text{OH}^-$  ions induced a fluorescence quenching response up to 72 % of the original fluorescence signal in polymer **P1**.

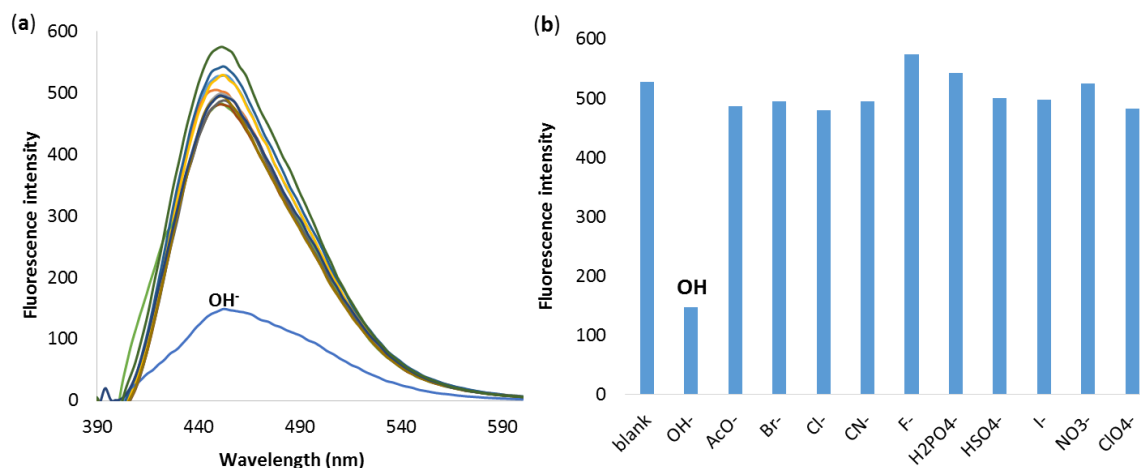


**Figure 4.23:** a) Emission spectra and b) Fluorescence response of polymer **P1** ( $3 \times 10^{-5}$  g/L); in the presence of ( $20 \mu\text{M}$ ) of  $\text{H}_2\text{PO}_4^-$ ,  $\text{F}^-$ ,  $\text{Cl}^-$ ,  $\text{Br}^-$ ,  $\text{HSO}_4^-$ ,  $\text{ClO}_4^-$ ,  $\text{OH}^-$ ,  $\text{I}^-$ ,  $\text{NO}_3^-$ ,  $\text{AcO}^-$  and  $\text{CN}^-$ . Excitation was performed at 385 nm.

The sensitivity of polymer **P1** towards OH<sup>-</sup> was further investigated using absorption and emission spectra upon addition of OH<sup>-</sup> aliquots. **Figure 4.24** shows variations in the absorption and emission spectra of polymer **P1** on the addition of OH<sup>-</sup> aliquots. As shown in **Figure 4.24 a**, the addition of OH<sup>-</sup> in the range of 1 to 10 μM to polymer **P1** in DMF resulted in a gradual decrease in the absorption band at 378 nm. A clear isobestic point at 347 nm was also observed, which indicates a formation of a **P1**-OH<sup>-</sup> complex. Similarly, the emission intensity at 425 nm gradually decreased upon titration of **P1** with OH<sup>-</sup> aliquots with no shifting in maximum emission wavelength (**Figure 4.24 b**). The plot of emission intensities of polymer **P1** at 325 nm versus the concentration of added OH<sup>-</sup>, resulted in a sigmoidal curve and the detection limit was determined within the linear response range of OH<sup>-</sup> (from 1-3 μM). The calculated detection limit was found to be 0.5 μM.

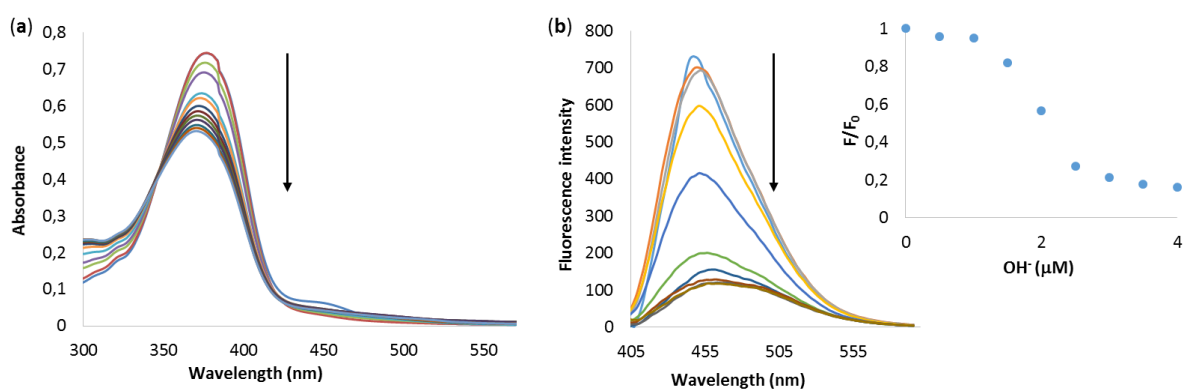


**Figure 4.24:** a) The absorption spectra of polymer **P1** ( $0.096 \text{ gL}^{-1}$ ) and b) Emission spectra of **P1** ( $4 \times 10^{-5} \text{ g/L}$ ) in DMF upon addition of OH<sup>-</sup> aliquots. The excitation was performed at 325 nm.

#### ❖ *Competitive studies*

The influence of other anions on the binding of OH<sup>-</sup> to polymer **P1** was investigated through competitive experiments in DMF. Spectra of polymer **P1** in the presence of OH<sup>-</sup> and 1.0 equivalent of other anions (F<sup>-</sup>, Cl<sup>-</sup>, Br<sup>-</sup>, HSO<sub>4</sub><sup>-</sup>, ClO<sub>4</sub><sup>-</sup>, OH<sup>-</sup>, I<sup>-</sup>, NO<sub>3</sub><sup>-</sup>, AcO<sup>-</sup> and CN<sup>-</sup>) were recorded at room temperature and resulted fluorescence responses are shown in the **Figure 4.25**. Notable, the fluorescence quenching induced by OH<sup>-</sup> ions was affected by the presence of 1.0 equivalents of other anions with less effect from the halides.

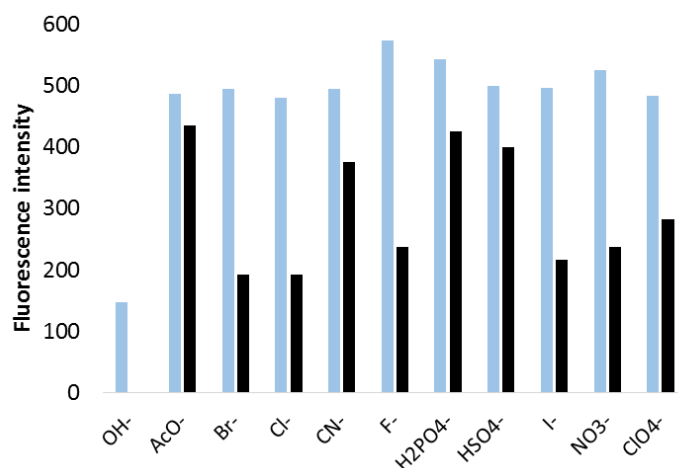


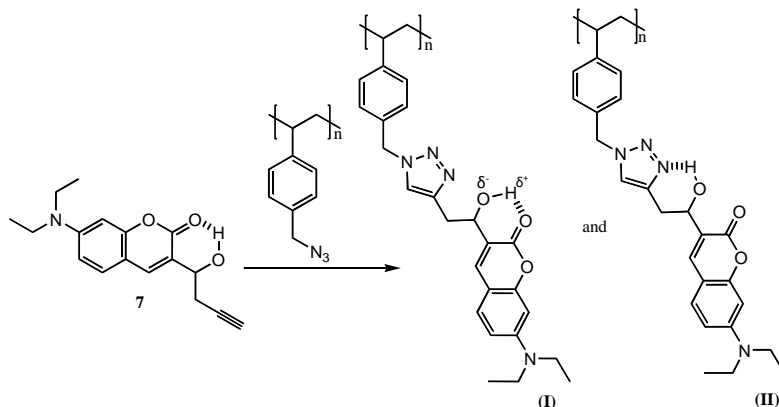
**Figure 4.25:** Fluorescence response of polymer **P1** ( $3 \times 10^{-5}$  g/L) in the presence of anionic species ( $20 \mu\text{M}$ )  $\text{H}_2\text{PO}_4^-$ ,  $\text{F}^-$ ,  $\text{Cl}^-$ ,  $\text{Br}^-$ ,  $\text{HSO}_4^-$ ,  $\text{ClO}_4^-$ ,  $\text{OH}^-$ ,  $\text{I}^-$ ,  $\text{NO}_3^-$ ,  $\text{AcO}^-$  and  $\text{CN}^-$  (blue bars) and in the presence of a mixture of  $\text{OH}^-$  ( $20 \mu\text{M}$ ) with one equivalent of other metal ions ( $20 \mu\text{M}$ ) (black bars). Excitation was performed at 385 nm.

❖ *The proposed binding modes of P1 with  $\text{Hg}^{2+}$ ,  $\text{Fe}^{3+}$  and  $\text{OH}^-$*

In order to understand the binding mechanism of polymer **P1** towards  $\text{Hg}^{2+}$ ,  $\text{Fe}^{3+}$  and  $\text{OH}^-$ , the absorption and emission behaviour of polymer **P1** in the presence of these ions was compared to that of the alkynylated coumarin derivative **7**. Since alkynylated coumarin derivative **7** and its corresponding polymer **P1** showed the same absorption and emission behaviours, it is believed that the interchains interactions in polymer **P1** have no influence on the absorption and emission properties of **P1**. Consequently, they do not play any significant role in ions sensing. Furthermore, as **P1** derives from the incorporation of alkyne-functionalized alkynylated coumarin derivative **7** into non-fluorescent **P0** via triazole forming reaction, any sensitivity difference in polymer **P1** can be attributed to the incoming triazole.

In the case of  $\text{Fe}^{3+}$ , a higher sensitivity was observed in polymer **P1** than in the alkynylated coumarin derivative **7**. As  $\text{Fe}^{3+}$  ions prefer binding to the carbonyl of the coumarin as illustrated in the conjugated triazolyl coumarin system in the Chapter 3, a difference in sensitivity between polymer **P1** and the alkynylated coumarin derivative **7** can be attributed to a strong hydrogen bonding between the hydroxyl and the carbonyl of the coumarin in the alkynylated coumarin derivative **7**. This compete with the interaction between  $\text{Fe}^{3+}$  ions and carbonyl of coumarin (**Scheme 4.6**). The presence of the triazole ring in polymer **P1** reduces the efficiency of hydrogen bonding between the coumarin carbonyl group and the hydroxyl hydrogen since a new hydrogen bond acceptor (the nitrogen of triazole) that competes with the carbonyl group

is introduced. This allows the carbonyl group to be more available for  $\text{Fe}^{3+}$  ion complexation resulting in fluorescence quenching as in conjugated triazolyl coumarin system (Chapter 3).



**Scheme 4.6:** Proposed hydrogen bonding interactions in the alkynylated coumarin derivative **7** and polymer **P1**.

In the case of  $\text{Hg}^{2+}$ , the comparison of the spectroscopic behaviour of alkynylated coumarin derivative **7** and polymer **P1** in the presence of  $\text{Hg}^{2+}$  gave related emission spectra which showed a quenching effect in the presence of  $\text{Hg}^{2+}$ . However, small variations were detected in their absorption spectra, as shown in **Figure 4.26**. By adding the same amount of  $\text{Hg}^{2+}$  to the DMF solution of both alkynylated coumarin derivative **7** and polymer **P1**, the absorption bands at 378 and 456 nm were highly affected in alkynylated coumarin derivative **7** than in polymer **P1**.

Similar to  $\text{Fe}^{3+}$  interaction, the hydrogen bonding between hydroxyl and carbonyl groups of the coumarin has an implication on these variations. As hydrogen bonding between the carbonyl group of the coumarin and the hydroxyl group of the linker makes a direct connection between this binding site (hydroxyl of the linker) and the coumarin fluorophore, any interaction with this binding site will affect the electronic arrangement in the coumarin system and the signal produced in the reporter will be proportional to the efficiency of hydrogen bonding.

Hydrogen bonding increases the push-pull effect in the coumarin system by making the carbonyl group of the coumarin more electron deficient. Binding of  $\text{Hg}^{2+}$  to the oxygen of the hydroxyl group in the alkynylated coumarin derivative **7** as demonstrated in previous section reduces this push-pull effect by interrupting the hydrogen bonding between the hydroxyl group and the carbonyl group. This charge transfer increase, due to the presence of  $\text{Hg}^{2+}$ , is reflected as an increase in absorption intensity of the red shifted absorption band at 456 nm for the alkynylated coumarin derivative **7**.

Unlike alkynylated coumarin derivative **7**, the presence of  $\text{Hg}^{2+}$  did not lead to any significant change in the absorption spectrum of polymer **P1**. This is due to decreased hydrogen bonding efficiency between the carbonyl group of the coumarin and the hydroxyl group of the linker because of the presence of competitive nitrogen atoms of triazole ring.

As the binding of  $\text{Hg}^{2+}$  leads to different absorption responses in the alkynylated coumarin derivative **7** and polymer **P1**, it is clear that electronic arrangements in the alkynylated coumarin derivative **7** and polymer **P1** are affected differently by the  $\text{Hg}^{2+}$  ions. This could be due to the different binding modes in the alkynylated coumarin derivative **7** and in polymer **P1** upon addition of  $\text{Hg}^{2+}$ .

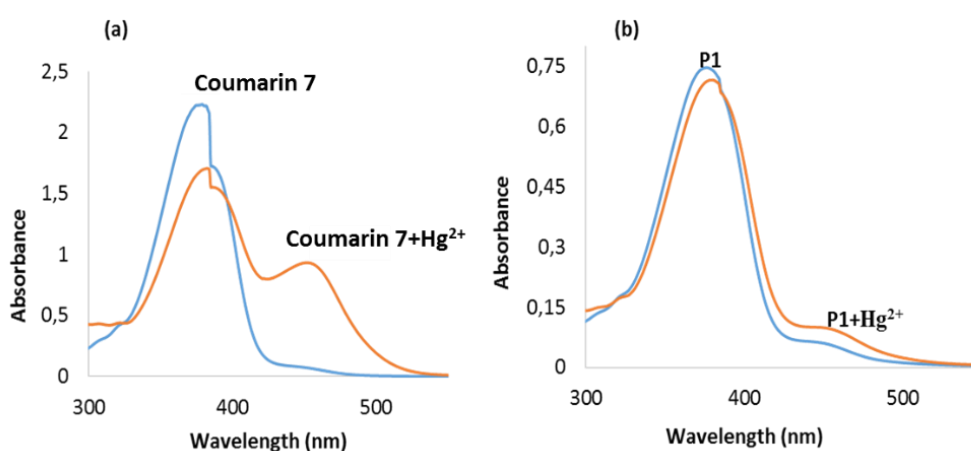
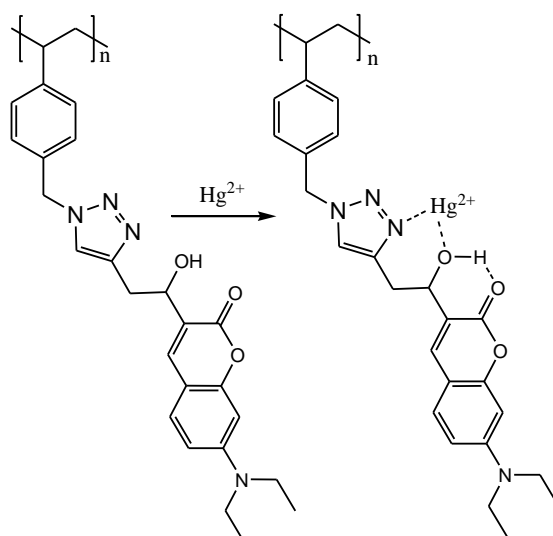


**Figure 4.26:** Absorption spectra of the alkynylated coumarin derivative **7** and polymer **P1** in the presence of  $\text{Hg}^{2+}$  ( $10^{-6}$  mol).

Due to the fact that  $\text{Hg}^{2+}$  did not significantly affect the absorption band of the coumarin fluorophore at 378 nm in polymer **P1** compared to its corresponding alkynylated coumarin derivative **7**, it was concluded that the carbonyl of the coumarin fluorophore was not directly involved in the complexation of  $\text{Hg}^{2+}$  in polymer **P1**. Instead, it is involved in the hydrogen bonding which played meaningful role in alkynylated coumarin derivative **7** for  $\text{Hg}^{2+}$  selectivity.

Since the alkyne group in the alkynylated coumarin derivative **7** was converted into triazole in polymer **P1**, the electron deficient triazole was believed to be involved in the  $\text{Hg}^{2+}$  complexation in polymer **P1**. Since interchain interactions are insignificant in polymer **P1**, the proposed binding mode of polymer **P1** with  $\text{Hg}^{2+}$  is shown in **Scheme 4.7**. A similar complexation mechanism was observed in a small molecular chemosensor system where hydroxyl group was replaced by carbonyl group.<sup>4</sup>

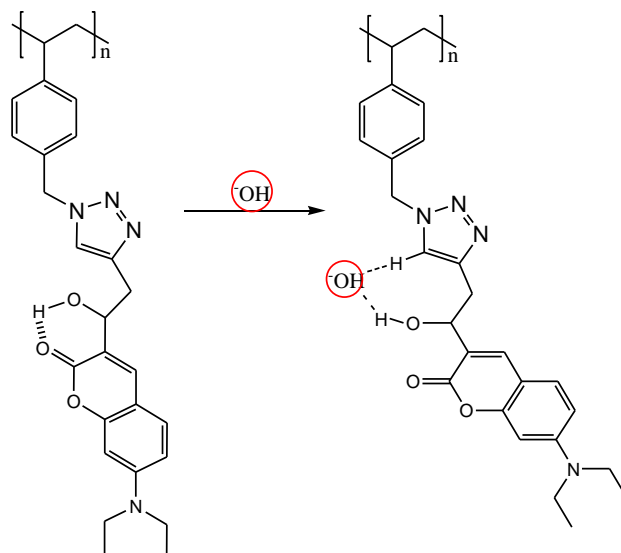




**Scheme 4.7:** A proposed binding mode of polymer **P1** with Hg<sup>2+</sup>.

In the case of hydroxide ions which led to fluorescence quenching in polymer **P1**, the fact that the alkynylated coumarin derivative **7** did not show any spectral changes in the presence of hydroxyl ions suggests the involvement of the polymer **P1** triazole ring as sensing unit. The only possible interaction that may occur between the triazole and the hydroxide ions, is through hydrogen bonding which involves the polar C-H of triazole ring. Since OH<sup>-</sup> ions gives a fluorescence quenching response, it is believed that their presence induces a change in charge density around the coumarin system. These changes in charge density resulted in an enhanced PET process which quenches the fluorescence of coumarin fluorophore.

Due to the electron deficient property of the triazole ring, the only possible way that the hydroxyde ion can bind and induce change that can lead to an enhanced PET process is *via* second hydrogen bonding which involves the proton from the hydroxyl of the functional linkage. This interaction increases charge density around the hydroxyl oxygen in the functional linkage, which participates in the quenching of coumarin fluorescence *via* the PET process. The proposed mechanism for OH<sup>-</sup> binding to polymer **P1** *via* unusual seven-membered ring is depicted in the **Scheme 4.8**.



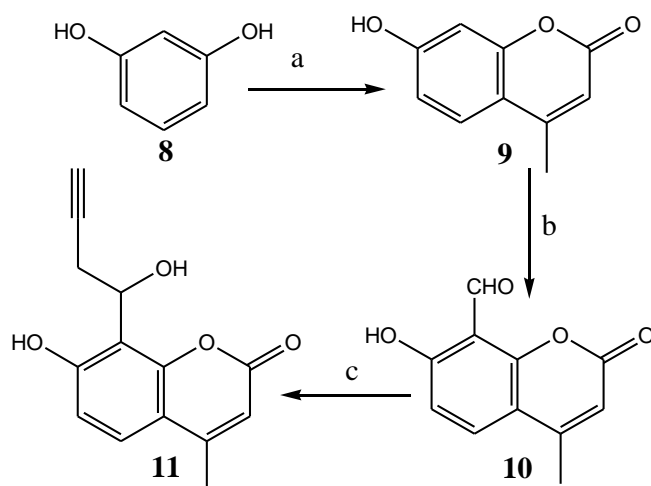
**Scheme 4.8:** A proposed binding mode of polymer **P1** with  $\text{OH}^-$ .

### 4.3.2 Triazolyl coumarin based polymers with the hydroxyethylene linkage at position 8 of the coumarin motif (**P2**)

As carried out in the synthesis of polymer **P1**, the synthesis of polymer **P2** was accomplished in two stages. The alkynylated coumarin derivative **11** with alkyne functional group at position 8 of coumarin motif was firstly synthesized as shown in **Scheme 4.9**. In the second stage, the alkynylated coumarin derivative **11** was incorporated into polymer **P0** side chains *via* a Cu(I) catalyzed post-polymerization functionalization. Polymer **P2** with pendant chains containing triazolyl coumarin system with hydroxyethylene linkage was produced.

#### 4.3.2.1 Synthesis of alkynylated coumarin derivative **11**

The synthesis was accomplished in three steps from resorcinol as shown in **Scheme 4.9**. The syntheses of coumarin **9** and **10** were achieved in good yields according to reported literature.<sup>19</sup> By using a well-established zinc mediated regioselective Barbier reaction of propargylic bromide,<sup>12</sup> the alkyne functional group was attached at position 8 of coumarin **10** in the presence of propargyl bromide to produce 7-hydroxy-8-(1-hydroxybut-3-ynyl)-4-methyl-2H-chromen-2-one (alkynylated coumarin derivative **11**) in good yield.



**Scheme 4.9.** Synthesis of alkyne-coumarin **11**: **a)** Conc  $\text{H}_2\text{SO}_4$ ,  $\text{CH}_3\text{COCH}_2\text{COOC}_2\text{H}_5$ ,  $0^\circ\text{C}$ , rt; **b)** Hexamethylenetetramine, AcOH (reflux) **c)** Zn, THF, propargyl bromide,  $\text{NH}_4\text{Cl}(\text{aq})$ .

The structures of coumarins **9**, **10** and **11** were characterized by mass and NMR spectroscopy (for  $^{13}\text{C}$  NMR of coumarin **11** and  $^1\text{H}$  NMRs for coumarins **9**, **10** see **Appendices Figure A.13-A.15**). **Figure 4.27** illustrates the assignment of proton signals in  $^1\text{H}$  NMR spectrum of the alkyne-coumarin derivative **11**. The proton signals from the terminal alkyne (a) and the methylene group next to alkyne functionality (b and c) appeared between 2.65 ppm and 2.89 ppm, while the proton attached to the asymmetric carbon connected to the coumarin (d) appeared at 4.52 ppm. The proton from the hydroxyl group attached to the same asymmetric carbon appeared at 4.90 ppm and three coumarin proton signals were observed between 6.19-7.65 ppm.

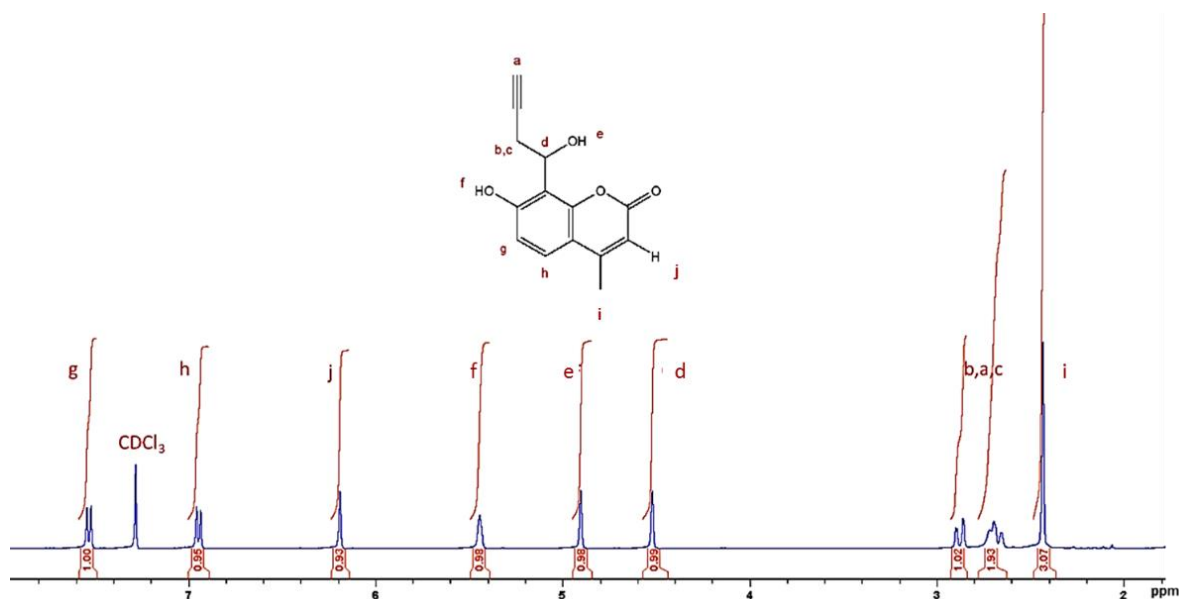
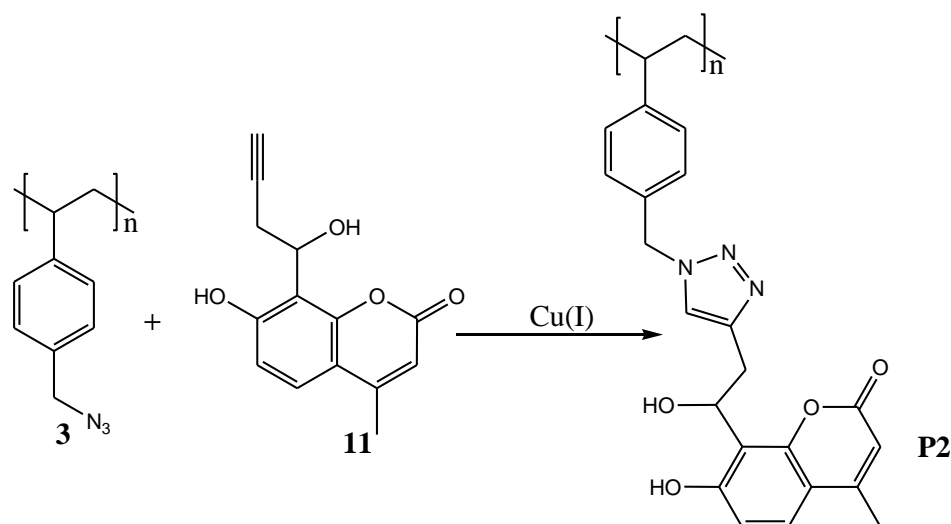


**Figure 4.27:**  $^1\text{H}$  NMR spectrum of the alkynylated coumarin derivative **11** in  $\text{CDCl}_3$ .

#### 4.3.2.2 Functionalization of polymer **P0** using alkynylated coumarin derivative **11**

**Scheme 3.10** shows functionalization of **P0** with the alkynylated coumarin derivative **11**. The functionalization was carried out under the same reaction conditions as applied in the functionalization of polymer **P0** using alkynylated coumarin derivative **7**. On completion of the reaction, the precipitated polymer was filtered and washed with water to afford pure polymer **P2** as off-white solid in 78 % yield.



**Scheme 4.10:** Functionalization of **P0** with the alkynylated coumarin derivative **11**.

The structure of polymer **P2** was confirmed by  $^1\text{H}$  NMR and Ft-IR spectroscopy. **Figure 4.28** compares the  $^1\text{H}$  NMR spectra of **P0**, alkynylated coumarin derivative **11** and polymer **P2**. Of

note, the proton signals from both starting materials were prominent in the polymer **P2**  $^1\text{H}$  NMR spectrum, confirming a successful synthesis of polymer **P2**. The average molecular weight and polydispersity index of **P2** were determined to be  $2.16 \times 10^4$  g/mol and 2.18 respectively.

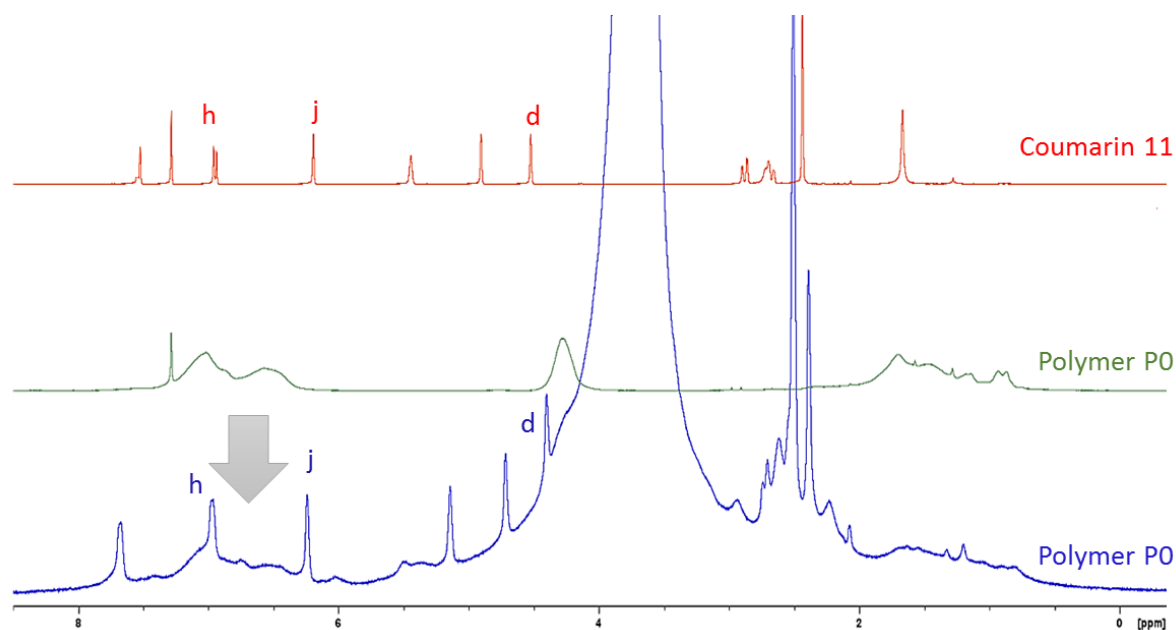


**Figure 4.28:**  $^1\text{H}$  NMR spectra of **P0**, the alkynylated coumarin derivative **11** and the polymer **P2**. For coumarin **11** and polymer **P0**  $\text{CDCl}_3$  solvent was used and  $\text{DMSO-d}_6$  was used for polymer **P2**.

The structure of polymer **P2** was further characterized by FT-IR. **Figure 4.29** compares FT-IR spectra of the starting **P0** and the functionalized polymer **P2**. The peak characteristic of the azide group at  $2089\text{ cm}^{-1}$  was significantly decreased in **P2** but not to the same extent as in polymer **P1**. This indicates that the functionalization of **P0** by alkyne-substituted coumarins depends on the chemical environments of alkyne functionality. The appearance of the hydroxyl hydrogen peak at  $3400\text{ cm}^{-1}$  also confirms the successful incorporation of the alkynylated coumarin derivative **11** into **P0** side chains. The percentage conversion of azide group was calculated using the peak height method and was found to be 73%.

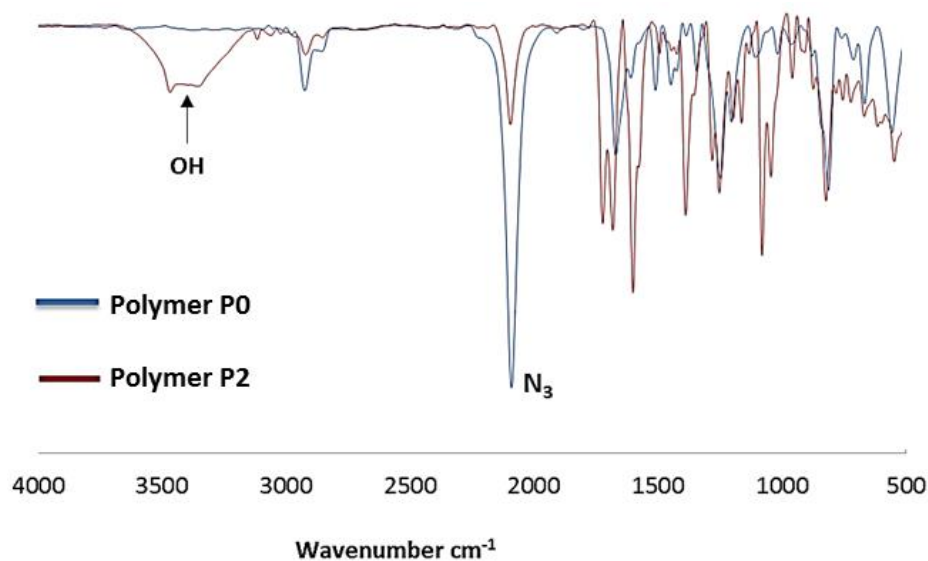


**Figure 4.29:** FT-IR spectra of polymer **P0** and the functionalized polymer **P2**.

#### 4.3.2.3 Absorption and emission studies on functionalized of polymer **P0**

To further confirm the functionalization of polymer **P0** with alkynylated coumarin derivative **11**, the photophysical properties of polymer **P0** was compared with the photophysical properties of polymer **P2** and alkynylated coumarin derivative **11**. To verify if the isolated polymer is not one of the starting materials, DMF solutions containing the same amount (in grams) were used. As expected, polymer **P2** showed absorption and emission with the intensities between the intensities of its starting materials (**Figure 4.30**). Same as in the previous section, the alkynylated coumarin derivative **11** showed higher absorption and emission intensities while polymer **P0** showed a negligible absorption and emission. Furthermore, both alkynylated coumarin derivative **11** and polymer **P2** exhibited similar absorption and emission behaviour with the maximum absorption and emission wavelengths observed at 325 nm and 386 nm respectively.

These observations confirmed a successful functionalization of polymer **P0** with alkynylated coumarin derivative **11**. It also indicated that the photophysical properties of polymer **P2** depend on the incorporated triazolyl coumarin system.

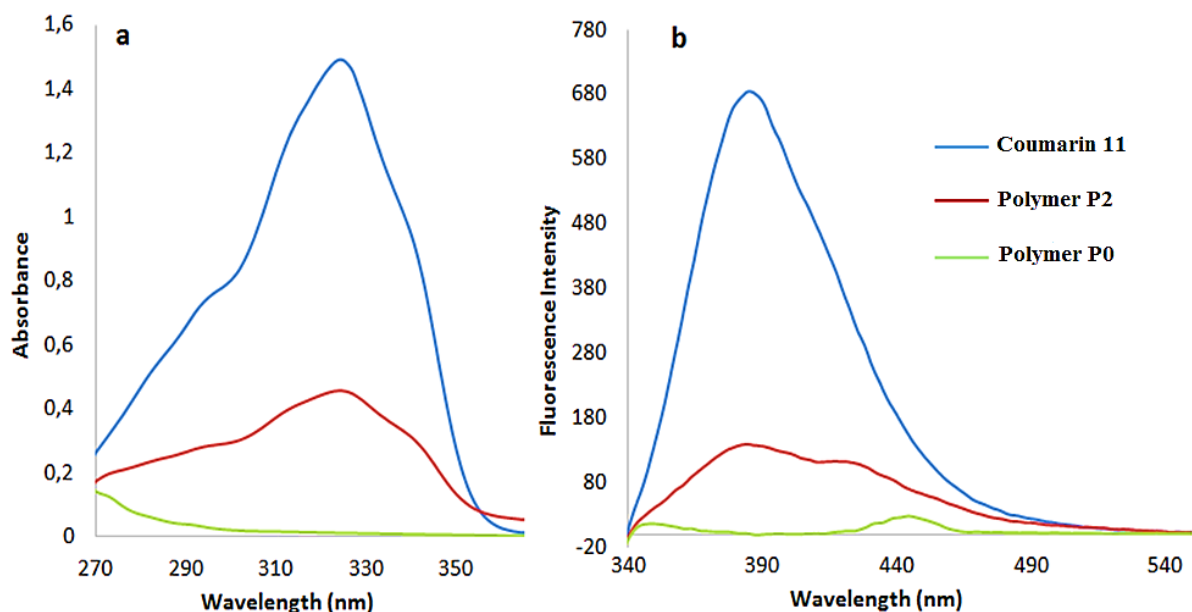


**Figure 4.30:** a) Absorption and b) Emission spectra of the alkynylated coumarin derivative **11** ( $8 \times 10^{-4}$  g/L), polymer **P0** ( $8 \times 10^{-4}$  g/L) and polymer **P2** ( $8 \times 10^{-4}$  g/L) in DMF. The excitation was performed at 325 nm.

#### 4.3.2.4 Chemosensing studies

Same as in section 4.3.1, the chemosensing capabilities of both the alkynylated coumarin derivative **11** and polymer **P2** for selected metal ions and anions were investigated and compared.

##### (i) Chemosensing studies of alkynylated coumarin 11

###### a) Absorption studies

The chemosensing capabilities of alkynylated coumarin derivative **11** were firstly investigated using UV-Vis spectral analysis. The studies were carried out in DMF at room temperature in the presence of different metal ions such as;  $\text{Na}^+$ ,  $\text{Ca}^{2+}$ ,  $\text{Ag}^+$ ,  $\text{Al}^{3+}$ ,  $\text{Ba}^{2+}$ ,  $\text{Cr}^{3+}$ ,  $\text{Cu}^{2+}$ ,  $\text{Fe}^{3+}$ ,  $\text{Hg}^{2+}$ ,  $\text{Mn}^{2+}$ ,  $\text{Co}^{2+}$ ,  $\text{Zn}^{2+}$ ,  $\text{Cd}^{2+}$ ,  $\text{Ni}^{2+}$  and  $\text{Pb}^{2+}$  and different anionic species, including  $\text{F}^-$ ,  $\text{Cl}^-$ ,  $\text{Br}^-$ ,  $\text{HSO}_4^-$ ,  $\text{ClO}_4^-$ ,  $\text{OH}^-$ ,  $\text{I}^-$ ,  $\text{NO}_3^-$ ,  $\text{AcO}^-$  and  $\text{CN}^-$ . As shown in **Figure 4.31 a**, all the tested metal ions, except  $\text{Hg}^{2+}$ , did not show any detectable changes in the alkynylated coumarin derivative **11** absorption bands. The presence of  $\text{Hg}^{2+}$  induced a decrease in the absorption band at 325 nm and a hypsochromic shift from 325 to 320 nm. This can be attributed to the heavy atom character of  $\text{Hg}^{2+}$  and its particular binding mode, which reduces the push-pull character of the coumarin moiety.

UV-Vis spectral analysis in the presence of anions was also carried out. As shown in **Figure 4.31 b**, only  $F^-$  and  $OH^-$  showed a notable changes in alkynylated coumarin derivative **11** absorption band at 325 nm with less absorption properties.

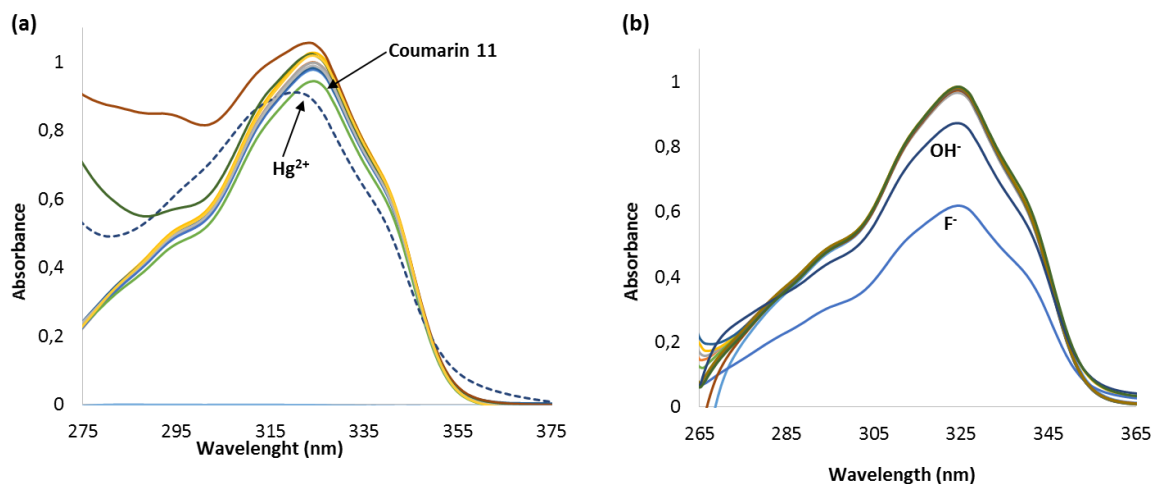


**Figure 4.31:** a) Absorption spectra of alkynylated coumarin derivative **11** ( $7.4 \times 10^{-5}$  M) in the presence of the aliquot ( $3 \times 10^{-4}$  M) of a) different metal ions ( $Na^+$ ,  $Ca^{2+}$ ,  $Ag^+$ ,  $Al^{3+}$ ,  $Ba^{2+}$ ,  $Cr^{3+}$ ,  $Cu^{2+}$ ,  $Fe^{3+}$ ,  $Hg^{2+}$ ,  $Mn^{2+}$ ,  $Co^{2+}$ ,  $Zn^{2+}$ ,  $Cd^{2+}$ ,  $Ni^{2+}$  and  $Pb^{2+}$ ); b) different anions ( $H_2PO_4^-$ ,  $F^-$ ,  $Cl^-$ ,  $Br^-$ ,  $HSO_4^-$ ,  $ClO_4^-$ ,  $OH^-$ ,  $I^-$ ,  $NO_3^-$ ,  $AcO^-$  and  $CN^-$ ).

#### b) Emission studies

The chemosensing capability of the alkynylated coumarin derivative **11** was further investigated using emission spectral analysis in the presence of different ionic species. The investigations were conducted using the same conditions and same ionic species as in UV-Vis spectral analysis, using an excitation wavelength of 325 nm. Among the tested metal ions, only  $Fe^{3+}$  and  $Hg^{2+}$  induced obvious changes in the alkynylated coumarin derivative **11** emission band at 386 nm with a fluorescence quenching response (**Figure 4.32 a**). For coumarin derivative **11**, the presence of  $Fe^{3+}$  induced a fluorescence quenching response up to 31% in its original fluorescence, while  $Hg^{2+}$  induced a stronger quenching response up to 87%. The quenching response in the presence of  $Hg^{2+}$  can be attributed to heavy atom effect and  $\pi$ -philic nature of  $Hg^{2+}$  associated to quenching metal ions.<sup>15,16</sup> Unlike cations, emission spectral analysis of alkynylated coumarin derivative **11** in the presence of different anionic species did not show any significant response towards the tested anionic species (**Figure 4.32 b**).



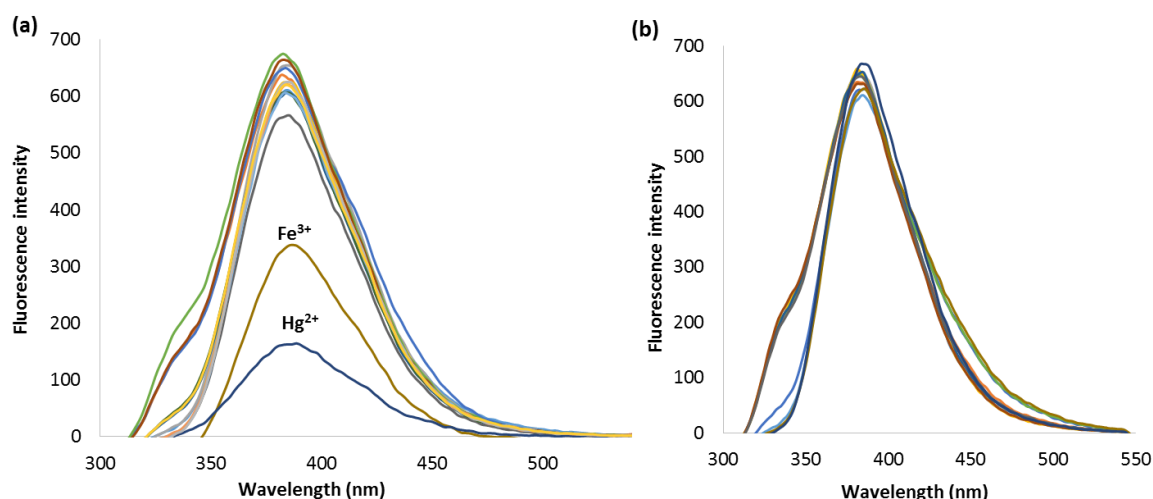


**Figure 4.32:** Emission spectra of the alkynylated coumarin derivative **11** ( $2.2 \times 10^{-3} \text{ M}$ ) in the presence of the aliquot ( $6.5 \times 10^{-5} \text{ M}$ ) of **a**) different metal ions ( $\text{Na}^+$ ,  $\text{Ca}^{2+}$ ,  $\text{Ag}^+$ ,  $\text{Al}^{3+}$ ,  $\text{Ba}^{2+}$ ,  $\text{Cr}^{3+}$ ,  $\text{Cu}^{2+}$ ,  $\text{Fe}^{3+}$ ,  $\text{Hg}^{2+}$ ,  $\text{Mn}^{2+}$ ,  $\text{Co}^{2+}$ ,  $\text{Zn}^{2+}$ ,  $\text{Cd}^{2+}$ ,  $\text{Ni}^{2+}$  and  $\text{Pb}^{2+}$ ); **b**) different anions ( $\text{H}_2\text{PO}_4^-$ ,  $\text{F}^-$ ,  $\text{Cl}^-$ ,  $\text{Br}^-$ ,  $\text{HSO}_4^-$ ,  $\text{ClO}_4^-$ ,  $\text{OH}^-$ ,  $\text{I}^-$ ,  $\text{NO}_3^-$ ,  $\text{AcO}^-$  and  $\text{CN}^-$ ). Excitation was performed at 325 nm.

*c) Titration experiments of  $\text{Hg}^{2+}$*

Since the alkynylated coumarin derivative **11** showed a selective response towards  $\text{Hg}^{2+}$  in both absorption and emission spectral analysis, its chemosensing properties were further investigated by UV-Vis and fluorescence titration experiments. In UV-Vis titration experiments, the addition of  $\text{Hg}^{2+}$  aliquots to a DMF solution of the alkynylated coumarin derivative **11** induced a gradual decrease in absorption accompanied by a hypsochromic shift in the absorption band from 325 to 320 nm as shown **Figure 4.33 a**. In fluorescence experiments (**Figure 4.33 b**), the addition of  $\text{Hg}^{2+}$  also caused a gradual decrease in the intensity of the emission band at 386 and the saturation point was reached when 10 equivalents of  $\text{Hg}^{2+}$  were added. The hypsochromic shift in UV-Vis can be attributed to the binding mode of  $\text{Hg}^{2+}$  which reduces the push-pull character of the coumarin system. The detection limit of the alkynylated coumarin derivative **11** towards  $\text{Hg}^{2+}$  was calculated from fluorometric titration within a linear range of 0.048-0.112  $\mu\text{M}$  and was found to be 0.0054  $\mu\text{M}$ .

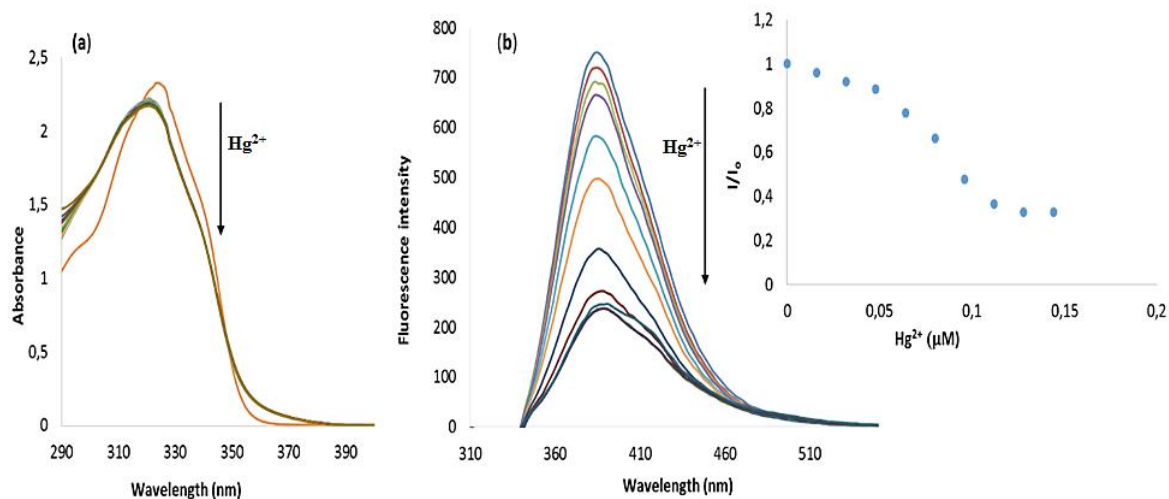


**Figure 4.33:** a) Absorption b) and Emission spectra of alkynylated coumarin derivative **11** ( $2.2 \times 10^{-3}$  M) in DMF upon addition of  $\text{Hg}^{2+}$ . Absorption (1-8  $\mu\text{M}$ ) and emission (0.016-0.144  $\mu\text{M}$ ). The excitation was performed at 325 nm.

#### d) Competitive studies

To investigate application of alkynylated coumarin derivative **11** as a selective chemosensor of  $\text{Hg}^{2+}$ , competitive experiments were carried out. These were conducted by monitoring the emission spectra of coumarin derivative **11** in the presence of  $\text{Hg}^{2+}$  with 2 equivalents of other metal ions ( $\text{Na}^+$ ,  $\text{Ca}^{2+}$ ,  $\text{Ag}^+$ ,  $\text{Al}^{3+}$ ,  $\text{Ba}^{2+}$ ,  $\text{Cr}^{3+}$ ,  $\text{Cu}^{2+}$ ,  $\text{Fe}^{3+}$ ,  $\text{Hg}^{2+}$ ,  $\text{Mn}^{2+}$ ,  $\text{Co}^{2+}$ ,  $\text{Zn}^{2+}$ ,  $\text{Cd}^{2+}$ ,  $\text{Ni}^{2+}$  and  $\text{Pb}^{2+}$ ). As shown in the **Figure 4.34**, the fluorescence quenching caused by the presence of  $\text{Hg}^{2+}$  was not significantly affected by the presence of two equivalents of other metal ions except in the presence of  $\text{Fe}^{3+}$  where enhanced quenching was noted. This shows that the alkynylated coumarin derivative **11** has high selectivity towards  $\text{Hg}^{2+}$  even in the presence of other heavy metals ions.

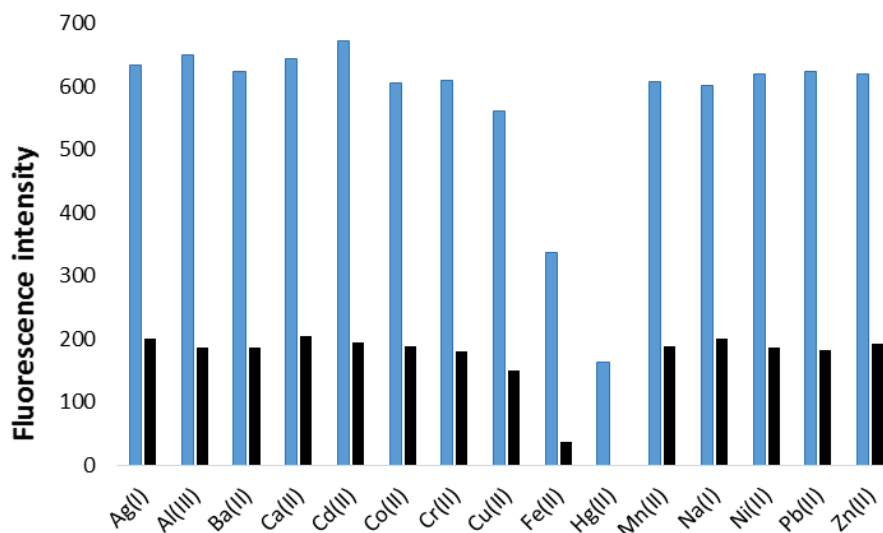


**Figure 4.34:** Fluorescence response of alkynylated coumarin **11** ( $2.2 \times 10^{-3}$  M) in the presence of metal ions ( $0.2 \mu\text{M}$ )  $\text{Na}^+$ ,  $\text{Ca}^{2+}$ ,  $\text{Ag}^+$ ,  $\text{Al}^{3+}$ ,  $\text{Ba}^{2+}$ ,  $\text{Cr}^{3+}$ ,  $\text{Cu}^{2+}$ ,  $\text{Fe}^{3+}$ ,  $\text{Hg}^{2+}$ ,  $\text{Mn}^{2+}$ ,  $\text{Co}^{2+}$ ,  $\text{Zn}^{2+}$ ,  $\text{Cd}^{2+}$ ,  $\text{Ni}^{2+}$  and  $\text{Pb}^{2+}$  (blue bars) and in the presence of mixture of  $\text{Hg}^{2+}$  ( $0.2 \mu\text{M}$ ) with 2 equivalents ( $0.4 \mu\text{M}$ ) of other metal ions (black bars). Excitation was performed at 325 nm.

*e) The proposed binding modes of alkynylated coumarin derivative 11 with  $\text{Hg}^{2+}$*

To study the binding mode between the alkynylated coumarin derivative **11** and  $\text{Hg}^{2+}$ , a Job plot analysis was performed. The continuous variation method with a total concentration of  $10^{-9}$  M was used. **Figure 4.35 a** shows a plot of emission intensity versus the molar fraction of  $\text{Hg}^{2+}$  at 325 nm. Notable, the maximum was reached when the molar fraction was 0.5 suggesting 1:1 stoichiometry of  $\text{Hg}^{2+}$ -coumarin **11** complex.

The binding constant ( $K_a$ ) between the coumarin derivative **11** and  $\text{Hg}^{2+}$  was evaluated graphically using the Benesi-Hildebrand method.<sup>20</sup> As shown in **Figure 4.35 b**,  $1/F_0 - F$  was plotted versus  $1/[\text{Hg}^{2+}]$  and the data was linearly fitted. The calculated value of  $K_a$  from the slope and intercept of the line was  $5.2 \times 10^6$  M.

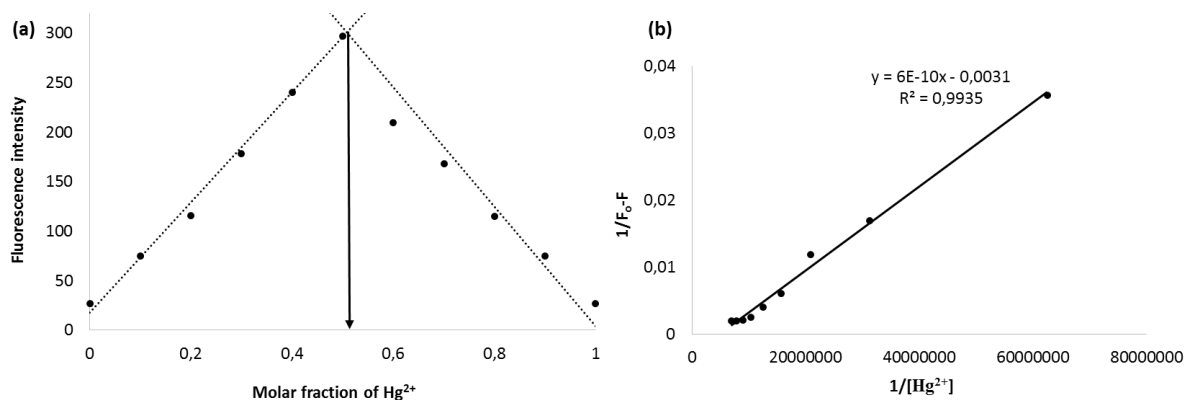


**Figure 4.35:** a) Job plot for Hg<sup>2+</sup>-coumarin **11** complexation with a constant total concentration of 10<sup>-9</sup> M and b) Benesi-Hildebrand plot of alkynylated coumarin **11** derivative with Hg<sup>2+</sup>. The spectra were recorded in DMF at 325 nm.

To understand the binding mode of the alkynylated coumarin derivative **11** with Hg<sup>2+</sup>, <sup>1</sup>H NMR of the alkynylated coumarin derivative **11** in the presence of increasing amounts of Hg<sup>2+</sup> were recorded in DMSO-d<sub>6</sub> as shown in the **Figure 4.36**. As noted, the splitting of the hydrogen from the chiral centre in position 8 of the coumarin backbone was more pronounced in DMSO-d<sub>6</sub> compared to CDCl<sub>3</sub>. Those protons were observed at 4.4 ppm and 4.73 ppm.

The addition of Hg<sup>2+</sup> aliquots affected two proton signals which were assigned to the proton of hydroxyl group directly attached to position **7** of the coumarin system at 5.5 ppm and terminal alkyne proton signal at 2.58 ppm as highlighted in **Figure 4.36**. As more Hg<sup>2+</sup> was added to the coumarin derivative **11** solution, the intensity of the hydroxyl proton signal at 5.5 ppm was reduced. This suggested that Hg<sup>2+</sup> deprotonates the hydroxyl group during binding. The interaction between the hydroxyl group at position **7** of the coumarin derivative **11** and Hg<sup>2+</sup> was also confirmed by UV-Vis analysis in the presence of Hg<sup>2+</sup> (**Figure 4.33 a**). The presence of Hg<sup>2+</sup> resulted to a hypsochromic shift in the absorption of coumarin derivative **11**. This means that, the presence of Hg<sup>2+</sup> decreases the push-pull character of coumarin system by interacting with the electron-donating hydroxyl group in position 7. The same deprotonation of hydroxyl group by Hg<sup>2+</sup> was observed in rhodamine B based chemosensor developed by Jiantai and co-workers.<sup>21</sup>

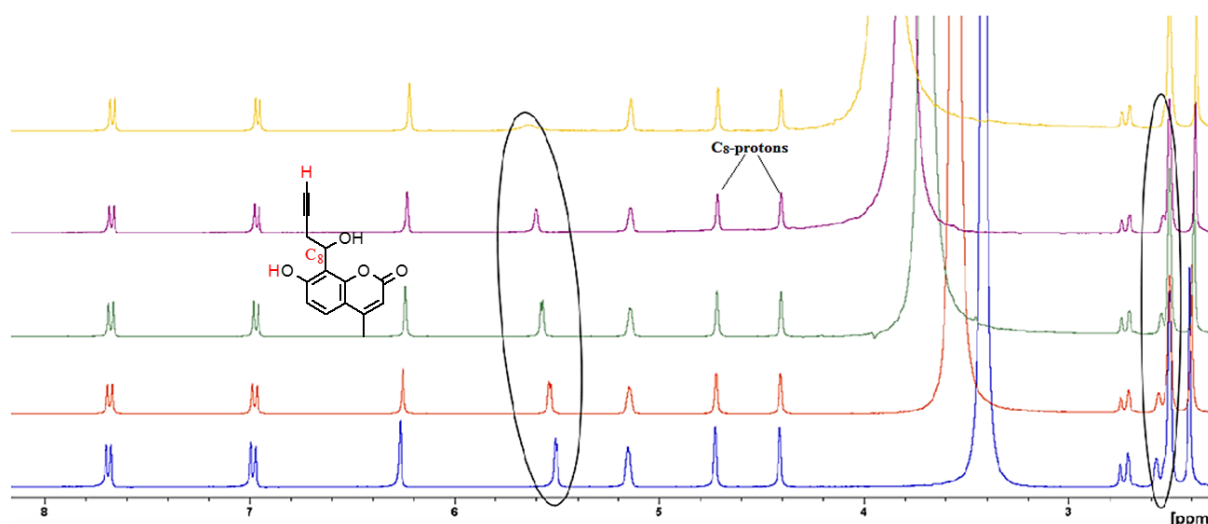
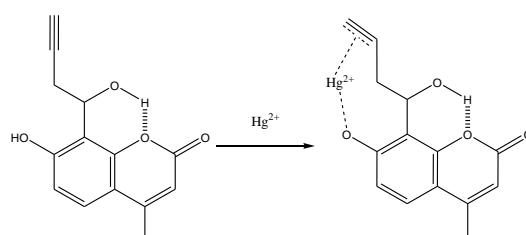


**Figure 4.36:** Changes in the  $^1\text{H}$  NMR signal of the alkynylated coumarin derivative **11** with increasing amounts of  $\text{Hg}^{2+}$  in  $\text{DMSO}_d_6$ .

Since the Job plot analysis indicated a 1:1 stoichiometry in the  $\text{Hg}^{2+}$ -coumarin derivative **11** complex, it was suggested that  $\text{Hg}^{2+}$  chelated triple bond of the terminal alkyne and deprotonated the hydroxyl group at position 7 of the coumarin. The possible binding mode is depicted in **Scheme 4.11**.



**Scheme 4.11:** A proposed binding mode of coumarin derivative **11** with  $\text{Hg}^{2+}$ .

## (ii) Chemosensing studies of **P2**

### a) Absorption studies

UV-Vis chemosensing studies of polymer **P2** were carried out in DMF at room temperature using the same set of metal ions and anions as in alkynylated coumarin derivative **11**. As observed in the UV-Vis spectral analysis of alkynylated coumarin **11**, the presence of  $\text{Hg}^{2+}$  induced a decrease in the polymer **P2** absorption band at 325 nm with a hypsochromic shift from 325 to 321 nm as shown in the **Figure 4.37 a**. All other tested metal ions except  $\text{Cu}^{2+}$  did not produce detectable changes in the polymer **P2** absorption bands.  $\text{Cu}^{2+}$  led to absorption enhancement. Furthermore, UV-Vis spectral analysis of polymer **P2** in the presence of anions

showed a slight decrease in absorption band in the presence of only  $\text{OH}^-$ ,  $\text{F}^-$  and  $\text{CN}^-$  as shown in the **Figure 4.37 b**.

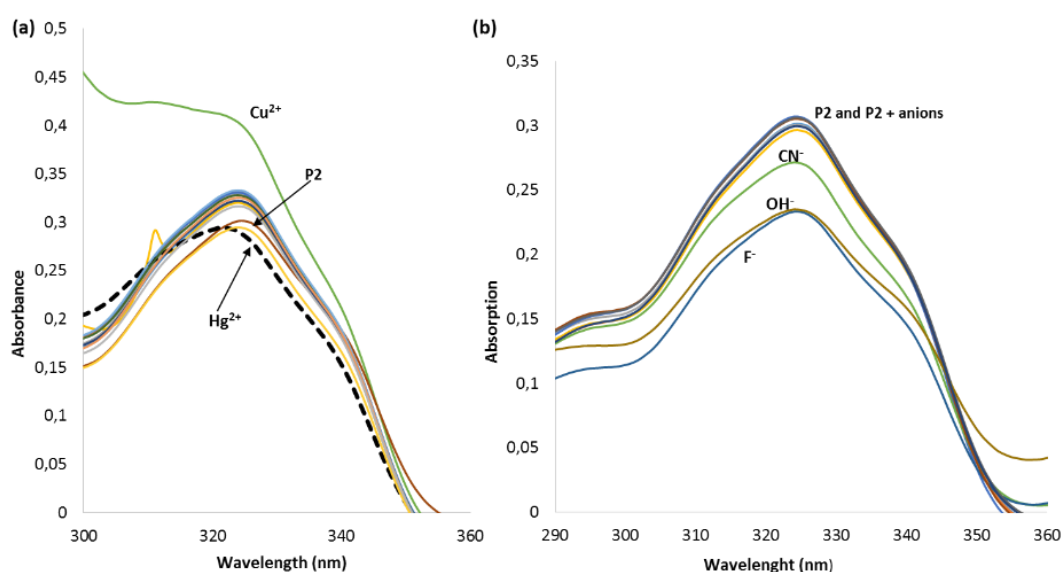


**Figure 4.37:** Absorption spectra of polymer **P2** ( $1.6 \times 10^{-2}$  g/L) in the presence of the aliquot ( $6.5 \times 10^{-5}$  M) of **a)** different metal ions ( $\text{Na}^+$ ,  $\text{Ca}^{2+}$ ,  $\text{Ag}^+$ ,  $\text{Al}^{3+}$ ,  $\text{Ba}^{2+}$ ,  $\text{Cr}^{3+}$ ,  $\text{Cu}^{2+}$ ,  $\text{Fe}^{3+}$ ,  $\text{Hg}^{2+}$ ,  $\text{Mn}^{2+}$ ,  $\text{Co}^{2+}$ ,  $\text{Zn}^{2+}$ ,  $\text{Cd}^{2+}$ ,  $\text{Ni}^{2+}$  and  $\text{Pb}^{2+}$ ); **b)** different anions ( $\text{H}_2\text{PO}_4^-$ ,  $\text{F}^-$ ,  $\text{Cl}^-$ ,  $\text{Br}^-$ ,  $\text{HSO}_4^-$ ,  $\text{ClO}_4^-$ ,  $\text{OH}^-$ ,  $\text{I}^-$ ,  $\text{NO}_3^-$ ,  $\text{AcO}^-$  and  $\text{CN}^-$ ).

#### *b) Emission studies*

To further investigate the chemosensing capability of polymer **P2**, emission spectral analysis was conducted using the same set of ions as in UV-Vis analysis. The studies were conducted at room temperature using DMF as the solvent. Of importance, all the tested metal ions except  $\text{Al}^{3+}$ ,  $\text{Fe}^{3+}$  and  $\text{Hg}^{2+}$  induced weak spectral changes in polymer **P2** emission band at 386 nm (**Figure 4.38 a**).  $\text{Al}^{3+}$  induced a bathochromic shift in the maximum wavelength from 386 nm to 401 nm with fluorescence enhancement as high as 80% of the original polymer **P2** fluorescence intensity. Due to the heavy atom effect,  $\text{Fe}^{3+}$  and  $\text{Hg}^{2+}$  induced a fluorescence quenching up to 39% and 72%, respectively, of the original polymer **P2** fluorescence intensity.<sup>15</sup> In the case of anions, none of the tested anions induced significant changes in the emission spectrum of polymer **P1** as shown in the **Figure 4.38 b**.

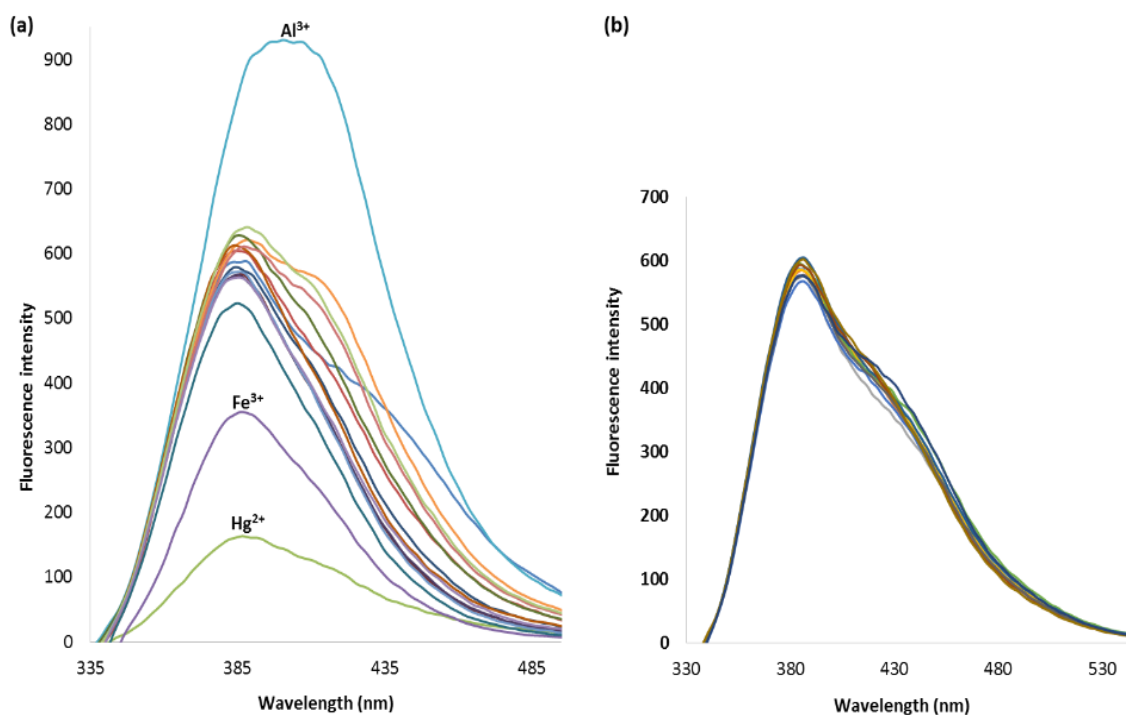


**Figure 4.38:** Emission spectra of the polymer **P2** ( $5 \times 10^{-4}$  g/L) in the presence of the aliquot ( $0.2 \mu\text{M}$ ) of **a)** different metal ions ( $\text{Na}^+$ ,  $\text{Ca}^{2+}$ ,  $\text{Ag}^+$ ,  $\text{Al}^{3+}$ ,  $\text{Ba}^{2+}$ ,  $\text{Cr}^{3+}$ ,  $\text{Cu}^{2+}$ ,  $\text{Fe}^{3+}$ ,  $\text{Hg}^{2+}$ ,  $\text{Mn}^{2+}$ ,  $\text{Co}^{2+}$ ,  $\text{Zn}^{2+}$ ,  $\text{Cd}^{2+}$ ,  $\text{Ni}^{2+}$  and  $\text{Pb}^{2+}$ ); **b)** different anions ( $\text{H}_2\text{PO}_4^-$ ,  $\text{F}^-$ ,  $\text{Cl}^-$ ,  $\text{Br}^-$ ,  $\text{HSO}_4^-$ ,  $\text{ClO}_4^-$ ,  $\text{OH}^-$ ,  $\text{I}^-$ ,  $\text{NO}_3^-$ ,  $\text{AcO}^-$  and  $\text{CN}^-$ ).

### c) Titration experiments

Since polymer **P2** exhibits a fluorescence quenching response in the presence of both  $\text{Fe}^{3+}$  and  $\text{Hg}^{2+}$ , the absorption and emission behaviours of polymer **P2** in the presence of increasing amounts of  $\text{Fe}^{3+}$  and  $\text{Hg}^{2+}$  was investigated in order to understand how the two metal ions ( $\text{Fe}^{3+}$  and  $\text{Hg}^{2+}$ ) can be distinguished. The addition of  $\text{Fe}^{3+}$  aliquots to the DMF solution of polymer **P2** (**Figure 4.39 a**) induced a gradual increase in the absorption band at 325 nm while the first addition of  $\text{Hg}^{2+}$  ( $1 \mu\text{M}$ ) induced a blue shift down to 321 nm and a decrease in absorption of the band which was originally at 325 nm (**Figure 4.39 b**). Additional aliquots of  $\text{Hg}^{2+}$  reversed the response and a gradual increase in intensity was observed in the absorption band at 321 nm. Though these differences can be used to distinguish  $\text{Fe}^{3+}$  and  $\text{Hg}^{2+}$ , it can also suggest different binding modes of polymer **P2** in the presence of  $\text{Fe}^{3+}$  or  $\text{Hg}^{2+}$ .

Since polymer **P2** showed fluorescence enhancement in the presence of  $\text{Al}^{3+}$ , the absorption behaviour of polymer **P2** in the presence of increasing amounts of  $\text{Al}^{3+}$  was also investigated. **Figure 4.39 c** shows variations in the absorption spectrum of polymer **P2** on addition of  $\text{Al}^{3+}$

aliquots. Notable, the addition 1  $\mu\text{M}$  of  $\text{Al}^{3+}$  to polymer **P2** solution caused a slight increase in intensity in the absorption band at 325 nm. Additional aliquots of  $\text{Al}^{3+}$  reversed the response. A gradual decrease in intensity and a weak blue shift in the absorption band from 325 to 323 nm was also observed. Furthermore, two clear isosbestic points at 295 and 317 nm were observed, indicating a clean formation of a polymer **P2**- $\text{Al}^{3+}$  complex.

A switch in absorption response in the presence of  $\text{Al}^{3+}$  or  $\text{Hg}^{2+}$  from enhancing to quenching in the case of  $\text{Al}^{3+}$  or from quenching to enhancing in the case of  $\text{Hg}^{2+}$ , suggests more than one binding mode in the polymer **P2**- $\text{Al}^{3+}$  and polymer **P2**- $\text{Hg}^{2+}$  complexes.

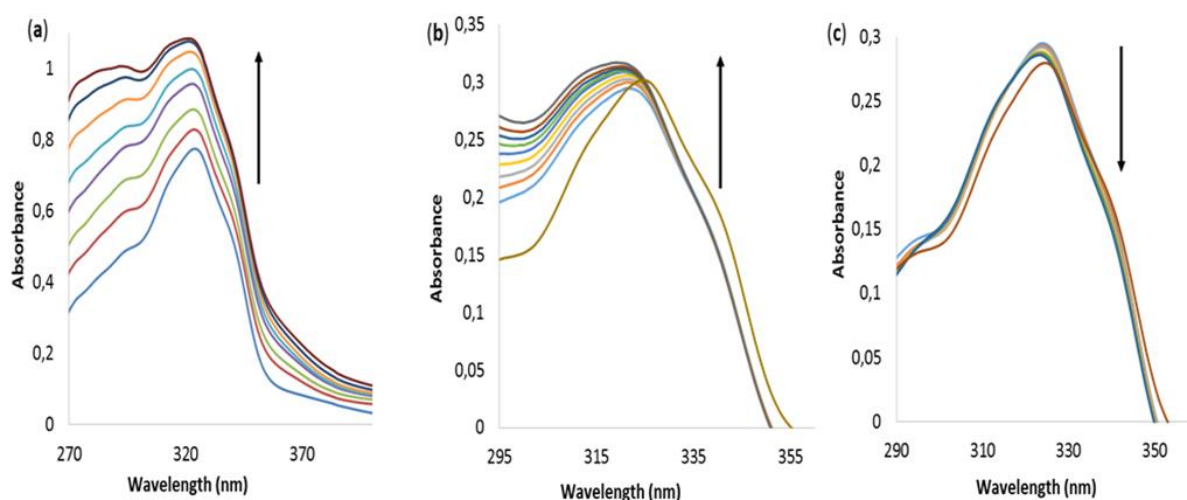


**Figure 4.39:** Absorption spectra of polymer **P2** in DMF upon addition of (a)  $\text{Fe}^{3+}$  (0.05-0.35  $\mu\text{M}$ ); (b)  $\text{Hg}^{2+}$  (1-9  $\mu\text{M}$ ) and (c)  $\text{Al}^{3+}$  (1-11  $\mu\text{M}$ ). The concentration of polymer **P2** was 0.16 g/L in the case of  $\text{Al}^{3+}$  and  $\text{Hg}^{2+}$ , while in the case of  $\text{Fe}^{3+}$  it was double.

To further investigate the photophysical properties of polymer **P2** in the presence of  $\text{Al}^{3+}$ ,  $\text{Hg}^{2+}$  and  $\text{Fe}^{3+}$  fluorescence, titration experiments were performed. The spectra were recorded at room temperature in DMF solvent at an excitation wavelength of 325 nm. **Figure 3.40** shows variations in the fluorescence of polymer **P2** with addition of  $\text{Hg}^{2+}$  and  $\text{Fe}^{3+}$  aliquots.

As noted in the case of  $\text{Hg}^{2+}$  (**Figure 4.40 a**), the addition of  $\text{Hg}^{2+}$  aliquots from 0.05 to 0.15  $\mu\text{M}$  caused gradual fluorescence quenching in the emission band at 386 nm. Surprisingly, additional aliquots of  $\text{Hg}^{2+}$  reversed the response and a gradual fluorescence increase in intensity of the fluorescence band at 386 nm was observed. As the addition of  $\text{Hg}^{2+}$  continued a bathochromic shift in maximum wavelength from 386 to 391 nm was also noted.



After 0.7  $\mu\text{M}$  of  $\text{Hg}^{2+}$  had been added, the fluorescence band at 391 nm started dropping with very small variation, at the same time a new emission band started appearing at 444 nm. As  $\text{Hg}^{2+}$  addition continued, a gradual increase in fluorescence and a bathochromic shift from 444 to 448 nm in then emission peak at 444 nm was noted. In addition, as the concentration of  $\text{Hg}^{2+}$  increased a fourth small emission band at ca. 490 nm started to appear. Since polymer **P2** and alkynylated coumarin derivative **11** show similar photophysical properties, it is unlikely that interchain interactions are involved in the binding events. Since this abnormal emission behaviour could not be detected in the corresponding alkynylated coumarin derivative **11**, the behaviour can be attributed to the incoming triazole ring or the change in conformation in polymer **P2** pendant chains which allow the occurrence of more than one binding mode in the presence of  $\text{Hg}^{2+}$ . The detection limit of polymer **P2** towards  $\text{Hg}^{2+}$  was calculated from fluorescence titration experiments and was found to be 0.036  $\mu\text{M}$ .

Unlike  $\text{Hg}^{2+}$ , the addition of increasing amounts of  $\text{Fe}^{3+}$  (from 0.05-0.5  $\mu\text{M}$ ) caused a gradual decrease in intensity of the fluorescence band at 386 nm until the saturation point was reached and no reverse fluorescence response were observed (**Figure 4.40 b**).

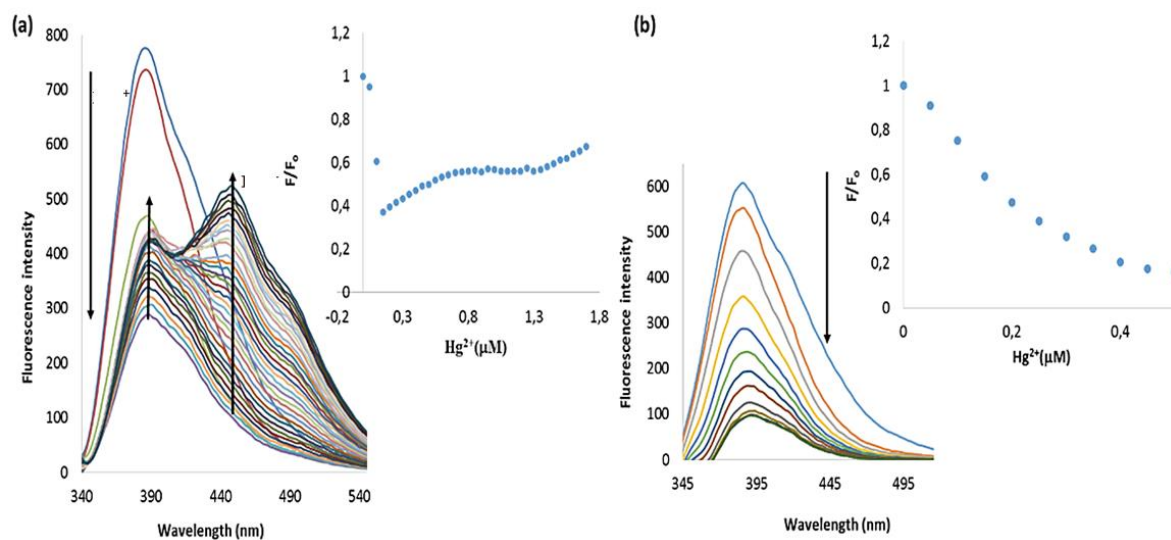


**Figure 4.40:** Emission spectra of polymer **P2** in DMF upon addition of **a)**  $\text{Hg}^{2+}$  (0-0.17  $\mu\text{M}$ ) and **b)**  $\text{Fe}^{2+}$  from (0-0.5  $\mu\text{M}$ ). Concentrations of  $7.7 \times 10^{-4}$  g/L and  $5 \times 10^{-4}$  g/L of polymer **P2** were titrated with  $\text{Hg}^{2+}$  and  $\text{Fe}^{2+}$  respectively. The excitation was performed at 325 nm.

From absorption and emission studies, it is clear that  $\text{Hg}^{2+}$  and  $\text{Fe}^{3+}$  can easily be distinguished from one another from their influence on the absorption or emission behaviour of polymer **P2**.

In the case of  $\text{Al}^{3+}$ , the addition of  $\text{Al}^{3+}$  aliquots ( $0.05\text{-}0.5\mu\text{M}$ ) to the DMF solution of polymer **P2** induced a gradual increase in fluorescence intensity from 636 to 874 nm and a bathochromic shift in maximum wavelength from 386 to 396 nm (**Figure 4.41**).

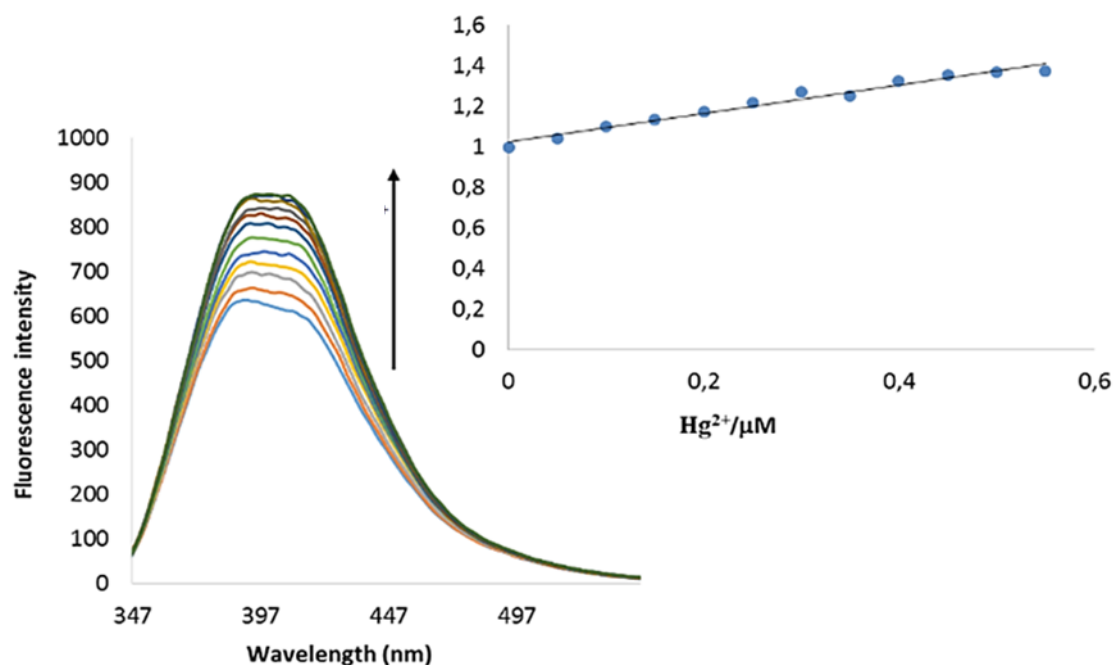


**Figure 4.41:** Changes in the emission spectra of polymer **P2** ( $5 \times 10^{-4}$  g/L) in DMF with increasing amounts of  $\text{Al}^{3+}$  ( $0.05\text{-}0.5\mu\text{M}$ ). The excitation was performed at 325 nm.

This shift suggests that the presence of  $\text{Al}^{3+}$  affects conjugation in the coumarin system. The inset (**Figure 4.41**) shows the plot of emission intensity of polymer **P2** at 325 nm versus the concentration of added  $\text{Al}^{3+}$  and a good linear relationship with a correlation coefficient of  $R^2=0.9725$  was obtained in the range of  $0.05\text{-}0.5 \mu\text{M}$ . The detection limit was calculated fluorescence titration experiments and was found to be  $0.096 \mu\text{M}$ .

#### d) Competitive studies

To investigate the effect of other metal ions on the binding in polymer **P2**- $\text{Al}^{3+}$  and polymer **P2**- $\text{Hg}^{2+}$  complexes, competitive experiments were conducted. These were conducted by recording emission spectra at an excitation wavelength of 325 nm in the presence of  $\text{Al}^{3+}$  or  $\text{Hg}^{2+}$  mixed with two equivalents of other metal ions ( $\text{Na}^+$ ,  $\text{Ca}^{2+}$ ,  $\text{Ag}^+$ ,  $\text{Ba}^{2+}$ ,  $\text{Cr}^{3+}$ ,  $\text{Cu}^{2+}$ ,  $\text{Fe}^{3+}$ ,  $\text{Mn}^{2+}$ ,  $\text{Co}^{2+}$ ,  $\text{Zn}^{2+}$ ,  $\text{Cd}^{2+}$ ,  $\text{Ni}^{2+}$  and  $\text{Pb}^{2+}$ ) in DMF. As shown in **Figure 4.42**, the fluorescence enhancement caused by  $\text{Al}^{3+}$  ions in polymer **P2** was slightly affected by the presence of two equivalents of other metal ions, except in the case of  $\text{Fe}^{3+}$  and  $\text{Hg}^{2+}$  ions. In addition, a

bathochromic shifting and broadening in the emission band induced by the presence of  $\text{Al}^{3+}$  were not significantly affected by the presence of other metal ions (**Appendices Figure A.16**). These observations indicate the stability of **P2**- $\text{Al}^{3+}$  complex in the presence of the other metal ions.

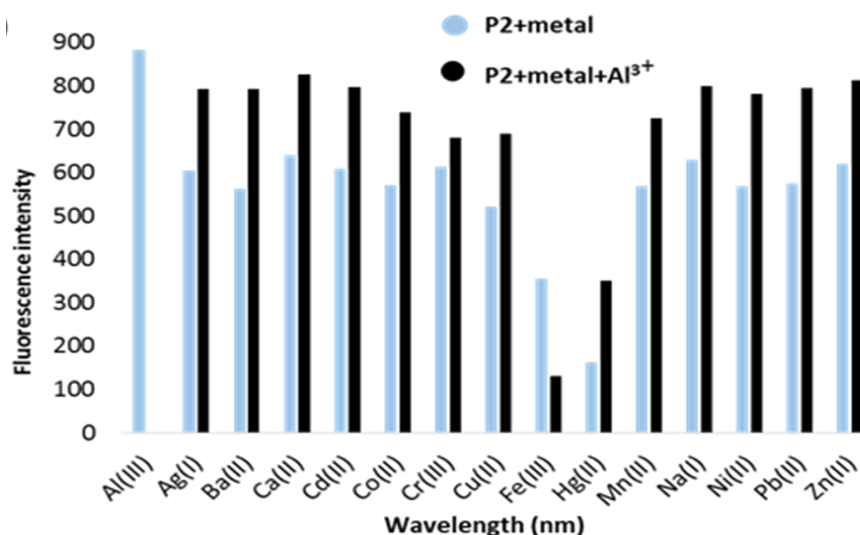


**Figure 4.42: a)** Fluorescence response of polymer **P2** ( $5 \times 10^{-4}$  g/L) in the presence of metal ions ( $0.2 \mu\text{M}$ )  $\text{Na}^+$ ,  $\text{Ca}^{2+}$ ,  $\text{Ag}^+$ ,  $\text{Al}^{3+}$ ,  $\text{Ba}^{2+}$ ,  $\text{Cr}^{3+}$ ,  $\text{Cu}^{2+}$ ,  $\text{Fe}^{3+}$ ,  $\text{Hg}^{2+}$ ,  $\text{Mn}^{2+}$ ,  $\text{Co}^{2+}$ ,  $\text{Zn}^{2+}$ ,  $\text{Cd}^{2+}$ ,  $\text{Ni}^{2+}$  and  $\text{Pb}^{2+}$  (blue bars) and **P2** in the presence of a mixture of  $\text{Al}^{3+}$  ( $0.2 \mu\text{M}$ ) and other metal ions ( $0.4 \mu\text{M}$ ) (black bars). Excitation was performed at 325 nm.

As was done for  $\text{Al}^{3+}$ , a competitive experiments for  $\text{Hg}^{2+}$  were conducted in DMF at 325 nm in the presence of two equivalents of other metal ions. As shown in **Figure 4.43** the fluorescence quenching caused by  $\text{Hg}^{2+}$  ions was not obviously affected by the presence of two equivalents of other metal ions, except in the case of  $\text{Al}^{3+}$  ions where slight enhancement was observed and in  $\text{Co}^{2+}$  and  $\text{Fe}^{2+}$  where enhanced quenching was observed. This indicates that the presence of other metal ions does not significantly affect **P2**-  $\text{Hg}^{2+}$  complex.

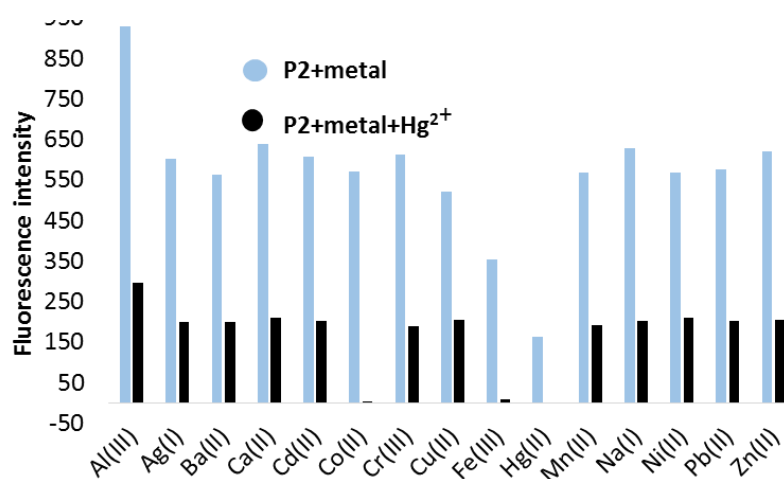


**Figure 4.43:** Fluorescence response of polymer **P2** ( $5 \times 10^{-4}$  g/L) in the presence of metal ions ( $0.2 \mu\text{M}$ )  $\text{Na}^+$ ,  $\text{Ca}^{2+}$ ,  $\text{Ag}^+$ ,  $\text{Al}^{3+}$ ,  $\text{Ba}^{2+}$ ,  $\text{Cr}^{3+}$ ,  $\text{Cu}^{2+}$ ,  $\text{Fe}^{3+}$ ,  $\text{Hg}^{2+}$ ,  $\text{Mn}^{2+}$ ,  $\text{Co}^{2+}$ ,  $\text{Zn}^{2+}$ ,  $\text{Cd}^{2+}$ ,  $\text{Ni}^{2+}$  and  $\text{Pb}^{2+}$  (blue bars) and in the presence of a mixture of  $\text{Hg}^{2+}$  ( $0.2 \mu\text{M}$ ) with two equivalents ( $0.4 \mu\text{M}$ ) of other metal ions (black bars). Excitation was performed at 325 nm.

*e) Proposed binding modes for P2 with Hg<sup>2+</sup> and Al<sup>3+</sup>*

In order to get an insight on the sensing mechanism of polymer **P2** towards  $\text{Hg}^{2+}$  and  $\text{Al}^{3+}$ , the absorption and emission behaviour of polymer **P2** in the presence of  $\text{Hg}^{2+}$  and  $\text{Al}^{3+}$  was compared with that of the corresponding alkynylated coumarin derivative **11** using the same ions. Since the photophysical properties of polymer **P2** are dominated by pendant coumarin units any difference in sensitivity between polymer **P2** and the alkynylated coumarin derivative **11** can be attributed to the newly formed triazole ring, which can lead to changes in the polymer **P2** pendant chains suitable for metal binding.

By comparing the selectivity of the alkynylated coumarin derivative **11** and polymer **P2** in the presence of different metal ions, it is clear that both the alkynylated coumarin derivative **11** and polymer **P2** showed selective responses with fluorescence quenching towards  $\text{Hg}^{2+}$ . The presence of  $\text{Al}^{3+}$  did not induce any noticeable changes in the emission band of the alkynylated coumarin derivative **11**, while a fluorescence enhancement was obtained in the corresponding polymer **P2**. This suggests that the triazole ring plays a meaningful role in  $\text{Al}^{3+}$  detection. Although both the alkynylated coumarin derivative **11** and polymer **P2** showed selective responses towards  $\text{Hg}^{2+}$ , their absorption and fluorescence titration experiments in the presence of increasing amount of  $\text{Hg}^{2+}$  showed some variations, suggesting different binding modes in the alkynylated coumarin derivative **11** and polymer **P2**. Furthermore, the absorption titration experiments in the presence of increasing amounts of both  $\text{Hg}^{2+}$  and  $\text{Al}^{3+}$  showed a reverse

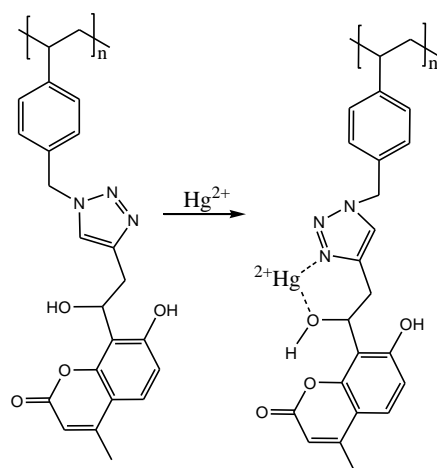
---

responses at some stages suggesting the occurrence of more than one binding mode during the recognition process. By analysing the absorption and emission behaviour of polymer **P2** in the presence of either  $\text{Hg}^{2+}$  or  $\text{Al}^{3+}$ , it is clear that the binding modes that occurred in the polymer **P2** affected the coumarin conjugated system. This could be justified by the spectral shifts obtained in presence of  $\text{Hg}^{2+}$  or  $\text{Al}^{3+}$ .

In the case of  $\text{Hg}^{2+}$ , the addition of  $\text{Hg}^{2+}$  aliquots to polymer **P2** solution resulted in the gradual decrease in the emission band at the beginning (**Figure 4.40 a**). When the addition continued, the response reversed from quenching to enhancement with a weak bathochromic shift from 386 to 391 nm. These observations were almost similar to those obtained during UV-Vis titration experiments in the presence of  $\text{Hg}^{2+}$  where a decrease in intensity and a hypsochromic shift in the absorption band were initially observed and the response later reversed to increase in intensity on further addition of  $\text{Hg}^{2+}$  (**Figure 4.39 b**).

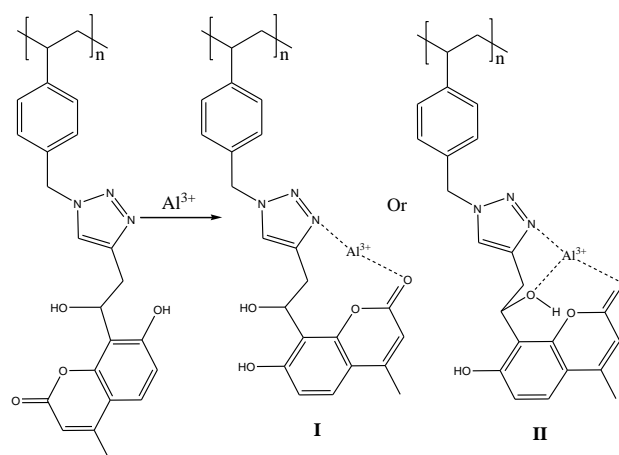
From absorption and emission spectral analysis, it is clear that at early stages of  $\text{Hg}^{2+}$  additions, the coumarin conjugated system was disrupted. This led to a hypsochromic shift in the absorption. However, additional aliquots of  $\text{Hg}^{2+}$  seemed to enhance conjugation in the coumarin system. This is justified by a reverse response from quenching to enhancement in both absorption and emission and a bathochromic shift in the emission band from 386 to 391 nm.

Based on the geometrically optimized structure of the pendant chain in the presence of  $\text{Hg}^{2+}$  determined through computation at the DFT level (B3PW91/LanL2MB). The minimum energy was obtained when  $\text{Hg}^{2+}$  coordinates the triazole nitrogen and hydroxyl of the functional linkage *via* a six membered ring structure (**Appendices A.30**). This binding mode as shown in **Scheme 4.12**, leads to the electron deficiency at position 8 of coumarin unit nitrogen, which disrupts push-pull effect in the coumarin system. This was supported by a clear hypsochromic shift in the absorption spectrum of **P2** upon  $\text{Hg}^{2+}$  addition. A change in conformation induced by this binding mode allows polymer **P2** to chelate to another  $\text{Hg}^{2+}$  ion using different binding sites which resulted in reverse responses in both absorption and emission spectra of polymer **P2** when the concentration of  $\text{Hg}^{2+}$  was increased.



**Scheme 4.12:** The proposed binding modes of polymer **P2** in the presence of  $\text{Hg}^{2+}$

Beside the involvement of the triazole ring in  $\text{Al}^{3+}$  binding, as suggested by alkynylated coumarin derivative **11** and polymer **P2** comparative spectral studies, the increase in fluorescence intensity and the red shift in the emission band from 386 to 396 nm in the presence of  $\text{Al}^{3+}$  also suggests enhanced conjugation in the coumarin system. The only way an increase in conjugation can occur in this system, is when the carbonyl of the coumarin system is involved in  $\text{Al}^{3+}$  binding. Two likely binding modes that involve the triazole and carbonyl coumarin carbonyl groups are depicted in **Scheme 4.13**. From the geometrically optimized structure of the pendant chain in the presence of  $\text{Al}^{3+}$ , determined through computation at the DFT level (B3PW91/LanL2MB), binding mode (**I**) (**Appendices A.31**) showed less energy than its corresponding binding mode (**II**). This suggests that  $\text{Al}^{3+}$  chelates to the nitrogen of the triazole and carbonyl of the coumarin resulting in increased push-pull effect in the coumarin unit. As a result an increase in intensity and red shift was observed in emission spectrum of **P2**.



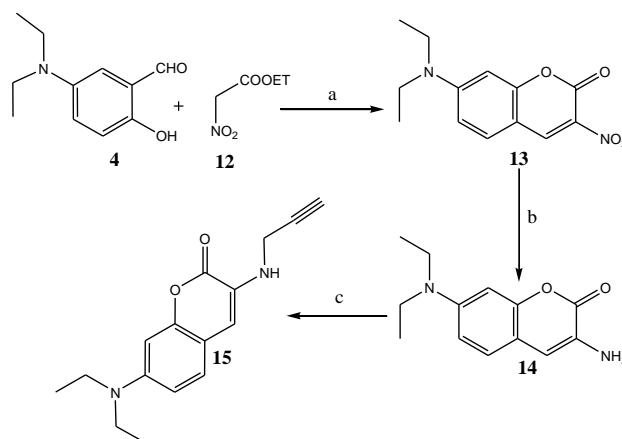
**Scheme 4.13:** The proposed binding modes of polymer **P2** in the presence of  $\text{Al}^{3+}$ .

## 4.4 Triazolyl coumarin-based polymers with amino-methylene linkages between triazole and coumarin units (P3)

The synthesis of polymer **P3** was accomplished in two stages as done for hydroxyethylene-bridged triazolyl coumarin based polymers. The first stage involved the synthesis of an alkynylated coumarin derivative **15** with an amino methylene bridge at position 3 of the coumarin system. The alkynylated coumarin derivative **15** was attached to the azide-functionalized side chains of polymer **P0** under click reaction conditions to yield polymer **P3** with an amino methyl bridge between the triazole and the coumarin system.

### 4.4.1 Synthesis of the alkynylated coumarin derivative **15**

The synthesis was accomplished in three steps from 4-(diethylamino)-2-hydroxybenzaldehyde as shown in **Scheme 4.14**. Coumarins **13** and **14** were synthesized according to the procedure previously used for the synthesis of coumarin **6** and **7** in Chapter 3. Synthesis of the alkynylated coumarin derivative **15** was done at room temperature in a mixture of dichloromethane and 50% NaOH solution according to the reported tandem alkylation reaction of the primary amine with alkyl halides.<sup>22</sup> Tetrabutylammonium bromide (TBAB) was used as a phase transfer catalyst and propargyl bromide was used in the place of the alkyl halide to yield desired product **15** in 61 % yield.



**Scheme 4.14:** Synthesis of the alkynylated coumarin derivative **15** **a)** Piperidine, AcOH, butanol, reflux; **b)** SnCl<sub>2</sub>, HCl(aq), rt; **c)** DCM and 50% NaOH (1:1), propargyl bromide.

The structures of alkynylated coumarin derivative **15** were characterized by NMR spectroscopy (For <sup>13</sup>C NMR see **Appendices Figure A.17**). **Figure 4.44** illustrates the assignment of proton signals in the <sup>1</sup>H NMR spectrum of coumarin **15**. The appearance of a signal for the terminal alkyne proton (i) at 2.59 ppm, methylene protons of the side chain (h) at 4.81 ppm and protons

of 7-(diethylamino)coumarin confirms the successful synthesis of alkynylated coumarin derivative **15**.

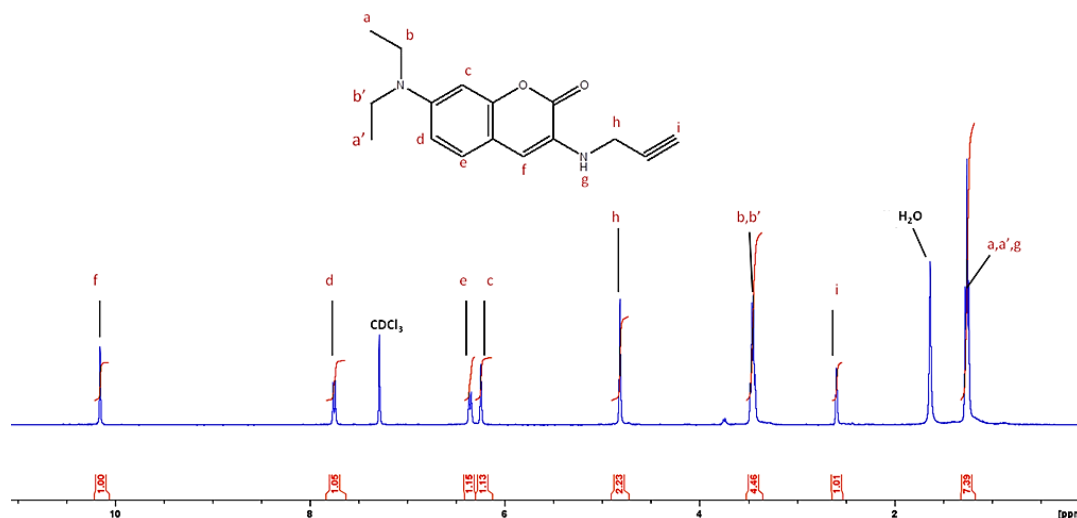
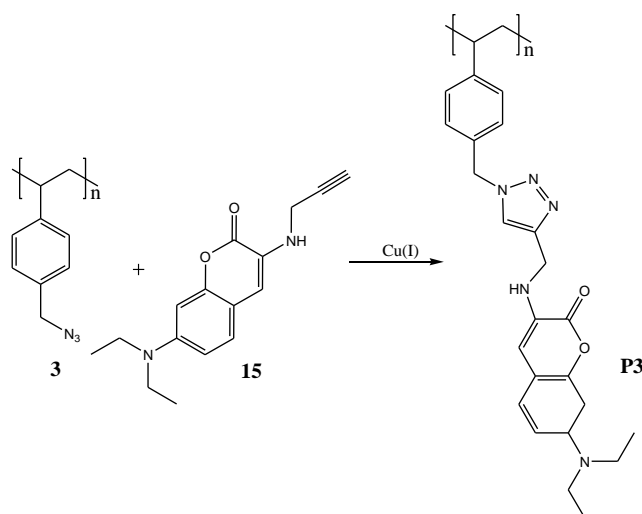


**Figure 4.44:**  $^1\text{H}$  NMR spectrum of alkynylated coumarin derivative **15** in  $\text{CDCl}_3$ .

#### 4.4.2 Functionalization of polymer **P0** with alkynylated coumarin derivative **15**

Polymer **P0** was functionalized with the alkynylated coumarin derivative **15** under Cu(I)-mediated click reaction conditions as shown in **Scheme 4.15**. The reaction was performed at room temperature in THF with a minimum amount of water. On completion of the reaction, the precipitated polymer was filtered and washed with water to afford pure polymer **P3** as a brown solid in 85% yield.



**Scheme 4.15:** Functionalization of polymer **P0** with alkynylated coumarin derivative **15**.



The structure of polymer **P1** was confirmed by  $^1\text{H}$  NMR and FT-IR spectroscopy. **Figure 4.45** illustrates partial comparative  $^1\text{H}$  NMR spectra of polymer **P0**, alkynylated coumarin derivative **15** and polymer **P3**. Due to the chemical modification from the electron donating alkyne group to the electron withdrawing triazole ring, the proton signal at 4.8 ppm which was attributed to the methylene group of the side chain in alkynylated coumarin derivative **15** (h) was shifted downfield with signal broadening which is typical for polymers. Furthermore, other proton signals from the starting materials were prominent as broad signals in the spectrum for polymer **P3**, along with a new signal in the aromatic region which was assigned to the triazole ring. Due to the low solubility of **P3**, the average molecular weight and polydispersity index could not be determined from size exclusion chromatography experiments.

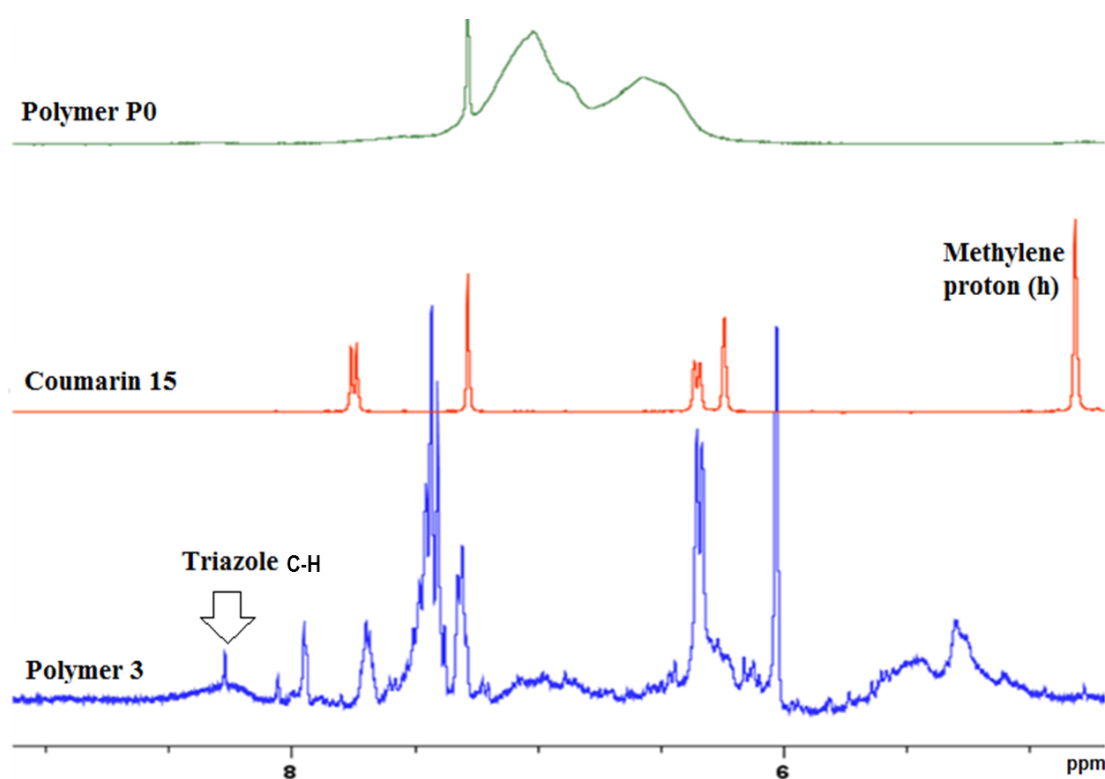


**Figure 4.45:** Comparative  $^1\text{H}$  NMR spectra for polymer **P0**, alkynylated coumarin derivative **15** and polymer **P3**. In the case of coumarin **15** and polymer **P0**,  $\text{CDCl}_3$  solvent was used for NMR characterization while DMSO was used for polymer **P3**.

The comparison of FT-IR spectra of the polymer **P0** and the functionalized polymer **P3** (**Figure 4.46**) showed a significant decrease in the intensity of the azide stretching at  $2090\text{ cm}^{-1}$  in polymer **P3** compared to the starting polymer **P0**. Furthermore, a broad new peak appeared at  $3400\text{ cm}^{-1}$  in the spectrum for polymer **P3** and was assigned to the stretch mode of the

secondary amine group from alkyne-coupled coumarin derivative **15**. The percentage conversion of the azide groups to triazole was found to be 92%.

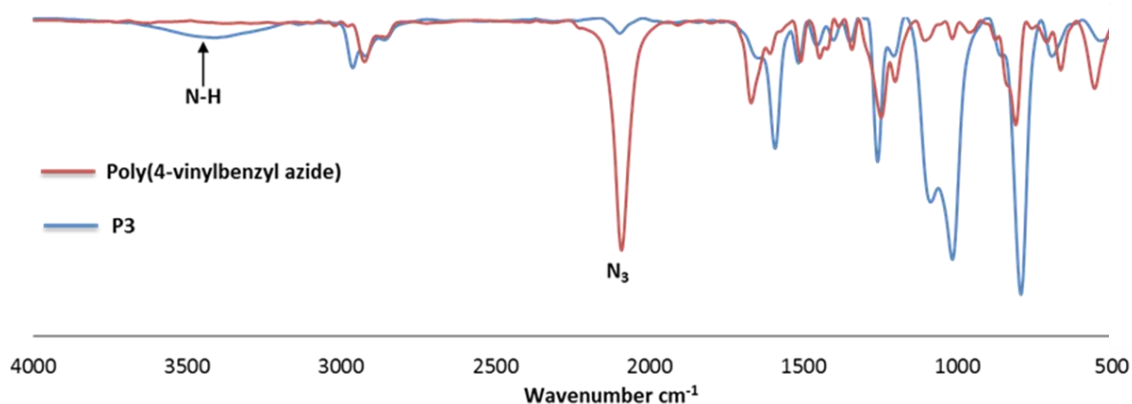
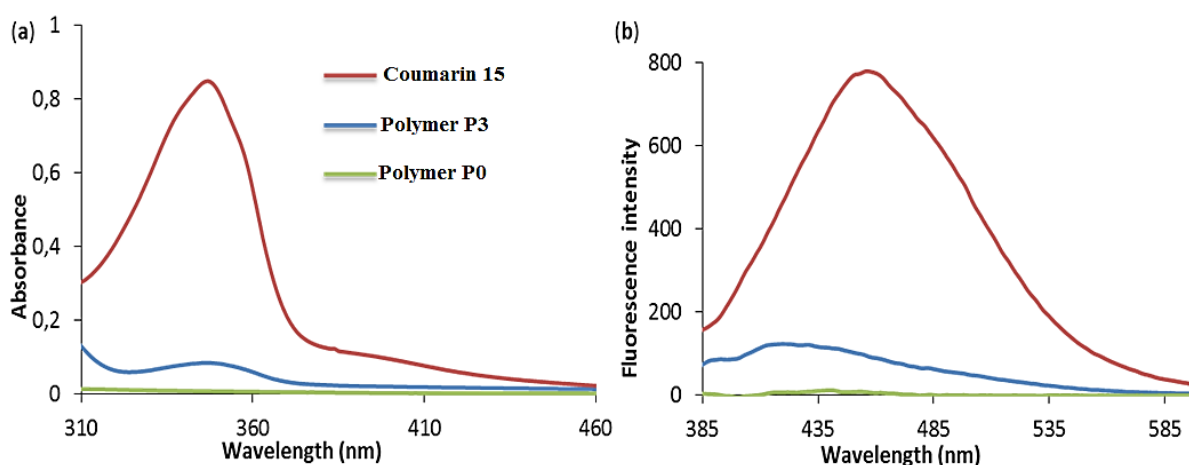


**Figure 4.46:** Comparative FT-IR spectra of polymer **P0** and the functionalized polymer **P3**.

#### 4.4.3 Absorption and emission studies on polymer **P0** functionalization

To further confirm the functionalization of polymer **P0** with alkyne-coupled coumarin derivative **15**, the photophysical properties of polymer **P0** were compared with the photophysical properties of polymer **P3** and alkyne-coupled coumarin derivative **15**. Same as in previous sections, DMF solutions containing equal amount (in grams) of each compound were used. As expected, polymer **P3** showed absorption and emission intensities with the magnitude between the absorption and emission intensities of the starting materials (**Figure 4.47**). The Alkyne-coupled coumarin derivative **15** with high content in coumarin chromophores showed higher absorption and emission intensities while polymer **P0** with quenching azide group showed negligible absorption and emission.

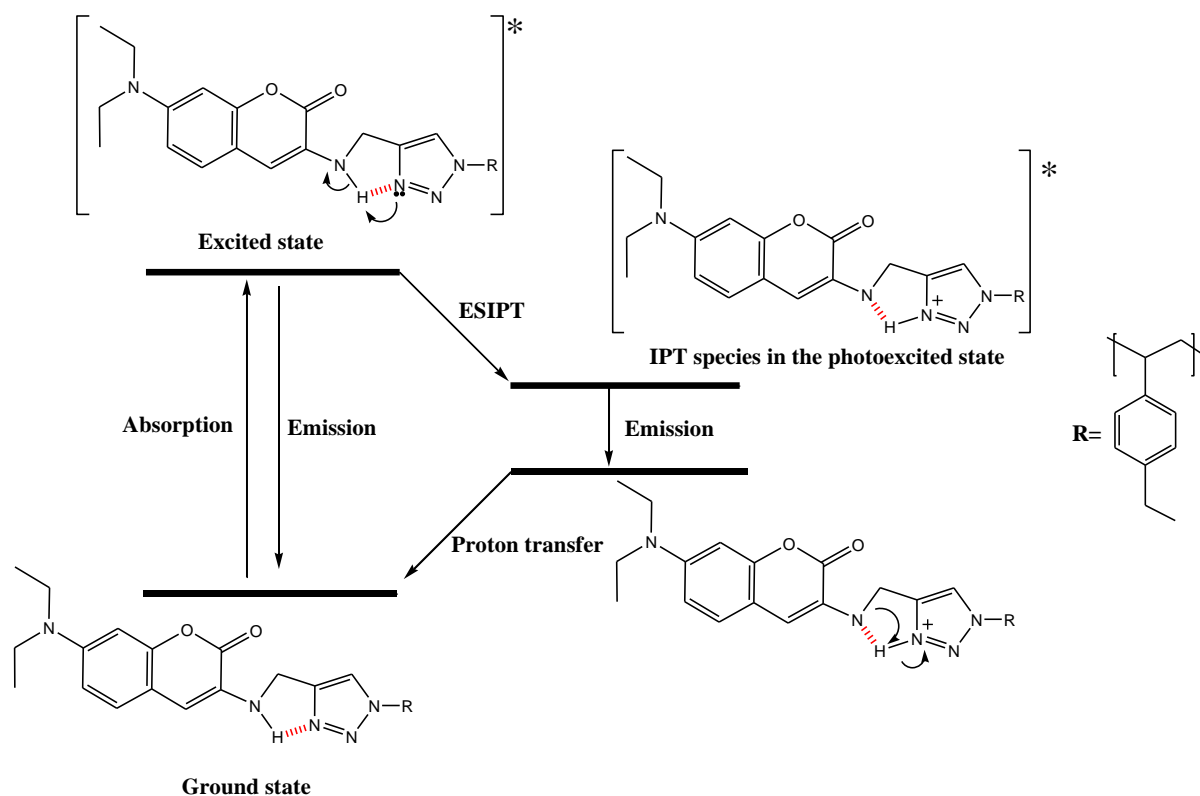


---

**Figure 4.47:** a) Absorption and b) Emission spectra of the alkynylated coumarin derivative **15** (0.12 g/L), polymer **P0** (0.12 g/L) and polymer **P3** (0.12 g/L) in DMF. Excitation was performed at 350 nm.

It was noted that the alkynylated coumarin derivative **15** and polymer **P3** showed similar absorption properties with maximum absorption at 348 nm and different emission properties. Polymer **P3** emitted at higher energy compared to its corresponding alkynylated coumarin derivative **15**. The maximum emission for **P3** was observed at 420 nm while maximum emission for alkynylated coumarin derivative **15** was observed at 457 nm. Since this shift was not detected in the absorption spectrum, it was concluded that there is connection between excited state of polymer **P3** and the blue shift which is detected in the emission spectrum. Only two photochemical processes can contribute to this shift. One is photoinduced electron transfer (PET) which involves the lone pair of nitrogen atom at position 3 of the coumarin unit to the excited coumarin system. The second one is the excited state intramolecular proton transfer (ESIPT) from the secondary amine hydrogen to either the carbonyl of the coumarin or to the triazole ring. Since this shift was not noticed in alkynylated coumarin derivative **15**, the most likely mechanism that could result in the shift is ESIPT from the secondary amine proton of the coumarin side chain to the nitrogen of the triazole as shown in **Scheme 4.16**.

When the proton is transferred to the nitrogen of the triazole, an excited state ESIPT complex with a negative charge on the nitrogen in position 3 of the coumarin is generated. The charge is delocalized into the coumarin system resulting in a decreased push-pull character of the coumarin system. A decrease in the push-pull character is expressed as a blue shift in the emission spectrum since the conjugation of the coumarin system is disturbed. The occurrence of the ESIPT mechanism was also supported by a large Stokes' shift (>70nm), which is one of the characteristics of this mechanism, and broadening of the emission spectrum of polymer **P3**. Broadening of the emission spectrum also suggests the presence of two excited states (normal and Zwitterionic tautomer excited states).<sup>23</sup>



**Scheme 4.16:** Schematic representation of the ESIPT mechanism in polymer **P3**.

Generally, the PET mechanism is disrupted by the presence of metal ions as they bind with the lone pair which is involved in the quenching of the excited fluorophore leading to fluorescence enhancement.<sup>24</sup> For this reason, the response of polymer **P3** in the presence of different metal ions was investigated in order to confirm the occurrence of the ESIPT mechanism. Different metal ions such as  $\text{Na}^+$ ,  $\text{Ca}^{2+}$ ,  $\text{Ag}^+$ ,  $\text{Al}^{3+}$ ,  $\text{Ba}^{2+}$ ,  $\text{Cr}^{3+}$ ,  $\text{Cu}^{2+}$ ,  $\text{Fe}^{3+}$ ,  $\text{Hg}^{2+}$ ,  $\text{Mn}^{2+}$ ,  $\text{Co}^{2+}$ ,  $\text{Zn}^{2+}$ ,  $\text{Cd}^{2+}$ ,  $\text{Ni}^{2+}$  and  $\text{Pb}^{2+}$  were investigated. As shown in **Figure 4.48**, the presence of metal ions showed a slight enhancement in polymer **P3** emission band. This confirms a small contribution of PET mechanism on the polymer **P3** emission.

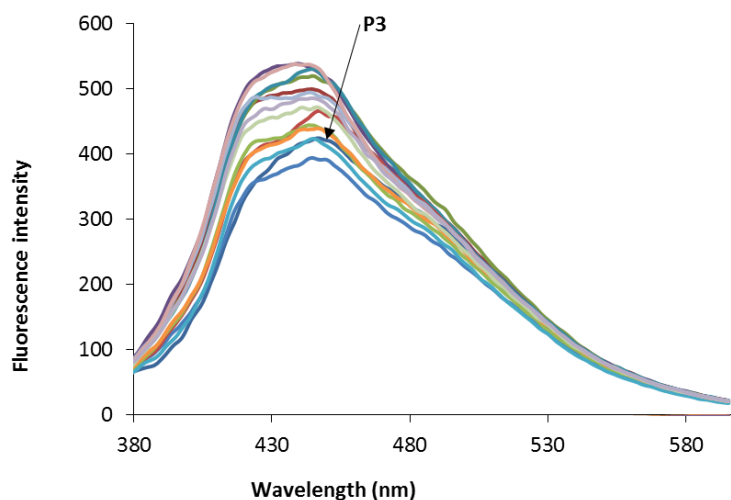


**Figure 4.48:** Emission spectra of polymer **P3** ( $1.3 \times 10^{-3}$  g/L) in the presence of ( $2 \mu\text{M}$ )  $\text{Na}^+$ ,  $\text{Ca}^{2+}$ ,  $\text{Ag}^+$ ,  $\text{Al}^{3+}$ ,  $\text{Ba}^{2+}$ ,  $\text{Cr}^{3+}$ ,  $\text{Cu}^{2+}$ ,  $\text{Fe}^{3+}$ ,  $\text{Hg}^{2+}$ ,  $\text{Mn}^{2+}$ ,  $\text{Co}^{2+}$ ,  $\text{Zn}^{2+}$ ,  $\text{Cd}^{2+}$ ,  $\text{Ni}^{2+}$  and  $\text{Pb}^{2+}$ . Spectra were recorded in DMF at 350 nm excitation wavelength.

#### 4.4.4 Chemosensing studies of polymer **P3**

Due to a strong affinity between the anions and the proton of the amino group connected to an electron-deficient system such as in urea,<sup>25</sup> thiourea,<sup>26</sup> tetrazole,<sup>27</sup> and diaminomethanenitrile,<sup>28</sup> based chemosensors, the chemosensing capability of polymer **P3** has been investigated in presence of anionic species. The interaction between the anions with the amino proton in the polymer **P3** disrupts ES IPT mechanism and leads to detectable changes in emission spectra. In all chemosensing studies, solutions of tetrabutylammonium salts were used as anions source.

##### 4.4.4.1 Absorption and emission studies

Investigation of the chemosensing capability of polymer **P3** towards anions was accomplished using absorption and emission spectra analysis in the presence of different ionic species such as  $\text{H}_2\text{PO}_4^-$ ,  $\text{F}^-$ ,  $\text{Cl}^-$ ,  $\text{Br}^-$ ,  $\text{HSO}_4^-$ ,  $\text{OH}^-$ ,  $\text{I}^-$ ,  $\text{NO}_3^-$ ,  $\text{AcO}^-$  and  $\text{CN}^-$ . The studies were carried out at room temperature in DMF. As shown in **Figure 4.49 a**, all the tested anions except  $\text{OH}^-$  and  $\text{F}^-$  slightly affected the absorption band of polymer **P3** at 348 nm. The presence of  $\text{OH}^-$  induced a blue shift, while  $\text{F}^-$  induced a significant decrease in the intensity of the absorption band of polymer **P3** which suggests a strong interaction between the polymer **P3** and the  $\text{F}^-$  ions. On the other hand, when emission spectra were recorded for the same set of anions at 350 nm, a reverse response was detected in the presence of  $\text{F}^-$  (**Figure 4.49 b**). The later almost doubled the fluorescence intensity of polymer **P3** while the other anions except  $\text{OH}^-$  did not induce

significant fluorescence enhancement. This fluorescence enhancement can be attributed to the disruption of the ESIPT mechanism due to the binding of the F<sup>-</sup> ions to the amino hydrogen of the coumarin-triazole linkage.

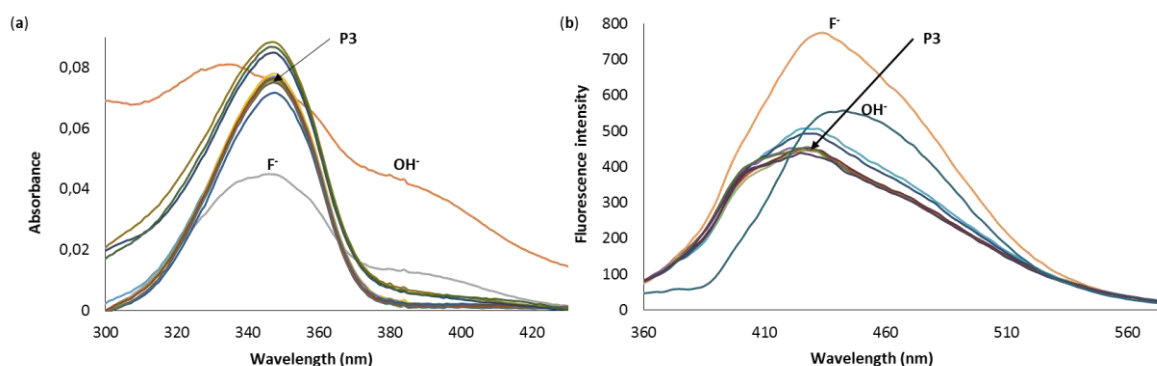


**Figure 4.49:** a) Absorption spectra of polymer **P3** ( $1.6 \times 10^{-3}$  g/L) and b) Emission spectra of polymer **P3** ( $1.3 \times 10^{-3}$  g/L) in the presence of the aliquot (2  $\mu$ M) of different anions ( $\text{H}_2\text{PO}_4^-$ ,  $\text{ClO}_4^-$ ,  $\text{F}^-$ ,  $\text{Cl}^-$ ,  $\text{Br}^-$ ,  $\text{HSO}_4^-$ ,  $\text{OH}^-$ ,  $\text{I}^-$ ,  $\text{NO}_3^-$ ,  $\text{AcO}^-$  and  $\text{CN}^-$ ). Spectra were recorded in DMF and excitation was performed at 350 nm.

#### 4.4.4.2 Titration experiments

In order to investigate the absorption and emission behaviour of polymer **P3** in the presence of F<sup>-</sup> ions, UV-Vis and fluorescence titration experiments were conducted. As shown in **Figure 4.50 a**, the addition of F<sup>-</sup> aliquots ( $5 \times 10^{-7}$  M) to a DMF solution of polymer **P3** induced a gradual decrease in the intensity of the maximum absorption band at 348 nm and a gradual increase in the intensity of the absorption band at 390 nm with an isosbestic point at 365 nm. The maximum absorption band was assigned to absorption in the coumarin system while the increase in the bathochromic absorption band was attributed to the increase in charge transfer in the coumarin system. The isosbestic point indicates the formation of a polymer **P3**-F<sup>-</sup> complex.

On the other hand, the recorded emission spectra from the mixtures of polymer **P3** with different concentrations of F<sup>-</sup> showed a gradual increase in polymer **P3** emission band at 438 nm (**Figure 4.50 b**). The inset in **Figure 4.50 b** shows the plot of emission intensity of polymer **P3** at 350 nm against the concentration of added F<sup>-</sup>. A linear relationship with a correlation coefficient of  $R^2=0.9949$  was obtained in the range of 0-2  $\mu$ M. The detection limit was calculated in the same range and found to be 0.195  $\mu$ M.

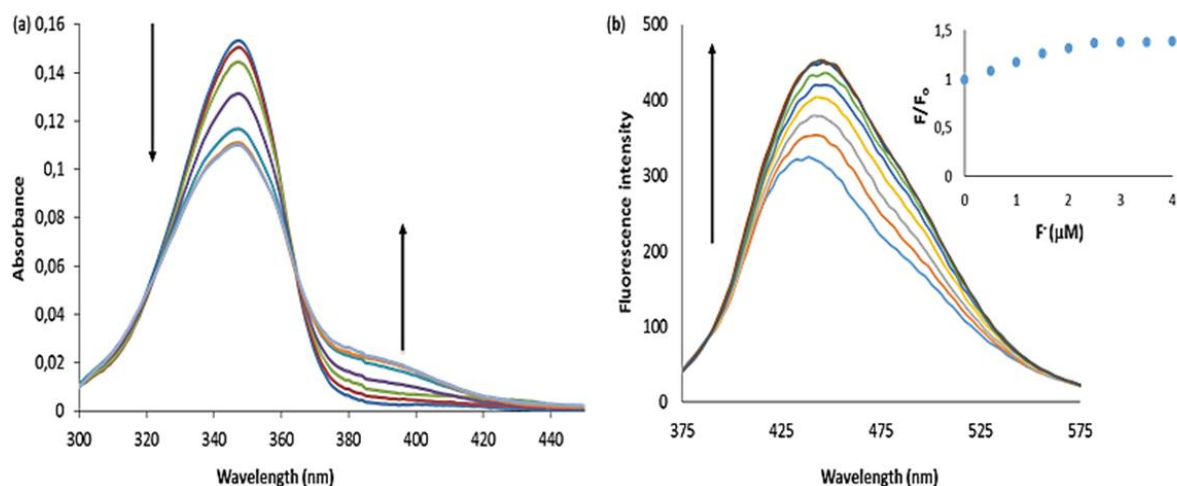


**Figure 4.50:** a) Absorption and b) Emission spectra of polymer **P3** in DMF upon addition of  $F^-$  ( $5 \times 10^{-7}$  M). Excitation was performed at 385 nm and a polymer **P3** concentration equivalent to  $3.2 \times 10^{-3}$  g/L and  $6.5 \times 10^{-4}$  g/L was used in absorption and emission analysis respectively.

#### 4.4.4.3 Competitive studies

The influence of other anions on  $F^-$  binding to polymer **P3** was investigated through competitive experiments. This was achieved through the analysis of the emission spectra of polymer **P3** in the presence of  $F^-$  and a molar equivalent of the other anion ( $H_2PO_4^-$ ,  $Cl^-$ ,  $Br^-$ ,  $HSO_4^-$ ,  $OH^-$ ,  $I^-$ ,  $NO_3^-$ ,  $AcO^-$ ,  $ClO_4^-$  and  $CN^-$ ). The emission spectra were recorded in DMF at room temperature at 350 nm. As shown in **Figure 4.51** the fluorescence enhancement response induced by the presence of  $F^-$  could not be significantly affected by the presence other anions in most of the cases. The highest interference was observed in the presence of  $CN^-$ . The presence of other halides showed very small interferences. This indicates that polymer **P3** can selectively bind with  $F^-$  in the presence of other anionic species.

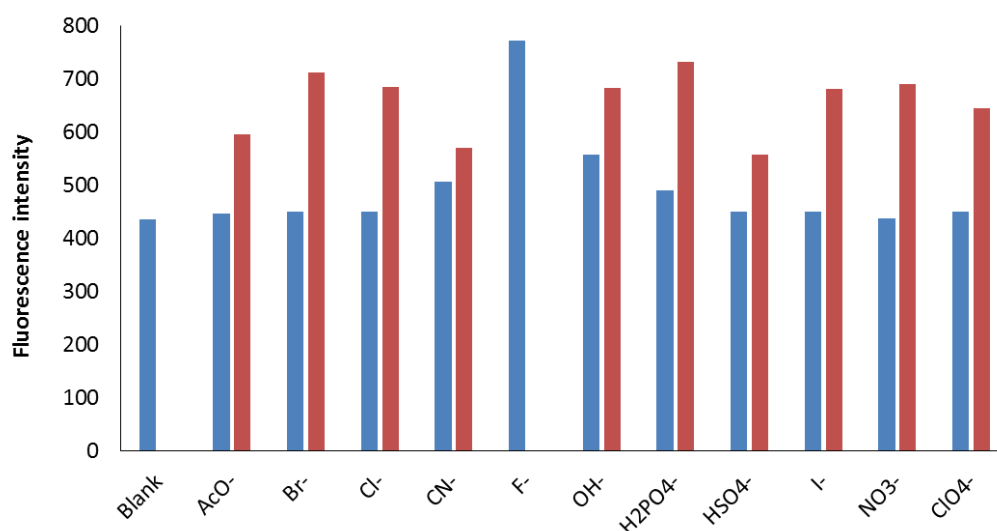
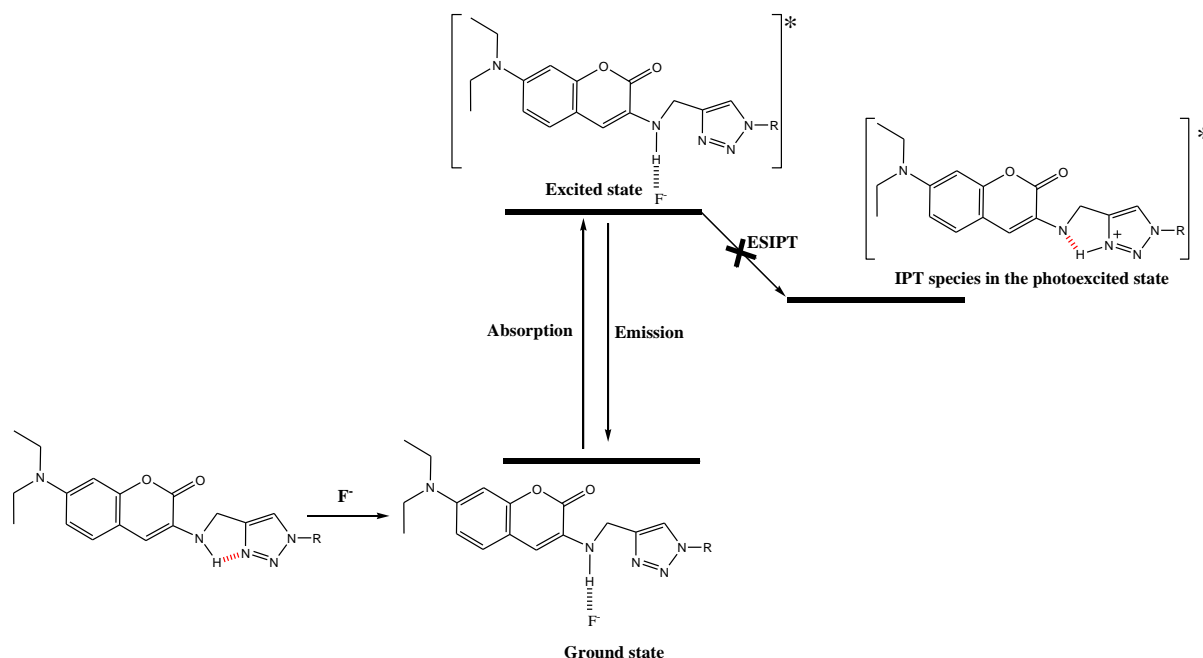


**Figure 4.51:** Fluorescence responses of polymer **P3** ( $1.3 \times 10^{-3}$  g/L) in the presence of different anions ( $2 \mu\text{M}$ )  $\text{H}_2\text{PO}_4^-$ ,  $\text{ClO}_4^-$ ,  $\text{F}^-$ ,  $\text{Cl}^-$ ,  $\text{Br}^-$ ,  $\text{HSO}_4^-$ ,  $\text{OH}^-$ ,  $\text{I}^-$ ,  $\text{NO}_3^-$ ,  $\text{AcO}^-$  and  $\text{CN}^-$  (blue bars) and in the presence of mixture of  $\text{F}^-$  ( $2 \mu\text{M}$ ) with one equivalent ( $2 \mu\text{M}$ ) of other anions (red bars). Excitation was performed at 350 nm.

#### 4.4.4.4 Sensing mechanism of the polymer **P3** with $\text{F}^-$ ions

Since the above studies confirmed the ESIPT mechanism as the sole mechanism involved in the sensing of  $\text{F}^-$  ions, the proposed sensing mechanism is summarized in **Scheme 4.17**. Due to the small size of the  $\text{F}^-$  ions, their interaction with the amino proton from the polymer **P3** via hydrogen bonding is easier compared to other anions. This fact was the basis for the selective response towards  $\text{F}^-$ . Once  $\text{F}^-$  binds to the secondary amine proton, it forms a polymer **P3**- $\text{F}^-$  complex in which the ESIPT mechanism is disrupted. This allows only one excitation state which decays via a radiative pathway and results in increase in emission intensity.

Since the binding of  $\text{F}^-$  increases the electron-donating ability of nitrogen in position 3 of the coumarin system, its presence increases the chance of the PET mechanism from the nitrogen in the position 3 to the coumarin system upon excitation. For this reason, the emission of polymer **P3** in the presence of  $\text{F}^-$  was not highly pronounced.



**Scheme 4.17:** A proposed inhibition of the ESIPT mechanism in polymer **P3**.



---

## 4.5 Conclusion

Polymers with bridged triazolyl coumarin systems were synthesized through multiple step syntheses. Their optical properties and chemosensing capabilities were investigated in DMF at room temperature. In the investigation of photophysical properties, where the absorption and emission properties of the polymers were compared with the absorption and emission properties of their corresponding starting materials, it was demonstrated that the photophysical properties of the polymers are generally governed by the coumarin system from the alkynylated coumarin compounds. The investigation of chemosensing capabilities of the polymers in the presence of various cationic and anionic species showed higher sensitivity towards  $\text{Hg}^{2+}$ ,  $\text{Fe}^{3+}$  and  $\text{OH}^-$  in polymer **P1**,  $\text{Hg}^{2+}$  and  $\text{Al}^{3+}$  in polymer **P2** and  $\text{F}^-$  in polymer **P3**. By comparing responses between each polymer and its corresponding alkynylated coumarin derivative in the presence of these ions, it was concluded that some chemical processes form the basis of their selective sensitivities. These include hydrogen bonding and ESIPT.

## 4.6 Experimental

### 4.6.1 General information

All chemicals and solvents were purchased from Sigma Aldrich or Merck and used as received without further purification. Reactions monitoring, products purification and characterization as well as photophysical studies were done using same materials and instrumentation as the ones stated in Chapter 3.

### 4.6.2 Synthesis of the poly(4-vinylbenzyl azide) (P0)

Both 4-vinylbenzyl azide and poly(4-vinylbenzyl azide) were synthesized according to literature procedures,<sup>9</sup> and their structures were confirmed using NMR and FT-IR.

#### 4.6.2.1 4-Vinylbenzyl azide (2)

Yield: 70%.  $^1\text{H}$  NMR ( $\text{CDCl}_3$ , 400 MHz):  $\delta$  = 7.44 (d,  $J$  = 8.08 Hz, 2H), 7.29 (d,  $J$  = 8.04 Hz, 2H), 6.74 (q,  $J$  = 10.88 Hz, 1H), 5.78 (d,  $J$  = 17.04 Hz, 1H), 5.29 (d,  $J$  = 10.44 Hz, 1H), 4.34 (s, 2H).  $^{13}\text{C}$  NMR ( $\text{CDCl}_3$ , 400 MHz):  $\delta$  = 137.67, 136.23, 134.80, 128.45, 126.64, 114.46, 54.54.

---

### 4.6.3 Synthesis of 7-(diethylamino)-3-(1-hydroxybut-3-ynyl)-2*H*-chromen-2-one (7)

Coumarins **5** and **6** were synthesized according to the reported literature procedures.<sup>11</sup>

#### 4.6.3.1 7-(Diethylamino)-2*H*-chromen-2-one (5)

Yield: 62%. <sup>1</sup>H NMR (CDCl<sub>3</sub>, 400 MHz): δ = 7.54 (d, *J* = 9.28 Hz, 1H), 7.26 (d, *J* = 8.76, 1H), 6.57 (d, *J* = 8.80 Hz, 1H), 6.50 (s, 1H), 6.04 (d, *J* = 9.28 Hz, 1H), 3.42 (q, *J* = 7.08 Hz, 4H), 1.22 (t, *J* = 7.08 Hz, 6H). <sup>13</sup>C NMR (CDCl<sub>3</sub>, 400 MHz): δ = 162.26, 156.75, 150.69, 143.66, 128.74, 109.21, 108.64, 108.29, 97.56, 44.78, 12.43.

#### 4.6.3.2 7-(Diethylamino)-2-oxo-2*H*-chromene-3-carbaldehyde (6)

Yield: 53%. <sup>1</sup>H NMR (CDCl<sub>3</sub>, 400 MHz): δ = 10.06 (s, 1H), 8.18 (s, 1H), 7.34 (d, *J* = 8.84 Hz, 1H), 6.56 (d, *J* = 8.84, 1H), 6.42 (s, 1H), 3.40 (q, *J* = 6.68 Hz, 4H), 1.18 (t, *J* = 6.84 Hz, 6H). <sup>13</sup>C NMR (CDCl<sub>3</sub>, 400 MHz): δ = 187.96, 158.95, 153.46, 145.37, 132.50, 114.38, 110.16, 108.25, 97.19, 45.27, 12.45.

#### 4.6.3.3 7-(Diethylamino)-3-(1-hydroxybut-3-ynyl)-2*H*-chromen-2-one (7)

To a solution of zinc (0.26 g, 4 mmol) in THF (20 ml) was added propargyl bromide (0.45 g, 4 mmol) in THF (10 mL) and a mixture was stirred at room temperature for 1h. After this, 7-(diethylamino)-2-oxo-2*H*-chromene-3-carbaldehyde (**6**) (1 g, 4 mmol) in THF (5 mL) was added. The mixture was stirred overnight at 60 °C and saturated NH<sub>4</sub>Cl (30 mL) was added. After 1 h, zinc residues were removed by filtration and hydrochloric acid (10 mL, 10%) was added. The organic layer was collected and THF was removed under reduced pressure. The residues were dissolved in dichloromethane (50 mL), washed with water (50 mL X 3) and dried over anhydrous Na<sub>2</sub>SO<sub>4</sub>. The organic solvent was removed under reduced pressure and the crude product was purified by column chromatography over silica gel (Hexane: EtOAc, 30:70) to afford a pure product as yellow (0.72 g, 63% yield). m.p. 125-130 °C. IR ν<sub>max</sub> (cm<sup>-1</sup>): 3393 (O-H), 3302 (≡C-H), 1683 (C=O), 1601 (C=C). <sup>1</sup>H NMR (CDCl<sub>3</sub>, 400 MHz): δ = 7.59 (s, 1H), 7.22 (d, *J* = 8.84 Hz, 1H), 6.51 (d, *J* = 8.84, 1H), 6.42 (s, 1H), 4.72 (q, *J* = 5.56 Hz, 1H), 3.34 (q, *J* = 7.04 Hz, 4H), 2.71 (dd, *J* = 3.6, 2H), 1.97 (s, 1H), 1.13 (t, *J* = 7.08 Hz, 6H). <sup>13</sup>C NMR (CDCl<sub>3</sub>, 400 MHz): δ = 162.06, 155.90, 150.64, 139.76, 129.11, 120.75, 109.07, 108.11, 97.17, 80.44, 71.26, 69.14, 44.82, 26.48, 12.42.

---

#### 4.6.4 Synthesis of 7-hydroxy-8-(1-hydroxybut-3-ynyl)-4-methyl-2H-chromen-2-one (11)

The syntheses of coumarin **9** and **10** were achieved according to reported literature.<sup>17</sup>

##### 4.6.4.1 7-Hydroxy-4-methyl-2H-chromen-2-one (9)

Yield: 85%. <sup>1</sup>H NMR (CDCl<sub>3</sub>, 400 MHz): δ = 10.51 (s, 1H), 7.59 (d, *J* = 8.68 Hz, 1H), 6.80 (d, *J* = 8.64 Hz, 1H), 6.70 (s, 1H), 6.10 (s, 1H), 2.36 (s, 3H). <sup>13</sup>C NMR (CDCl<sub>3</sub>, 400 MHz): δ = 161.62, 160.74, 155.30, 154.00, 127.08, 113.32, 112.49, 110.71, 102.64, 18.56.

##### 4.6.4.2 7-Hydroxy-4-methyl-2-oxo-2H-chromene-8-carbaldehyde (10)

Yield: 41%. <sup>1</sup>H NMR (CDCl<sub>3</sub>, 400 MHz): δ = 12.13 (s, 1H), 10.54 (s, 1H), 7.65 (d, *J* = 8.84 Hz, 1H), 6.83 (d, *J* = 8.92 Hz, 1H), 6.13 (s, 1H), 2.35 (s, 3H). <sup>13</sup>C NMR (CDCl<sub>3</sub>, 400 MHz): δ = 193.42, 165.28, 159.21, 156.17, 152.64, 132.88, 132.50, 114.29, 111.98, 108.69, 18.93.

##### 4.6.4.3 7-Hydroxy-8-(1-hydroxybut-3-ynyl)-4-methyl-2H-chromen-2-one (11):

Synthetic procedure and the same molar ratio used in the synthesis of synthesis of 7-(diethylamino)-3-(1-hydroxybut-3-ynyl)-2H-chromen-2-one (**7**) was used in the synthesis of 7-hydroxy-8-(1-hydroxybut-3-ynyl)-4-methyl-2H-chromen-2-one (**11**) and white solid product was obtained in 43% in yield. m.p. 147-152 °C. IR  $\nu_{\max}$  (cm<sup>-1</sup>): 3359 (O-H), 3255 ( $\equiv$ C-H), 1685 (C=O), 1597 (C=C). <sup>1</sup>H NMR (CDCl<sub>3</sub>, 400 MHz): δ = 7.53 (d, *J* = 8.84 Hz, 1H), 6.94 (d, *J* = 8.84 Hz, 1H), 6.19 (s, 1H), 5.44 (s, 1H), 4.9 (s, 1H), 4.52 (s, 1H), 2.77 (dd, *J* = 14, 2H), 2.71 (s, 1H), 2.43 (s, 3H). <sup>13</sup>C NMR (CDCl<sub>3</sub>, 400 MHz): δ = 160.63, 155.58, 152.97, 152.28, 151.12, 125.59, 114.02, 113.35, 112.09, 95.48, 57.98, 33.64, 18.82.

#### 4.6.5 Synthesis of 7-(diethylamino)-3-(prop-2-ynylamino)-2H-chromen-2-one (15)

7-(Diethylamino)-3-nitro-2H-chromen-2-one (coumarin **13**) and 3-amino-7-(diethylamino)-2H-chromen-2-one (coumarin **14**) were synthesized according to the literature procedure provided in Chapter 3.

##### 4.6.5.1 7-(diethylamino)-3-(prop-2-ynylamino)-2H-chromen-2-one (15)

To a solution of propargyl bromide (0.15 g, 1.26 mmol) and 3-amino-7-(diethylamino)-2H-chromen-2-one (0.30 g, 1.29 mmol) in 10 mL dichloromethane was added 50% aqueous NaOH solution (1 mL). The mixture was stirred at room temperature for 48 hrs and poured into water

---

(100 mL). The aqueous solution was extracted with dichloromethane (50 mL X 3) and dichloromethane extracts was dried over anhydrous Na<sub>2</sub>SO<sub>4</sub>. The organic solvent was removed under reduced pressure and the crude product was purified by column chromatography over silica gel (Hexane: EtOAc, 90:10) to afford pure product as brown oil in 61% yield. IR  $\nu_{\max}$  (cm<sup>-1</sup>): 3286 ( $\equiv$ C-H), 3234 (N-H), 1675 (C=O), 1585 (C=C). <sup>1</sup>H NMR (CDCl<sub>3</sub>, 400 MHz):  $\delta$  = 10.15 (d,  $J$  = 8.84 Hz, 1H), 7.74 (d,  $J$  = 8.92 Hz, 1H), 6.35 (d,  $J$  = 8.92 Hz, 1H), 6.24 (s, 1H), 4.81 (s, 1H), 3.45 (q,  $J$  = 7.04, 2H), 2.58 (s, 1H), 1.25 (q,  $J$  = 7.08, 3H). <sup>13</sup>C NMR (CDCl<sub>3</sub>, 400 MHz):  $\delta$  = 186.98, 162.05, 153.62, 130.70, 114.62, 105.07, 94.35, 78.29, 76.14, 56.12, 44.92, 12.63.

#### 4.6.5.2 General procedure for functionalization of poly(4-vinylbenzyl azide)

A mixture of poly(4-vinylbenzyl azide (0.5 mmol repeating units ), alkynylated coumarin derivatives (1 mmol), CuSO<sub>4</sub>.5H<sub>2</sub>O (0.054 mmol), sodium ascorbate (0.15 mmol) and N,N,N',N'',N''-pentamethyldiethylenetriamine (PMDETA) (0.15 mmol) in THF (100 mL) was stirred at room temperature for 48 hrs. The precipitated polymers were filtered, washed with water and dried under vacuum to afford polymer **P1**, **P2** or **P3** in 83%, 78% and 85% yields respectively.

## 4.7 References

1. Y. H. Lau, P. J. Rutledge, M. Watkinson and M. H. Todd, *Chem. Soc. Rev.*, **2011**, 40, 2848-2866.
2. J. Morales-Sanfrutos, M. Ortega-Muñoz, J. Lopez-Jaramillo, F. Hernandez-Mateo and F. Santoyo-Gonzalez, *J. Org. Chem.*, **2008**, 73, 7768–7771.
3. Y. H. Lau, J. R. Price, M. H. Todd and P. J. Rutledge, *Chem.–Eur. J.*, **2011**, 17, 2850-2858.
4. I. T. Ho, T. L. Lai, R. T. Wu, M. T. Tsai, C. M. Wu, G. H. Lee and W. S. Chung, *Analyst*, **2012**, 137, 5770–5776.
5. Y. Zhou, K. Liu, J. Y. Lin, Y. Fang, T. C. Zhao and C. Yao, *Org. Lett.*, **2011**, 13, 1290-1293.
6. S. H. Kim, H. S. Choi, J. Kim, S. J. Lee, D. T. Quang and J. S. Kim, *Org. Lett.*, **2010**, 12, 560–563.
7. M. Meldal and C. W. Torne, *Chem. Rev.*, **2008**, 108, 2952–3015.
8. I. Misztalewska, A. Z. Wilczewska, O. Wojtasik, K. H. Markiewicz, P. Kuchlewski and A. M. Majcher, *RSC Adv.*, **2015**, 5, 100281–100289.

- 
9. C. Uhler, "Synthesis of Well-Controlled Nanogels via Block Copolymer Self-Assembly: A Systematic Characterization of the Properties and Potential Applications". *Undergraduate Honors Theses*, University of Colorado, (2013), Paper 564
  10. S. Bräse, C. Gil, K. Knepper and V. Zimmermann, *Angew. Chem. Int. Ed.*, **2005**, 44, 5188-5240.
  11. J. Wu, W. Liu, X. Zhuang, F. Wang, P. Wang, S. Tao, X. Zhang, S. Wu and S. Lee, *Org. Lett.*, **2007**, 9, 33-36.
  12. A. Jögi and U. Mäeorg, *Molecules*, **2001**, 6, 964-968.
  13. P. K. Adapa, L. G. Schonenau, T. Canam, and T. Dumonceaux, *J. Agric. Sci. Technol.*, **2011**, 1, 177-188
  14. B. Raju and T. S. Varadarajan, *J. Phys. Chem.*, **1994**, 98, 8903–8905
  15. a) D. S. McClure, *J. Chem. Phys.*, **1952**, 20, 682-686. b) H. Masuhara, H. Shioyama, T. Saito, K. Hamada, S. Yasoshima and N. Mataga; *J. Phys. Chem.*, **1984**, 88, 5868–5873.
  16. a) M. Bassetti, B. Floris and G. Spadafora, *J. Org. Chem.*, **1986**, 51, 4140; b) R. C. Larock, L. D. Burns, S. Varaprath and C. E. Russell, *Organometallics*, **1987**, 6, 1780; c) M. Nishizawa, H. Imagawa and H. Yamamoto, *Org. Biomol. Chem.*, **2010**, 8, 511.
  17. J. S. Renny, L. L. Tomasevich, E. H. Tallmadge and D. B. Collum, *Angew. Chem., Int. Ed.*, **2013**, 52, 11998–12013.
  18. H. A. Benesi and J. H. Hildebrand, *J. Am. Chem. Soc.*, **1949**, 71, 2703–2707.
  19. J. C. Qin, T. R. Li, B. D. Wang, Z. Y. Yang and L. Fan, *Spectrochim. Acta A*, **2014**, 133, 38-43.
  20. H. A. Benesi and J. H. Hildebrand, *J. Am. Chem. Soc.*, **1949**, 71 2703–2707.
  21. Z. Dong, X. Tian, Y. Chen, J. Hou, Y. Guo, J. Sun and J. Ma, *Dyes and Pigments*, **2013**, 97, 324-329.
  22. X. Li, E. A. Mintz, X. R. Bu, O. Zehnder, C. Bosshard and P. Günter, *Tetrahedron*, **2000**, 56, 5785-5791.
  23. H. Yao and T. Funada, *Chem. Commun.*, **2014**, 50, 2748–2750.
  24. L. Q. Yan, Y. Ma, M. F. Cui and Z. J. Qi, *Anal. Methods*, **2015**, 7, 6133-6138.
  25. R. M. Duke and T. Gunnlaugsson, *Tetrahedron Lett.*, **2011**, 52, 1503-1505.
  26. G. Liu and L. M. Zhao, *Spectrosc. Lett.*, **2012**, 45, 424-429.
  27. J. Y. Li, X. Q. Zhou, Y. Zhou, Y. Fang and C. Yao, *Spectrochim. Acta, Part A*, **2013**, 102, 66-70.
  28. G. J. Park, H. Y. Jo, K. Y. Ryu and C. Kim, *RSC Adv.*, **2014**, 4, 63882–63890.

---

## Chapter 5 Linear triazolyl coumarin-based polymers

### 5.1 Introduction

Properties of polymers can be influenced by the arrangement of repeating units within the polymer chains. The properties of the triazolyl coumarin based polymers were also investigated from that perspective. This involved the investigations of chemosensing capabilities of a polymer in which the triazolyl coumarin units are incorporated into the main chain. From the literature, linear polytriazoles are mainly synthesized using Cu(I)-catalysed 1,3-dipolar cycloaddition step-growth polymerization (click polymerization) of either AA- and BB-type bifunctional monomers or between AB-type monomers (**Figure 5.1**).<sup>1,2</sup>

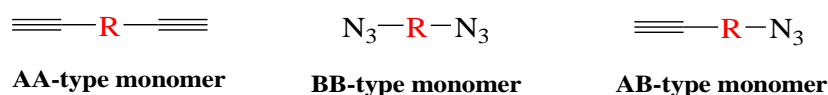


**Figure 5.1:** Different types of monomers for the synthesis of polytriazoles.

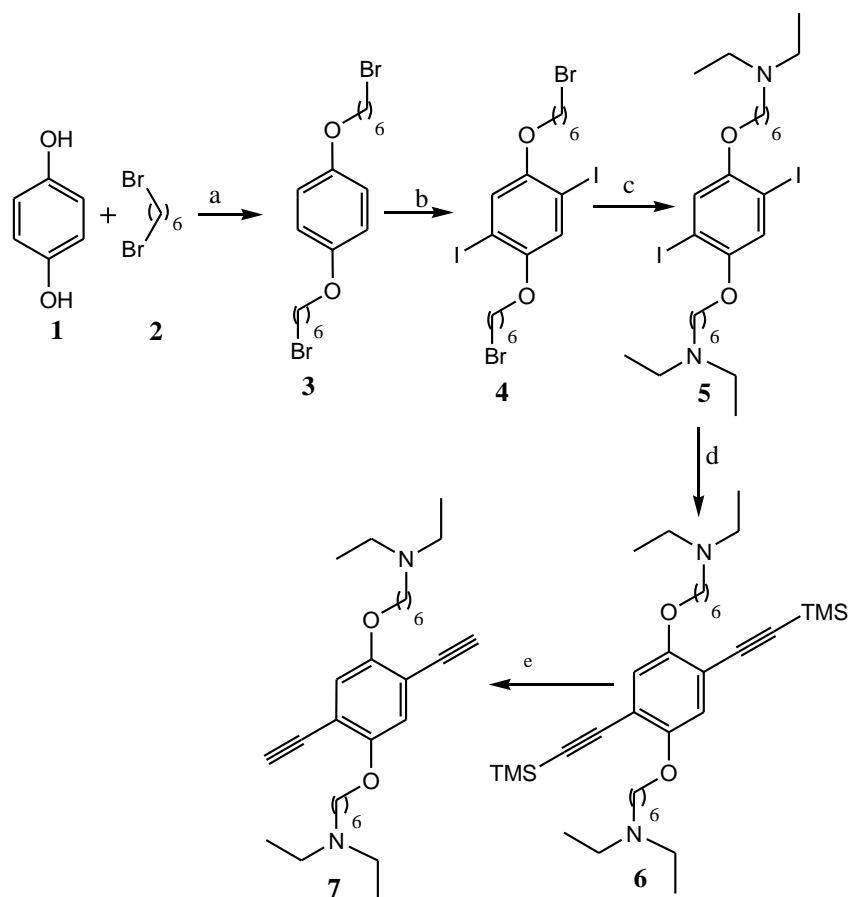
Despite the simplicity and modular nature of the click reaction which is applied during polymerization, a major frequently reported drawback of the resulting polytriazoles is their poor solubilities in organic solvents which complicates their characterization, property investigations and applications<sup>1,3</sup> To overcome this poor solubility issue and other practical problems associated with these polymers, solubilizing groups are often incorporated into the polymer chains. Long chain alkyl groups and alkyl dendrimers are among the solubilizing groups which have shown to improve the solubility of the polytriazoles, when incorporated into the repeating units.<sup>4,5</sup>

In our studies, linear coumarin-based polytriazoles were synthesized *via* AA-BB step-growth click polymerization using two diazide-functionalized coumarin monomers and a dialkyne-functionalized monomer. The latter contained six carbon alkyl chain capped with diethylamino group to enhance the solubility of the polymer. Furthermore, the amino functionality in the side chains can be converted into an ammonium salt, which extends the applications of the resulting polymer to aqueous media.

## 5.2 Monomer synthesis

### 5.2.1 AA-type monomer synthesis

Dialkyne monomer **7** was synthesized in five steps from benzene-1,4-diol as shown in **Scheme 5.1**. Compound **3** was synthesized according to a literature procedure<sup>6</sup>, before its iodination which was carried out in acetic acid in the presence of  $\text{H}_2\text{SO}_4$ ,  $\text{H}_2\text{O}$ ,  $\text{KIO}_3$  and  $\text{I}_2$  by following a reported literature procedure for the iodination of 1,4-diiodo-2,5-dimethoxybenzene.<sup>7</sup> Bromo-capped alkyl chain in compound **4** was converted into tertiary amine by refluxing in diethylamine according to a literature method.<sup>8</sup> Compound **5** was alkynylated to form monomer precursor **6** in the presence of trimethylsilyl acetylene,  $\text{Pd}(\text{PPh}_3)_2\text{Cl}_2$  and  $\text{CuI}$ .<sup>9</sup> Monomer precursor **6** was then treated with  $\text{K}_2\text{CO}_3$  in a mixture of methanol and THF (1:1) to give monomer **7** in good yield.



**Scheme 5.1:** Synthesis of the dialkyne monomer **7**; a)  $\text{NaOH}$ , ethanol (reflux); b)  $\text{H}_2\text{SO}_4$ ,  $\text{H}_2\text{O}$ ,  $\text{KIO}_3$ ,  $\text{I}_2$  and  $\text{AcOH}$  (reflux); c) Diethylamine; d) Triethylamine, trimethylsilyl acetylene,  $\text{Pd}(\text{PPh}_3)_2\text{Cl}_2$  and  $\text{CuI}$ ; e)  $\text{K}_2\text{CO}_3$ ,  $\text{CH}_3\text{OH}/\text{THF}$  (1:1).

The structures of compounds **3**, **4**, **5**, **6** and monomer **7** were characterized by NMR and mass spectrometry (for  $^1\text{H}$  NMR spectra of compounds **3**, **4** and **5** and  $^{13}\text{C}$  spectra of compounds **6** and **7** see **Appendices Figure A.18-A.22**). **Figure 5.2** shows the assignment of proton signals in the  $^1\text{H}$  NMR spectrum of the monomer precursor **6**. The appearance of 24 alkyl chain protons at 1.35, 1.52, 1.80, 2.45 and 3.95 ppm, 20 diethylamino protons at 1.04 and 2.55 ppm, 2 aromatic protons at 6.89 ppm and 18 trimethylsilyl protons at 0.26 ppm confirmed the structure of compound **6**. **Figure 5.3** shows the assignment of proton signals in the  $^1\text{H}$  NMR spectrum of monomer **7**. Once again the appearance of 2 terminal alkyne protons at 3.25 ppm and disappearance of 18 trimethylsilyl protons at 0.26 ppm confirms the structure of the monomer **7**.

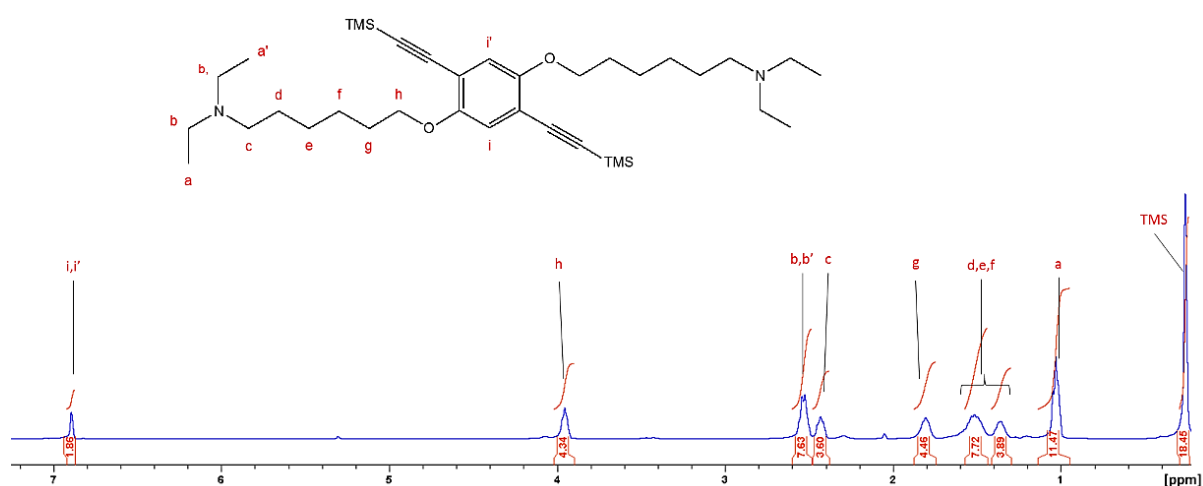


**Figure 5.2:**  $^1\text{H}$  NMR spectrum of the monomer precursor **6** in  $\text{CDCl}_3$ .

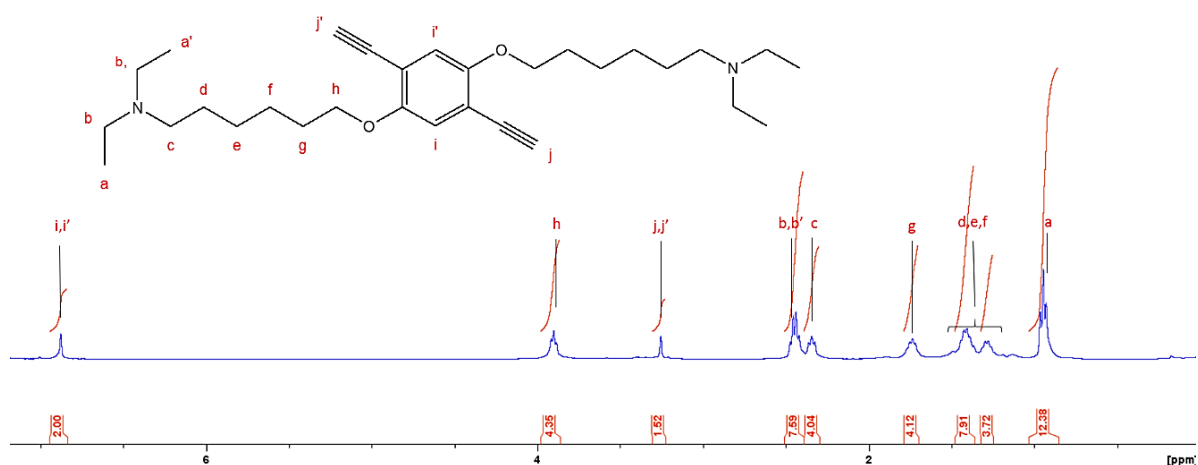


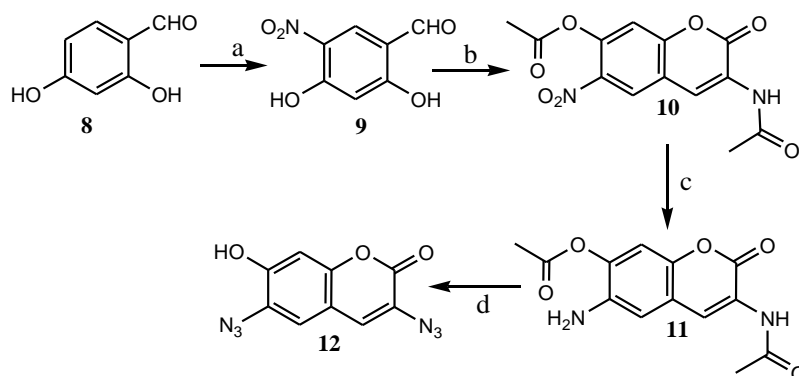
**Figure 5.3:**  $^1\text{H}$  NMR spectrum of monomer **7** in  $\text{CDCl}_3$ .



## 5.2.2 BB-type monomer synthesis

Two diazide-functionalized coumarin monomers (**12** and **17**), to couple with the dialkyne functionalized monomer **7** during click polymerization, were synthesized *via* multi-step syntheses. The two monomers differed by the position of the hydroxyl group in the coumarin system. The aim of preparing those monomers was to study the impact of the hydroxyl groups on the photophysical and chemosensing properties of the resulting polymers.

Monomer **12**, with the hydroxyl group at position 7, was prepared in four steps from 2,4-dihydroxybenzaldehyde as shown in **Scheme 5.2**. 2,4-Dihydroxybenzaldehyde **8** was firstly nitrated in acetic acid using a mixture of H<sub>2</sub>SO<sub>4</sub> and HNO<sub>3</sub> (1:1). Nitrated coumarin **10** was then obtained from compound **9** *via* a Perkin condensation reaction in the presence of *N*-acetylglycine.<sup>10</sup> The nitro group on coumarin **10** was then reduced in aqueous acetic acid into its corresponding amino coumarin **11** in the presence of iron. The amide group in position 3 of the coumarin system was next hydrolyzed under acidic conditions and a diazotization-azidation reaction in the presence of NaNO<sub>2</sub> and NaN<sub>3</sub> resulted in desired monomer **12** in good yield.



**Scheme 5.2:** Synthesis of the diazide-functionalized coumarin monomer **12**; a) H<sub>2</sub>SO<sub>4</sub> and HNO<sub>3</sub> (1:1) and AcOH (rt); b) *N*-acetylglycine, anhydrous sodium acetate and acetic anhydride (reflux); c) AcOH and H<sub>2</sub>O (1:1) and Fe, rt; d) Ethanol and HCl (2:3), then NaNO<sub>2</sub>, NaN<sub>3</sub>.

Compounds **9**, **10**, and **11**, and monomer **12** were characterized by FT-IR, NMR and mass spectroscopy (for the <sup>1</sup>H NMR spectra of compounds **9**, **10** and **11** and <sup>13</sup>C NMR spectrum of monomer **12** see **Appendices Figure A.23-A.26**). **Figure 5.4** below shows the assignment of proton signals in the <sup>1</sup>H NMR spectrum of monomer **12**. The three coumarin protons are observed at 7.95, 7.28 and 7.54 ppm, while the hydroxyl proton appeared at 11.48 ppm.

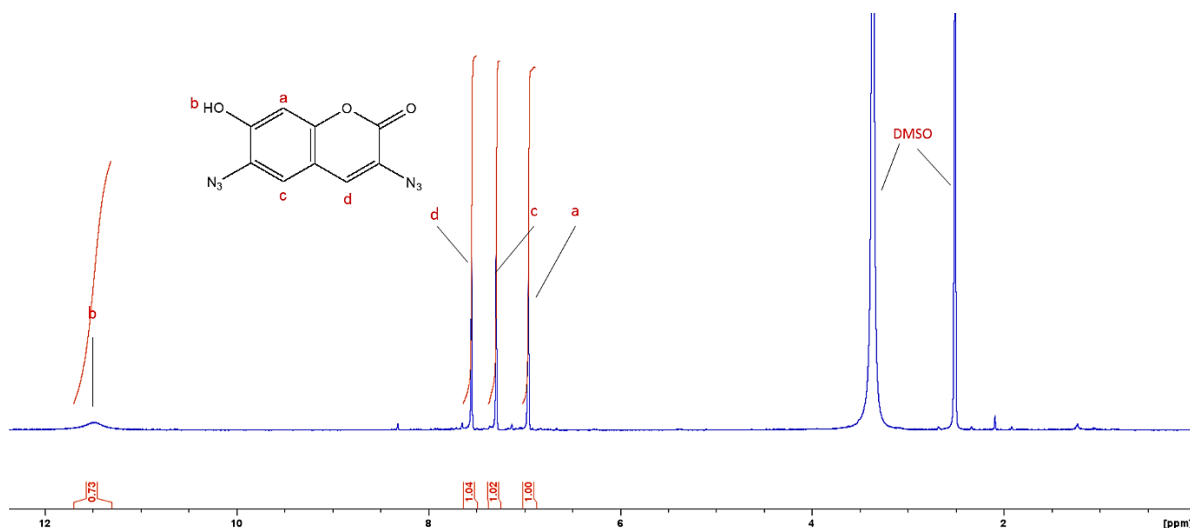


**Figure 5.4:**  $^1\text{H}$  NMR spectrum of monomer **12** in DMSO

The presence of the azide functional group in the monomer **12** was confirmed by FT-IR spectroscopy (**Figure 5.5**). The appearance of a stretching at  $2113\text{ cm}^{-1}$  in the spectrum of monomer **12**, confirms the presence of the azide functional group. Furthermore, the hydroxyl group at position 7 was also detected at  $3400\text{ cm}^{-1}$ .

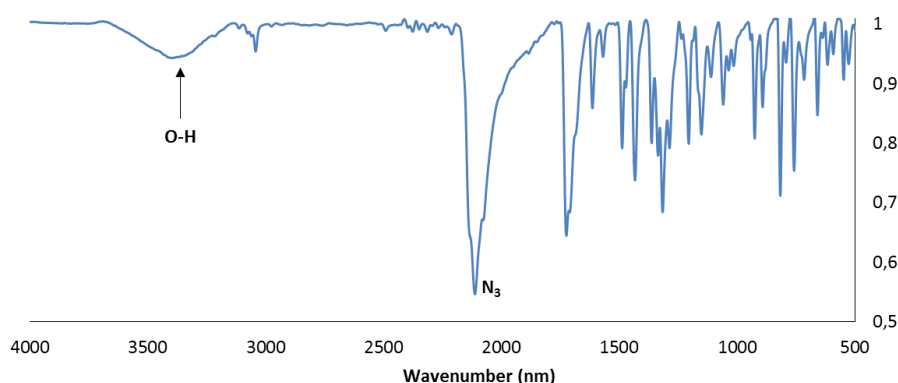
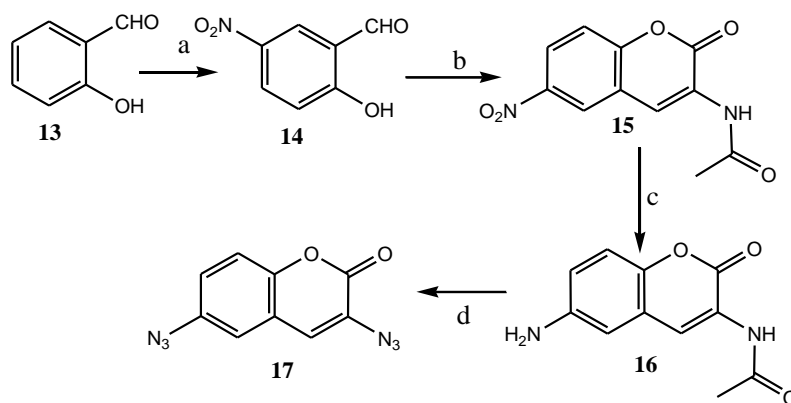


**Figure 5.5:** FT-IR spectrum of monomer **12**.

The second diazide coumain monomer **16**, without the hydroxyl group at position 7, was also prepared in four steps from 2-hydroxybenzaldehyde (**Scheme 5.3**). Using the methods used for the synthesis of monomer **12**, nitration of the starting compound **13**, followed by Perkin condensation reaction in the presence of *N*-acetylglycine, formed the nitrated coumarin compound **15**. Reduction using  $\text{Fe}^{3+}$ , followed by acid hydrolysis and then a diazotization-azidation reaction in the presence of  $\text{NaNO}_2$  and  $\text{NaN}_3$ , yielded the desired diazide functionalized coumarin monomer **17** in good yield.



**Scheme 5.3:** Synthesis of the diazide coumarin monomer **17**: a)  $\text{Ca}(\text{NO}_3)_2$ , AcOH (reflux); b) *N*-acetylglycine, anhydrous sodium acetate and acetic anhydride (reflux); c) AcOH and  $\text{H}_2\text{O}$  (1:1) and Fe; d) Ethanol and HCl (2:3), and then  $\text{NaNO}_2$ ,  $\text{NaN}_3$ .

Compounds **14**, **15** and **16**, and monomer **17** were once again characterized by FT-IR and NMR and mass spectrometry (for  $^1\text{H}$  NMR spectra of compounds **15** and **16** and the  $^{13}\text{C}$  NMR spectrum of monomer **17** see **Appendices Figure A27-A29**). **Figure 5.6** shows the assignment of proton signals in the  $^1\text{H}$  NMR spectrum of monomer **17**. All four coumarin protons resonate between 7 and 8 ppm. The disappearance of the amino group protons and amide methyl group protons observed in  $^1\text{H}$  NMR spectrum of compound **16** confirm the successful synthesis of monomer **17**.

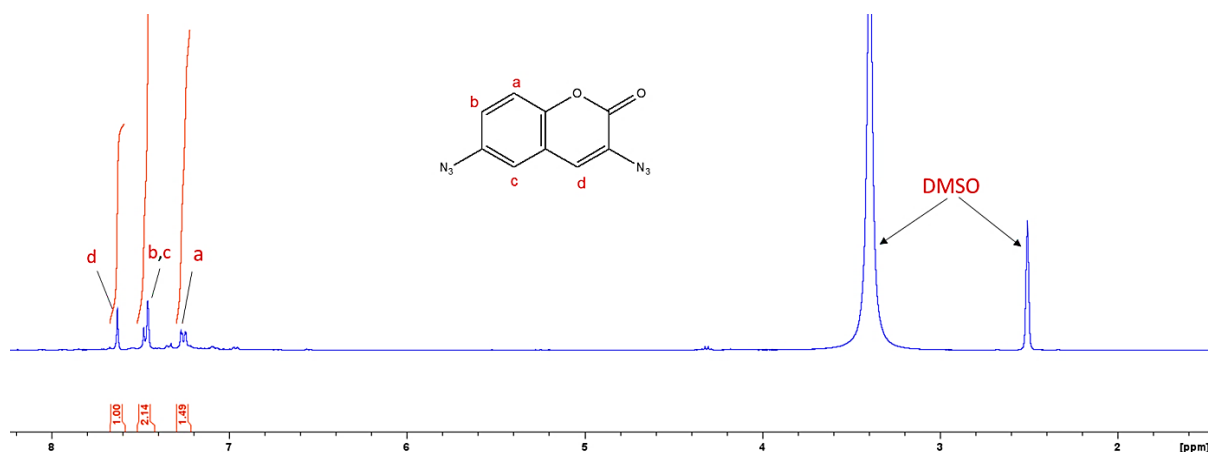


**Figure 5.6:**  $^1\text{H}$  NMR spectrum of monomer **17** in  $\text{CDCl}_3$ .

The presence of the azide functional group in monomer **17** was confirmed by FT-IR spectroscopy as shown in **Figure 5.7**. The azide functional group stretch was observed at  $2110\text{ cm}^{-1}$ .

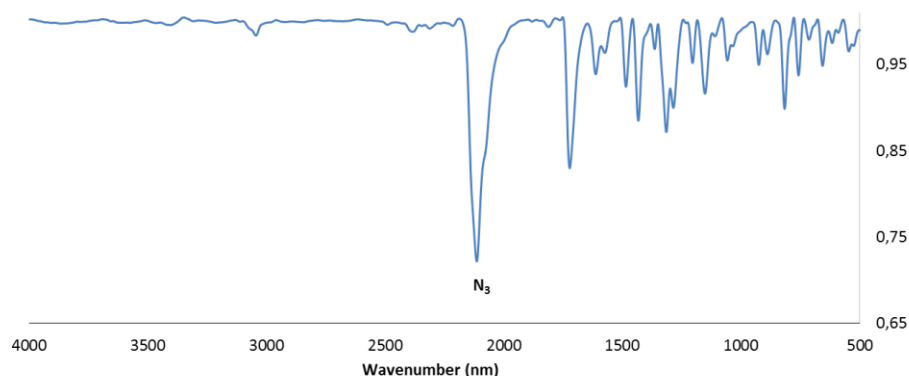
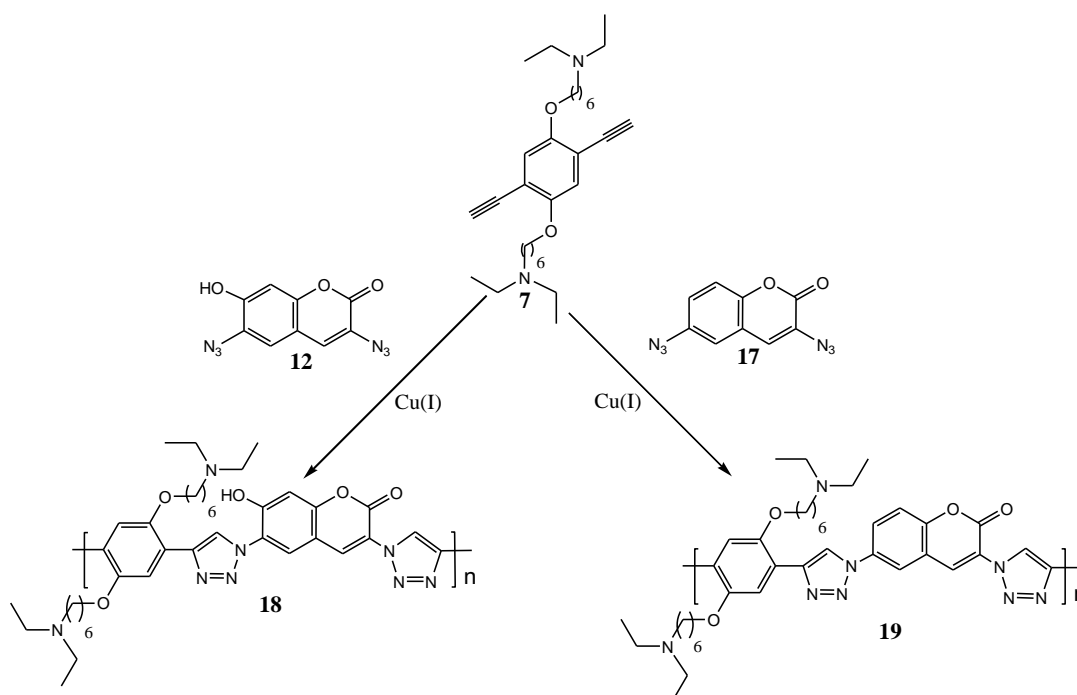


**Figure 5.7:** FT-IR spectrum of monomer **17**.

### 5.3 AA-BB step-growth click polymerization

The synthesis of linear triazolyl coumarin based polymers was achieved *via* a triazole-forming AA-BB step-growth click polymerization using diazide-functionalized coumarin monomers **17** and **12**, respectively and the dialkyne-functionalized monomer **7** (**Scheme 5.4**). The reaction was carried out at room temperature in THF with minimum amount of water, and the click conditions included Cu(I), a reducing agent and a ligand according to the literature procedure.<sup>11</sup> After completion of the reaction in 48 h, the precipitated polymers were filtered and washed with water to afford pure polymer **18** and **19** in good yield.



**Scheme 5.4:** AA-BB step-growth click polymerization of dialkyne-functionalized monomer **7** with diazide-functionalized coumarin monomers **12** and **17**.

The structures of polymers **18** and **19** were confirmed by NMR and FT-IR spectroscopy. **Figures 5.8** and **5.9** show the assignment of proton signals in the  $^1\text{H}$  NMR spectra of polymers **18** and **19**, respectively. Notable, are the aromatic protons from the coumarin and the substituted benzene derivative, as well as alkyl proton from the side chains. Due to the low solubility of polymer **18** and **19**, the average molecular weight and polydispersity index could not be determined from size exclusion chromatography experiments.

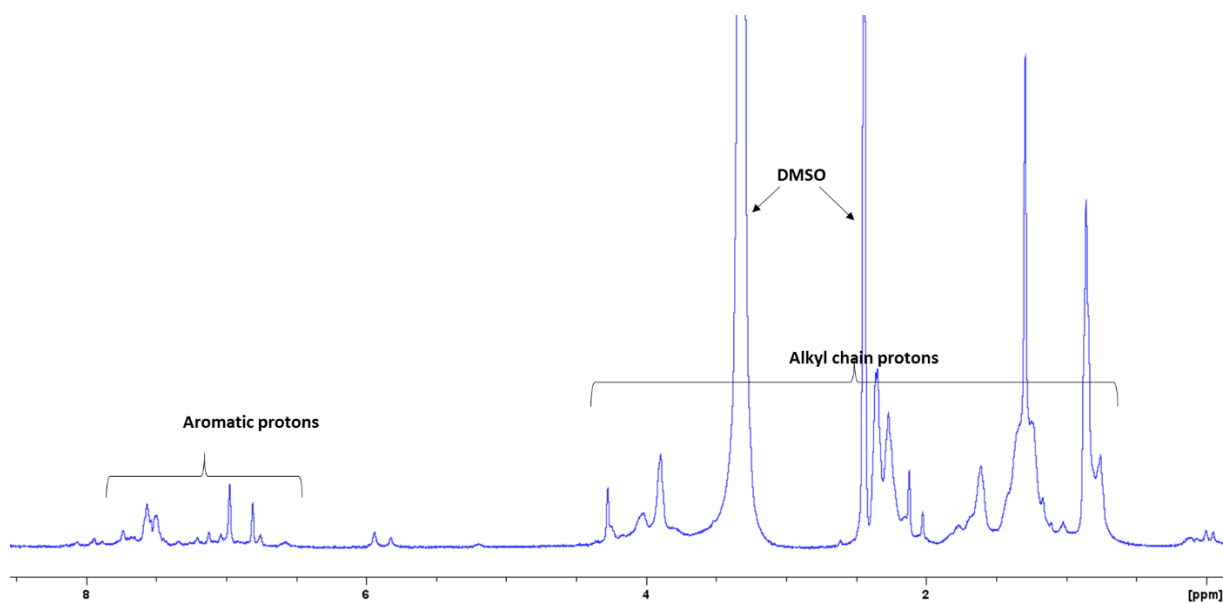


**Figure 5.8:**  $^1\text{H}$  NMR spectrum of polymer **18** in DMSO.

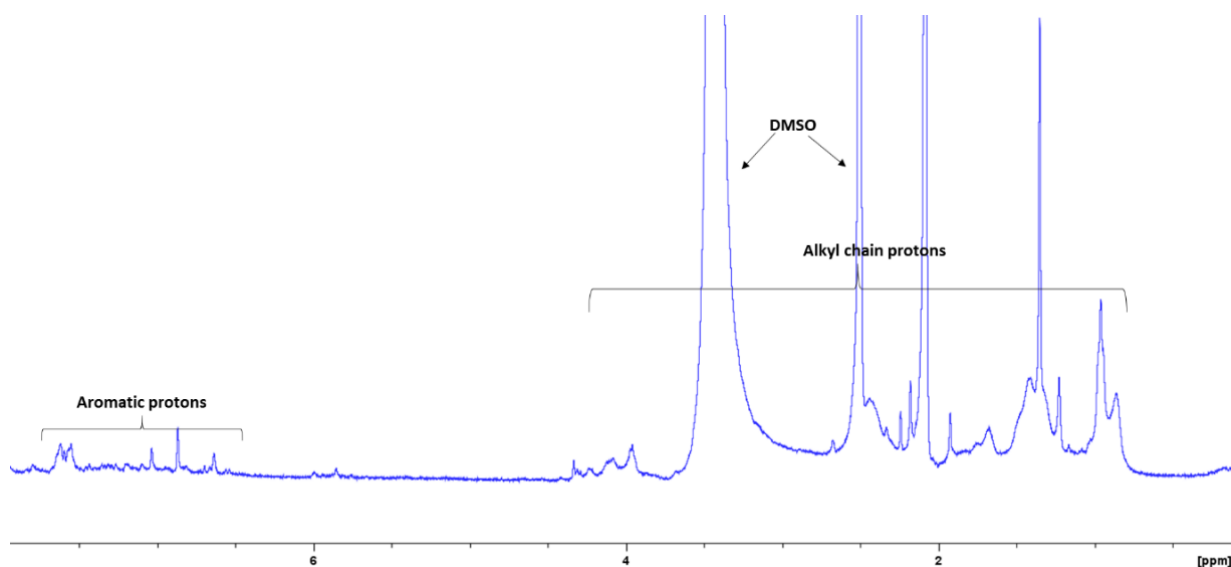


**Figure 5.9:**  $^1\text{H}$  NMR spectrum of polymer **19** in DMSO.

The structures of polymers **18** and **19** were further confirmed by FT-IR spectroscopy. **Figure 5.10** shows comparative FT-IR spectra of diazide-functionalized coumarin monomers **12** and

**17**, and their corresponding polymers **18** and **19**. It should be noted that the stretching at  $2113\text{ cm}^{-1}$  assigned to the azide groups in monomers **12** and **17** disappeared in their corresponding polymers **18** and **19** respectively. This confirms a successful conversion of the azide and alkyne functionalities in the monomers **12** and **17** into the triazole ring during polymerization.

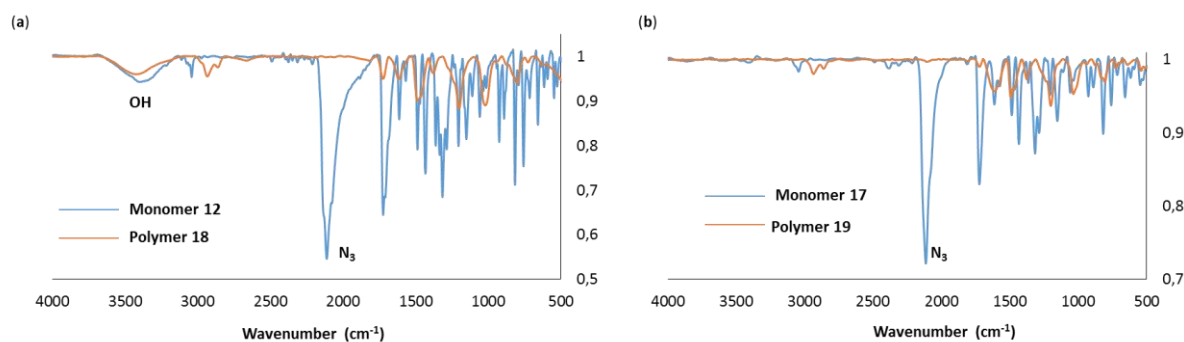


**Figure 5.10:** Comparative FT-IR spectra between monomers **12** and **17** and their corresponding polymers **18** and **19**.

## 5.4 The effect of click polymerization on photophysical properties of the monomers

The effect of click polymerization on the starting monomers was investigated through the comparison of absorption and emission spectra of monomers **7** and **12**, and polymer **18** which has hydroxyl as additional binding site. The spectra were recorded at room temperature using DMF solutions containing an excess of monomers **7** and **12** compared to their corresponding number of repeating units in polymer **18**. The concentration of each monomer (monomer **7** and **12**) was equivalent to the total number of repeating units in the polymer, which have been calculated from the mass of the polymer and its respective repeating units. Since polymer **18** was synthesized from two different monomers (monomer **7** and **12**), each monomer solution would have an excess number of moles of the respective monomer compared to the polymer solution. Regardless of that disparity, polymer **18** shows higher absorption intensities compared to the respective monomers (**Figure 5.11 a**). The maximum absorption band of polymer **18** was observed at 355 nm as well as a shoulder at peak 437 nm. Weaker absorption peaks were observed at 350 and 332 nm for monomers **7** and **12** respectively. The presence of two absorption bands in polymer **18** could be attributed to the intra or interchain interactions in the polymer backbone.

Similar results were obtained in the analysis of emission spectra when DMF solutions of monomer **7** and **12**, and polymer **18** were excited at 337 nm (**Figure 5.11 a**). Polymer **18** showed higher emission intensity than its corresponding monomers **7** and **12** which showed negligible intensities. Polymer **18** showed two peaks within a broad emission band in the 300-600 nm range with the highest peak at 383 nm. The structureless emission band suggested different excited state energy levels and could be attributed to formation of the excimer/excimer or ESIPT mechanism from hydroxyl proton in position 7 of coumarin unit to the nitrogen of the triazole ring.

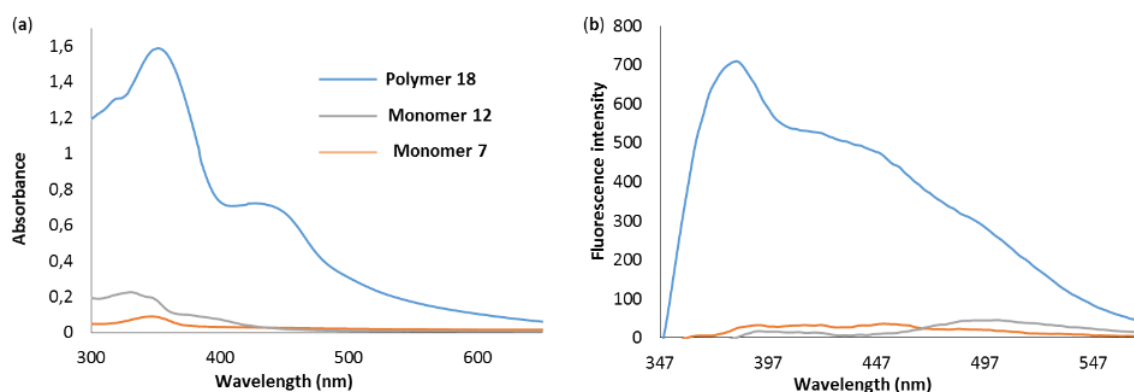


**Figure 5.11:** a) Absorption and b) Emission spectra of monomers **7** and **12** and polymer **18** in DMF. Absorption concentration was  $1.5 \times 10^{-3}$  M; Emission concentration was  $8 \times 10^{-8}$  M. The excitation was performed at 337 nm.

From absorption and emission studies of polymer **18** and its starting monomers, it is clear that the click polymerization enhanced both the absorption and emission of the starting monomers once they are in the polymer. This is probably due to the quenching properties of the azide group in the monomer **12** being suppressed in the polymer due to the formation of triazole ring. These differences in the photophysical properties also confirm the success of the CuAAC AA-BB step-growth click polymerization.

## 5.5 Photophysical properties of polymers **18** and **19**

In order to understand the impact of the hydroxyl group on the photophysical properties of polymer backbone, the absorption and emission of DMF solutions of polymers **18** and **19** containing the same number of moles of repeating units were investigated. As shown in **Figure 5.12 a**, both polymers exhibited similar absorption behaviours, albeit with different intensities. Polymer **18** showed higher absorption intensity than polymer **19**. These observations could be

as a result of increased push-pull effect on the coumarin system of the polymer **18** due to the presence of the hydroxyl group at position 7. Same as in absorption spectra, the emission studies showed higher emission intensity for polymer **18** than **19**, although their emission behaviours were slightly different (**Figure 5.12 b**). The emission peak at 383 nm in the polymer **18** was not detected in polymer **19**.

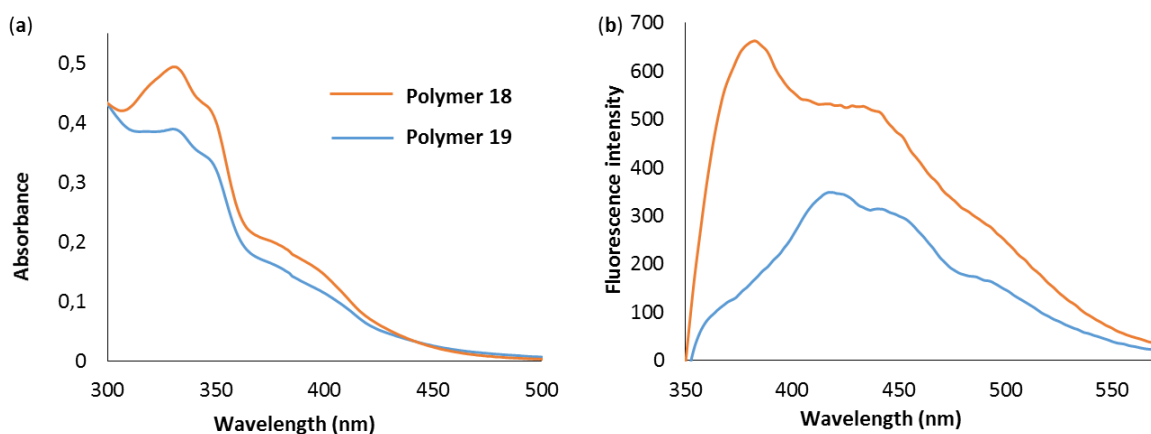
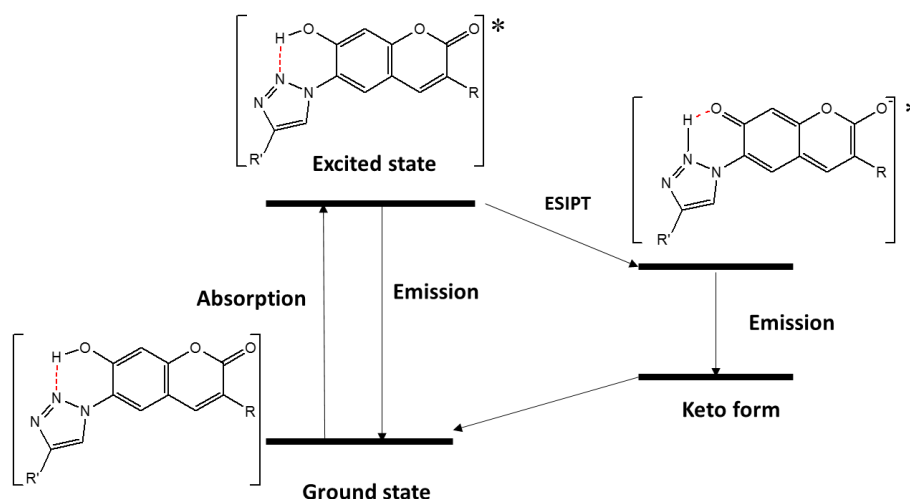


**Figure 5.12:** a) Absorption and b) Emission spectra of polymers **18** and **19** in DMF. Absorption concentration:  $1.7 \times 10^{-4}$  M; Emission concentration:  $8 \times 10^{-6}$  M. The excitation was performed at 337 nm.

Since these differences could not be detected in the absorption spectra, some excited state-based mechanisms can be associated to these variations. Due to the broadening of the emission band in polymer **18**, which suggests the occurrence of more than one excited state, two photophysical mechanisms were proposed to be responsible for these variations, these are: excited state proton transfer (ESIPT) and excimer/exciple formation.<sup>12,13</sup>

As the emission spectrum of an excimer/exciple often appears at a lower energy compared to the monomer emission spectrum,<sup>14</sup> ESIPT mechanism from hydroxyl proton in the position 7 to the triazole nitrogen is likely to be the mechanism that leads to the emission at 383 nm, while the emission peak at 435 nm can be assigned to normal emission of the polymer. **Scheme 5.5** illustrates the proposed ESIPT mechanism in polymer **18** which leads to two emission bands from normal excited state of the polymer and the excited state of tautomeric form. Since both polymers **18** and **19** showed shoulder bands in their emission spectra at the longer wavelength, it is possible that both mechanisms (ESIPT and excimer/exciple formation) take place when polymer **18** is excited.





**Scheme 5.5:** Schematic representation of ESIPT in polymer **18**

It has been reported that the rate of proton transfer is environment reliant,<sup>15</sup> thus changes in the emission spectrum of polymer **18** upon excitation at different wavelengths was investigated in order to confirm the proposed mechanism. The investigation were carried out using excitation wavelengths in a range encompassing the excitation wavelengths of monomer **7** and **12**, and polymer **18**. As shown in **Figure 3.13**, an increase in the excitation wavelength from 337 nm (which is an excitation wavelength of polymer **18**) to 355 nm (the excitation wavelength of coumarin monomer **12**), resulted in a significant decrease in the intensity of the maximum emission peak at 383 nm and a negligible decrease in the shoulder band at 435 nm. This suggests that the increase in excitation energy favours the ESPT mechanism and the emission band at 383 nm was assigned to the keto form from ESIPT.

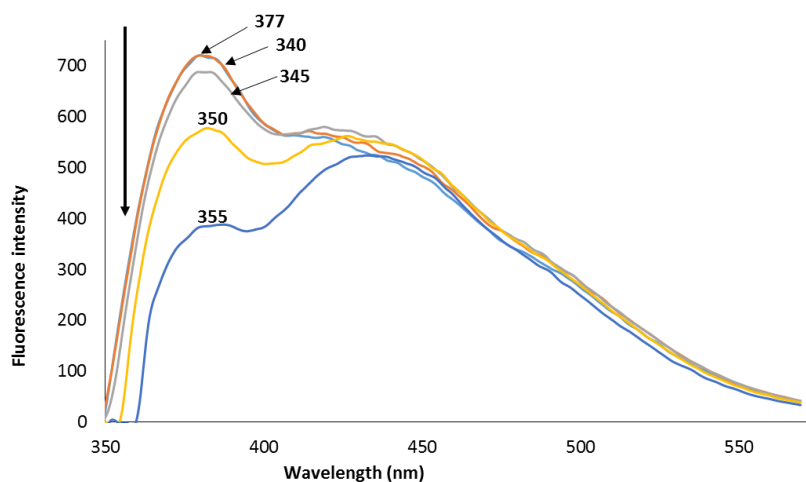


**Figure 5.13:** Emission spectra of polymer **18** in DMF ( $8 \times 10^{-6}$  M) at different the excitation wavelengths (337-355 nm).

---

## 5.6 Chemosensing studies of polymer 18

Polymer **18** showed two emission bands from the normal excited state of the polymer and the keto form excited state due to the ESIPT mechanism. Due to the fact that the ESIPT mechanism is environment reliant, it was believed that changing the environment of polymer **18** using different ions can result in selective sensitivity towards certain ions. Hence the absorption and emission behaviours of polymer **18**, in the presence of different metal ions and anions were investigated in order to investigate its chemosensing capability. In all chemosensing studies, solutions of nitrate and tetrabutylammonium salts were used as cation and anion source respectively.

### 5.6.1 Absorption studies

The absorption behaviour of polymer **18** in the presence of different ions was studied in DMF at room temperature using different metal ions ( $\text{Na}^+$ ,  $\text{Ca}^{2+}$ ,  $\text{Ag}^+$ ,  $\text{Al}^{3+}$ ,  $\text{Ba}^{2+}$ ,  $\text{Cr}^{3+}$ ,  $\text{Cu}^{2+}$ ,  $\text{Fe}^{3+}$ ,  $\text{Hg}^{2+}$ ,  $\text{Mn}^{2+}$ ,  $\text{Co}^{2+}$ ,  $\text{Zn}^{2+}$ ,  $\text{Cd}^{2+}$ ,  $\text{Ni}^{2+}$  and  $\text{Pb}^{2+}$ ) and anions ( $\text{F}^-$ ,  $\text{Cl}^-$ ,  $\text{Br}^-$ ,  $\text{H}_2\text{PO}_3^-$ ,  $\text{HSO}_4^-$ ,  $\text{ClO}_4^-$ ,  $\text{OH}^-$ ,  $\text{I}^-$ ,  $\text{NO}_3^-$ ,  $\text{AcO}^-$  and  $\text{CN}^-$ ). As shown in **Figure 5.14 a**, most of the tested metal ions did not induce any significant change in the absorption spectrum of polymer **18**. However  $\text{Cu}^{2+}$  induced an increase in the intensity of the maximum absorption peak at 330 nm while  $\text{Ag}^+$  induced an increase in intensity in both the maximum absorption peak and in the shoulder peak. In addition, the presence of  $\text{Fe}^{3+}$  gave a very intense band which was due to  $\text{Fe}^{3+}$  self-absorption.

Unlike  $\text{Cu}^{2+}$  and  $\text{Ag}^+$ , which induced an increase in the intensity of the maximum absorption peak,  $\text{Hg}^{2+}$  led to a decrease in the intensity of the maximum absorption peak and a small increase in intensity of the shoulder peak. This suggests that  $\text{Hg}^{2+}$  interacts differently with polymer **18** than other metal ions. In the presence of all the tested anions as shown in **Figure 5.14 b**, negligible changes were detected in the absorption spectrum of polymer **18**.

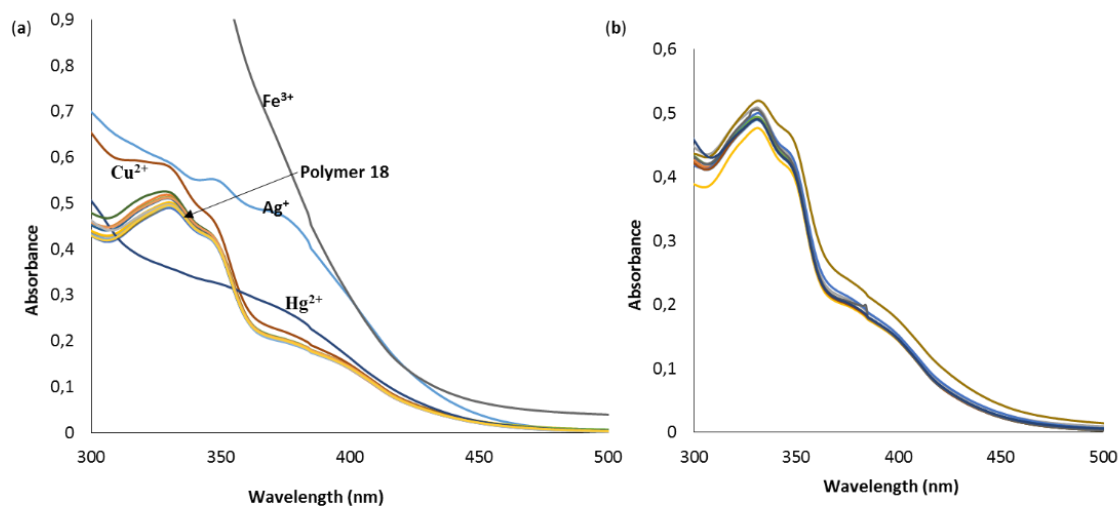


**Figure 5.14:** Absorption spectra of polymer **18** (0.12 g/L) in the presence of the aliquot ( $2 \times 10^{-4}$  M) of **a**) various metal ions ( $\text{Na}^+$ ,  $\text{Ca}^{2+}$ ,  $\text{Ag}^+$ ,  $\text{Al}^{3+}$ ,  $\text{Ba}^{2+}$ ,  $\text{Cr}^{3+}$ ,  $\text{Cu}^{2+}$ ,  $\text{Fe}^{3+}$ ,  $\text{Hg}^{2+}$ ,  $\text{Mn}^{2+}$ ,  $\text{Co}^{2+}$ ,  $\text{Zn}^{2+}$ ,  $\text{Cd}^{2+}$ ,  $\text{Ni}^{2+}$  and  $\text{Pb}^{2+}$ ); **b**) various anions ( $\text{F}^-$ ,  $\text{Cl}^-$ ,  $\text{Br}^-$ ,  $\text{H}_2\text{PO}_3^-$ ,  $\text{HSO}_4^-$ ,  $\text{ClO}_4^-$ ,  $\text{OH}^-$ ,  $\text{I}^-$ ,  $\text{NO}_3^-$ ,  $\text{AcO}^-$  and  $\text{CN}^-$ ).

### 5.6.2 Emission studies

The investigation of the chemosensing capabilities of the polymer **18** *via* emission spectral analysis was conducted under the same conditions and using the same set of ions as the in UV-Vis analysis. Noteworthy, all tested metal ions, except  $\text{Hg}^{2+}$  enhanced the fluorescence of polymer **18** when their mixtures with polymer **18** were excited at 337 nm (**Figure 5.15 a**). The presence of  $\text{Hg}^{2+}$  induced a fluorescence quenching in both the polymer and tautomer emission peaks with higher quenching observed for the tautomer emission peak. Since the presence of all metal ions except  $\text{Hg}^{2+}$  led to an increase in intensity of tautomer emission peak, it would appear that the presence of other metal ions encourage the ESIPT mechanism, while the presence of  $\text{Hg}^{2+}$  disrupts it. As observed in UV-Vis analysis, the presence of different anionic species did not induce any obvious changes to the spectrum of polymer **18** (**Figure 5.15 b**)

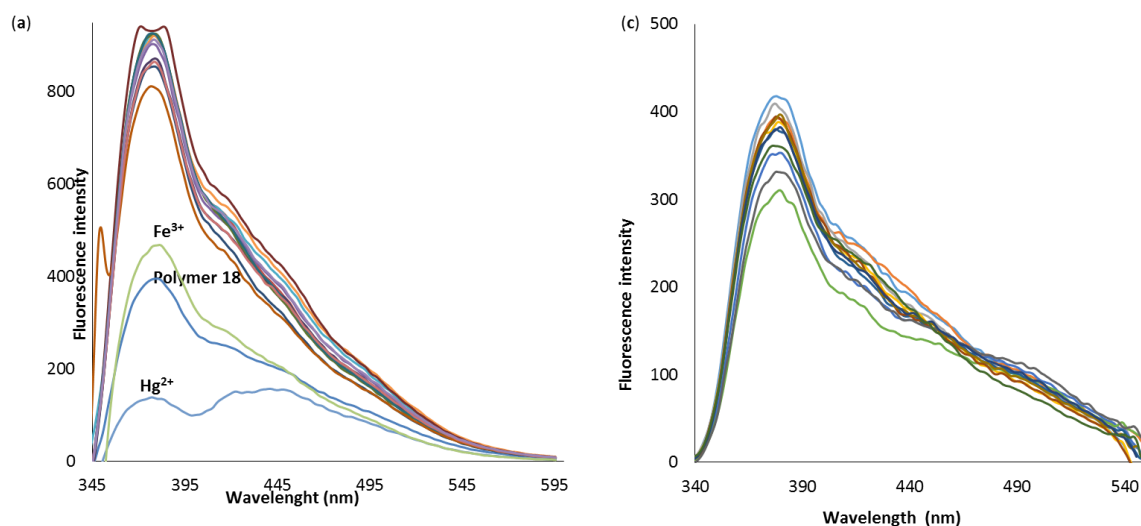


**Figure 5.15:** a) Emission spectra of the polymer **18** ( $1.8 \times 10^{-3}$  g/L) in the presence of the aliquot ( $0.15 \mu\text{M}$ ) of different metal ions ( $\text{Na}^+$ ,  $\text{Ca}^{2+}$ ,  $\text{Ag}^+$ ,  $\text{Al}^{3+}$ ,  $\text{Ba}^{2+}$ ,  $\text{Cr}^{3+}$ ,  $\text{Cu}^{2+}$ ,  $\text{Fe}^{3+}$ ,  $\text{Hg}^{2+}$ ,  $\text{Mn}^{2+}$ ,  $\text{Co}^{2+}$ ,  $\text{Zn}^{2+}$ ,  $\text{Cd}^{2+}$ ,  $\text{Ni}^{2+}$  and  $\text{Pb}^{2+}$ ); b) Emission spectra of the polymer **18** ( $5 \times 10^{-4}$  g L $^{-1}$ ) in the presence of the aliquot ( $0.3 \mu\text{M}$ ) of different anions ( $\text{F}^-$ ,  $\text{Cl}^-$ ,  $\text{Br}^-$ ,  $\text{HSO}_4^-$ ,  $\text{ClO}_4^-$ ,  $\text{OH}^-$ ,  $\text{I}^-$ ,  $\text{NO}_3^-$ ,  $\text{AcO}^-$  and  $\text{CN}^-$ ). Excitation was performed at 337 nm.

### 5.6.3 Titration experiments

Since both the absorption and emission spectral analyses of polymer **18** in the presence of different ions showed a selective response towards  $\text{Hg}^{2+}$ , the sensitivity of polymer **18** towards  $\text{Hg}^{2+}$  was further investigated through titration experiments. **Figure 5.16 a** shows changes in the absorption spectrum as aliquots of  $\text{Hg}^{2+}$  ( $2.5 \times 10^{-7}$  M) were added to a DMF solution of polymer **18**. Initially the addition of  $\text{Hg}^{2+}$  did not show any significant changes to the maximum absorption peak of polymer **18** at 330 and only induced a small increase in the intensity of the absorption peak at  $\sim 380$  nm. As more  $\text{Hg}^{2+}$  was added a decrease in maximum absorption peak and a gradual increase in the absorption peak at  $\sim 380$  nm were observed. Additional aliquots of  $\text{Hg}^{2+}$  resulted in a gradual decrease in both absorption bands. These changes in the absorption spectrum of polymer **18** with addition of  $\text{Hg}^{2+}$  could be attributed to structural changes that occur in polymer **18** as the concentration of  $\text{Hg}^{2+}$  increases.

On the other hand, fluorescence titration experiments (**Figure 5.16 b**) showed a gradual decrease in both the polymer and tautomer peaks with addition of  $\text{Hg}^{2+}$  ( $0.025 \mu\text{M}$ ). Furthermore, it was noted that the tautomer emission peak was affected more by the increasing amount of  $\text{Hg}^{2+}$  than the polymer emission peak. Once again this confirms the fact that  $\text{Hg}^{2+}$

disrupts the ESIPT mechanism by interacting with the binding sites which participate in proton transfer. The inset in **Figure 5.16 b** shows a plot of the emission intensity of polymer **18** at 337 nm against the concentration of  $\text{Hg}^{2+}$ . A linear relationship with a correlation coefficient of  $R^2=0.9942$  was obtained in the range of 0-0.175  $\mu\text{M}$  and detection limit was calculated in the same range and found to be 0.0135  $\mu\text{M}$ .

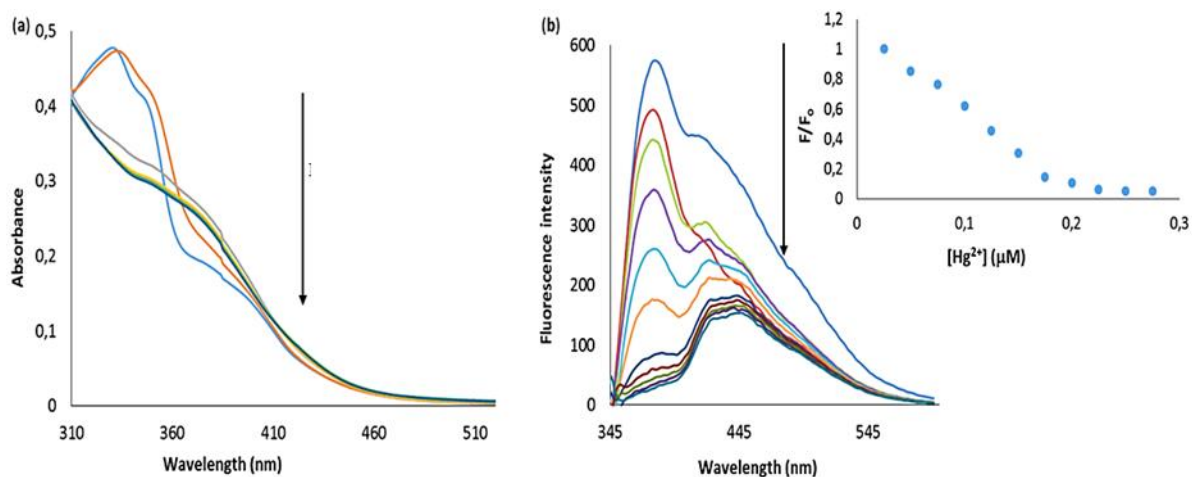


**Figure 5.16:** a) Absorption spectra of polymer **18** (0.12 g/L) upon addition of  $\text{Hg}^{2+}$  ( $2.5 \times 10^{-7}$  M) aliquots; and b) Emission spectra of polymer **18** ( $3.6 \times 10^{-3}$  g/L) upon addition of  $\text{Hg}^{2+}$  (0.025  $\mu\text{M}$ ) aliquots. Excitation was performed at 337 nm in DMF solvent.

#### 5.6.4 Competitive studies

To investigate the influence of other metal ions on the interaction between  $\text{Hg}^{2+}$  and polymer **18**, competitive experiments were conducted using an emission spectral analysis method. The experiments were conducted in the presence of  $\text{Hg}^{2+}$  and two equivalents of other metal ions ( $\text{Na}^+$ ,  $\text{Ca}^{2+}$ ,  $\text{Ag}^+$ ,  $\text{Ba}^{2+}$ ,  $\text{Cr}^{3+}$ ,  $\text{Cu}^{2+}$ ,  $\text{Fe}^{3+}$ ,  $\text{Mn}^{2+}$ ,  $\text{Co}^{2+}$ ,  $\text{Zn}^{2+}$ ,  $\text{Cd}^{2+}$ ,  $\text{Ni}^{2+}$  or  $\text{Pb}^{2+}$ ) and the spectra were recorded in DMF at 337 nm. As shown in **Figure 5.17**, the fluorescence quenching induced by  $\text{Hg}^{2+}$  ions in polymer **18** was not significantly influenced by the presence of two equivalents of other metal ions. In some cases enhanced quenching were observed. This indicates that the interactions between polymer **18** and  $\text{Hg}^{2+}$  result in a more stable complex, which cannot be destabilized by the presence of other metal ions.

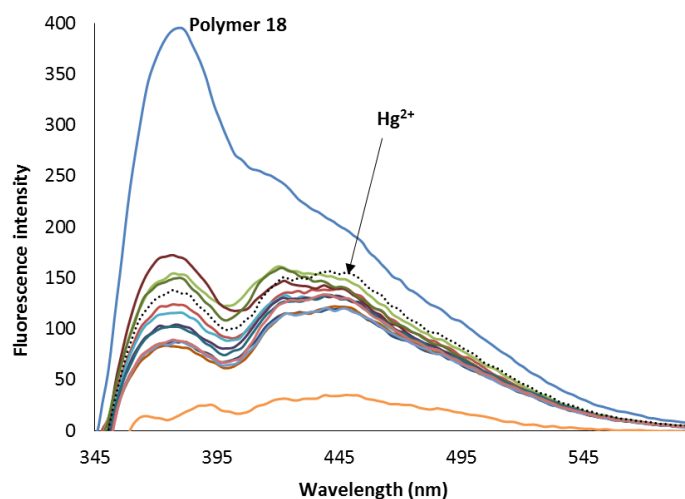


**Figure 5.17:** Emission spectra of polymer **18** ( $1.8 \times 10^{-3}$  g/L) in the presence of mixture of  $\text{Hg}^{2+}$  ( $0.15 \mu\text{M}$ ) and two equivalents of other metal ions ( $0.3 \mu\text{M}$ ) ( $\text{Na}^+$ ,  $\text{Ca}^{2+}$ ,  $\text{Ag}^+$ ,  $\text{Al}^{3+}$ ,  $\text{Ba}^{2+}$ ,  $\text{Cr}^{3+}$ ,  $\text{Cu}^{2+}$ ,  $\text{Fe}^{3+}$ ,  $\text{Hg}^{2+}$ ,  $\text{Mn}^{2+}$ ,  $\text{Co}^{2+}$ ,  $\text{Zn}^{2+}$ ,  $\text{Cd}^{2+}$ ,  $\text{Ni}^{2+}$  and  $\text{Pb}^{2+}$ ). Excitation was performed at 337 nm in DMF solvent.

### 5.6.5 Sensing mechanism of polymer **18** with $\text{Hg}^{2+}$

Since the emission band at 383 nm in the polymer **18** was assigned to the keto form resulting from ESIPT mechanism between hydroxyl group and triazole, any changes in the keto form emission peak can be related to the changes in electron density around the two functionalities (hydroxyl group and triazole). Since all the metal ions except  $\text{Hg}^{2+}$  led to the enhancement of tautomer emission band, it is clear that the binding sites for  $\text{Hg}^{2+}$  are different from other metal ions binding sites. Furthermore, the enhancement in the keto state emission band suggests that the presence of other metal ions increases the rate of ESIPT mechanism. This can be achieved *via* stabilization of the negative charge which is generated after proton transfer. Since this charge is delocalized on the carbonyl group at position 2 of coumarin system (**Figure 5.18**), it is most likely that other metal ions except  $\text{Hg}^{2+}$  interact with the carbonyl group of coumarin. This results in charge stabilization, and hence ESIPT enhancement. On other hand the interaction of  $\text{Hg}^{2+}$  with the triazole and/or  $\text{OH}$  on the other side of the coumarin system where ESIPT mechanism takes place disrupts the occurrence of this mechanism. This reduces the rate of ESIPT mechanism and hence the decrease in the keto state emission band.

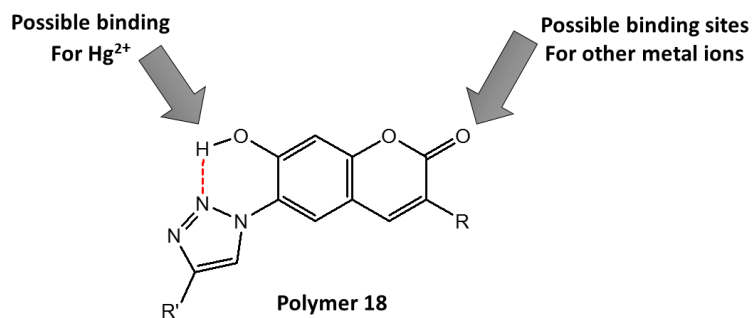
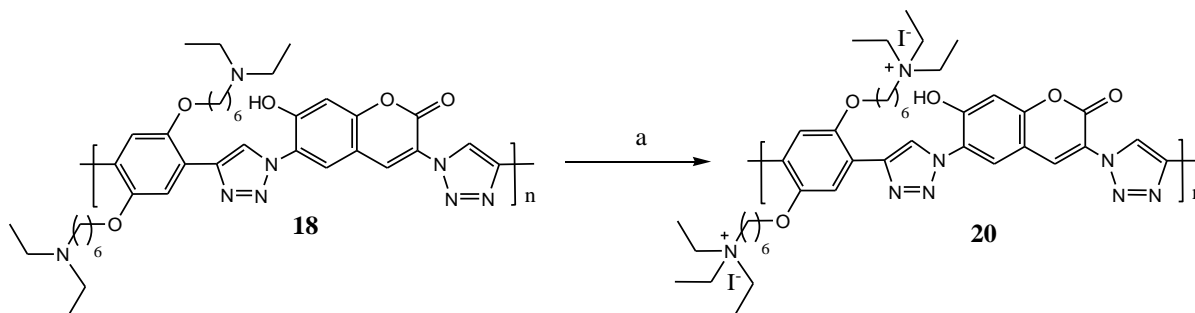


**Figure 5.18:** The proposed binding sites of  $\text{Hg}^{2+}$  and other metal ions.

## 5.7 Quarternarization of polymer 18

The quaternarization of polymer **18** was accomplished in THF at room temperature according to **Scheme 5.6**.



**Scheme 5.6:** Quaternarization of polymer **18** a)  $\text{CH}_3\text{CH}_2\text{I}$ , THF.

Quaternary polymer **20** was characterized by  $^1\text{H}$  NMR spectroscopy. **Figure 5.19** shows comparative  $^1\text{H}$  NMR spectra of polymer **18** and that of quaternarized polymer **20**. Notable, is the downfield shift for the proton signals assigned to the  $-\text{CH}_2-\text{N}$  in polymer **18**. The degree of quaternarization is assumed to be nearly 100% since all the  $^1\text{H}$  NMR peaks corresponding to  $-\text{CH}_2-\text{N}$  shifted in the spectrum of the quaternarized polymer **20**.

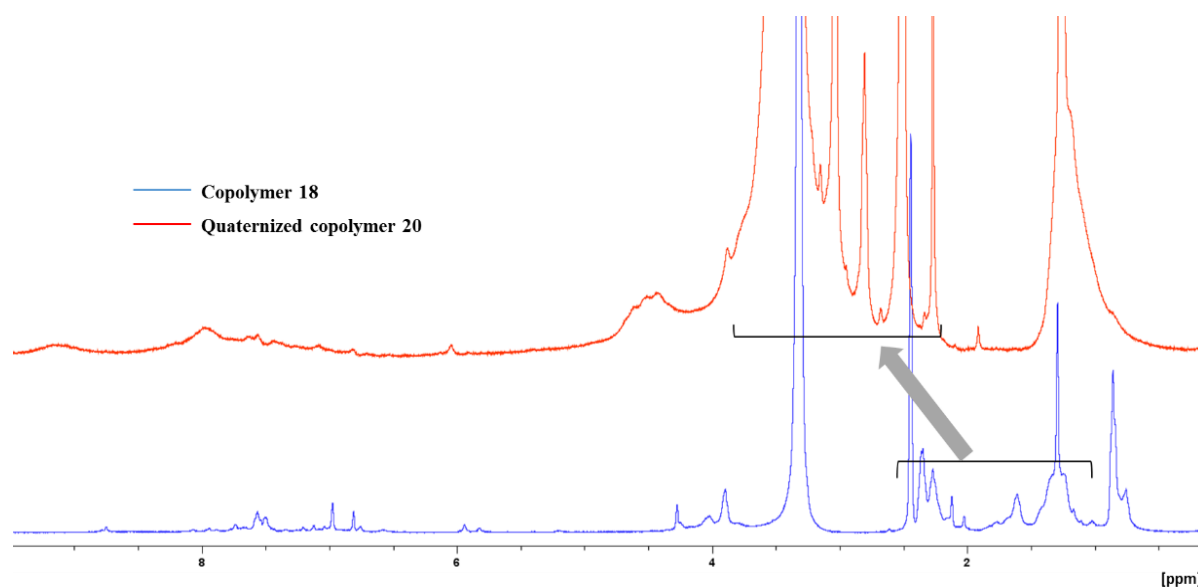


**Figure 5.19:** Comparative  $^1\text{H}$  NMR spectra between polymer **18** and the quaternarized polymer **20**.

### 5.7.1 Emission studies

To investigate the effect of quaternarization on the emission properties of polymer **18**, the emission spectrum of polymer **18** was compared to the emission spectrum of its corresponding quaternarized polymer **20** as shown in **Figure 5.20**. Of note, the emission peak assigned to the excited state tautomer in polymer **18** at 383 nm disappeared in the quaternarized polymer **20**. Only the emission peak from normal excited state of polymer remained prominent at 441 nm. Due to environment reliance of ES IPT mechanism, this can be attributed to the change in environment from neutral to ionic.

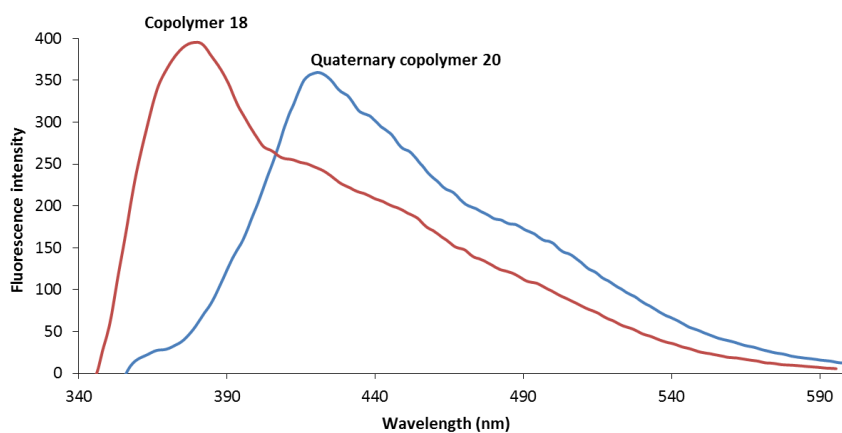


**Figure 5.20:** Comparative emission spectra between polymer **18** and the quaternarized polymer **20**. Excitation was performed at 337 nm in DMF solvent.



### 5.7.2 Effect of solvent on the emission of the quaternarized polymer **20**

In order to investigate the possibilities of aggregate formation which can lead to the fluorescence quenching in the quaternarized polymer **20** in aqueous solutions, the emission behaviour of the quaternarized polymer **20** in DMF with increasing amounts of water, was investigated. As shown in **Figure 5.21**, increase in the amount of water resulted in a gradual increase in the intensity of the maximum emission peak at 424 nm, accompanied with a gradual red shift from 424 to 441 nm. The highest emission intensity was detected when the DMF/H<sub>2</sub>O composition was 40:60 and further increase in water content resulted in a decrease of polymer **20** emission intensity. This effect could be attributed to the formation of aggregates as a result of increased interchain hydrophobic interactions at higher H<sub>2</sub>O content.<sup>16</sup> Increase in fluorescence upon addition of H<sub>2</sub>O from 10 to 60 % can be assigned to an increase in hydrogen bonding, which affects both ends of the coumarin system (7-OH and C-2 carbonyl groups). The hydrogen bonding increases the electron-donating ability of the hydroxyl group at position 7 and electron-withdrawing ability of the carbonyl group at position 2 of the coumarin unit. This leads to an increase in the push-pull effect in the coumarin unit and hence an increase in emission intensity. These conclusions were also supported by the red shift in the emission spectrum as H<sub>2</sub>O content increases.

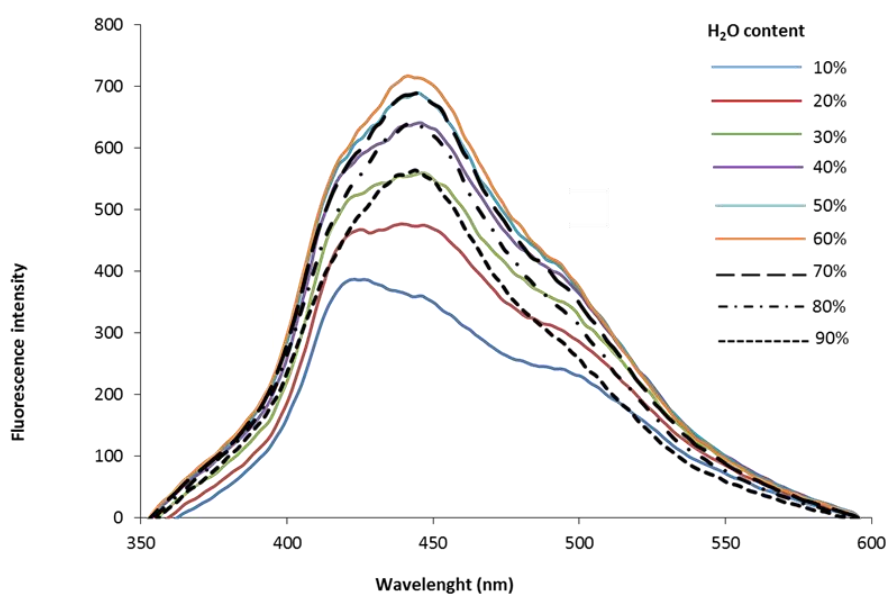


**Figure 5.21:** Changes in the emission spectra of the quaternarized polymer **20** ( $10^{-2}$  g/L) with different DMF/H<sub>2</sub>O ratios. Excitation was performed at 337 nm.

### 5.7.3 Effect of metal ions on the emission of the quaternarized polymer **20**

The effect in the heading was investigated in a DMF/ H<sub>2</sub>O mixture (40:60) in the presence of metal ions (Na<sup>+</sup>, Ca<sup>2+</sup>, Ag<sup>+</sup>, Al<sup>3+</sup>, Ba<sup>2+</sup>, Cu<sup>2+</sup>, Fe<sup>3+</sup>, Hg<sup>2+</sup>, Mn<sup>2+</sup>, Co<sup>2+</sup>, Zn<sup>2+</sup>, Cd<sup>2+</sup>, Ni<sup>2+</sup> and Pb<sup>2+</sup>).

**Figure 5.22** shows the emission spectra recorded, at an excitation wavelength of 337 nm, from a mixture of the polymer **20** with each metal ion. Once again, none of the tested metal ions, except Hg<sup>2+</sup>, showed any significant changes in the emission spectrum of the quaternarized polymer **20**. The presence of Hg<sup>2+</sup> enhanced the fluorescence intensity to almost double the intensity of the free quaternarized polymer **20**. This fluorescence enhancement corroborates with reported findings.<sup>9,17</sup> Due to the extended conjugation in the main chain of the quaternarized polymer **20**, the polymer can be considered as a PET-based system where the extended conjugation backbone acts as a fluorophore and the diethylamino group on the side chains as the receptor. In the absence of Hg<sup>2+</sup>, the lone pairs from the diethylamino group quench the fluorescence of the excited conjugated system through rapid intramolecular electron transfer (IET) from the HOMO of the diethylamino group to the semi-vacant HOMO of excited fluorophore. When Hg<sup>2+</sup> coordinates with this lone pair of electrons, the energy of the receptor group's HOMO becomes lower than that of fluorophore's HOMO. This disrupts the IET process and consequently the fluorescence of the fluorophore is restored.

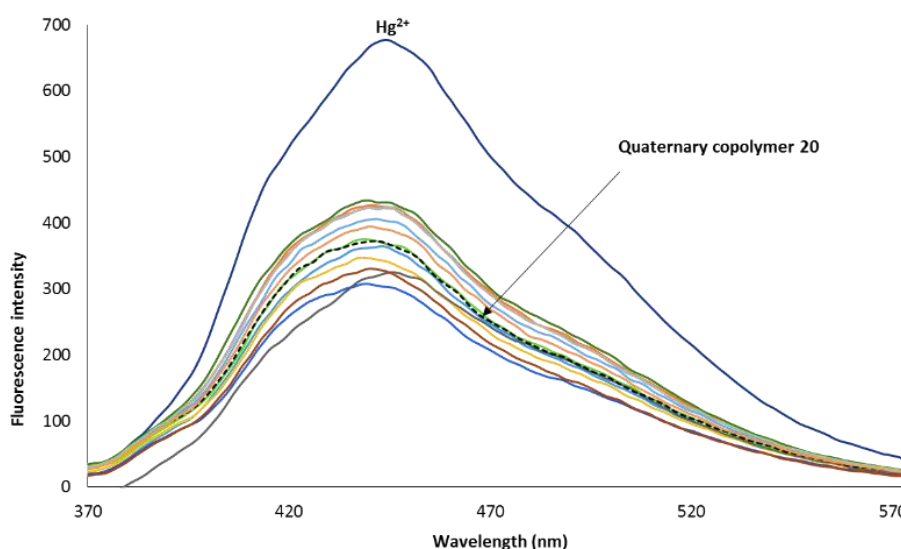


**Figure 5.22:** Emission spectra of the quaternarized polymer **20** ( $5 \times 10^{-3} \text{ g L}^{-1}$ ) in the presence of metal ions ( $0.1 \mu\text{M}$ ) (Na<sup>+</sup>, Ca<sup>2+</sup>, Ag<sup>+</sup>, Al<sup>3+</sup>, Ba<sup>2+</sup>, Cu<sup>2+</sup>, Fe<sup>3+</sup>, Hg<sup>2+</sup>, Mn<sup>2+</sup>, Co<sup>2+</sup>, Zn<sup>2+</sup>, Cd<sup>2+</sup>, Ni<sup>2+</sup> and Pb<sup>2+</sup>). Excitation was performed at 337 nm in a DMF/H<sub>2</sub>O mixture (40:60).

The sensitivity of the quaternarized polymer **20** towards  $\text{Hg}^{2+}$  was further investigated through fluorescence titration experiments as shown in **Figure 5.22**. Upon addition of  $\text{Hg}^{2+}$  aliquots ( $0.005\mu\text{M}$ ) to an aqueous DMF solution of the quaternarized polymer **20**, a gradual increase in the intensity of the emission band at 441 nm was observed. The inset in **Figure 5.23** shows a plot of emission intensity of the quaternarized polymer **20** at 337 nm against the concentration of added  $\text{Hg}^{2+}$ , and a linear relationship with a correlation coefficient of  $R^2=0.9808$  was obtained in the 0-0.2  $\mu\text{M}$  range. The detection limit of the quaternarized polymer **20** towards  $\text{Hg}^{2+}$  was determined in the same range and was found to be 0.004  $\mu\text{M}$ . This indicates that quaternarized polymer **20** has high sensitivity towards  $\text{Hg}^{2+}$  ions in the aqueous DMF solution.

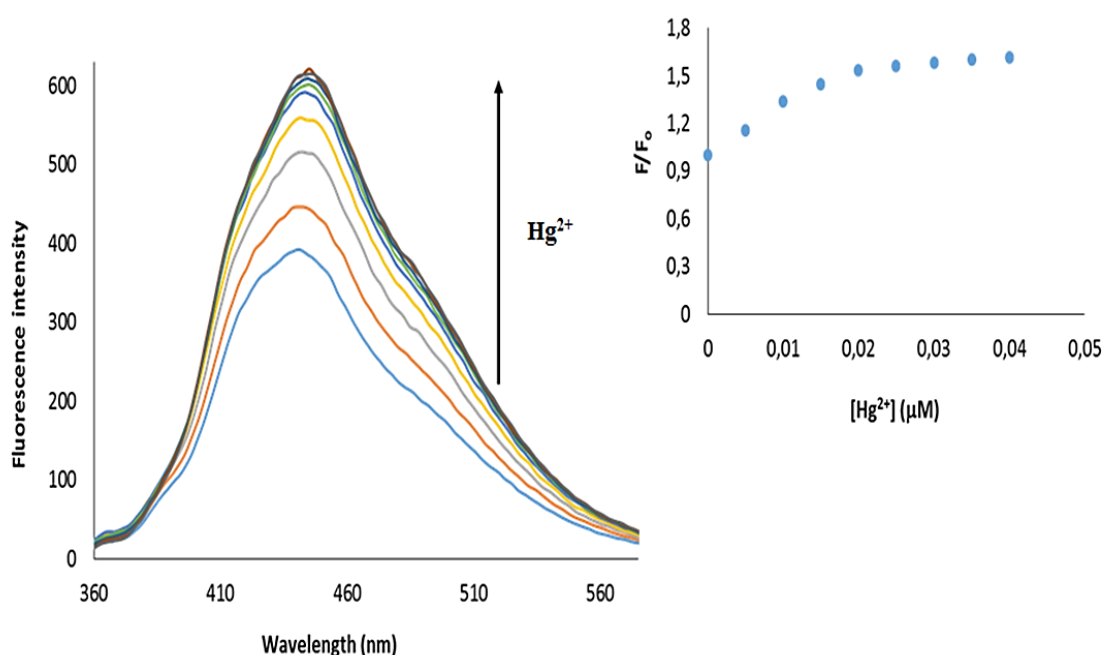


**Figure 5.23** Changes in the emission spectra of the quaternarized polymer **20** ( $5 \times 10^{-3}\text{g/L}$ ) with increasing amounts of  $\text{Hg}^{2+}$  ( $0.005 \mu\text{M}$ ). Excitation was performed at 385 nm in a DMF/ $\text{H}_2\text{O}$  mixture (40:60).

#### 5.7.4 Competitive studies

The impact of other metal ions on the binding of  $\text{Hg}^{2+}$  to the quaternarized polymer **20** were also investigated through an emission spectral analysis method. The emission spectra of the mixtures of the quaternarized polymer **20**,  $\text{Hg}^{2+}$  and one equivalent of other metal ion ( $\text{Na}^+$ ,  $\text{Ca}^{2+}$ ,  $\text{Ag}^+$ ,  $\text{Ba}^{2+}$ ,  $\text{Cr}^{3+}$ ,  $\text{Cu}^{2+}$ ,  $\text{Fe}^{3+}$ ,  $\text{Mn}^{2+}$ ,  $\text{Co}^{2+}$ ,  $\text{Zn}^{2+}$ ,  $\text{Cd}^{2+}$ ,  $\text{Ni}^{2+}$  and  $\text{Pb}^{2+}$ ) were recorded at room temperature in a mixture of DMF and  $\text{H}_2\text{O}$  (40:60). As shown in **Figure 5.24**, the fluorescence

enhancement induced by  $\text{Hg}^{2+}$  in the quaternarized polymer **20** was slightly affected by the presence of one equivalent of most of the tested metal ions. This indicates that the interactions between the quaternarized polymer **20** and  $\text{Hg}^{2+}$  in aqueous DMF solutions results in a stable complex which is weakly affected by the presence of other metal ions.

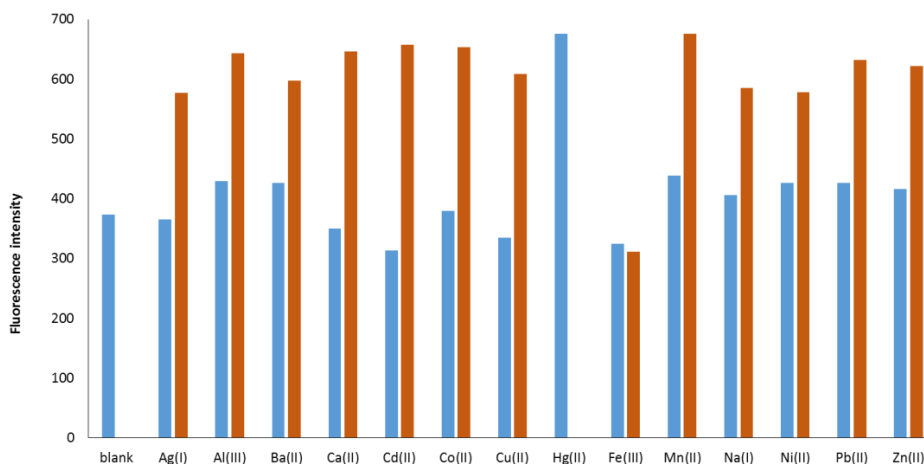


**Figure 5.24:** Fluorescence responses of the quaternarized polymer **20** ( $5 \times 10^{-3}$  M) in the presence of metal ions ( $0.1 \mu\text{M}$ ) ( $\text{Na}^+$ ,  $\text{Ca}^{2+}$ ,  $\text{Ag}^+$ ,  $\text{Al}^{3+}$ ,  $\text{Ba}^{2+}$ ,  $\text{Cu}^{2+}$ ,  $\text{Fe}^{3+}$ ,  $\text{Hg}^{2+}$ ,  $\text{Mn}^{2+}$ ,  $\text{Co}^{2+}$ ,  $\text{Zn}^{2+}$ ,  $\text{Cd}^{2+}$ ,  $\text{Ni}^{2+}$  and  $\text{Pb}^{2+}$ ) (blue bars) and in the presence of a mixture of  $\text{Hg}^{2+}$  ( $0.1 \mu\text{M}$ ) with one equivalent ( $0.2 \mu\text{M}$ ) of another metal ion (red bars). Excitation was performed at 337 nm in DMF/ $\text{H}_2\text{O}$  mixture (40-60).

## 5.8 Conclusion

A new polymer system which showed higher sensitivity towards  $\text{Hg}^{2+}$  in both neutral and cationic form was developed. The synthesis of the polymer **18** was accomplished using AA-BB step-growth click polymerization of diazide-functionalized monomer and dialkyne-functionalized monomers. Polymer **18** and its quaternarized derivative polymer **20** showed a strong selectivity towards  $\text{Hg}^{2+}$  in DMF and DMF/ $\text{H}_2\text{O}$  mixture, even in the presence of other metal ions.

---

## 5.9 Experimental

### 5.9.1 General information

All chemicals and solvents were purchased from Sigma Aldrich or Merck and used as received without further purification. Reactions monitoring, products purification and characterization as well as photophysical studies were done using same materials and instrumentations used in Chapter 3.

### 5.9.2 Synthesis of AA-type monomer

#### 5.9.2.1 1,4-Bis(6-bromohexyloxy)benzene (3)<sup>7</sup>

Yield: 85%. <sup>1</sup>H NMR (CDCl<sub>3</sub>, 400 MHz): δ = 6.74 (s, 4H), 3.83 (t, *J* = 6.28, 4H), 3.34 (t, *J* = 6.68, 4H), 1.83-1.68 (m, 8H), 1.43-1.41 (m, 8H). <sup>13</sup>C NMR (CDCl<sub>3</sub>, 400 MHz): δ = 153.13, 115.43, 68.38, 33.80, 32.70, 29.20, 27.94, 25.31.

#### 5.9.2.2 1,4-Bis(6-bromohexyloxy)-2,5-diiodobenzene (4)<sup>8</sup>

Yield: 76%. <sup>1</sup>H NMR (CDCl<sub>3</sub>, 400 MHz): δ = 7.19 (s, 4H), 3.95 (b, 4H), 3.45 (b, *J* = 6.68, 4H), 1.93-1.85 (m, 8H), 1.56 (b, 8H). <sup>13</sup>C NMR (CDCl<sub>3</sub>, 400 MHz): δ = 152.84, 122.82, 86.31, 70.07, 33.77, 32.67, 28.95, 27.81, 25.29.

#### 5.9.2.3 6-(4-[6-(Diethylamino)hexyloxy]-2,5-diiodophenoxy]-*N,N*-diethylhexan-1-amine (5)<sup>9</sup>

Yield: 72%. <sup>1</sup>H NMR (CDCl<sub>3</sub>, 400 MHz): δ = 7.09 (s, 2H), 3.85 (t, *J* = 6.00, 4H), 2.84 (q, *J* = 6.96, 8H), 2.65 (t, *J* = 7.32, 4H), 1.70-1.75 (m, 4H), 1.45-1.28 (m, 12H), 0.94 (t, *J* = 7.00, 12H). <sup>13</sup>C NMR (CDCl<sub>3</sub>, 400 MHz): δ = 152.75, 122.75, 86.36, 70.03, 52.00, 46.65, 28.91, 26.89, 25.77, 25.10, 10.24.

#### 5.9.2.4 6-{4-[6-(Diethylamino)hexyloxy]-2,5-bis[2-(trimethylsilyl)ethynyl]phenoxy]-*N,N*-diethylhexan-1-amine (6)<sup>10</sup>

Yield: 64%. <sup>1</sup>H NMR (CDCl<sub>3</sub>, 400 MHz): δ = 6.89 (s, 2H), 3.95 (t, *J* = 6, 4H), 2.56-2.45 (m, 12H), 1.80-1.36 (m, 16H), 1.04 (t, *J* = 6.12, 12H), 0.26 (s, 18H). <sup>13</sup>C NMR (CDCl<sub>3</sub>, 400 MHz): δ = 154.02, 117.26, 114.01, 101.07, 100.12, 69.37, 52.90, 46.90, 29.37, 27.53, 26.84, 26.04, 11.56.

---

### 5.9.2.1 6-(4-(6-(Diethylamino)hexyloxy)-2,5-diethynylphenoxy)-N,N-diethylhexan-1-amine (7)

A mixture of compound (6) and  $K_2CO_3$  in THF/MeOH (1:1, 20 ml) was stirred at room temperature for 2 h. The solvent was then evaporated under reduced pressure and the residues dissolved in ethyl acetate. The organic layer was collected, washed with water and dried over anhydrous  $Na_2SO_4$ . The solvent was evaporated and the crude product was purified by column chromatography over silica gel (Hexane: EtOAc, 20:80) to afford brown product in yield: 60%.  $^1H$  NMR ( $CDCl_3$ , 400 MHz):  $\delta$  = 6.87 (s, 2H), 3.90 (t,  $J$  = 6.2, 4H), 3.25 (s, 2H), 2.50-2.30 (m, 12H), 1.75-1.27 (m, 16H), 0.94 (t,  $J$  = 6.96, 12H).  $^{13}C$  NMR ( $CDCl_3$ , 400 MHz):  $\delta$  = 153.96, 117.79, 113.30, 82.45, 79.75, 69.57, 52.84, 46.88, 29.11, 27.40, 26.85, 25.91, 11.60.

## 5.9.3 Synthesis of BB-type monomer

### 5.9.3.1 Synthesis of diazide functionalized coumarin monomer (12)

#### (i) 2,4-Dihydroxy-5-nitrobenzaldehyde (9)

With stirring at rt, a mixture of 5.86 g (0.07 moles) of 72% nitric acid and 6.67 g (0.07 moles) of concentrated sulfuric acid was added dropwise to a suspension of 9.6.7 g (0.2 mole) of 2,4-dihydroxybenzaldehyde in 50 ml of glacial acetic acid, and the mixture was stirred for 5 h and poured into 150 ml of cold water. The precipitate was filtered off and washed with water to afford pure product as brown powder in 55% yield.  $^1H$  NMR ( $CDCl_3$ , 400 MHz):  $\delta$  = 11.55 (s, 1H), 11.11 (s, 1H), 9.76 (s, 1H), 8.41 (s, 1H), 6.55 (s, 1H).  $^{13}C$  NMR ( $CDCl_3$ , 400 MHz):  $\delta$  = 194.00, 167.97, 161.40, 133.57, 127.92, 115.21, 106.06.

#### (ii) Coumarin derivative (10)

A mixture of 2,4-dihydroxy-5-nitrobenzaldehyde (9) (4.0 g, 22 mmol), *N*-acetylglycine (2.6 g, 22 mmol) and anhydrous sodium acetate (5.4 g, 66 mmol in 100 mL acetic anhydride) was refluxed for 12 h. The reaction mixture was then poured onto ice and kept overnight in cold room. The formed precipitate was filtrated, washed with water and dried under vacuum to afford pure product as yellow powder in 55% yield. IR  $\nu_{max}$  ( $cm^{-1}$ ): 3349 (N-H), 1769, 1667, 1624 (C=O), 1540 (C=C).  $^1H$  NMR ( $CDCl_3$ , 400 MHz):  $\delta$  = 9.90 (s, 1H), 8.69 (s, 1H), 8.66 (s, 1H), 7.56 (s, 1H), 2.35 (s, 3H), 2.18 (s, 3H).  $^{13}C$  NMR ( $CDCl_3$ , 400 MHz):  $\delta$  = 170.95, 168.90, 156.94, 153.01, 143.81, 138.75, 126.32, 125.65, 121.67, 118.99, 113.25, 24.42, 20.90. Anal. Calc. for  $C_{13}H_{10}N_2O_7$ : C: 50.99, H: 3.29, N: 9.15. Found: C: 52.24, H: 3.47, N: 8.5.

---

(iii) *Coumarin derivative (11)*

Compound **(10)** (1 g, 3 mmol) was added to a stirred mixture of iron (2 g, 18 mmol) in aqueous acetic acid (20 mL, 1:1 v/v) and the mixture was stirred at room temperature for 5 h. The reaction mixture was then poured into saturated sodium hydrogen carbonate (100 mL) and extracted with ethyl acetate (3x50 mL). The combined organic extracts were dried over anhydrous Na<sub>2</sub>SO<sub>4</sub> and evaporate to dryness to afford light green powder in 38 % yield. IR  $\nu_{\max}$  (cm<sup>-1</sup>): 3312 (N-H), 1697, 1612, 1583 (C=O), 1542 (C=C). <sup>1</sup>H NMR (CDCl<sub>3</sub>, 400 MHz):  $\delta$  = 9.57 (s, 1H), 9.31 (s, 1H), 8.43 (s, 1H), 8.03 (s, 1H), 6.84 (s, 1H), 1.99 (s, 3H), 1.91 (s, 3H). <sup>13</sup>C NMR (CDCl<sub>3</sub>, 400 MHz):  $\delta$  = 170.29, 169.40, 158.29, 150.94, 147.74, 126.35, 124.95, 121.92, 120.65, 111.23, 102.46, 24.23, 24.11.

(iv) *3,6-Diazido-7-hydroxy-2H-chromen-2-one (12)*

Compound **(11)** (2.00 g, 7.24 mmol) was refluxed in a mixture of conc. HCl and ethanol 2:1 (30 mL) for 2 h. The reaction mixture was then diluted with water (40 mL) and cooled in an ice bath. When the reaction temperature was below 5 °C, NaNO<sub>2</sub> (1.9 g, 28 mmol) was added and the mixture was stirred for 30 minutes. This was followed by the addition of NaN<sub>3</sub> (1.8 g, 28 mmol) in portions and continued stirring for another 30 minutes. The resulting precipitate was filtered, washed with water and dried under vacuum to afford pure product as brown powder in 65% yield). IR  $\nu_{\max}$  (cm<sup>-1</sup>): 3359 (OH), 2113 (N<sub>3</sub>) 1725 (C=O), 1614 (C=C). <sup>1</sup>H NMR (CDCl<sub>3</sub>, 400 MHz):  $\delta$  = 11.47 (s, 1H), 7.54 (s, 1H), 7.28 (s, 1H), 6.95 (s, 1H). <sup>13</sup>C NMR (CDCl<sub>3</sub>, 400 MHz):  $\delta$  = 156.98, 153.07, 149.44, 126.85, 124.16, 122.17, 118.70, 111.59, 103.2.

### 5.9.3.2 Synthesis of diazide functionalized coumarin monomer (17)

(i) *2-Hydroxy-5-nitrobenzaldehyde (14)*<sup>18</sup>

Yield = 60%. <sup>1</sup>H NMR (CDCl<sub>3</sub>, 400 MHz):  $\delta$  = 11.53 (s, 1H), 9.93 (s, 1H), 8.34 (d, *J* = 9.36 1H), 7.06 (d, *J* = 9.20 1H), <sup>13</sup>C NMR (CDCl<sub>3</sub>, 400 MHz):  $\delta$  = 195.46, 166.14, 137.12, 131.68, 131.33, 129.73, 119.02.

(ii) *N-(6-Nitro-2-oxo-2H-chromen-3-yl)acetamide (15)*

Coumarin **(15)** was prepared from 2-hydroxy-5-nitrobenzaldehyde **(14)** using the procedure previously used for coumarin **(10)** and a yield of 52 % was obtained. m.p. 194-197 °C, IR  $\nu_{\max}$  (cm<sup>-1</sup>): 3328 (N-H), 1707, 1676 (C=O), 1604 (C=C). <sup>1</sup>H NMR (CDCl<sub>3</sub>, 400 MHz):  $\delta$  = 8.68 (s, 1H), 8.36 (s, 1H), 8.88 (d, *J* = 8.92, 1H), 8.03 (s, 1H), 7.38 (d, *J* = 9.04, 1H), 2.21 (s, 3H). <sup>13</sup>C

---

NMR (CDCl<sub>3</sub>, 400 MHz):  $\delta$  = 169.55, 157.53, 152.95, 144.83, 125.56, 124.25, 123.37, 121.27, 120.39, 117.49, 24.72. Anal. Calc. for C<sub>11</sub>H<sub>8</sub>N<sub>2</sub>O<sub>5</sub>: C: 53.24, H: 3.51, N: 11.27. Found: C: 62.17, H: 6.30, N: 17.59.

(iii) *N*-(6-Amino-2-oxo-2H-chromen-3-yl)acetamide (**16**)

Coumarin (**16**) was prepared from coumarin (**15**) using the procedure previously used for coumarin (**11**) synthesis and a yield of 49% was obtained. m.p. 198-201°C, IR  $\nu_{\max}$  (cm<sup>-1</sup>): 3314 (N-H), 1708, 1667 (C=O), 1604 (C=C). <sup>1</sup>H NMR (CDCl<sub>3</sub>, 400 MHz):  $\delta$  = 9.60 (s, 1H), 8.39 (s, 1H), 7.08 (d, *J* = 8.68, 1H), 6.74 (d, *J* = 8.72, 1H), 6.68 (s, 1H), 5.17 (s, 2H), 2.14 (s, 3H). <sup>13</sup>C NMR (CDCl<sub>3</sub>, 400 MHz):  $\delta$  = 170.10, 157.73, 145.90, 141.48, 124.19, 124.05, 119.74, 116.54, 116.12, 109.60, 23.87.

(iv) 3,6-Diazido-2H-chromen-2-one (**17**)

Compound (**17**) was prepared from coumarin (**16**) using the procedure previously used for the synthesis of corresponding diazide monomer (**12**). After purification the product was obtained as brown solid in 68 % yield. IR  $\nu_{\max}$  (cm<sup>-1</sup>): 2111 (N<sub>3</sub>), 1723 (C=O), 1624 (C=C). <sup>1</sup>H NMR (CDCl<sub>3</sub>, 400 MHz):  $\delta$  = 7.63 (s, 1H), 7.48-7.46 (m, 2H), 7.25 (d, *J* = 8.78 1H). <sup>13</sup>C NMR (CDCl<sub>3</sub>, 400 MHz):  $\delta$  = 157.17, 148.48, 136.68, 127.11, 125.82, 121.87, 120.89, 118.12, 117.54.

#### 5.9.4 General procedure for AA-BB step-growth click polymerization

A mixture of diazide functionalized monomer (0.5 mmol), dialkyne functionalized (0.5 mmol), CuSO<sub>4</sub>·5H<sub>2</sub>O (0.054 mmol), sodium ascorbate (0.11 mmol) and PMDETA (0.15 mmol) in THF (30 mL) and minimum amount of water was stirred at room temperature for 72 hrs. The precipitated polymer were collected and washed with water to yield pure polymers in 78% and 82% yield for polymer **18** and **19** respectively.

#### 5.9.5 Quaternarization of polymer **18**

A mixture of polymer **18** (40 mg) and iodoethane (0.5 mL) in THF was stirred at room temperature for 48 h. The precipitated polymer were filtered and washed with THF to yield polymer **20** as brown solid in 81% yield.



---

## 5.10 References

1. S. Binauld, F. Boisson, T. Hamaide, J.P. Pascault, E. Drockenmuller and E. Fleury, J. *Polym. Sci., Part A: Polym. Chem.*, **2008**, 46, 5506-5506.
2. N. V. Tsarevsky, B. S. Sumerlin and K. Matyjaszewski, *Macromolecules*, **2005**, 38, 3558-3561.
3. Y. Nagao and A. Takasu, *Macromol. Rapid Commun.*, **2009**, 30, 199-203.
4. S. Binauld, D. Damiron, T. Hamaide, J. P. Pascault, E. Fleury and E. Drockenmuller, *Chem. Commun.*, **2008**, 4138-4140.
5. K. N. Lau, H. F. Chow, M. C. Chan and K. W. Wong, *Angew. Chem., Int. Ed.*, **2008**, 47, 6912-6916.
6. Y. Jin, Y. Xu, Z. Qiao, J. Peng, B. Wang and D. Cao, *Polymer*, **2010**, 51, 5726-5733.
7. Q. Zhou and T. M. Swager, *J. Am. Chem. Soc.*, **1995**, 117, 7017-7018.
8. D. Ye, L. Wang, H. Li, J. Zhou and D. Cao, *Sens. Actuators B*, **2013**, 181, 234-243.
9. J. Li, J. Meng, X. Huang, Y. Cheng and C. Zhu, *Polymer*, **2010**, 51, 3425-3430.
10. J. R. Johnson, " *Org. React.* **1942**, 1, 210-265.
11. M. Meldal and C. W. Torne, *Chem. Rev.*, **2008**, 108, 2952-3015.
12. J. Zhao, S. Ji, Y. Chen, H. Guo and P. Yang, *Phys. Chem. Chem. Phys.*, **2012**, 14, 8803-8817.
13. J. Kalinowski, *Mater. Sci. Poland*, **2009**, 27, 735-756.
14. B. Valeur, and I. Leray, *Coord. Chem. Rev.*, **2000**, 205, 3-40.
15. a) J. Seo, S. Kim and S. Y. Park, *J. Am. Chem. Soc.*, **2004**, 126, 11154-11155. b) O. K. Abou-Zied, R. Jimenez, E. H. Z. Thompson, D. P. Millar and F. E. Romesberg, *J. Phys. Chem. A.*, **2002**, 106, 3665-3672. c) K. Das, N. Sarkar, A. K. Ghosh, D. Majumdar, D. N. Nath and K. Bhattacharyya, *J. Phys. Chem.*, **1994**, 98, 9126-9132.
16. Y. Bao, H. Wang, Q. Li, B. Liu, Q. Li, W. Bai, B. Jin and R. Bai, *Macromolecules*, **2012**, 45, 3394-3401.
17. L. J Fan, Y. Zhang and W. E Jones. *Macromolecules*, **2005**, 38, 2844-2849.
18. V. B. Panchabhai, S. N. Budhwani, S. S. Jagtab, Y. B. Zambare and N. Y. Kalyane, *Asian J. Pharm. Hea. Sci.*, **2011**, 1, 158-162.

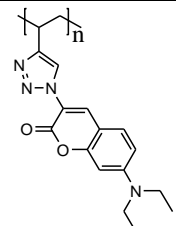
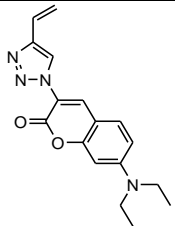
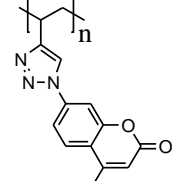
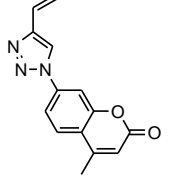
## Chapter 6 Summary, conclusions and recommendations for future work

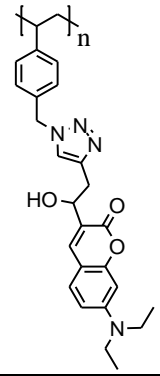
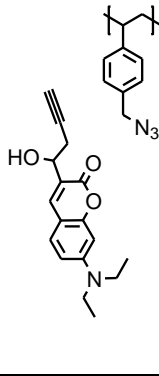
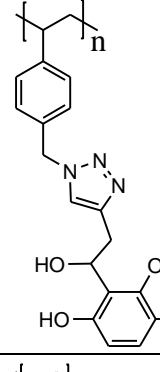
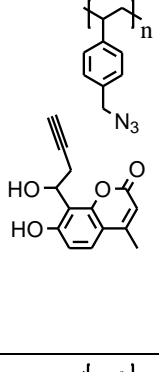
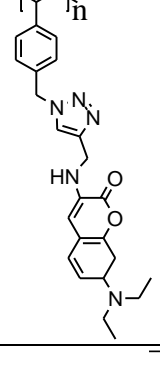
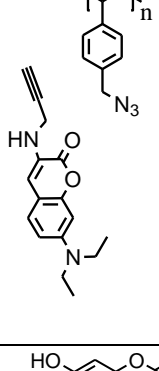
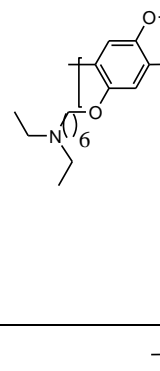
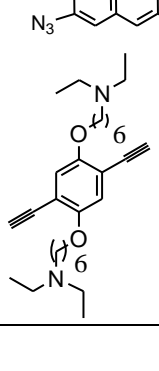
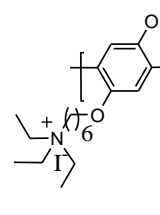
### 6.1 Summary and conclusions

We have synthesized different types of polymeric materials and their photophysical properties as well as their chemosensing capabilities towards ions were investigated in DMF and DMF/H<sub>2</sub>O. **Table 1** shows the synthesized polymers, their respective starting monomers, selective ions and observed responses. From the chemosensing investigations results it can be concluded that triazolyl coumarin-based polymer are highly sensitive to Fe<sup>3+</sup> and Hg<sup>2+</sup>. Fe<sup>3+</sup> interact with the carbonyl group of the coumarin unit, while Hg<sup>2+</sup> interacts simultaneously with the triazole ring and other auxiliary binding sites in the triazole's vicinity. These variations in the binding modes can be used to distinguish between Fe<sup>3+</sup> and Hg<sup>2+</sup> as different signals are induced in the coumarin chromophore during complexation.

Due to the acidic nature of C-H of triazole, triazolyl coumarin-based polymer with functional linkage at position 3 showed sensitivity towards OH<sup>-</sup>, unlike their corresponding conjugated triazolyl coumarin-based polymers. This suggests that for C-H of triazole to interact efficiently with anions, other auxiliary binding sites are required. Triazolyl coumarin-based polymers also showed a higher sensitivity towards Hg<sup>2+</sup> in DMF/H<sub>2</sub>O which indicates that the sensitivity of these polymers cannot be affected in the aqueous media.

**Table 1:** Summary of the polymers, their respective starting monomers, their selective ions and observe emission responses.

Polymer	Starting monomer	Selective ions	Emission response
		Fe <sup>3+</sup>	Quenching
		Fe <sup>3+</sup>	Quenching

		$\text{Fe}^{3+}$ $\text{Hg}^{2+}$ $\text{OH}^-$	Quenching Quenching Quenching
		$\text{Fe}^{3+}$ $\text{Hg}^{2+}$ $\text{Al}^{3+}$	Quenching Quenching Enhancement
		$\text{F}^-$	Enhancement
		$\text{Hg}^{2+}$	Quenching
	-	$\text{Hg}^{2+}$	Enhancement

---

## 6.2 Recommendations for future work

In this study, only DMF solvent was used during investigation of chemosensing capabilities of triazolyl coumarin-based polymers. However, the use of other solvents or mixture of solvents that cannot interact with metal ions is highly recommended for further investigations. This was emphasized by  $\text{Fe}^{3+}$ , which showed self-absorption in DMF even in the absence of fluorophore. The use of less interfering solvents can improve the chemosensing ability of the polymers, as ions would only interact with the binding sites on the polymer with less interference from the solvent. Owing to the limited solubility of triazolyl coumarin-based polymers which limited their characterization, properties investigations as well their applications, the incorporation of different solubilizing groups which can reduce the rigidity of triazolyl coumarin system is recommended. This will broaden the application of triazolyl coumarin based polymer in various environments including aqueous medium.

## Appendices

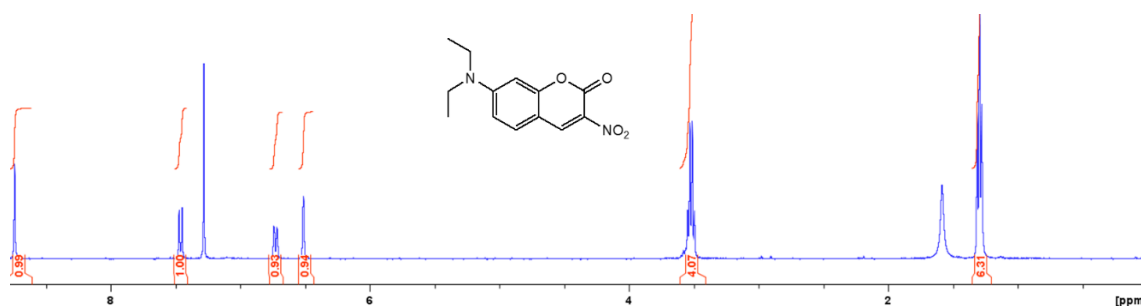


**Figure A.1:**  $^1\text{H}$  NMR spectrum of 7-(diethylamino)-3-nitro-2*H*-chromen-2-one in  $\text{CDCl}_3$ .

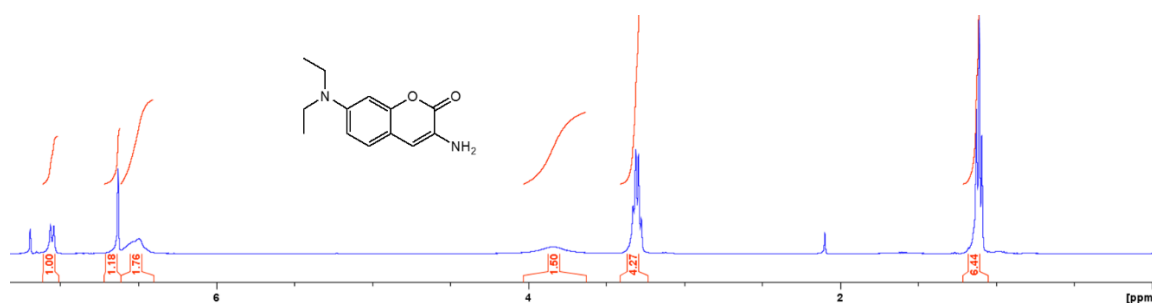


**Figure A.2:**  $^1\text{H}$  NMR spectrum of 3-amino-7-(diethylamino)-2*H*-chromen-2-one in  $\text{CDCl}_3$ .

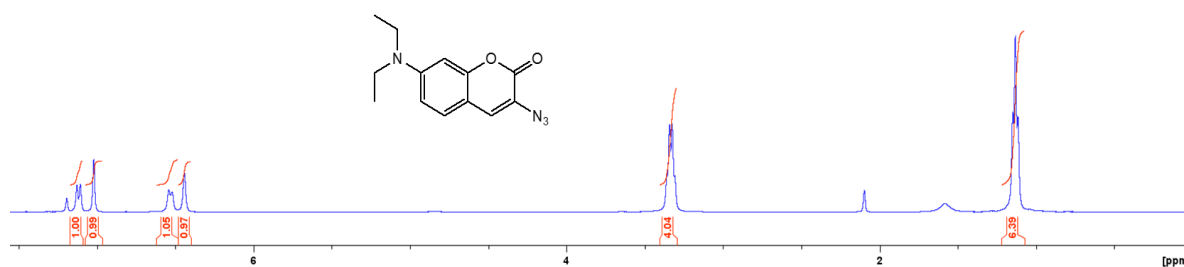


**Figure A.3:**  $^1\text{H}$  NMR spectrum of 3-azido-7-(diethylamino)-2*H*-chromen-2-one in  $\text{CDCl}_3$ .

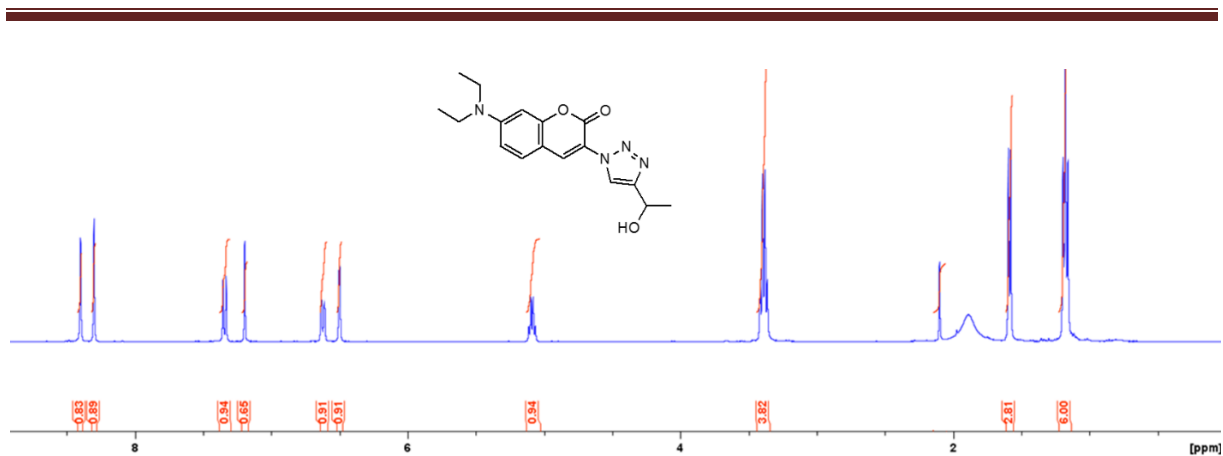


**Figure A.4:** <sup>1</sup>H NMR spectrum of 7-(diethylamino)-3-(4-(1-hydroxyethyl)-1H-1,2,3-triazol-1-yl)-2H-chromen-2-one in CDCl<sub>3</sub>.

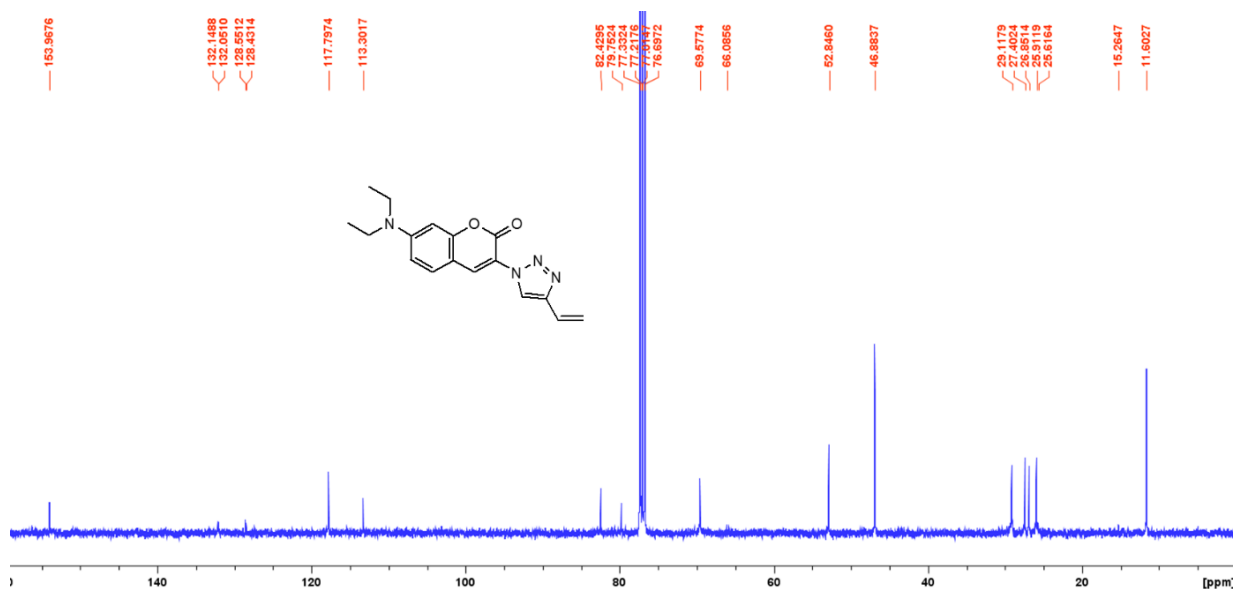


**Figure A.5:** <sup>13</sup>C NMR spectrum of 7-(diethylamino)-3-(4-vinyl-1H-1,2,3-triazol-1-yl)-2H-chromen-2-one in CDCl<sub>3</sub>.

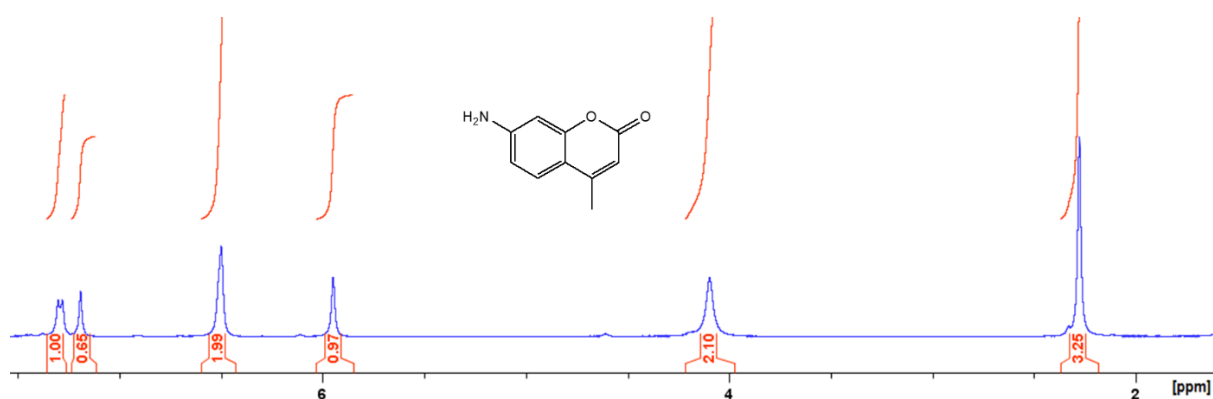


**Figure A.6:**  $^1\text{H}$  NMR spectrum of 7-amino-4-methyl-2*H*-chromen-2-one in  $\text{CDCl}_3$ .

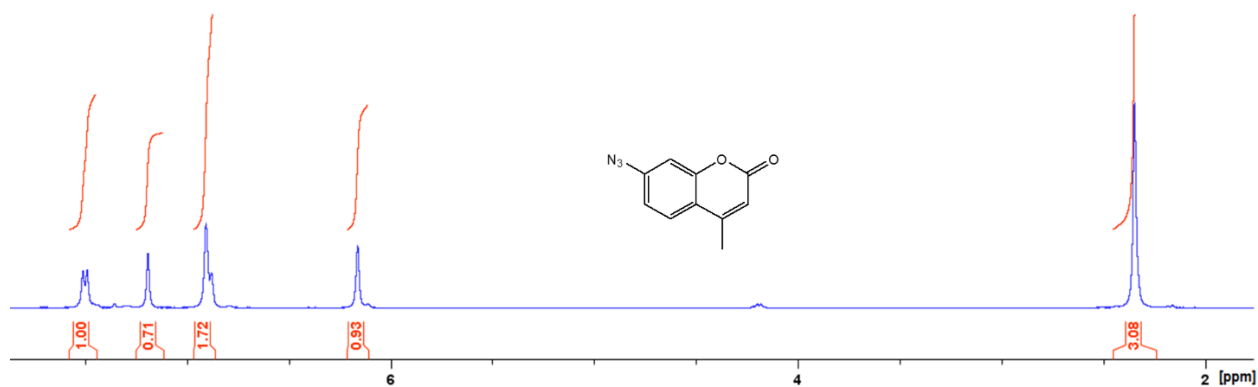


**Figure A.7:**  $^1\text{H}$  NMR spectrum of 7-azido-4-methyl-2*H*-chromen-2-one in  $\text{CDCl}_3$ .

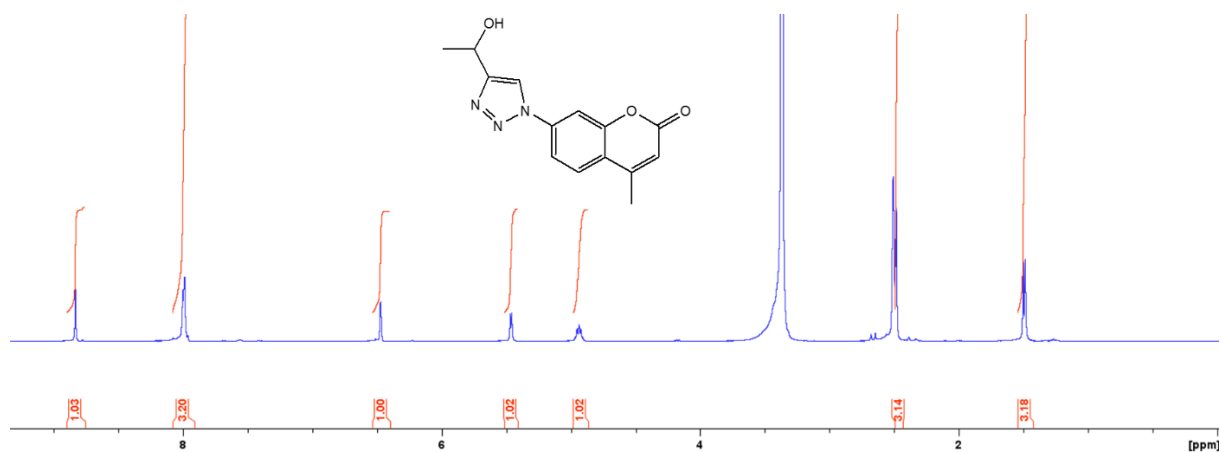


**Figure A.8:**  $^1\text{H}$  NMR spectrum of 7-(4-(1-hydroxyethyl)-1*H*-1,2,3-triazol-1-yl)-4-methyl-2*H*-chromen-2-one in  $\text{DMSO-d}_6$ .

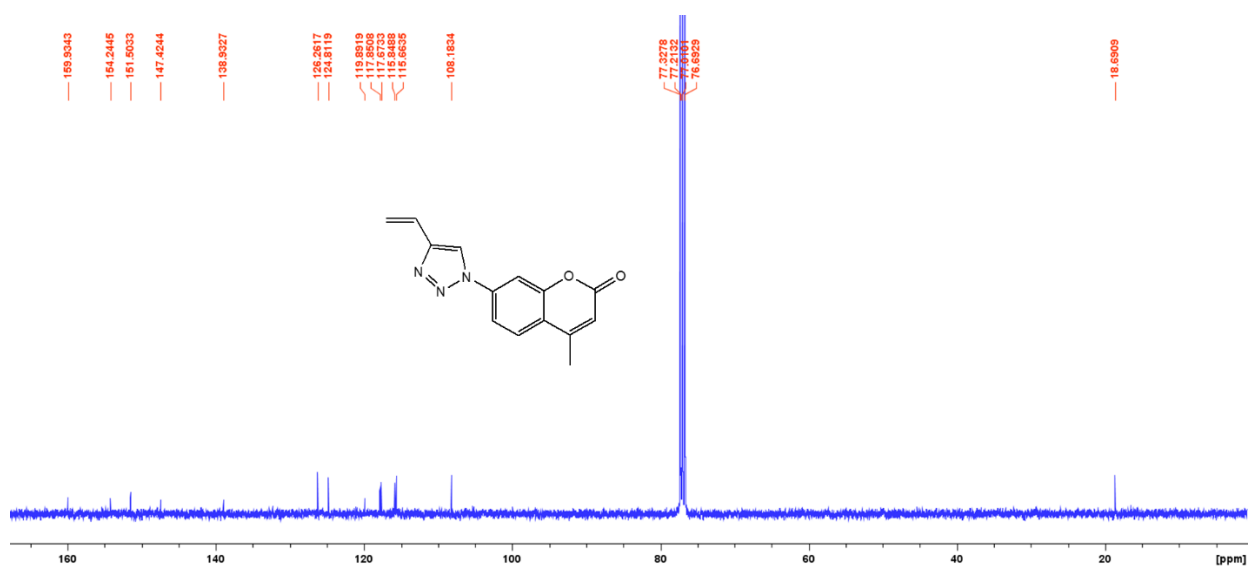


**Figure A.9:**  $^{13}\text{C}$  NMR spectrum of 4-methyl-7-(4-vinyl-1*H*-1,2,3-triazol-1-yl)-2*H*-chromen-2-one in  $\text{CDCl}_3$ .

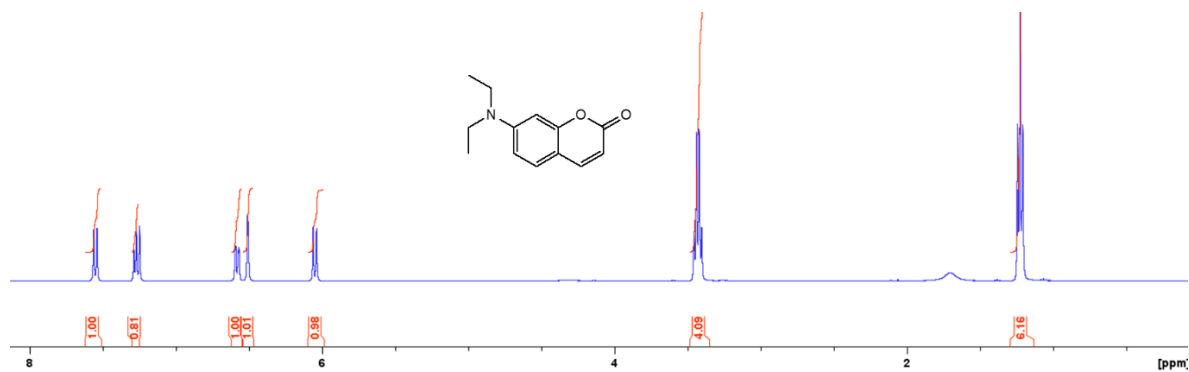


**Figure A.10:**  $^1\text{H}$  NMR spectrum of 7-(diethylamino)-2*H*-chromen-2-one in  $\text{CDCl}_3$ .

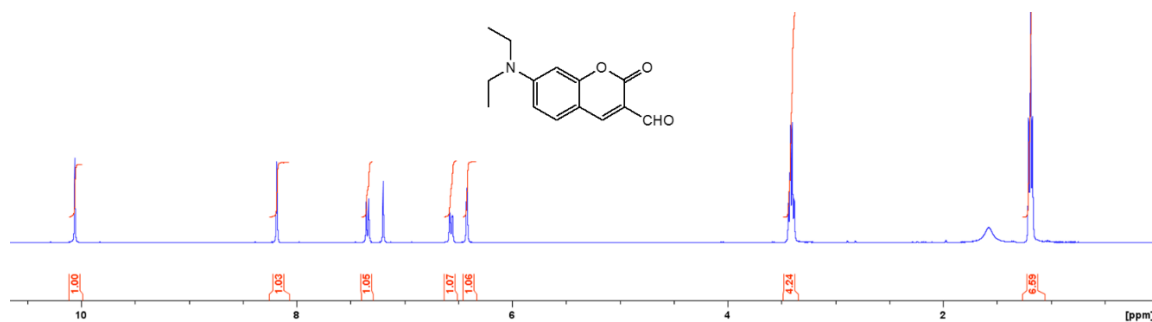
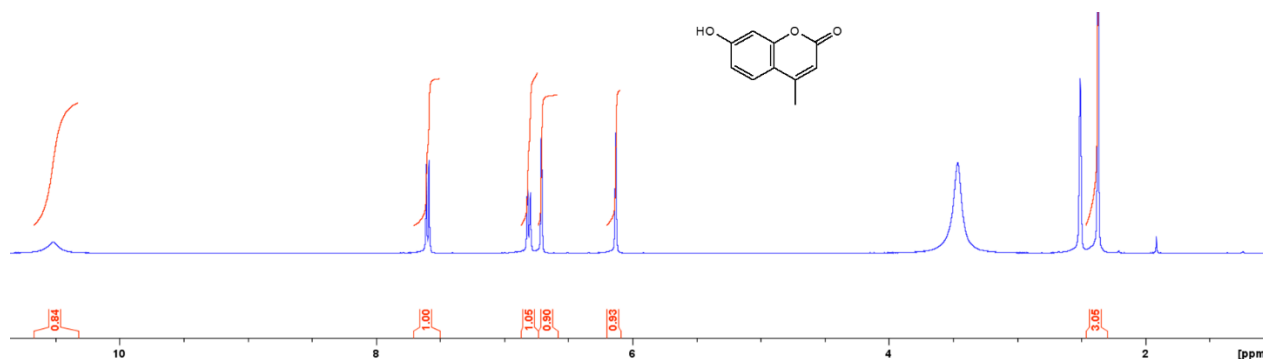


**Figure A.11:**  $^1\text{H}$  NMR spectrum of 7-(diethylamino)-2-oxo-2*H*-chromene-3-carbaldehyde in  $\text{CDCl}_3$ .

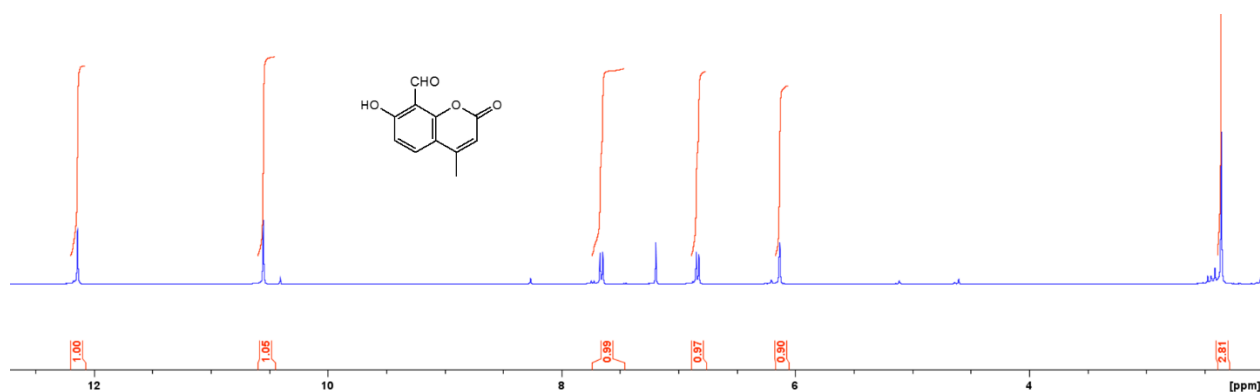




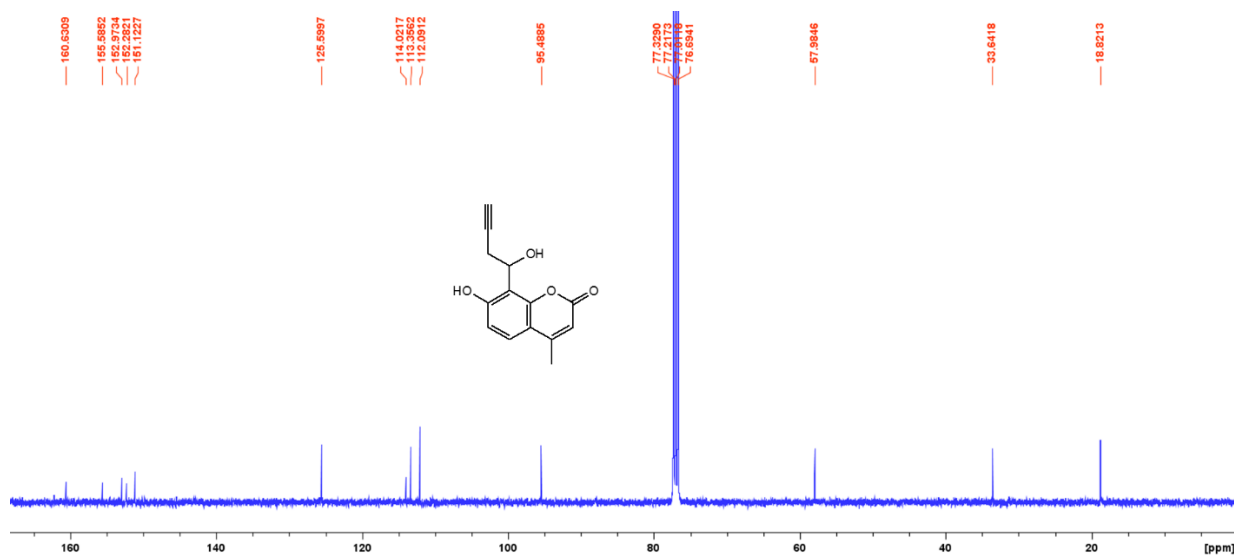
**Figure A.12:**  $^1\text{H}$  NMR spectrum of 7-(diethylamino)-3-(1-hydroxybut-3-ynyl)-2*H*-chromen-2-one in  $\text{CDCl}_3$ .



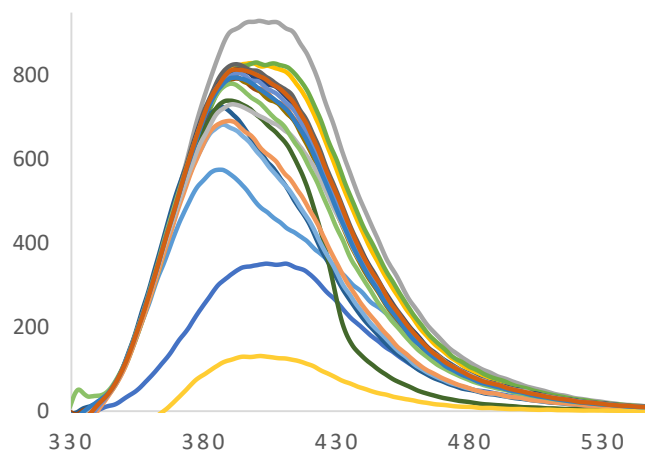
**Figure A.13:**  $^1\text{H}$  NMR spectrum of 7-hydroxy-4-methyl-2*H*-chromen-2-one in  $\text{CDCl}_3$ .



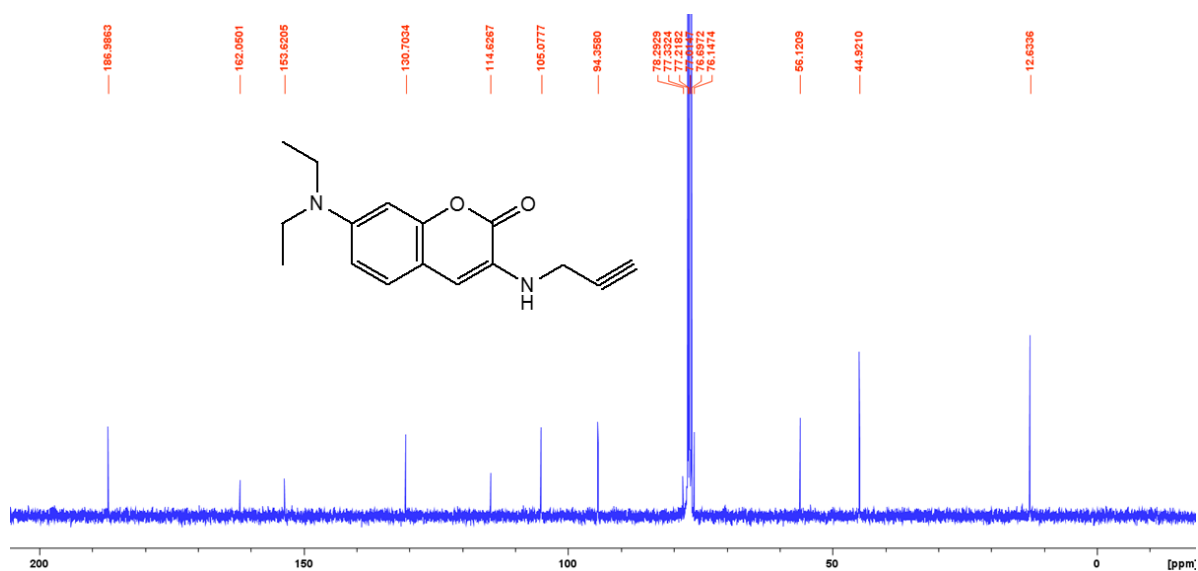
**Figure A.14:**  $^1\text{H}$  NMR spectrum of 7-hydroxy-4-methyl-2-oxo-2*H*-chromene-8-carbaldehyde in  $\text{CDCl}_3$ .



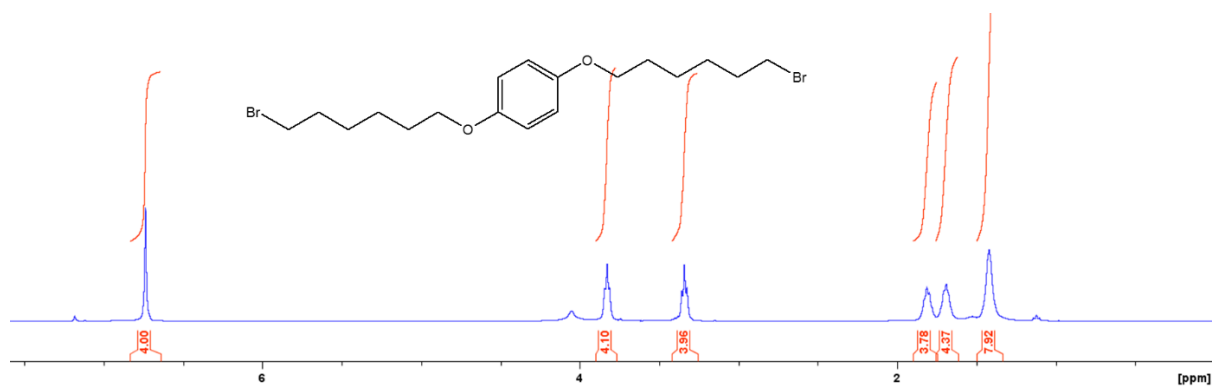
**Figure A.15:**  $^{13}\text{C}$  NMR spectrum of 7-hydroxy-8-(1-hydroxybut-3-ynyl)-4-methyl-2*H*-chromen-2-one in  $\text{CDCl}_3$ .



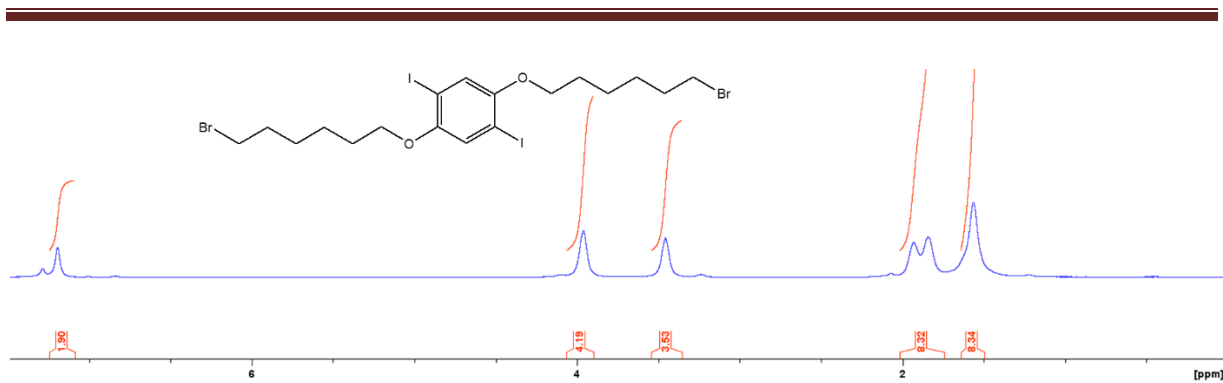
**Figure A.16:** Fluorescence spectra of polymer **P2** in the presence of mixture of  $\text{Al}^{3+}$  with two equivalents of other metal ions. Excitation was performed at 325 nm.



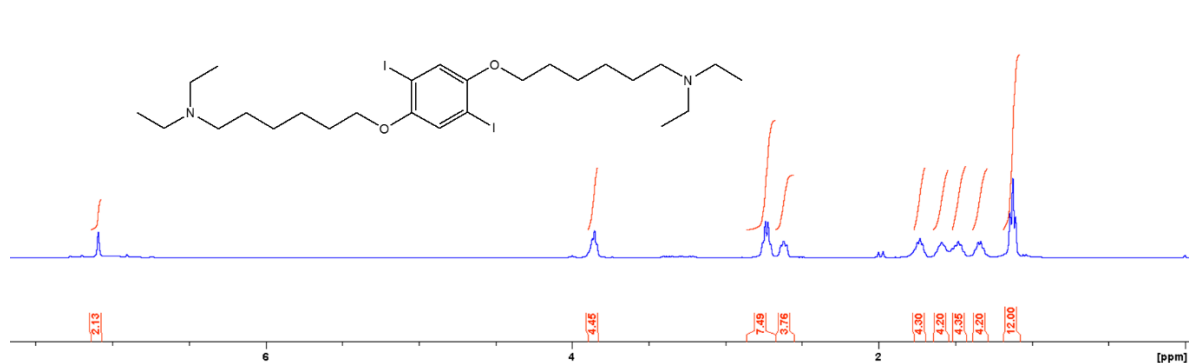
**Figure A.17:**  $^{13}\text{C}$  NMR spectrum of 7-(diethylamino)-3-(prop-2-ynylamino)-2H-chromen-2-one in  $\text{CDCl}_3$ .



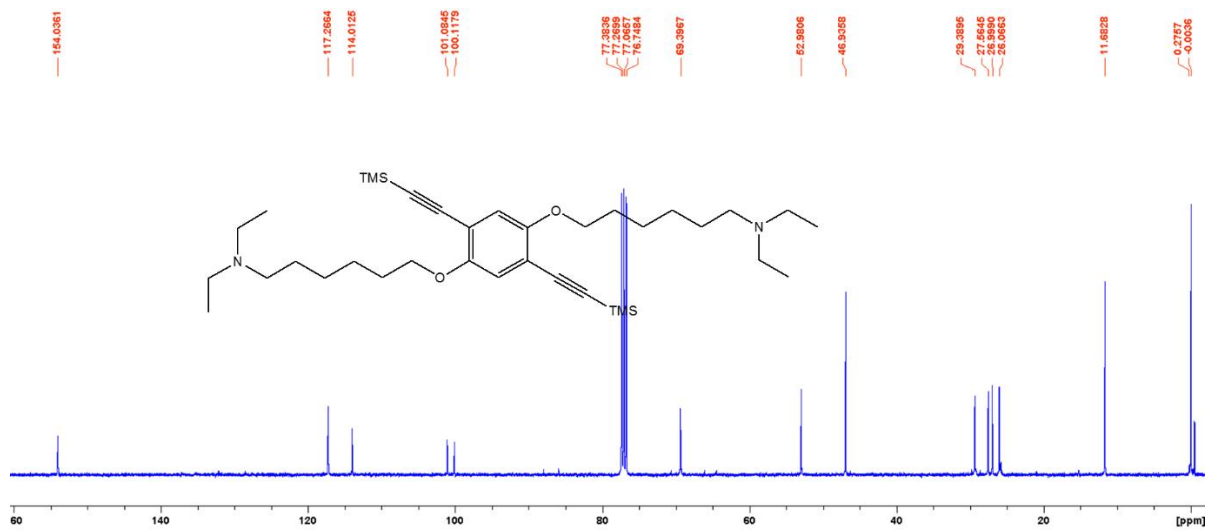
**Figure A.18:**  $^1\text{H}$  NMR spectrum of 1,4-bis(6-bromohexyloxy)benzene in  $\text{CDCl}_3$ .



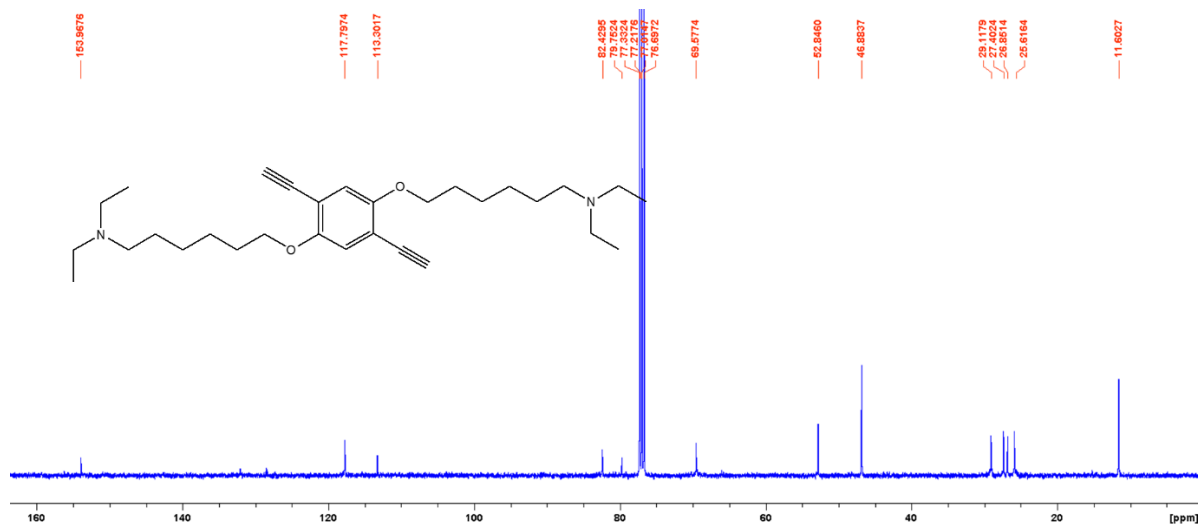
**Figure A.19:**  $^1\text{H}$  NMR spectrum of 1,4-bis(6-bromohexyloxy)-2,5-diiodobenzene in  $\text{CDCl}_3$ .



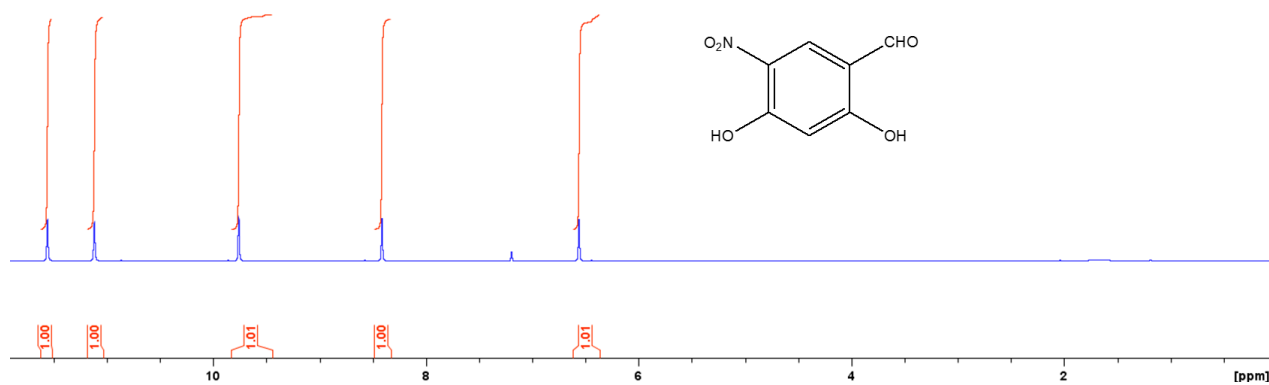
**Figure A.20:**  $^1\text{H}$  NMR spectrum of 6-(4-(6-(diethylamino)hexyloxy)-2,5-diiodophenoxy)-N,N-diethylhexan-1-amine in  $\text{CDCl}_3$ .



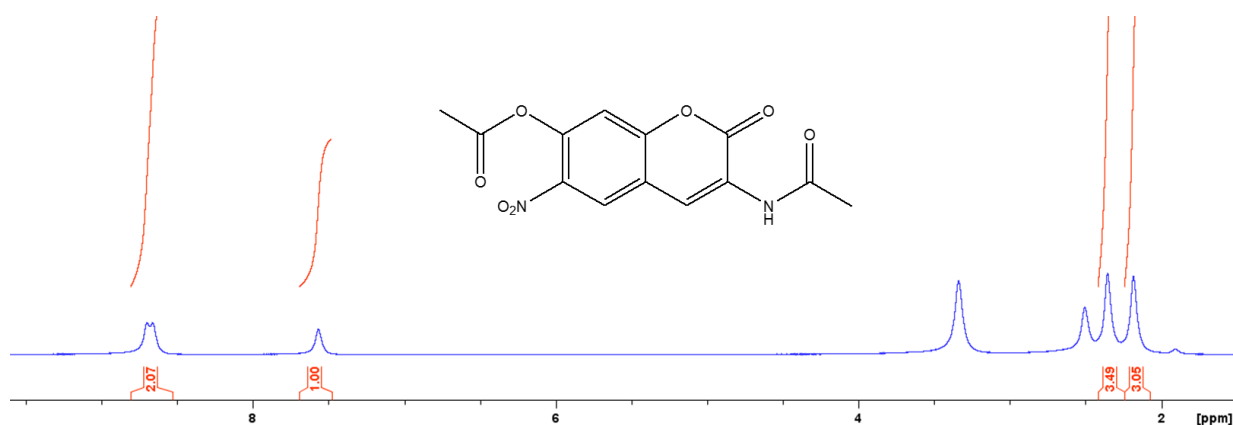
**Figure A.21:**  $^{13}\text{C}$  NMR spectrum of 6-(4-(6-(diethylamino)hexyloxy)-2,5-bis(2-(trimethylsilyl)ethynyl)phenoxy)-N,N-diethylhexan-1-amine in  $\text{CDCl}_3$ .



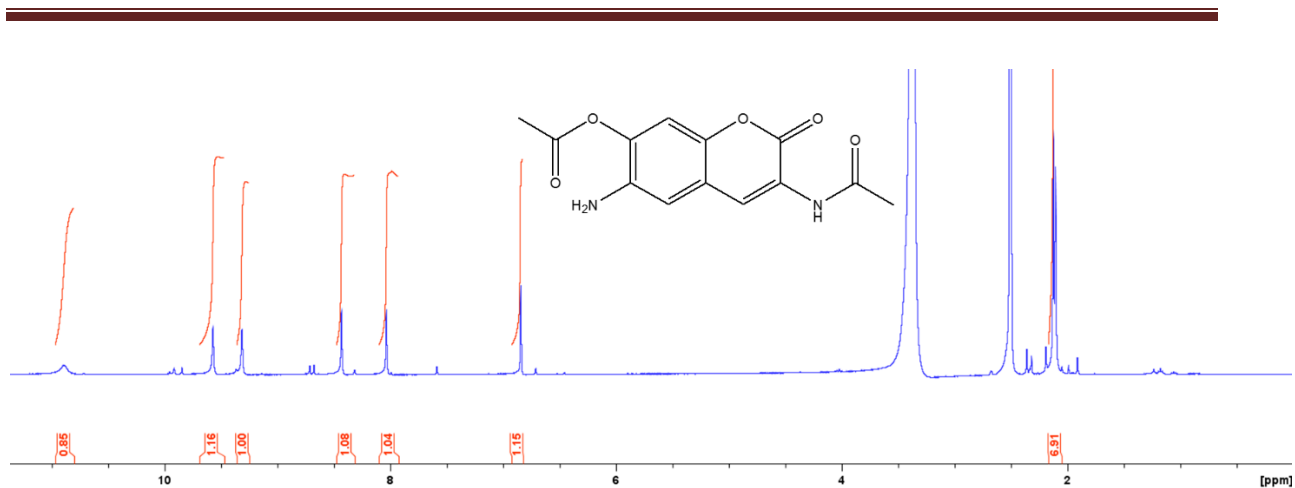
**Figure A.22:** <sup>13</sup>C NMR spectrum of 6-[4-(6-(diethylamino)hexyloxy)-2,5-diethynylphenoxy]-*N,N*-diethylhexan-1-amine in CDCl<sub>3</sub>.



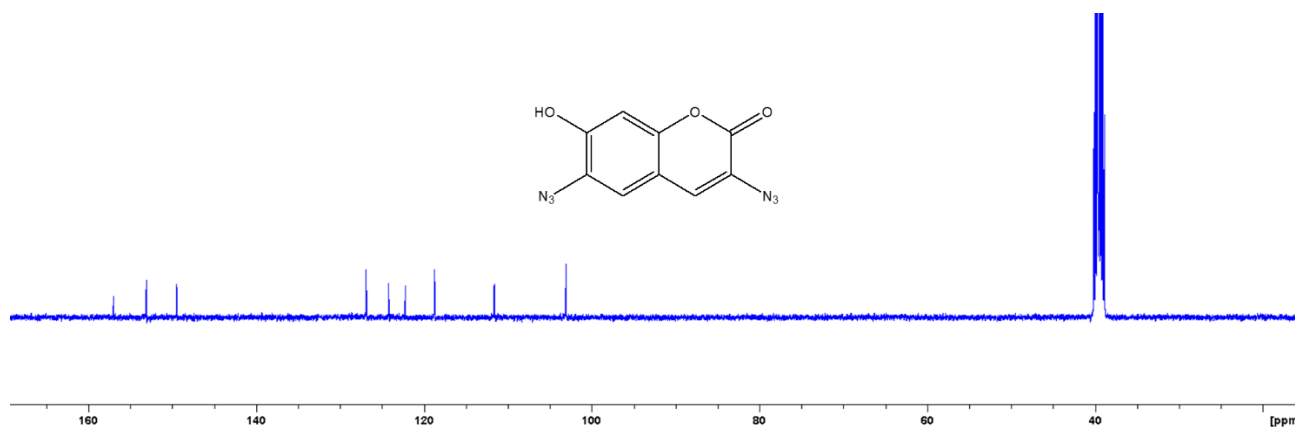
**Figure A.23:** <sup>1</sup>H NMR spectrum of 2,4-dihydroxy-5-nitrobenzaldehyde in CDCl<sub>3</sub>.



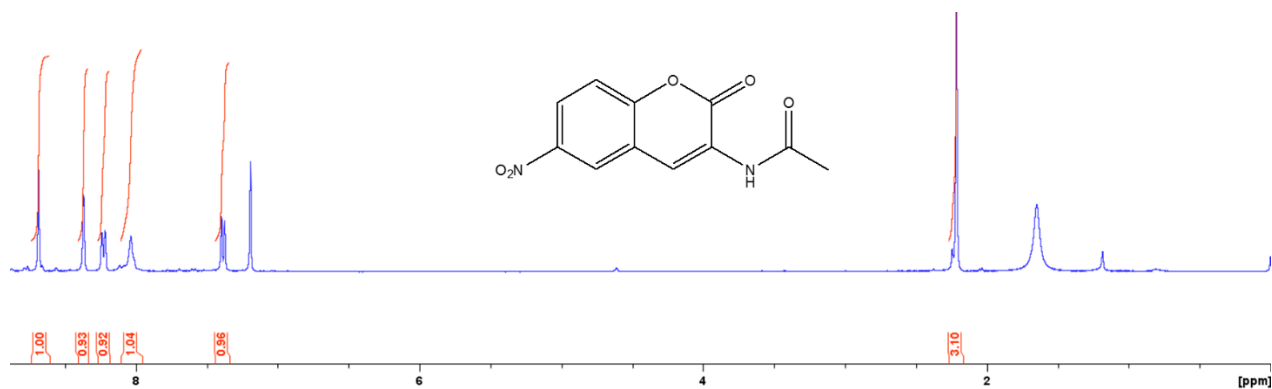
**Figure A.24:** <sup>1</sup>H NMR spectrum of Coumarin (**10**) in DMSO-d<sub>6</sub>.



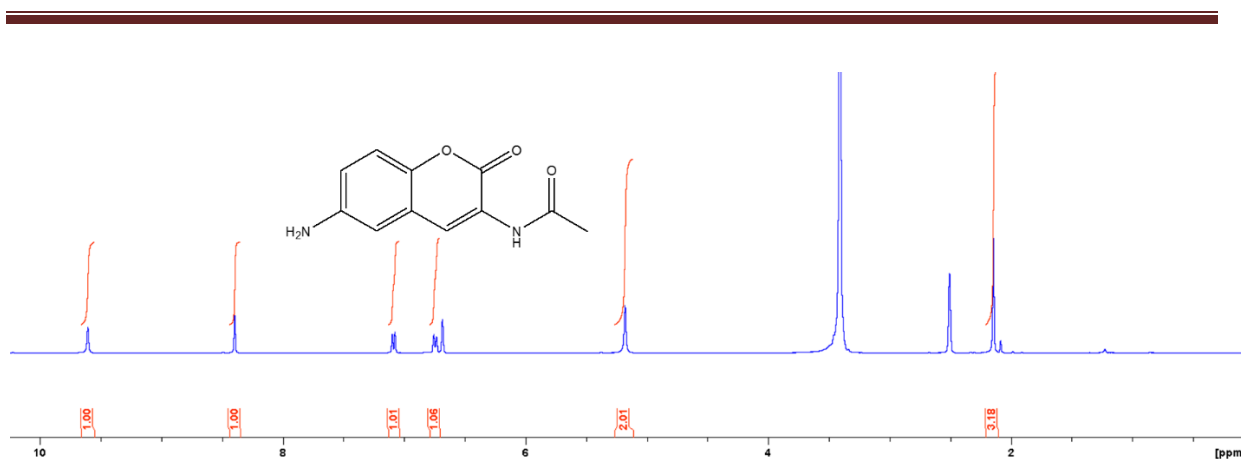
**Figure A.25:** <sup>1</sup>H NMR spectrum of Coumarin (11) in DMSO-d<sub>6</sub>.



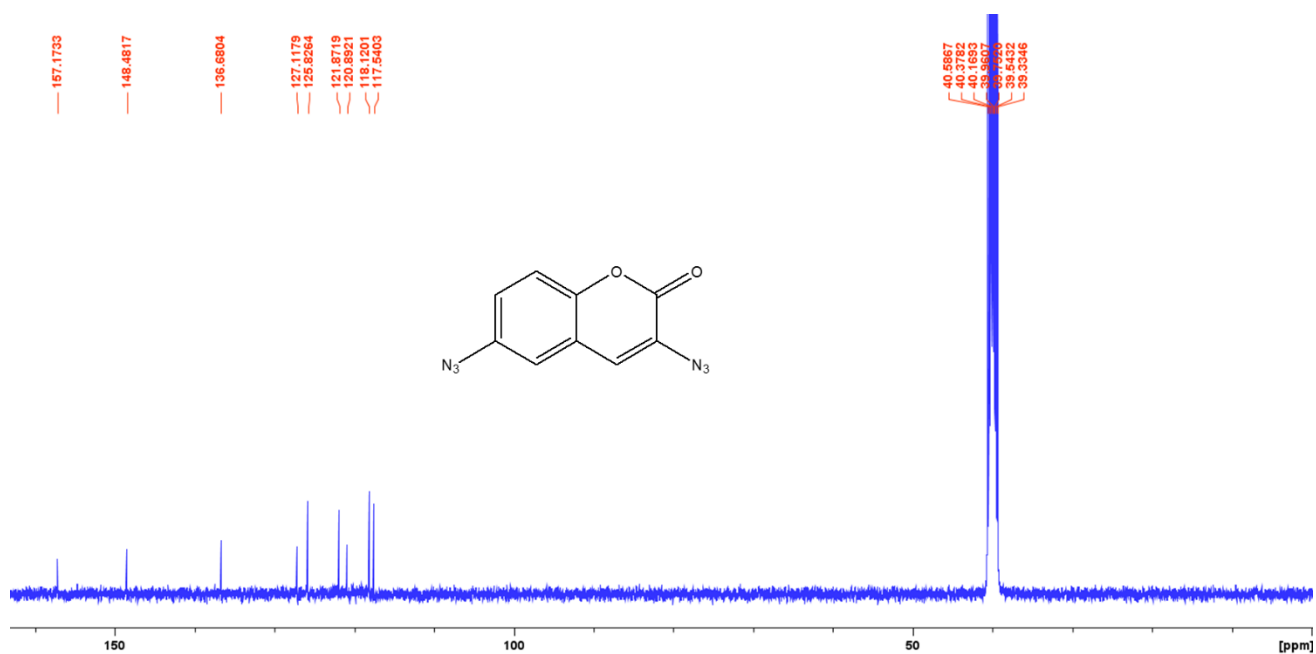
**Figure A.26:** <sup>13</sup>C NMR spectrum of 3,6-diazo-7-hydroxy-2H-chromen-2-one in DMSO-d<sub>6</sub>.



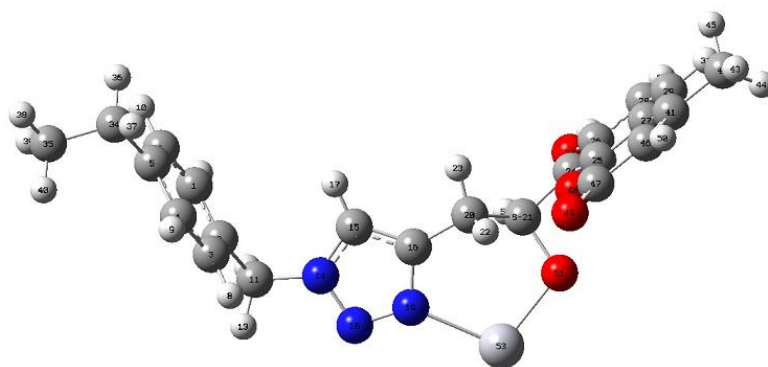
**Figure A.27:** <sup>1</sup>H NMR spectrum of N-(6-nitro-2-oxo-2H-chromen-3-yl)acetamide in CDCl<sub>3</sub>.

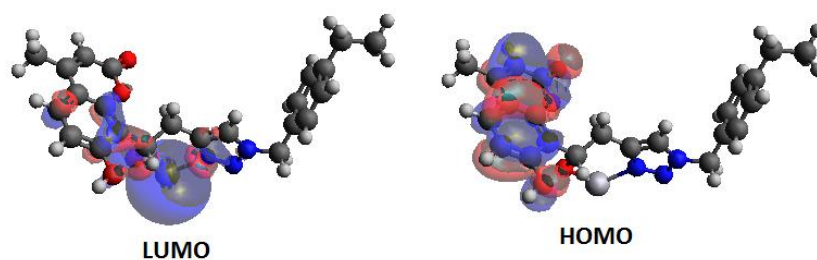


**Figure A.28:**  $^{13}\text{C}$  NMR spectrum of N-(6-amino-2-oxo-2H-chromen-3-yl)acetamide in DMSO- $\text{d}_6$ .

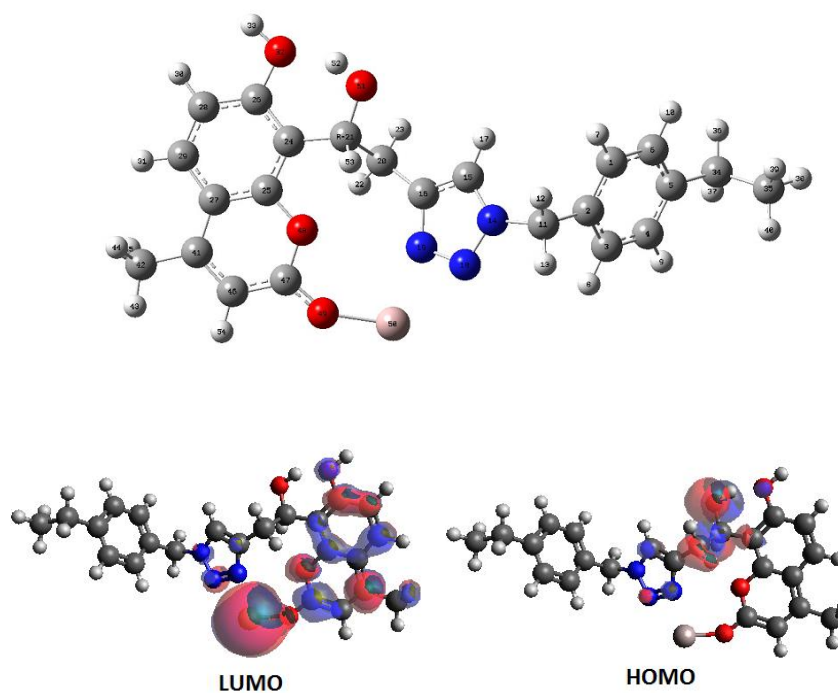


**Figure A.29:**  $^{13}\text{C}$  NMR spectrum of 3,6-diazo-2H-chromen-2-one in DMSO- $\text{d}_6$ .





**A. 30:** Computed structure of pendant chain of polymer **P2** in the presence of  $\text{Hg}^{2+}$  at the DFT (B3PW91/LanL2MB) level.



**A. 32:** Computed structure of pendant chain of polymer **P2** in the presence of  $\text{Al}^{3+}$  at the DFT (B3PW91/LanL2MB) level.